THE EFFECT OF MASONRY INFILL ON THE SEISMIC BEHAVIOUR OF REINFORCED CONCRETE MOMENT RESISTING FRAMES

By

WAEL MOHAMED ABOU ELMAGD MAHMOUD BASIOUNY

A Thesis
Submitted to the School of graduate Studies
in Partial Fulfillment of the Requirements
for the degree
Doctor of Philosophy

McMaster University
Hamilton, Ontario, Canada

DOCTOR OF PHILOSOPHY (2009)
(Civil Engineering)

McMaster University
Hamilton, Ontario, Canada

TITLE: THE EFFECT OF MASONRY INFILL ON THE SEISMIC BEHAVIOUR OF REINFORCED CONCRETE MOMENT RESISTING FRAMES

AUTHOR: WAEL MOHAMED ABOU ELMAGD MAHMOUD BASIOUNY
B.Sc. (Cairo, Egypt)
M.Sc. (Cairo, Egypt)

SUPERVISOR: PROFESSOR AHMED GHOBARAH

NUMBER OF PAGES: xx, 219

ABSTRACT

A moment resisting frame is one of the most commonly used lateral load resisting system in modern structures because it is suitable for low and medium rise buildings and industrial structures. It can be designed to behave in a ductile manner under seismic loads.

Masonry infills have traditionally been used in buildings as partitions and for architectural or aesthetic reasons. They are normally considered as non-structural elements, and their effect on the structural system has been ignored in the design. However, even though they are considered non-structural elements, there is mounting evidence that they interact with the frame when the structures are subjected to lateral loads

Infill walls have been identified as a contributing factor to catastrophic structural failures during earthquakes. Frame-infill interaction can induce brittle shear failures of reinforced concrete columns by creating a short column. Furthermore, infills can over-strengthen the upper stories of a structure and when they fail a soft first storey is created, which is highly undesirable from the earthquake resistance standpoint.

There is a need for an efficient and accurate computational model to simulate the nonlinear hysteretic force-deformation behaviour of masonry infills, which is also suitable for implementation in time-history analysis of large structures. The aim is to develop a simplified advanced and cost-effective model for nonlinear time history analysis and seismic design of masonry infill frame structures.

The objective of this research was to develop a practical and economical technique applicable for global analysis of general three-dimensional reinforced concrete infilled frames under lateral loads. Novel finite element model for the infill and the surrounding frame was developed using a special finite element configuration to represent the masonry panel. Some prescribed failure planes in different directions were defined depending on the common failure mode of masonry panels. Moreover, some of contact elements were used on the failure planes to connect among the panel elements, and between the panel elements and the boundary reinforced concrete frame. Different material models were used to represent the behaviour of concrete, reinforcing steel, mortar joints and inclined saw-tooth cracks in the infill panel. Different material models were used to describe the behaviour

through and perpendicular to the prescribed failure planes. The proposed model and the used material models were described in details in the first part of this research.

The proposed finite element model was verified against experimental and analytical results previously published by others. Different frames configurations, reinforcing details, boundary conditions and material properties were consider in that section to verify the capability of the proposed model to simulate the behaviour of different frames. The overall behaviour "Load-deflection relationship", failure point and failure mode were compared with the experimental and analytical results. Satisfactory agreement with the previously published results was obtained.

The study investigates the capability of the proposed model to simulate the behaviour of infilled frames subjected to cyclic loads. Hysteretic loops obtained by using the new model were verified against experimental and analytical results and good correlation were obtained. The failure modes and crack patterns were compared with the experimental results and good agreements were obtained. The proposed model failed to capture some shear cracks in the RC frames as per the experimental results.

ACKNOWLEDGEMENTS

I wish to express my sincere appreciation to my research supervisor Professor Ahmed Ghobarah, for his firm support, guidance, advices, encouragement and time spent throughout the course of this research. I thank the members of my supervisory committee Dr. Stan Pietruszczak and Philip Koshy for their valuable comments, advices and suggestions and their time spent in reviewing this thesis. Thanks are also due to the Civil Engineering Department Chair, Faculty and staff for their support and encouragement.

The author gratefully acknowledges the financial support received from the ministry of high education, Culture Affairs & missions sector, Government of Arab republic of Egypt.

Finally, much appreciation is extended to my mother and my family for their support, patience and sincere supplication.

This work is dedicated to my mother, memory of my father and my family.

TABLE OF CONTENT

LIST OF FIGURES

LIST OF TABLES

LIST OF SYMBOLS

b	The model hardening ratio.
B	Length of the infill.
c	The cohesion.
C	Applied lateral cyclic load.
d_m	Length of diagonal strut.
epsc0	Strain at the model compressive strength.
epscu	Strain at the model crushing strength.
E_0	The model initial elastic tangent.
E_b	Elastic modulus of the brick.
E_c	Elastic modulus of the concrete.
E_f	Elastic moduli of the frame material.
E_m	Elastic moduli of the masonry wall.
E_s	Elastic modulus of steel.
f'_c	Concrete compressive strength.
f_{cm}	Uniaxial compressive strength of masonry material.
f'_m	Compressive strength of the infill.
fpc	The model compressive strength.
fpcu	The model crushing strength.
f_{sy}	Yield stress of steel.
f_t	Tensile strength of the concrete.
f_{tm}	Uniaxial tensile strength of masonry material.
fy	The model yield strength.
$f(\sigma_{ij}, \varepsilon^p_{ij}, k)$	Load function.
$g(\sigma_{ij}, \varepsilon^p_{ij}, k)$	Potential function.
H	Height of infill panel.
k	Hardening parameter.
k_n & k_s	The stiffness of the contact springs.
L	Length of enfill panel.
m	Parameter to measure relative lateral strength.
M_p	Plastic moment capacity of the corners of the frame.

M_z	Applied moment about z-axes.
N	Axial load in surrounding columns.
P	Applied vertical concentrated load.
t_w	Thickness of the infill.
V_y	Initial elastic stiffness upto the yield force.
V_m	Maximum strength of masonry panel.
V_z	Shear force in z-direction.
w	The equivalent strut width.
W	Applied vertical distributed load.
α	Angle between the diagonals and the beams.
ε	Total strain.
ε^e	Reversible elastic strain.
ε^p	Permanent plastic strain.
ε^p_{ij}	Plastic strain component.
$d\varepsilon^p_{ij}$	The increment of plastic strain components.
ε_u	Ultimate compressive strain.
$d\lambda$	Positive scalar factor of proportionality.
ν_c	Concrete poisson's ratio.
ν_s	Steel poisson's ratio.
ν_m	Masonry poisson's ratio.
ρ	Ratio of longitudinal reinforcement (%).
σ	Vertical axial stress.
σ_{ij}	The state of stress.
$d\sigma_{ij}$	The stress increment.
σ_{sy}	Steel yield stress.
σ_u	Masonry compressive strength.
τ_f	Mortar shear strength.
τ_{max}	Maximum shear stress.
τ_{sl}	Shear stress at slip surface.
θ	The angle of inclined failure planes with the horizontal axis.
φ	The angle of internal friction.

CHAPTER 1

INTRODUCTION

1.1 GENERAL

There are several structural systems used in reinforced concrete (RC) buildings to resist lateral loads such as wind, mechanical loads or ground motions. Each lateral load resisting system has advantages and disadvantages. The main structural systems suitable for earthquake resistance include:

1- Moment resisting frames

2- Shear walls and structural walls

3- Hybrid structural system (combination of two systems)

4- Braced frames

5- Tube systems

A moment resisting frame is one of the most commonly used lateral load resisting system in modern structures because it is suitable for low and medium rise buildings and industrial structures. It can be designed to behave in a ductile manner under seismic loads. However, due to the frame flexibility the deflections may be excessive (Tarr, 1977). Many existing RC frame buildings were not designed for seismic resistance or detailed for ductile behaviour.

Masonry infills have traditionally been used in buildings as partitions and for architectural or aesthetic reasons. They are normally considered as non-structural elements, and their effect on the structural system has been ignored in the design. However, even though they are considered non-structural elements, there is mounting evidence that they interact with the frame when the structures are subjected to lateral loads (Lee and Woo, 2002). This interaction may or may not be beneficial to the performance of the structure, and it has been a topic of much recent debate (Shing and Mehrabi, 2002).

Infill walls have been identified as a contributing factor to catastrophic structural failures during earthquakes (Lee and Woo, 2002). Frame-infill interaction can induce brittle shear failures of reinforced concrete columns by creating a short column. Furthermore, infills can over-strengthen the upper stories of a structure and when they fail a soft first storey is created, which is highly undesirable from the earthquake resistance standpoint.

Masonry infills have been used to strengthen existing structures, and increase the lateral load resistance. The rigidity and strength of frames are significantly improved when masonry panels are built in line with the frames. In studies using reinforced concrete frames, the improvement in strength ranges from twice to over quadruple the strength of a frame with no infill. Stiffness improvement is still more substantial, with increase up to 60 times over that of a bare frame (Mehrabi 1994). If properly designed, detailed and constructed masonry infill can improve the earthquake resistance of a frame structure. The increase in strength is also associated with increase of the initial stiffness of the structure and may result in adverse increase of the inertia force. The damage to the structure may be reduced by dissipating a considerable portion of the input energy in the masonry infills or at the interface between the infills and the frame (Lee and Woo, 2002).

The behaviour of the masonry-infilled frame under lateral loads has been investigated by several researchers. Bertero et al. (1983) performed an experimental investigation of a series of quasi-static cyclic and monotonic load tests on 1/3-scale models of the lower 3-1/2 storeys of an 11-storey, 3-bay RC frame infilled in the outer two bays. Different panel material and reinforcement combinations were tested. In this study, the effective inter-storey lateral stiffness of infilled frames was 5.3-11.7 times the lateral stiffness of the bare frame depending on the type of infill used. The maximum lateral resistance of infilled frames was 4.8-5.8 times that obtained for the bare frame.

There is the misconception that a frame with infills, as it is subjected to an earthquake, the infills will fail first and the behaviour will be that of a bare frame, as shown in figure 1.1. This behaviour has been observed following major earthquake but not very often. This scenario is likely to occur when very weak infill masonry tiles are used in a heavy RC moment resisting frame. The sequence of failure of infills affects the failure of the frames and may produce brittle failure. Moreover, if the configuration of the infills is irregular, they can induce significant local damages to the structural elements (Lee and Woo, 2002).

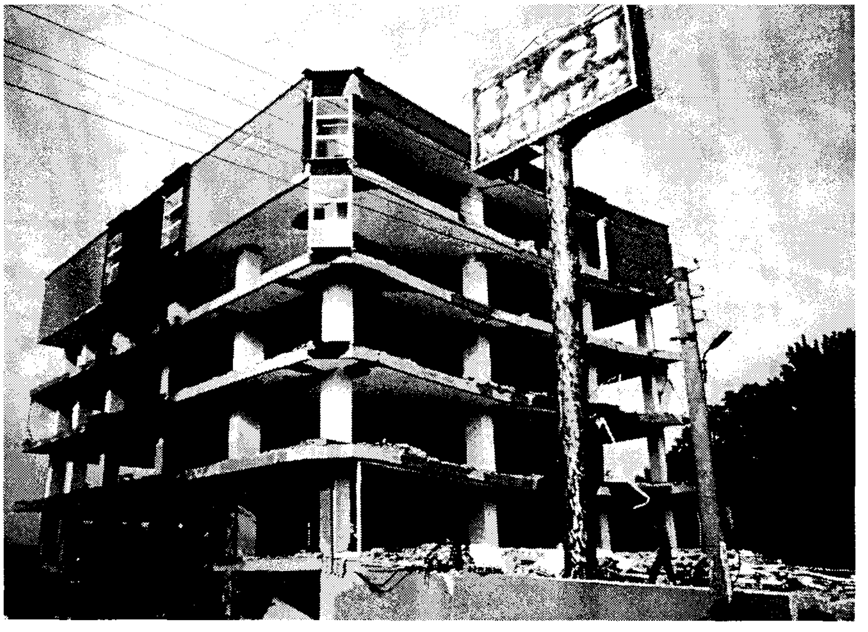

Fig. 1.1 Complete failure of the infill panel during earthquake.

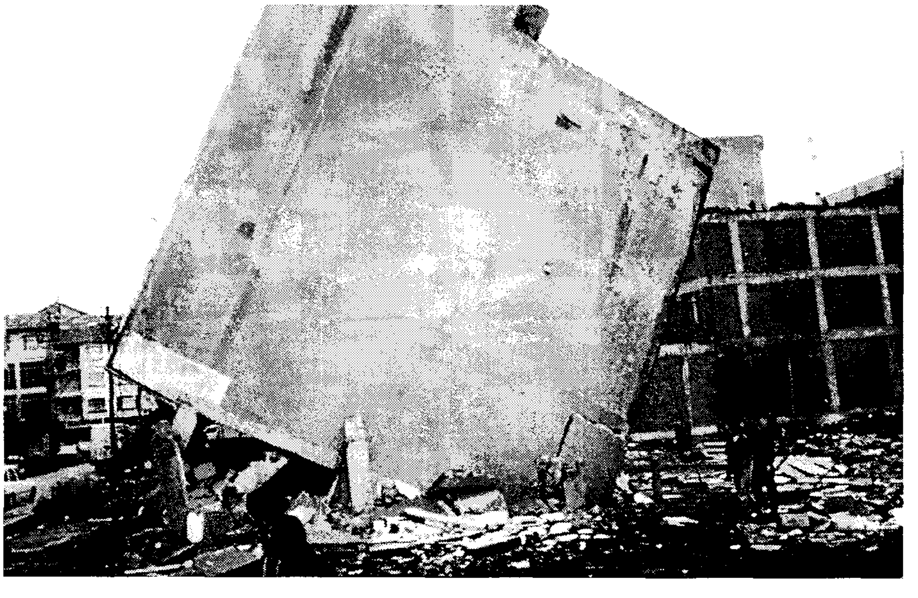

Fig. 1.2 Soft-story mechanisms due to failure of first floor masonry infill.

Soft-story failure mechanism may occur due to a stiffness decrease in a story, compared to the adjacent ones. Significant change in stiffness results in concentration of high stresses in the elements of the soft story, leading, in most cases, to extensive damages. Failure of the masonry infill walls in the first story creates a soft story failure mechanism as shown in figure 1.2.

Masonry built up to mid-height of the panel (or due to partial failure during earthquake) leads to increase in the stiffness of column and the creation of a short column with brittle shear failure. This type of failure is known as short column failure mechanism, as shown in figure 1.3.

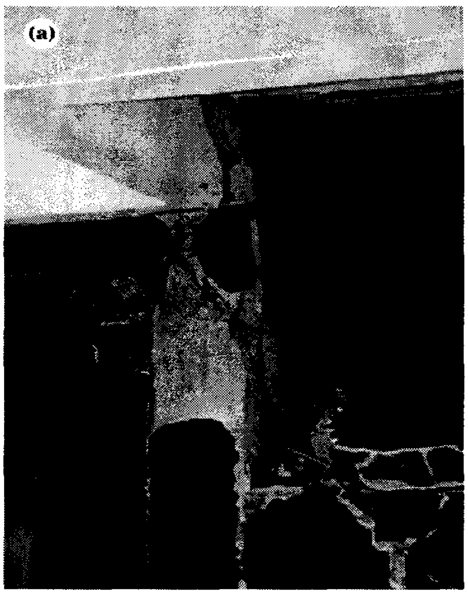

Fig. 1.3 Brittle shear failure in short column (Saatcioglu et al., 2001)

The experience gained from recent earthquakes showed that irregular distribution of infills and neglecting the interaction between the frame structure and infills may cause the collapse of the entire structure. The actual capacity of these structures and their ability to withstand moderate and strong earthquakes needs to be evaluated using accurate models for predicting the behaviour of structures subjected to in-plain and out-of-plain loads (Shing and Mehrabi, 2002).

In most of the current seismic codes, the influence of non-structural masonry infills is ignored (Lee and Woo, 2002). In spite of the numerous studies in past years, many of the controversial issues still remain. The main difficulty in evaluating the performance of an infilled structure is to determine the nature of interaction between the infill and the frame, which has a major impact on the structural behaviour and load-resisting mechanism.

1.2 BEHAVIOUR OF MASONRY INFILLED RC FRAMES

Masonry is a complex material consisting of an assemblage of bricks and mortar joints, each with different properties. The behaviour is made more complex by the mortar joints acting as planes of weakness due to their low tensile, shear and bond strengths. The out-of-plane stiffness of the unreinforced masonry panels is very low as compared to its in-plane stiffness. The behaviour of an infilled frame depends on the interaction between the infill and the frame.

The behaviour of masonry-infilled reinforced concrete frames subjected to in-plane lateral loads was investigated by a number of researchers. Studies have shown that infilled frames can develop a number of possible failure mechanisms, depending on the strength and stiffness of the bounding frame with respect to those of the infill and the geometric configuration of the framing system (Shing and Mehrabi, 2002).

At a low lateral load level, an infilled frame acts as a monolithic load resisting system with high in-plane stiffness. As the load increases, the infill tends to partially separate from the bounding frame and form a compression strut mechanism as observed in several studies. However, the compression strut may or may not evolve into a primary load-resistance mechanism of the structure, depending on the strength and stiffness properties of the infill with respect to those of the bounding frame (Shing and Mehrabi, 2002).

1.2.1 Failure Mechanism

From experimental observations, five main failure mechanisms of infilled frames were identified. They are illustrated in figure 1.4, and are summarized as follows: (Shing and Mehrabi, 2002);

Mode-A: is a purely flexural mode in which the frame and the infill act as an integral flexural element. This behaviour can occur at a low load level, where the separation of the frame and the infill has not occurred; it rarely evolves into a primary failure mechanism, except for the case of tall slender frames with low flexural reinforcement in the columns. A low reinforcement ratio causes the early yielding of the flexural steel in the windward column when it is subjected to tension. In most cases, infill panels tend to partially separate from the bounding frame at a moderate load level if the two are not securely tied. This is normally the case when the infills are treated as non-structural elements (Shing and Mehrabi, 2002).

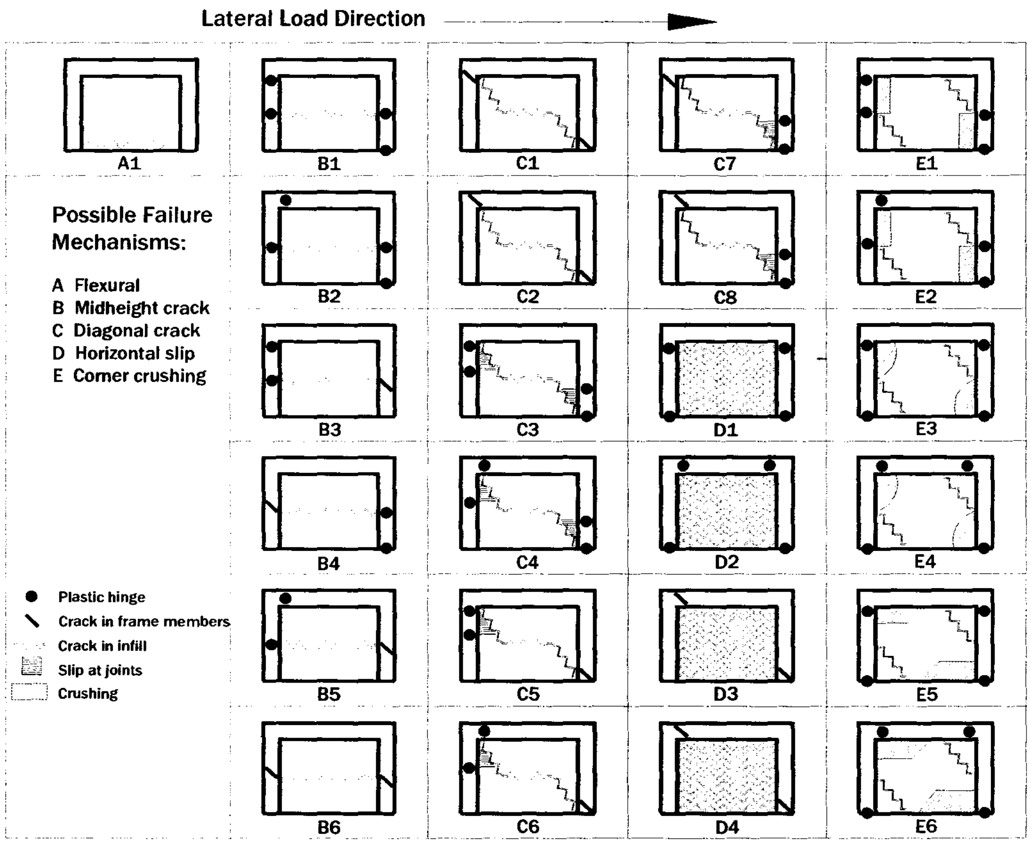

Fig. 1.4 Failure mechanisms of infilled frames (Shing and Mehrabi, 2002).

Mode-B: is a failure mechanism that is characterized by a horizontal sliding crack at the mid-height of an infill as shown in figure 1.5. This creates short-column behaviour and is therefore highly undesirable. In this situation, plastic hinges can form at the mid-height of the frame. For reinforced concrete frames, the columns will have a tendency to develop shear failure, especially in the windward column that is subjected to tension. The lateral resistance corresponding to this mechanism is the sum of the shear forces in the columns and the shear resistance of the wall. However, the development of plastic hinges in the columns usually occurs at a relatively large lateral displacement. Therefore, the infill is assumed to be cracked at that time, and the residual shear force of the cracked infill should be considered as the shear resistance of the wall (Shing and Mehrabi, 2002).

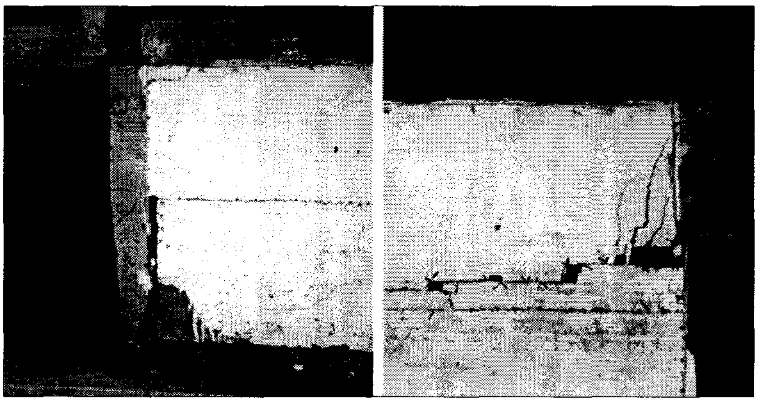

Photo-**A** Photo-**B**

Fig. 1.5 Development of cracks in pushover test-Mode-B (Lee and Woo, 2002).

Mode-C: diagonal cracks propagate from one loaded corner to the other; and these can sometimes be jointed by a horizontal crack at mid-height. In this case, the infill develops a diagonal strut mechanism that may eventually lead to corner crushing and plastic hinges or shear failure in the frame members. The main distinction of this mechanism from the mechanism of mode-B is the development of shear failure at one or more locations in the columns. As shown in figure 1.6, the lateral resistance provided by this mechanism is the sum of the ultimate shear resistance of the windward column, the shear force in the leeward column, and the residual shear resistance along the horizontal crack in the wall.

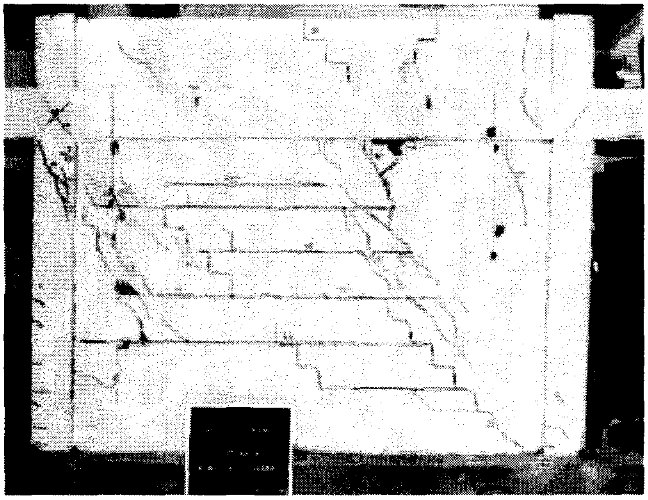

Fig. 1.6 Failure pattern-Mode-C (Shing and Mehrabi, 2002).

Mode-D: is characterized by the sliding of multiple bed-joints in the masonry infill. This type of failure often occurs in infills with weak mortar joints, and can result in a fairly ductile behaviour, provided that the brittle shear failure of the columns can be avoided. In the mechanism of mode-D, the frame and the infill are considered as two parallel systems with displacement compatibility at the compression corners. Hence, the lateral resistance of this mechanism is considered to be the sum of the flexural resistance of the frame and the residual shear resistance of the fractured wall (Shing and Mehrabi, 2002).

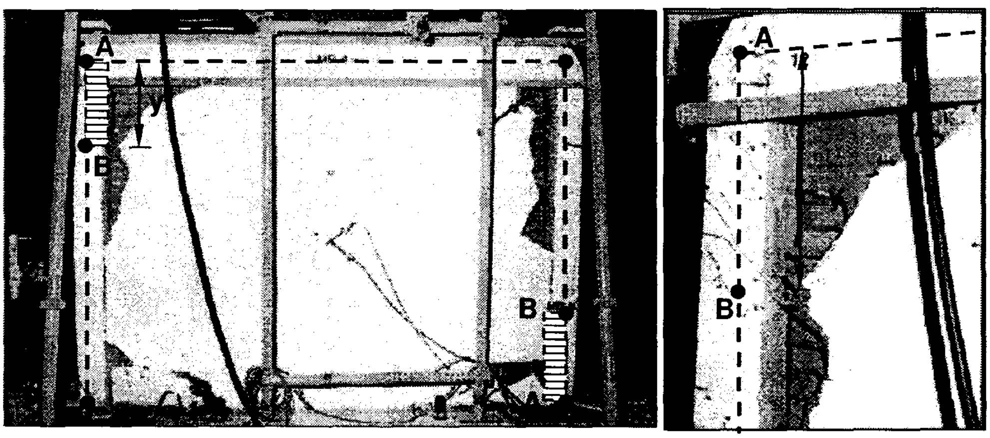

Fig. 1.7 Failure pattern-Mode-E (Combescure and Pegon, 2000).

Mode-E: exhibits a distinct diagonal strut mechanism with two distinct parallel cracks. It is often accompanied by corner crushing. Sometimes, crushing also occurs at the centre of the infill. In the mechanism of mode-E, as shown in figure 1.7, masonry is assumed to reach the crushing strength along the length y at the wall-to-frame interface, and plastic hinges are assumed to develop in the columns near the beam-to-column joints and at points B in the columns. This mechanism is based on the plastic analysis method proposed by Liauw and Kwan (1985). It is assumed that there is no significant shear transfer between the beam and the infill. The contact stress between the infill and the columns is assumed uniform, which implies that the entire region has reached the plastic state (Shing and Mehrabi, 2002).

1.2.2 Parameters that Affect the Failure Mechanisms

The complex interaction between an infill and a surrounding structural frame was identified in earlier work conducted by Polyakov (1956 and 1960). In the last five decades, several researchers have studied systems consisting of various combinations of frame and infill materials (Seah et al. 1997). Due to a multitude of highly variable parameters affecting the behaviour of infilled frames, approximate analyses are generally acceptable for this type of structure. In the following section discussions of some of the parameters that affect the behaviour of infilled frame are presented.

Aspect ratio of infill panel

Experiments conducted by Oliveira and Lorenc (2004) showed that the aspect ratio (height/length) is an important parameter that affects the wall's overall behaviour. These effects are related to the activation of different mechanisms of non-linearity, namely cracking of the joints, frictional sliding along the joints, tensile and shear failure of the units and compressive failure of masonry.

An infilled frame that failed in diagonal compression mode may, due to decrease in length, fail in shear rotation mode. In addition, if the length of the infill is increased, the infill that failed in diagonal compression mode may fail in shear rotation mode. In a square frame panel, the resultant of the horizontal and the vertical reactions passes through the loaded point at the top opposite corner. Depending on the aspect ratio, this resultant rotates. The direction of this resultant determines whether hinges are formed in the beam or in the column. Frames with low aspect ratios are common. The columns of a building could be spaced at 6 m and by as much as 10 m while the typical floor to floor height is normally less than 4 m. However, experimental work using specimens of this aspect ratio is rare or nonexistent (Ghosh and Made, 2002).

Strength of the infill panel (Weak/Strong infill)

While most of the studies have focused on unreinforced masonry panels, Klingner and Bertero (1976), and Bertero and Brokken (1983) investigated the behaviour of engineered infilled frames. They tested 1/3-scale, three-storey, reinforced concrete frames infilled with fully grouted concrete masonry that had both horizontal and vertical reinforcement. The infill panels were securely tied to the bounding frames. They demonstrated that properly engineered infilled frames can provide superior performance, in terms of strength, stiffness, and energy dissipation, compared with a bare frame. An over-reinforced infill may risk the brittle shear failure of the bounding reinforced concrete columns. Studies by Mehrabi et al. (1994 and 1996) have shown that relatively weak unreinforced masonry infills can enhance the stiffness and strength of a non-ductile reinforced concrete frame significantly without jeopardizing ductility.

It was found that for most frames with weak infills, the shear beam model provides close correlation with test results. For frames with strong infills, the shear beam model tends to overestimate the secant stiffness by more than two-fold. The last case is associated with separation of the infills from the bounding frames at a low load level (Shing and Mehrabi, 2002).

The analytical results, by Shing and Mehrabi (2002), indicated that Mechanism E is the dominant failure mechanism of the specimens with weak infills. In this mechanism, large slips along the bed-joints and the plastic hinges in the columns govern. On the other hand, for the specimens with strong infills, the results indicated that the mechanism of mode-C dominated. This mechanism is governed by the diagonal/sliding shear failure of the infill and the shear failure of the windward column (Shing and Mehrabi, 2002).

In summary, the failure mechanism and load resistance of an infilled frame depends very much on the strength and stiffness of the infill with respect to those of the bounding frame. It is evident that the strength of the mortar joints is also an important factor. A relatively weak infill is most desirable. Studies have shown that infill panels can significantly enhance the performance of a bare frame under earthquake loads, provided the short-column phenomenon and the brittle shear behaviour of the columns can be avoided.

Relative strength between infill and frame

At low lateral load level, an infilled frame acts as a monolithic load resisting system. As the load increases, the infill tends to partially separate from the bounding frame and form a compression strut mechanism as observed in several early studies (e.g., Stafford Smith, 1962). However, the compression strut may or may not evolve into a primary load-resistance mechanism of the structure, depending on the strength and stiffness properties of the infill with respect to those of the bounding frame (Shing and Mehrabi, 2002).

Strength of mortar

The sliding of multiple bed-joints in the masonry infill occurs in infills with weak mortar joints. This type of failure represents failure mechanism Mode-D (figure 1.4). This failure may result in a fairly ductile behaviour, provided that the brittle shear failure of the columns is avoided. In this case, the frame and the infill are considered as two parallel systems with displacement compatibility at the compression corners. Hence, the lateral resistance of this mechanism is considered to be the sum of the flexural resistance of the frame and the residual shear resistance of the fractured wall (Shing and Mehrabi, 2002).

Ductility of the RC frame

At moderate load the infill separates from the surrounding frame and the infill behaves as a diagonal strut. As the horizontal load is increased, failure occurs eventually in either the frame or the infill. The usual mode of frame failure results from tension in the windward column, or from shearing of the columns or beams. However, if the frame strength is sufficient to prevent its collapse by one of these modes, the increasing horizontal load eventually produces failure of the infill. In the most common situations, the in-plane lateral load applied at one of the top corners is resisted by a truss formed by the loaded column and the infill along the diagonal connecting the loaded corner and the opposite bottom corner. The state of stress in the infill is a principal compressive stress along the diagonal and a principal tensile stress in the perpendicular direction. If the infill is made of concrete, successive failures, initially by cracking along the compression diagonal and then by crushing near one of the loaded corners or by crushing alone, will lead to collapse. If the infill is made of brick masonry, an alternative possibility of shearing failure along the mortar planes may arise (Ghosh and Amde, 2002).

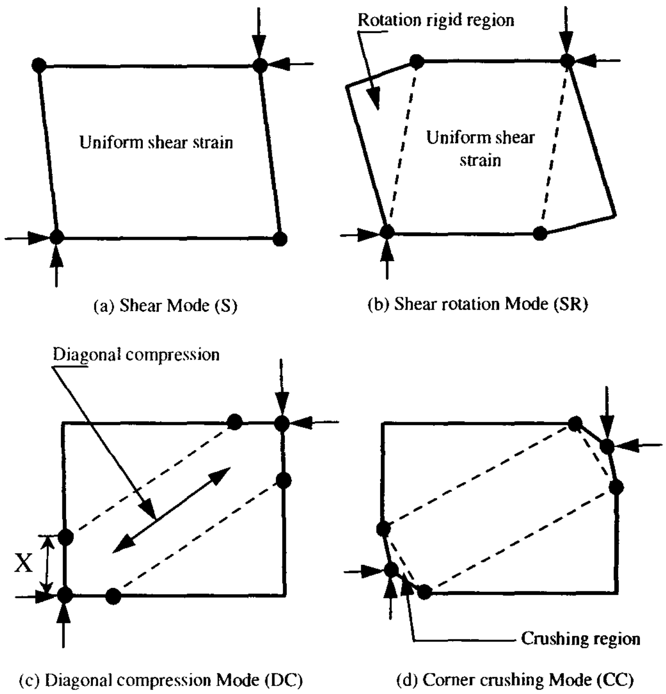

Fig. 1.8 Failure modes of infilled frames by Wood (1978)

The order of occurrence of different failure modes has been formulated based on the relative lateral strength between the infill and the frame by Wood (1978). The measure of this relative lateral strength is given by the parameter $m = 8M_p/(f'_m t_w B^2)$. In this equation, "M_p" is the plastic moment capacity of the corners of the frame, "f'_m" is the compressive strength of the infill, "t_w" is the thickness of the infill, and B is the length of the infill. Shear rotation (SR), diagonal compression (DC), and corner crushing (CC) may occur when m is less than 1. Failure in the composite shear (S) mode occurs if $m \geq 1$. Plastic hinges are formed at the beam-column connections similar to a bare frame. The infill is subjected to pure shear. This may arise at the lower levels of a multi-story frame where the columns are much stronger than a single story frame with masonry infill. The infill is subjected to pure shear because the columns go through rigid body rotation only. These modes of failure are illustrated in figure 1.8. The location of plastic hinge formation in the frame is also a function of the parameter m and is given by $X = 1 - \sqrt{m/2}(\sin\alpha)$ in which α is the angle between the diagonals and the beams. Once the mode of failure of an infilled frame is determined, the failure load can be obtained by the equations given by Ghosh and Amde, (2002).

Liauw and Kwan (1983) used a plastic collapse theory to calculate the ultimate loads for infilled frames. Three different failure modes were identified, which included corner crushing with failure in columns, corner crushing with failure in beams, and diagonal failure. The first mode of failure occurs if the frame is weak relative to the infill and the beams are stronger than the columns. The second mode occurs when the frame is weak relative to the infill and the beams are weaker than the columns. The third mode of failure occurs when the frame is stronger than the infill; therefore, plastic hinges cannot form in the columns or in the beams. They are developed at all corners and the infill crushed regions extend along the diagonal toward the infill center (Ghosh and Amde, 2002).

Openings

Infill walls may have windows or door openings. Fiorato et al. (1970) have found that the reduction of the load resistance of an infilled frame is not proportional to the reduction of the cross-sectional area of the infill, due to openings. In their tests, openings that reduced the horizontal cross-sectional area of an infill by 50% led to a strength reduction of about 20–28% only.

Mosalam et al. (1997) confirmed this observation. They tested two two-bay steel frames infilled with concrete block masonry that had window and door openings. One specimen had symmetric window openings with one opening in each bay, and the other had a window in one bay and a door in the other. These openings reduced the horizontal cross-sectional area of an infill by approximately 17%. The study showed that the presence of openings led to a lower initial stiffness, but a more ductile behaviour. The maximum load resistance of the frame with symmetric window openings was almost the same as that without openings. However, the presence of a door opening reduced the load resistance by approximately 20%. They also observed that crack patterns were affected by the openings. Cracks tended to initiate at the corners of the openings and propagate towards the loaded corners, as compared to the initiation of a horizontal crack at mid-height that propagated towards the loaded corners in a solid infill (Mode-C in figure 1.4) (Shing and Mehrabi, 2002).

1.3 BEHAVIOUR OF INFILLED RC FRAME UNDER CYCLIC LOAD

1.3.1 Introduction

Mander et al. (1993) reported the results of cyclic pseudo-dynamic test performed on masonry infilled frame subassemblies. The report presented the observed strength and deformation limit states as well as the hysteric behaviour characteristics such as strength and stiffness degradation due to repeated load reversals. The important in-plane failure modes of masonry infilled frames, include: (1) tension failure of the tension column due to overturning moments; (2) flexural or shear failure of the columns; (3) compression failure of the diagonal strut; (4) diagonal tension cracking of the panel; and (5) sliding shear failure of the masonry along horizontal mortar beds. Formulas were provided for capacity values corresponding to various failure models for the purposes of design. The load resisting mechanism of infilled frames was idealized as a combination of a moment resisting frame system formed by the frame and a pin-jointed truss system formed by the infill panel.

1.3.2 Performance of Mortar

Several experimental programs were carried out to investigate the behaviour of mortar joint within masonry panel under uniaxial cyclic loading conditions. The results were graphically scaled on peak experimental displacement and stress values, for a better comparison.

Atkinson et al. (1989) carried out a direct cyclic shear test on mortar joints. The comparison between the experimental data and the numerical results by Oliveira and Lourenco (2004) is shown in Fig. 1.9.

Experimental results of a test carried out by Gopalaratnam and Shah (1985) to study the behaviour of mortar joint under uniaxial cyclic tension are shown in figure 1.10.

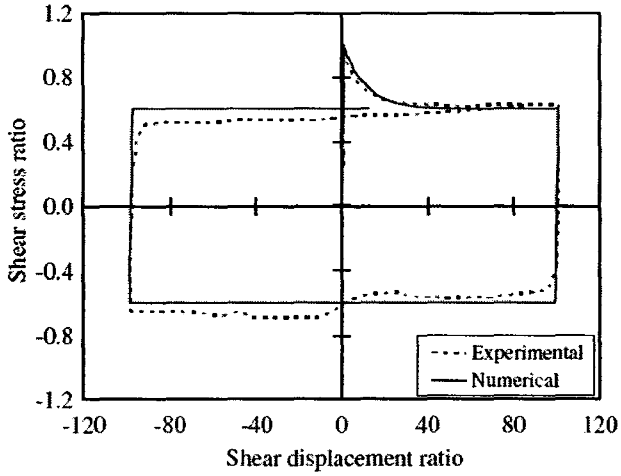

Fig. 1.9 Direct shear test under cyclic loading (scaled τ-$\Delta\gamma$ curve).

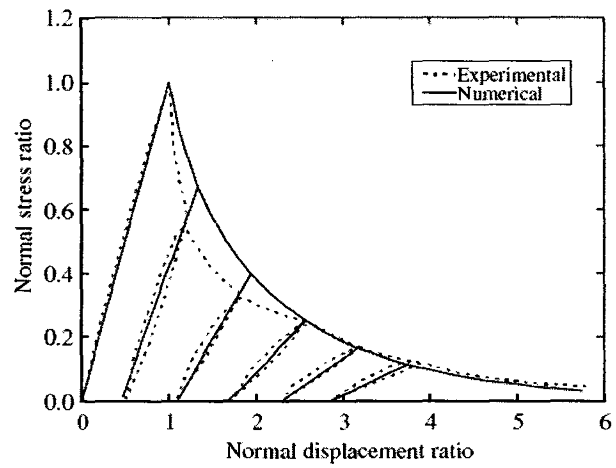

Fig. 1.10 Uniaxial tensile test under cyclic loading (scaled σ-Δu curve).

The results of experiments carried out by Karsan and Jirsa (1969) on concrete mortar joint under cyclic compressive loading are shown in figure 1.11.

Reinhardt (1984) tested a concrete specimen under cyclic tensile-compressive loading conditions. Only six loading cycles were carried out. The results are shown in figure 1.12.

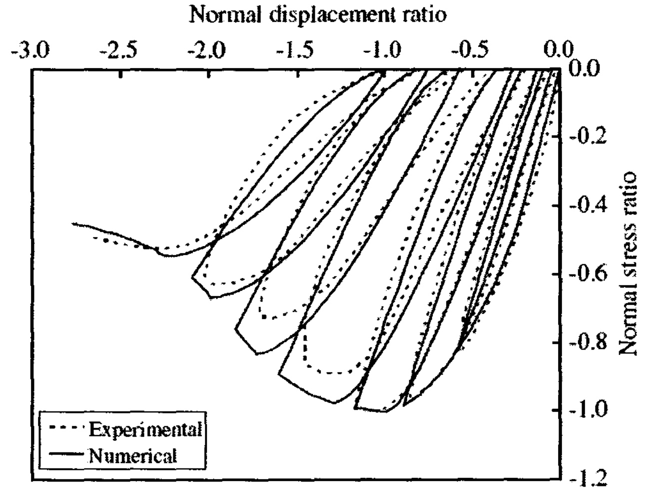

Fig. 1.11 Uniaxial compressive test under cyclic loading (scaled σ-Δu curve).

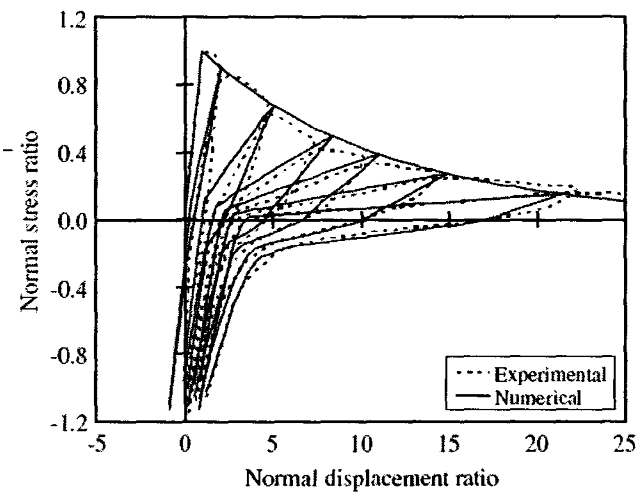

Fig. 1.12 Cyclic tensile–compressive loading test (scaled σ-Δucurve).

1.4 MODELING OF INFILLED RC FRAMES

There is still a lack of methods for analysis and design which would properly take into account the highly non-linear behaviour of the masonry infilled RC frame system during strong earthquakes and yet would be appropriate for practical applications. Seismic codes do not normally address the design of infilled frames. Heavy damage and collapse of infilled RC frames has been observed during recent earthquakes, most notably during the 1999 Kocaeli (Turkey) earthquake (Dolsek and Fajfar, 2004).

1.4.1 Modeling of RC Frame

In a study presented by Singh et al. (1998) a 3-noded beam-column element, as shown in figure 1.13, was used to model the skeletal frame. Inelastic behaviour of the element is governed by the interaction of the axial force, two flexural moments and a torsional moment. The yield surface proposed by Powell and Chen (1986) has been used.

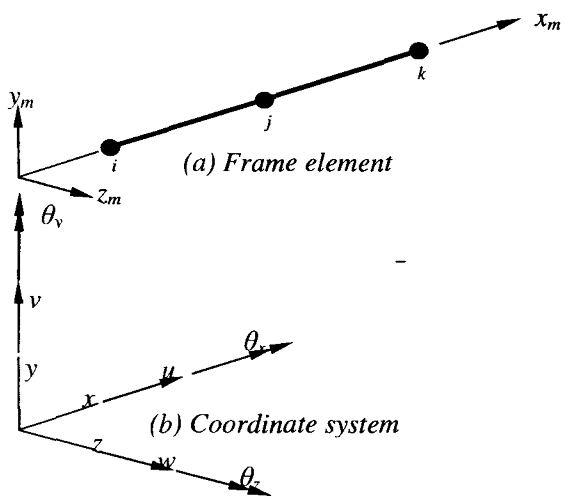

Fig. 1.13 Modeling of Frame Element (Singh et al., 1998)

Due to the plastic behaviour of the concrete material, the modulus of elasticity varies with the stress rate and magnitude of the stress. In addition, the effective reinforced concrete section varies with the stress level. Both the modulus of elasticity and the effective cross section decrease with the increase in stress level (Singh et al., 1998).

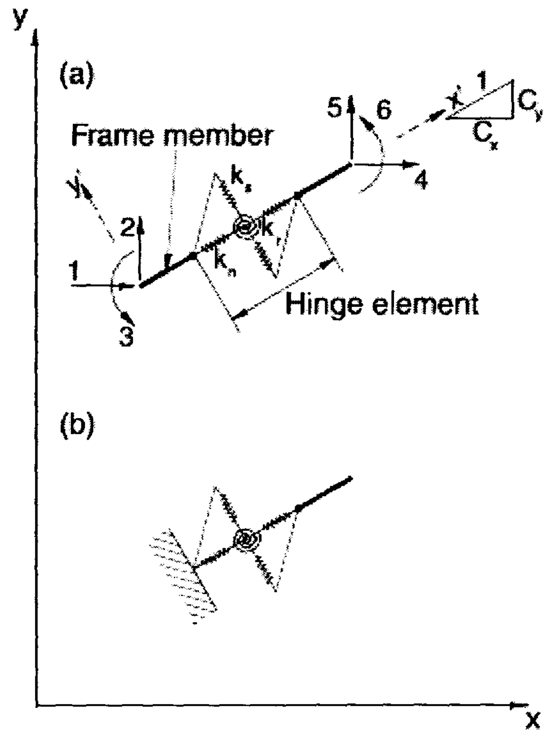

Fig. 1.14 Hinge element (a) connecting two frame members and (b) connecting a frame member and a fixed support (Dawe et al., 2001).

Dawe et al. (2001) used a typical frame element to represent the RC frame in their analysis. The typical plane frame element consisted of two three degree-of-freedom nodes, one at either end of a member with coordinate displacements corresponding to moment, shear, and axial load. Standard procedures can be used to evaluate the stiffness matrix of this element (Weaver and Gere 1980). It was assumed that the frame element was linearly elastic and that all inelastic behaviour may be concentrated at a nonlinear hinge introduced at the ends of an element. The input required for this element consisted of member length, cross-sectional dimensions, and modulus of elasticity of the material (Dawe et al., 2001).

The hinge elements were zero-length elements consisting of two translational springs and one rotational spring corresponding to three degrees of freedom at each node. As shown in figure 1.14 for a general case, a hinge element was used to connect two frame elements or to connect a frame element to its support (Dawe et al., 2001).

1.4.2 Modeling of Infill Panel

Although brick masonry is one of the most ancient and widespread composite materials, remarkable difficulties are still encountered in the formulation of adequate constitutive models due to its heterogeneity and anisotropy. In such formulations a preliminary experimental and theoretical characterization of each component; brick units and mortar and of the interfaces must precede the definition of the global constitutive equations. The calibration of masonry constitutive models considering the in-plane response either of the mortar-brick interfaces or of masonry walls under the horizontal loads is necessary in order to develop realistic constitutive relations (Morbiducci, 2003).

1.4.2.1 Equivalent diagonal strut model

Due to a multitude of highly variable parameters affecting the behaviour of infilled frames, approximate analyses are generally acceptable. Various approximate analytical techniques have been proposed. The simplest and most highly developed was the concept of equivalent diagonal strut. This concept was originally proposed by Polyakov (1956) and subsequently refined by Stafford-Smith (1962, 1966, 1967a and 1967b).

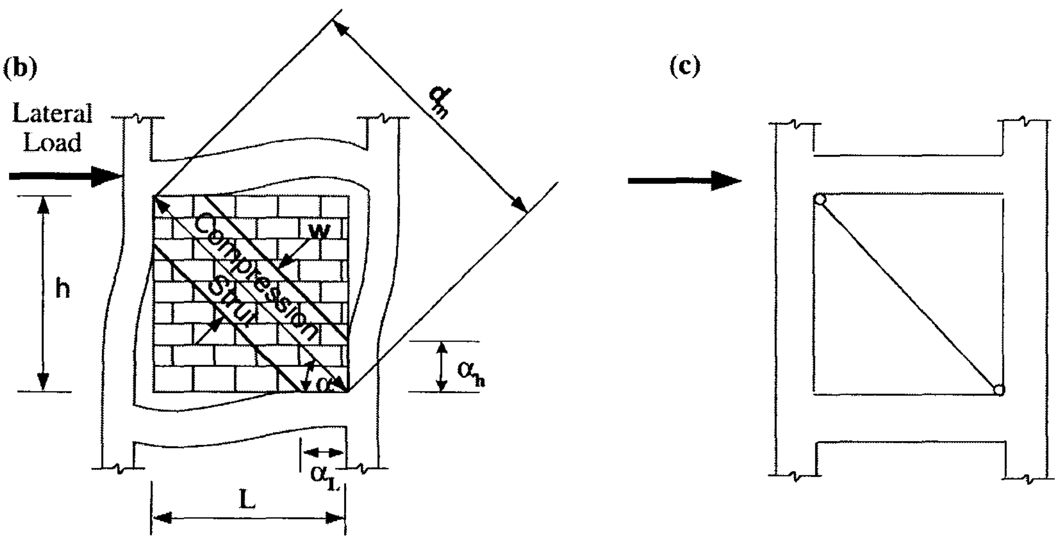

Fig. 1.15 Equivalent strut model for masonry infill panels (Stafford-Smith, 1966).

In this method, an infilled frame structure is modelled as an equivalent braced frame system, with a compression diagonal replacing infill panels, as shown in figure 1.15. The diagonal strut concept may be used to predict behaviour prior to panel cracking. However, Stafford-Smith (1962, 1966) and Stafford-Smith and Carter (1969) concluded that the analysis cannot predict nonlinear load-deformation behaviour and ultimate strength.

Holmes (1961) proposed replacing the infill by equivalent pin-jointed diagonal strut of the same material with a width equals one-third of the infill's diagonal length. He proposed that the effective width of an equivalent strut depends primarily on the thickness and the aspect ratio of the infill.

Stafford-Smith (1966) used an elastic theory to show that this width should be a function of the ratio of the stiffness of the infill with respect to that of the bounding frame. By analogy to a beam on elastic foundation, Stafford-Smith defined a dimensionless relative stiffness parameter to determine the degree of frame-infill interaction and thereby, the effective width of the strut, as follows:

$$\alpha_h = \frac{\pi}{2}\sqrt[4]{\frac{4E_f I_c h}{E_m t \sin 2\theta}} \quad \text{and} \quad \alpha_L = \pi\sqrt[4]{\frac{4E_f I_b L}{E_m t \sin 2\theta}} \qquad (1.1)$$

Where: E_m , E_f = elastic moduli of the masonry wall and frame material, respectively.
t, h, L = thickness, height, and length of the infill wall, respectively.
I_c, I_b = moments of inertia of the column and the beam of the frame, respectively.
θ = $\tan^{-1}$ (h/L)

Hendry (1981) proposed the following equation to determine the equivalent strut width w, where the strut is assumed to be subject to uniform stress:

$$w = \frac{1}{2}\sqrt{\alpha_h^2 + \alpha_L^2} \qquad (1.2)$$

Once the geometric and material properties of the struts were calculated, conventional braced frame analysis can be used to determine the stiffness of the infilled frame, the internal forces, and the deflections.

Stafford-Smith (1967b) found that his model tended to overestimate the effective width of an equivalent strut, based on his experimental results. He subsequently developed a set of empirical curves that related the stiffness parameter to the effective width of an equivalent strut. These curves showed better correlations with experimental data than his theoretical results.

Mainstone and Weeks (1970) proposed an empirical relation between the effective width of an equivalent strut and Stafford-Smith's stiffness parameter for masonry infills. This relationship gave a lower value of the effective width than that given by Stafford-Smith's model.

Fiorato et al. (1970) proposed the use of a shear beam model to estimate the initial stiffness of an infilled frame. They found good correlations with their experimental results. However, the stiffness of infilled frames was determined using a low load level (10-30% of the ultimate load). This may not reflect the overall behaviour of an infilled frame before peak strength.

The accuracy of the above models in predicting the lateral stiffness of masonry-infilled frames varied significantly from one study to another. Mehrabi et al. (1994 and 1996) found that Mainstone and Weeks' model significantly underestimates the lateral stiffness of the infilled frames considered. With Stafford-Smith's model, using the bending stiffness of uncracked reinforced concrete sections, Mehrabi et al. (1994) found that the lateral stiffness of their infilled frames was consistently underestimated by a factor of two.

A multi-strut model known as the "Compression-Only Three Struts Model" was investigated by Chrystoyomou et al. (1992). A significant limitation of the model is that it cannot effectively model the force transfer and slip along the frame panel interfaces. A simplified model based on the equivalent strut approach that accounts for slip along the frame panel interface was recently suggested by Mosalam (1996). The model uses empirically determined correction factors to determine the effective strut dimensions (Madan et al. 1997).

Mehrabi et al. (1996) compared the secant stiffness of the infilled frames they tested with the shear beam model. They found that for most frames with weak infills, the shear beam model provided close correlation with experimental results. Nevertheless, for frames with strong infills, the shear beam model tended to overestimate the secant stiffness by more than two-fold. The shear beam model indicated the separation of the infills from the bounding frames at a low load level.

Zarnic and Gostic (1998) proposed a hysteretic strut model in which the ultimate strength was governed by the shear capacity of the masonry infill. However, the model had a large number of empirical parameters that need to be calibrated.

Stafford-Smith's model seemed to show some consistency within each study, whether it tended to over- or under-estimate the lateral stiffness. This points to a couple of issues that need to be resolved in future studies. First; a proper and consistent definition of the initial lateral stiffness of an infilled frame that is reflective of the overall behaviour before major damage, is needed. Second; the value of the modulus of elasticity of masonry that should be used in Stafford-Smith's model requires evaluation. Values obtained from masonry prism tests might not be most appropriate in view of the highly anisotropic behaviour of unreinforced masonry (Shing and Mehrabi, 2002).

Strut models have been used to evaluate the strength as well as the stiffness of infilled frames. Even though some limited success has been achieved, the use of an equivalent strut model to calculate the strength of an infilled frame is rather inadequate for a number of reasons. Most importantly, an infilled frame has a number of possible failure modes caused by the frame-infill interaction, and a compression strut type failure is just one of several possibilities. It is evident that the diagonal strut model is not capable of representing a number of the failure mechanisms shown in figure 1.4, such as the short-column phenomenon and the sliding bed-joint failure of a masonry infill. Furthermore, the effective width proposed by Stafford Smith is based on an elastic theory and may not be adequate near the ultimate limit state. The contact length between the infill and the frame will change as the infill approaches its ultimate resistance (Shing and Mehrabi, 2002).

1.4.2.2 Finite element model

Problem scale

In the traditional finite element analysis of unreinforced masonry structures, the effect of mortar joints as planes of weakness and a source of material non-linearity has been accounted for with different levels of refinement. The least refined approach, termed macro-modeling (figure 1.16a), made no distinction between the individual units and joints, but considered masonry as a homogeneous, anisotropic continuum. This approach may be preferred for the analysis of large masonry structures. However, it is not suitable for detailed stress analysis of small panels because it can not capture all failure mechanisms (Stutcliffe et al., 2001).

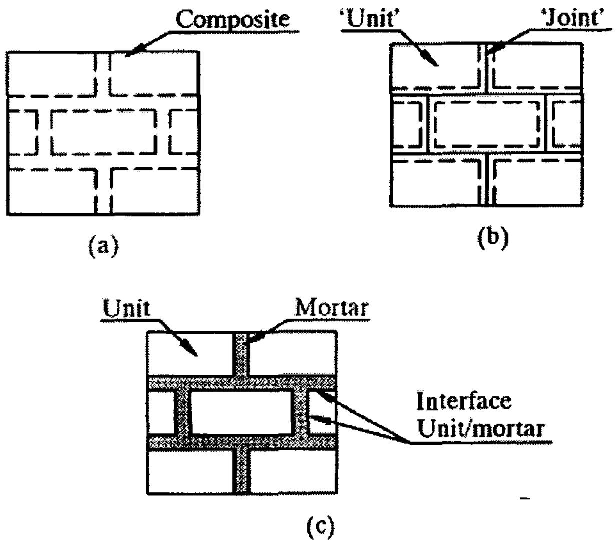

Fig. 1.16 Level of refinement for masonry models; (a) Macro-modelling; (b) simplified micro modeling; (c) detailed micro-modeling (Stutcliffe et al., 2001).

The second model is a simplified micro-model (figure 1.16b). It represented an intermediate approach. The properties of the mortar and the unit/mortar interface were lumped into a common element, while expanded elements were used to represent the brick units. Some accuracy was obviously lost, however the reduction in computational intensiveness results in a model which would be applicable to a wider range of structures (Stutcliffe et al., 2001).

In the most refined approach, termed detailed micro-modeling (figure 1.16c), the units, mortar and the unit/mortar interface were all modeled separately. While this led to more accurate results, the level of refinement meant that the analysis will be computationally intensive, with application limited to small laboratory specimens (Stutcliffe et al., 2001).

Macro-Modeling

In this approach, a typical element of brickwork was regarded as a structured composite medium for which the average macroscopic properties could be uniquely identified. Thus, a reprehensive volume of the "material" considered was assumed to consist of a number of brick units interrupted by two orthogonal families of joints. The presence of discrete sets of mortar joints resulted in a strong direction dependence of the average mechanical properties (Pietruszczak and Niu, 1992).

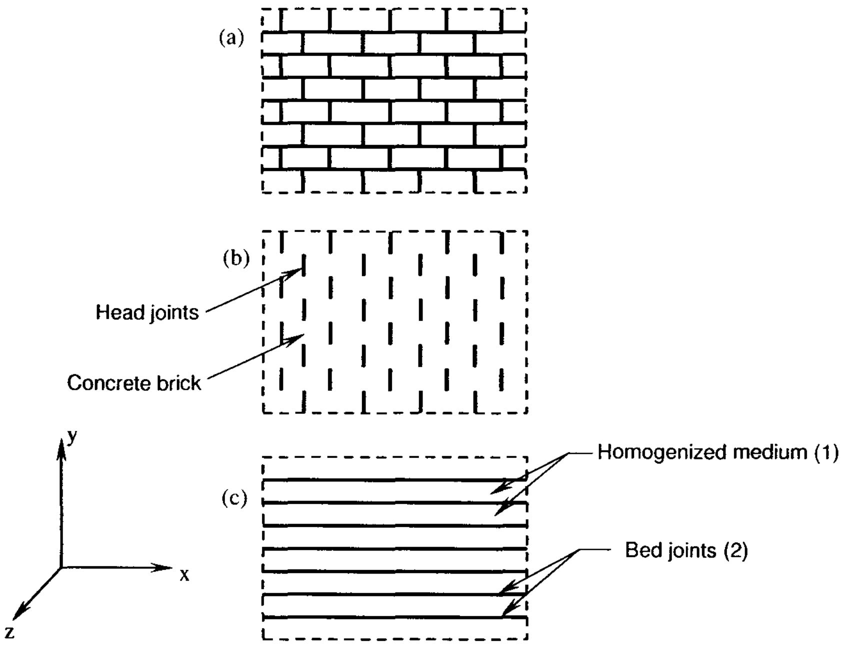

Fig. 1.17 (a) Geometry of a structural masonry panel; (b) brick matrix with a family of head joints; (c) family of bed joints (Pietruszczak and Niu, 1992).

A typical element of structural masonry, i.e. a brick panel, was taken as shown schematically in figure 1.17(a), subjected to a uniformly distributed load. On the macro-scale, the panel was treated as a two-phase composite consisting of brick units interspersed by two orthogonal sets of joints filled with mortar. In order to describe the average mechanical properties of the system, the influence of head (vertical) and bed joints were addressed separately, i.e. invoke the concept of superimposed medium (Pietruszczak and Niu, 1992).

The brick matrix shown in figure 1.17(b) was considered with a family of head joints (a so-called medium (1)). The head joints were treated as aligned, uniformly dispersed weak inclusions embodied in the matrix. The entire masonry panel can now be represented by homogenized medium (1) stratified by a family of bed joints (2), figure 1.17(c). The bed joints run continuously through the panel and form the weakest link in the microstructure of the system (Pietruszczak and Niu, 1992).

Simplified Micro-Model

Singh et al. (1998) used eight-noded isoparametric element as shown in figure 1.18 to model the infill panels. The masonry material was assumed to be linearly elastic up to failure. There can be separation, closing of gap and slipping between the frame and the infill. A six noded interface element as shown in figure 1.18 was used to model this behaviour between the frame element and the panel element. Two in-plane translational degrees of freedom per node were assumed.

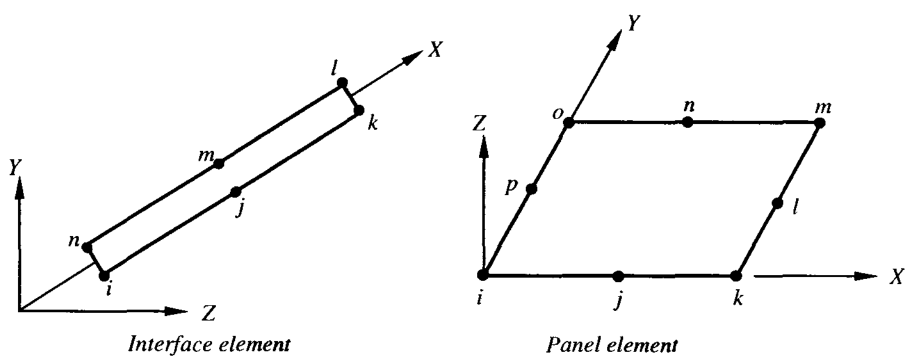

Fig. 1.18 Different elements used for modelling the infilled frame (Singh et al., 1998).

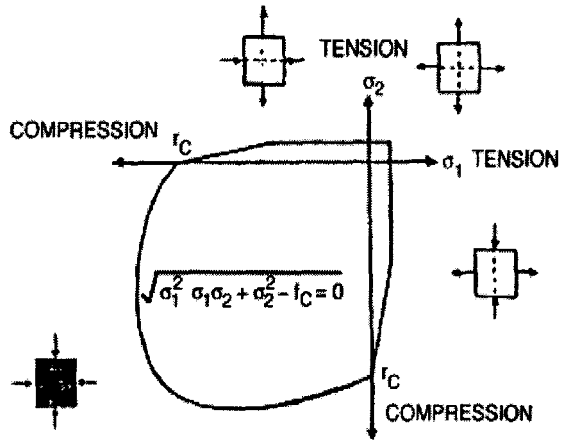

Fig. 1.19 Yield surface for the masonry panel (Singh et al., 1998).

To predict the cracking and crushing type of failure, Von-Mises failure criterion with a tension cut off as shown in figure 1.19 was adopted. Upon crushing in compression, the stiffness and all stresses were reduced to zero. Upon cracking in tension (Fig. 1.20), the stiffness normal to crack was reduced to zero but along the crack, partial shear stiffness was maintained. The stress normal to the crack was reduced to zero; however, a partial shear transfer due to interlocking between the particles was maintained. The normal stiffness and stresses along the crack were also maintained (Singh et al., 1998).

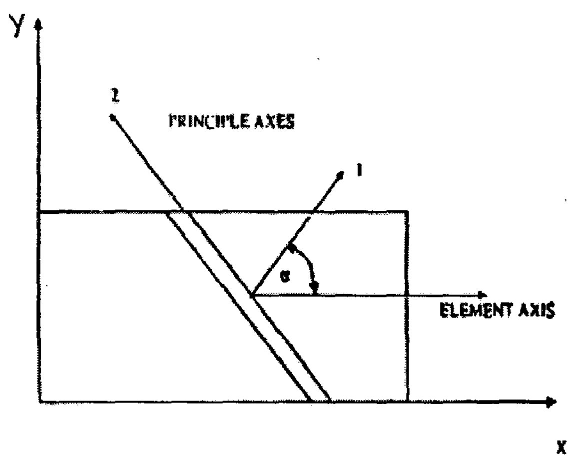

Fig. 1.20 Crack and principle axes directions (Singh et al., 1998).

Kappos et al. (2001) studied the behaviour of R.C. frames infilled with clay brick walls and subjected to earthquake loading. The vulnerability and seismic reliability of two 10-story, three-bay infilled frames (a fully infilled one and one with a soft ground story) were derived and compared with values corresponding to the bare frame (Kappos et al., 2001). The masonry infills were modeled using four-noded isoparametric shear panel elements of complex hysteretic.

Detailed Micro-Model

The modeling of in-plane loaded brick masonry shear walls was considered in a study by Gambarotta et al. (1997) through a composite model. The model was based on damage mechanics and takes into account both the mortar damage and the brick-mortar decohesion, which were considered to take place when opening and frictional sliding were activated. Moreover, by comparison with the typical experimental results from the triplet tests, the model parameters could be identified (Kappos et al., 2002).

The mortar joint model was the basis of a composite finite element model in which brick units and mortar joints were described. The brick units were modeled by isoparametric elements connected by interfaces located in both bed and head mortar joints. In particular, the brick units were modeled as elastic-plastic solids having brittle interfaces located to correspond with the head joints of the neighbouring layers.

In a study by Dawe et al. (2001), masonry infilled panel was modelled as an assemblage of rectangular elastic zones separated by joints with limited shear and tensile capacity. This approach was first introduced by Goodman et al. (1968) for the analysis of jointed rocks and subsequently adopted by Page (1979) for modeling brickwork supported on beams. The elastic zones are modelled by rectangular orthotropic plane stress elements (Weaver and Johnston 1983) and are interconnected by joint elements.

Joint elements are linkage members with infinite compression stiffness and capacity, low tensile strength, and a shear capacity depending on mortar bond strength and joint friction. It is assumed that each elastic zone, modelled with a plane stress rectangular element, may incorporate several masonry joints and units, with the effects of cracking concentrated in joint elements along the boundary. This representation allows for typical masonry failure modes corresponding to tensile failure in head and bed joints, shear failure in bed joints, tensile failure in masonry units, and combinations of one or more of these. These failure modes are illustrated in figure 1.21. In regions where compressive stresses predominate, crushing of masonry may occur and if significant shear stress also exists, a stepped failure involving head and bed joints as shown in figure 1.22 may also occur (Dawe et al., 2001).

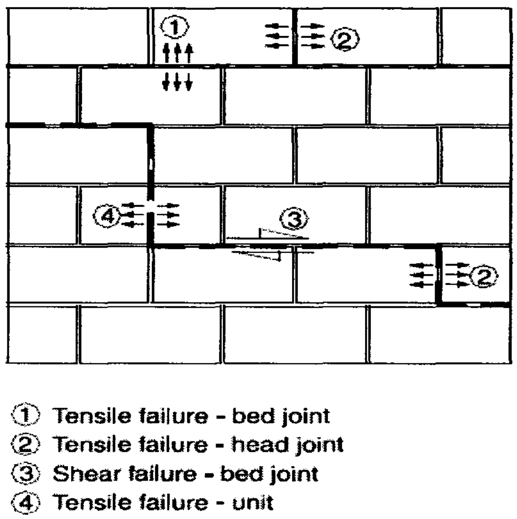

Fig. 1.21 Masonry failure modes (Dawe et al., 2001).

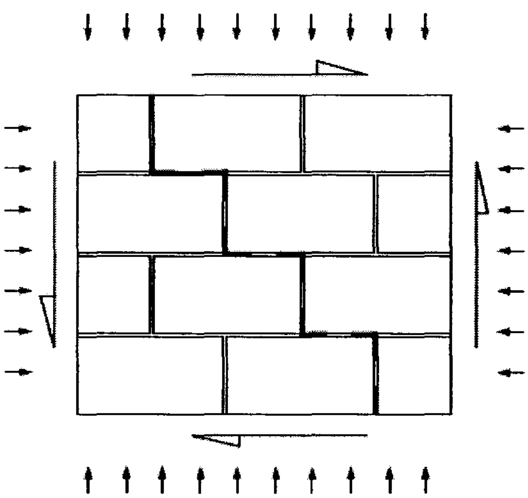

Fig. 1.22 Stepped failure involving head and bed joints (Dawe et al., 2001).

Figure 1.23 illustrates a typical joint element used to link four surrounding rectangular panel elements. The joint element consisted of four nodes and ten springs with no associated physical dimension. The purpose of Springs 1 to 8 was to ensure that nodes of the wall elements connected by the joint move in unison when load is applied. An arbitrarily high value was assigned to the stiffness of these springs. When failure occurred in the form of tensile cracking or shear along mortar joints, the stiffness of one or more springs may be reduced to zero to reflect the corresponding failure.

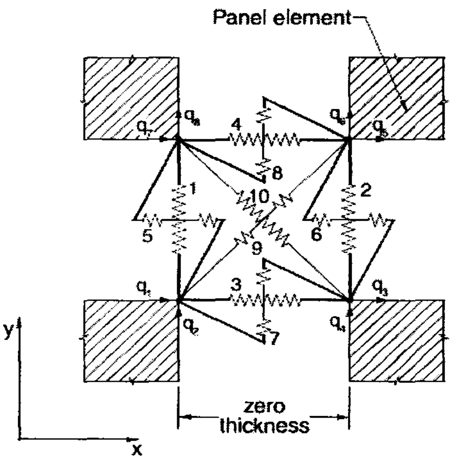

Fig. 1.23 Typical joint element (Dawe et al., 2001).

The boundary between a frame and panel was modelled by interface elements each consisting of a pair of normal and tangential springs. These elements were used to match displacements of a frame and infill at interfacial nodes. As shown in figure 1.24, an interface element had two nodes, each with two degrees of freedom. One node was attached to a node of a frame element and the other was attached to a corresponding node of a panel element.

A normal spring was assumed to have infinite compressive stiffness and a tensile stiffness depending on the adhesive bond between frame and infill. A high stiffness value was assigned to the normal spring if the frame was in compressive contact with the infill. If the tensile bond strength was exceeded, separation will occur and the stiffnesses of both the normal and tangential springs were reduced to zero to allow the frame and infill to deform independently. The stiffness and strength of a tangential spring depends on the shear bond and friction that exists at the interface.

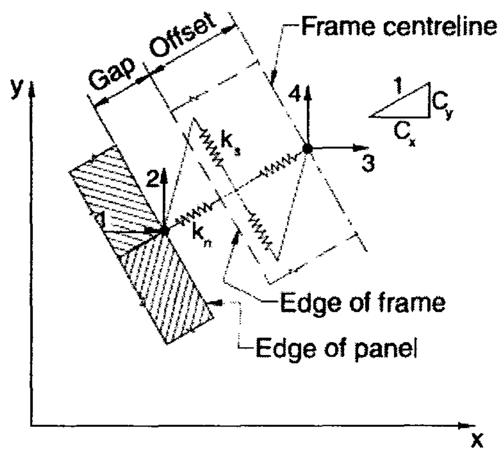

Fig. 1.24 Interface element (Dawe et al., 2001).

Kappos et al. (2002) analyzed a typical 2D masonry structure by using a finite element model consisting of plane stress elements. The material constitutive law (Willam-Warnke model) used for masonry is shown in figure 1.25. The equivalent uniaxial stress–strain relationship was a parabolic one. The biaxial strength envelope produced as a projection of the 3D failure surface, both shown in figure 1.25, was in good agreement with the one proposed on the basis of test results (Dhanasekar et al. 1985).

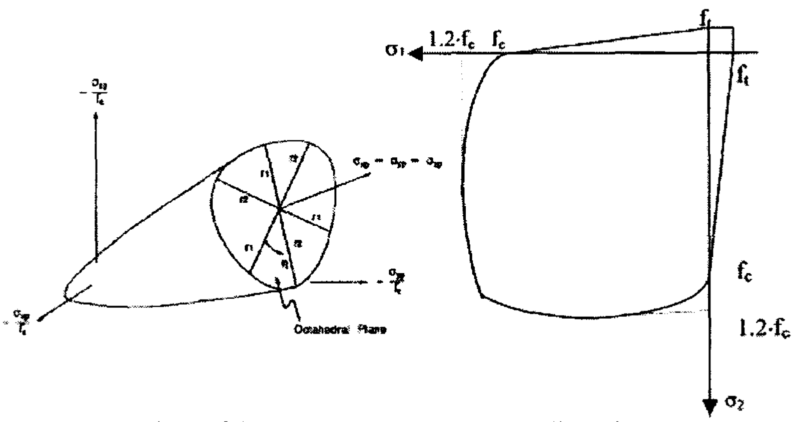

Fig. 1.25 Three-dimensional failure surface and corresponding biaxial strength envelope for unreinforced masonry Kappos et al. (2002).

Whenever the biaxial tensile strength was exceeded the element was assumed to have cracked, while a compressive strain in excess of ε_u was considered as crushing of the element. The element stiffness matrix was updated whenever failure according to either criterion occurred. After cracking, residual shear stiffness was retained, equal to 60% of the uncracked value (Kappos et al., 2002).

The use of a tensile strength equal to 10% of the compressive strength for the un-reinforced masonry (URM), as well as the use of 60% of the uncracked shear stiffness after closing of a crack, were selected on the basis of a sensitivity analysis performed for a half-scale URM building tested at Instituto Sperimentale Modelli e Strutture (ISMES) (Benedetti et al. 1998).

1.4.3 Cyclic Loading Models

1.4.3.1 Macro Modelling

A computational model of the hysteretic in-plane force-deformation behaviour of masonry infilled frames based on the tie and strut approach was proposed by Mander et al. (1994). The infill panel was modeled as a combination of three nonparallel struts (one diagonal and two off-diagonal) in each direction of loading. However, the analysis requires determination of the geometry and hysteretic rule parameters from theoretical or empirical models.

Saneinejad and Hobbs (1995) developed a method based on the equivalent diagonal strut approach for the analysis and design of steel or concrete frames with concrete or masonry infill walls subjected to in-plane forces. The method took into account the elastoplastic behaviour of infilled frames considering the limited ductility of infill aspect ratio, the shear stresses at the infill-frame interface and relative beam and column strengths were accounted for. However, the formulation provided only extreme or boundary values for design purposes.

Madan et al. (1997) considered a macro-model for masonry infill in his analysis. The model was based on an equivalent strut with a hysteretic force-deformation rule that accounted for strength and stiffness degradation as well as pinching resulting from opening and closing of masonry gaps. The model was verified and used to simulate experimental behaviour of tested masonry infill frame subassemblies under quasi-static displacement controlled cyclic loading.

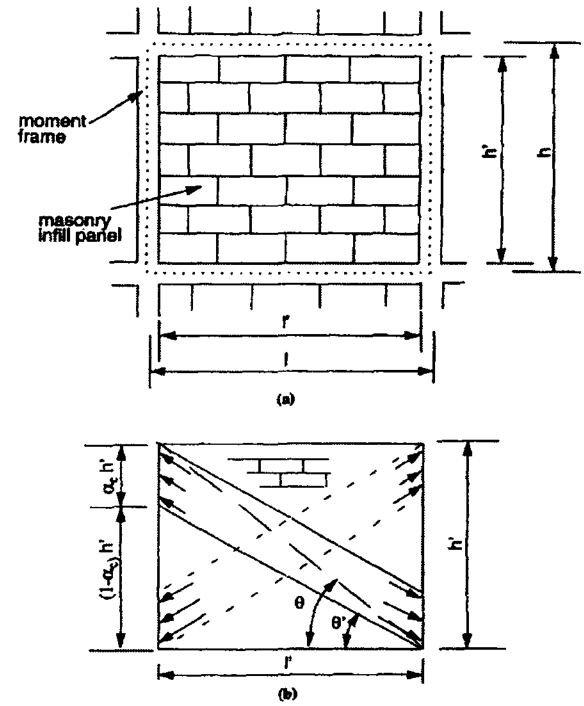

Fig. 1.26 Equivalent strut model for masonry infill panel in frame structure: (a) Masonry infill frame sub-assemblage; (b) Masonry infill panel.

The proposed analytical development assumes that the contribution of the masonry infill panel (Fig. 1.26(a)) to the response of the infilled frame can be modeled by "replacing the panel" by a system of two diagonal masonry compression strut (Fig. 1.26(b)). The stress-strain relationship for masonry in compression (Fig. 1.27(a)) was idealized by a polynomial function (Mander et al. 1988). This relationship was used to determine the strength of the equivalent strut. Since the tensile strength of masonry is negligible, the individual masonry struts were considered to be ineffective in tension. However, the combination of both diagonal struts provided a lateral load resisting mechanism for the opposite lateral directions of loading.

The lateral force-deformation relationship for the masonry infill panel was assumed to be a smooth curve bounded by a linear strength envelop with an initial elastic stiffness up to the yield force V_y. Post-yield degraded stiffness was used until the maximum force V_m is reached (figure 1.27(b)). The corresponding lateral displacement values were denoted as u_y and u_m respectively. The analytical formulations for the strength envelop parameters were developed on the basis of the available "equivalent strut model" for infilled masonry frame (Saneinejad et al., 1995).

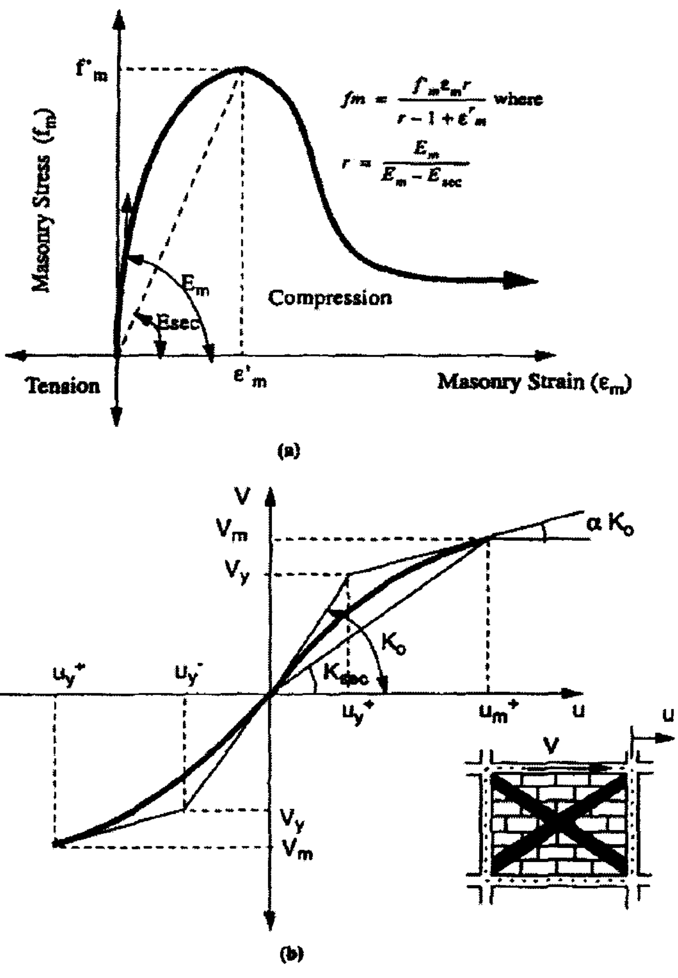

Fig. 1.27 Constitutive models for masonry infill panels: (a) Constitutive model for masonry; (b) strength envelope for masonry infill panel.

The macro-modeling approach presented by Madan et al. (1997) considered the entire infill panel as a single unit and takes into account only the equivalent global behaviour of the infill in the analysis. As a result, the approach did not permit study of local effects such as frame-infill interaction within the individual infilled frame subassemblies.

A smooth hysteretic model was proposed for the masonry infill panel. The model took into account hysteretic effects characteristic of structural masonry elements subjected to repeated loading reversal such as stiffness degradation, strength deterioration, and pinching.

The development of the hysteresis model was based on the Bouc-Wen model for hysteretic behavior. The model considered a smooth hysteretic force displacement relationship between force V and displacement u as shown in figure 1.28. Pinching of the hysteretic loops was due to opening and closing of masonry cracks.

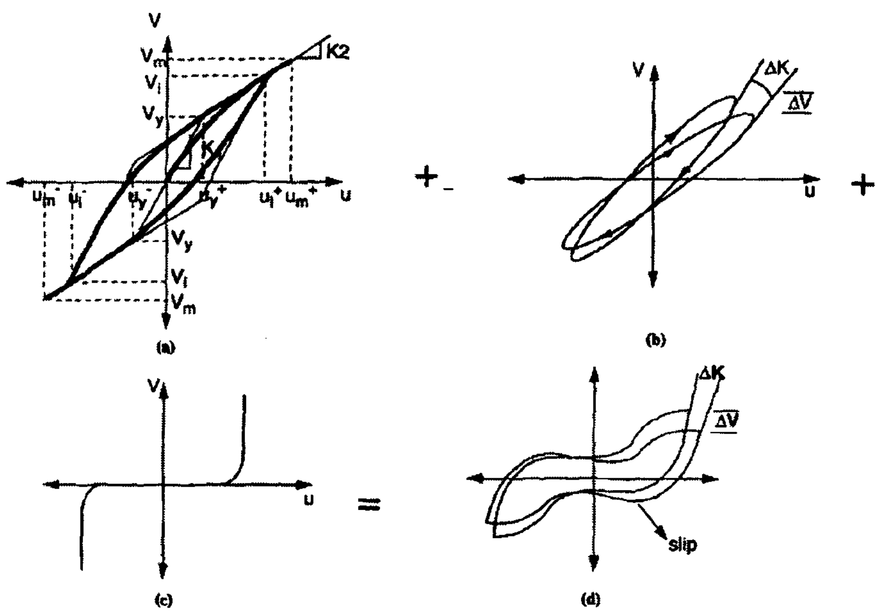

Fig. 1.28 Integrated hysteretic model for degrading pinching elements: (a) Wen-Bouc hysteresis model; (b) Hysteretic model with stiffness and strength degradation; (c) Slip-Lock model; (d) Integrated model in IDARC

1.4.3.2 Micro Modelling

Interface elements were initially employed in concrete by Ngo and Scordelis (1967), in rock mechanics by Goodman et al. (1968) and in masonry by Page (1978). Since then, they were being used in a variety of structural problems. The application of a micro-modelling strategy to the analysis of in-plane masonry structures using the finite element method requires the use of continuum elements and line interface elements. Usually, continuum elements are assumed to behave elastically whereas non-linear behaviour is concentrated in the interface elements. This type of modelling is important in structures where the interface appears well defined (as in masonry structures) and, therefore, the numerical simulation of the cyclic behaviour of interface elements is a key issue when dealing with micro-modelling (Oliveira and Lourenc, 2004).

Experimental work carried out to investigate cyclic behaviour of interfaces has shown some important characteristics, summarized as:

- stiffness degradation in both tension and compression regimes;
- residual relative normal displacements at zero stress;
- absence of stiffness degradation in direct shear;
- complete crack closing under compressive loading.

Dymiotis et al., (2001) modelled masonry infills using four-noded isoparametric shear panel elements of complex hysteretic behaviour. The shear stress-shear strain (τ-γ) hysteretic loops were described by 12 rules, as shown schematically in figure 1.29. These were initially developed by Kappos et al. (1998b). The model allowed for effects such as slip, pinching, and strength and stiffness degradation. Neglecting stresses in surrounding columns caused by the presence of axial loads:

$$\tau_{sl} = \pm 0.01\tau_{\max} \qquad (1.3)$$

where τ_{sl} is the shear stress at slip surface, and τ_{max} is the maximum shear stress

The τ-γ behaviour is governed by the slip surface and two points along the envelop curve that represent the cracking point and the point of maximum stress. Valiasis (1989) proposed the empirical equations for the coordinates of these points, following an experimental program:

$$\gamma_{cr} = \begin{cases} 0.11[(80 + h/t)\sqrt{f_m}\,]^{-1} & , N = 0 \\ 0.09[(80 + h/t)\sqrt{f_m}\,]^{-1} & , N \neq 0 \end{cases} \tag{1.4}$$

$$\tau_{cr} = 0.70\tau_{max} \tag{1.5}$$

$$\gamma_{max} = 4.55\gamma_{cr} \tag{1.6}$$

$$\tau_{max} = \begin{cases} 0.22\sqrt{f_m}, N = 0 \\ 0.35\sqrt{f_m}, N \neq 0 \end{cases} \tag{1.7}$$

where h and t are height and thickness of the panel, respectively; N is axial load in surrounding columns (neglected herein); and f_m is masonry compressive strength (MPa). The descending envelope branch is described by

$$\frac{\tau}{\tau_{max}} = 1 - 0.24\sqrt{\frac{(\gamma/\gamma_{max} - 1)}{\rho^{3.82(1-0.22\sigma)}(1 + 0.17\sigma)}}$$

$$= 1 - 0.24\sqrt{\frac{(\gamma/\gamma_{max} - 1)}{C}} \tag{1.8}$$

where ρ= ratio of longitudinal reinforcement (%); and σ= N/A_c= vertical axial stress (MPa).

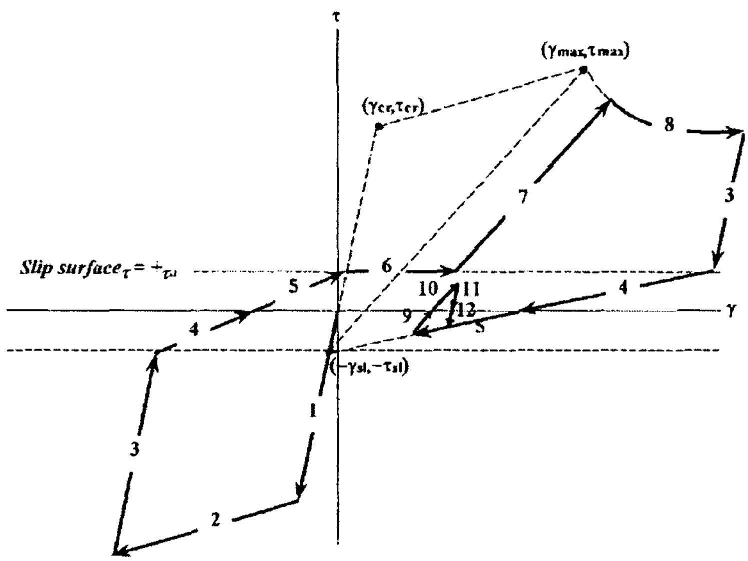

Fig. 1.29 Rules for hysteretic behaviour of infill panels

1.5 SUMMARY

During the last three decades, and particularly as a result of damage from major earthquakes, the behaviour of masonry infill has received increasing attention. New buildings could possibly be properly designed for high rigidity and to have predictable behaviour at ultimate loadings. Similarly, older buildings may be rehabilitated with infills that are compatible with the original framework. Achieving these objectives requires not only theoretical understanding of infilled frames, but also the development of simplified, and therefore practical, design methods.

Most analytical models proposed focused on one type of mechanism, and they were not universally applicable to all infilled structures. Hence, the design of engineered infilled frames and the evaluation of existing infilled structures still remain a challenge.

The equivalent strut model is a good approximation to study the overall beaviour of the structure but it could not simulate most of the failure mechanism of the masonry panel. While finite element method can simulate all failure modes of masonry infill panels, it is time consuming for analysis of large structures which makes it an impractical method for design.

1.6 RESEARCH OBJECTIVE

The objective of this research program is to develop a practical and economical technique applicable for global analyses of general three-dimensional reinforced concrete frames with infills.

The developed analysis will be used to investigate the effect of masonry infill failure on the behaviour of reinforced concrete moment resistance frames during earthquakes.

1.7 SCOPE OF THE WORK

To achieve the study objectives, the following issues are addressed.

1- Identify failure modes, and collect evidence from previous earthquakes.

2- Develop a simple computer model to simulate the failure mechanism of infill panels. This ultimately will lead to the development of a successful, economic, and powerful tool for design engineers to consider the effect of infill panels in the design of ordinary reinforced concrete buildings. In this study, only in-plane stiffness will be addressed.

3- Verification of the proposed model.

4- Analysis cases

5- Evaluation of the effect of different parameters on the behaviour of infilled frames under different loading and boundary conditions.

6- Impact of the study results on the modification of design codes.

1.8 ORGANIZATION OF THE THESIS

This thesis is organized into seven chapters. Chapter one includes an introduction in addition to a survey of different models previously used to represent infilled RC frames. A detailed description of the developed finite element model and the proposed material model are presented in Chapter two.

Verification of the proposed new model against experimental and previous analytical models is described in Chapter three. Chapters four and five include some parametric studies to evaluate the effect of different parameters on the behaviour of infilled frames under different loading and boundary conditions. These parametric studies include size and type of infill, aspect ratio, loading criteria, boundary conditions, ductility of RC frame.

Chapter six contains verification of the developed model against cyclic and dynamic results by others. In Chapter seven, conclusion of the study and recommendations for future research are presented.

CHAPTER 2

FINITE ELEMENT MODEL

2.1 INTRODUCTION

Extensive experimental and analytical research on masonry infilled concrete frames has been carried out worldwide in past 50 years in order to establish design procedures that would realistically predict the behaviour during an earthquake. Different models have been developed and verified mainly using the results of static, cyclic or pseudo-dynamic tests. However, the understanding of the seismic behaviour of structures can be achieved by taking into account the dynamic nature of their response. The capacity of RC frames with masonry infills and their ability to withstand moderate and strong earthquakes need to be evaluated using efficient and accurate models.

Few dynamic tests on infilled RC frame were conducted. There are significant problems associated with dynamic testing of scaled models which may include the modelling of scaled material properties, the financial restrictions leading to testing of limited number of specimens and limitations on specimen size due to capacity of available shake tables and other testing equipment.

The prediction of the seismic response of infilled RC frame is subject to large uncertainties due to the randomness of structural properties and ground motion parameters. The errors generated by these uncertainties and randomness are usually much larger than inaccuracies which occur due to the simplifications of mathematical models. It is therefore appropriate to employ relatively simple mathematical models. The usual model for infill consists of two equivalent diagonal struts, which only carry compressive loads. However, in practice it is difficult to determine the characteristics of the equivalent struts with much confidence (Dolsek M. and Fajfar P., 2002).

The equivalent strut model is a good approximation to evaluate the overall behaviour of the structure but it can not simulate most of the failure mechanism of the masonry panel. Moreover, the equivalent diagonal spring, that used to replace an infill, can not take many important effects into consideration, such as;

1. Interaction between frame and infill, including the effects of initial lack of fit, gaps between frame and infill, interface bond and friction, and separation and re-contact at the frame-to-infill interface;
2. Nonlinear behaviour of the infill resulting from cracking due to shear and tension, and possible crushing of the infill material under the action of biaxial compressive stress;
3. Nonlinear behaviour of peripheral frame members and the formation of plastic hinges due to a critical combination of axial load, shear, and moment in a member.

While finite element method can simulate all failure modes of masonry infill panels, it is too time consuming for analysis of large structures which makes it an impractical method for design purposes.

There is a need for an efficient and accurate computational model to simulate the nonlinear hysteretic force-deformation behaviour of masonry infills, which is also suitable for implementation in time-history analysis of large structures. The aim is to develop a simplified advanced and cost-effective model for nonlinear time history analysis and seismic design of masonry infill frame structures.

In this chapter a simple new model for masonry panel is presented. This model can simulate most of the masonry panel failure modes with small number of elements. The proposed model combines the advantages of both struts model (micro modeling) and finite element models (detailed micro modeling).

2.2 DESCRIPTION OF THE MODEL

A detailed finite element model of masonry infilled panel is an assemblage of rectangular elastic zones separated by joints with limited shear and tensile capacity. The elastic zones are modeled by rectangular orthotropic plane stress elements that are interconnected by joint elements. The specific nature of the orthotropy of these elements is described by Seah (1998). In general, such micro-modeling is too time-consuming for analysis of large structures.

2.2.1 Configuration of the Proposed Model

In the proposed model, the RC frame was modeled using two-dimensional (2-D), two node elements with three degrees of freedom per node. Details of the RC frame element are discussed in the following sections. The masonry panel is modeled using ten 2-D isoparametric elements (with two degrees of freedom per node) connected together with a number of zero-length elements (*contact elements*). The zero-length element accepts two different materials' stress-strain relationships in any two arbitrary directions. These two directions were the direction of prescribed failure planes and perpendicular to this plane. Zero-length elements were also used as *interface elements* between the masonry panel and the surrounding frame. All zero-length elements on horizontal and vertical planes represented the mortar joints between masonry elements or between the masonry panel and the boundary frame. The zero-length elements on inclined planes were used to simulate the behaviour of the diagonally cracked masonry. Details of the proposed model including model configuration, frame and masonry elements, contact elements and interface elements are shown in figure 2.1.

A special configuration of the finite element model was selected to represent the masonry panel. This configuration was based on the experience gained from experimental results and observations following earthquakes. Five prescribed failure planes were assumed to simulate the failure planes of actual structures. Figure 2.2 shows the capability of the proposed model to simulate different failure modes of masonry panel in infilled RC frames. The proposed model was incorporated in a generic nonlinear structural analysis program, for static and dynamic analysis of masonry infilled RC frames.

Inclined prescribed failure planes need special attention since the horizontal and vertical failure planes are predictable. The angle "φ" of the inclined planes with the horizontal axis is dependent on the input values of x and y (see figure 2.3). The angle "φ" should be 45^o or close to that value since the inclined failure plane represents the saw-tooth cracks through head and bed joints of the masonry panel.

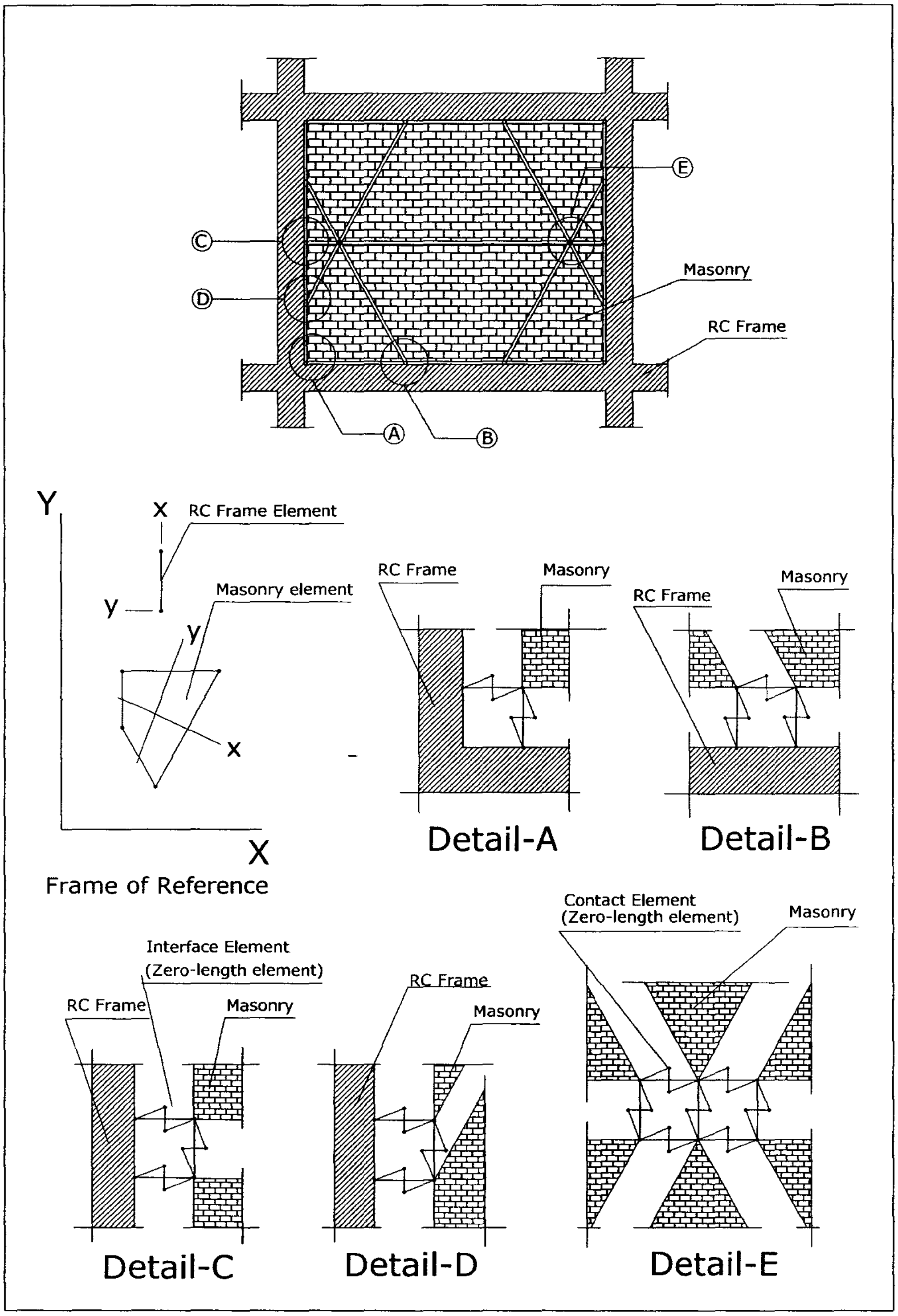

Fig. 2.1 Details of the proposed model.

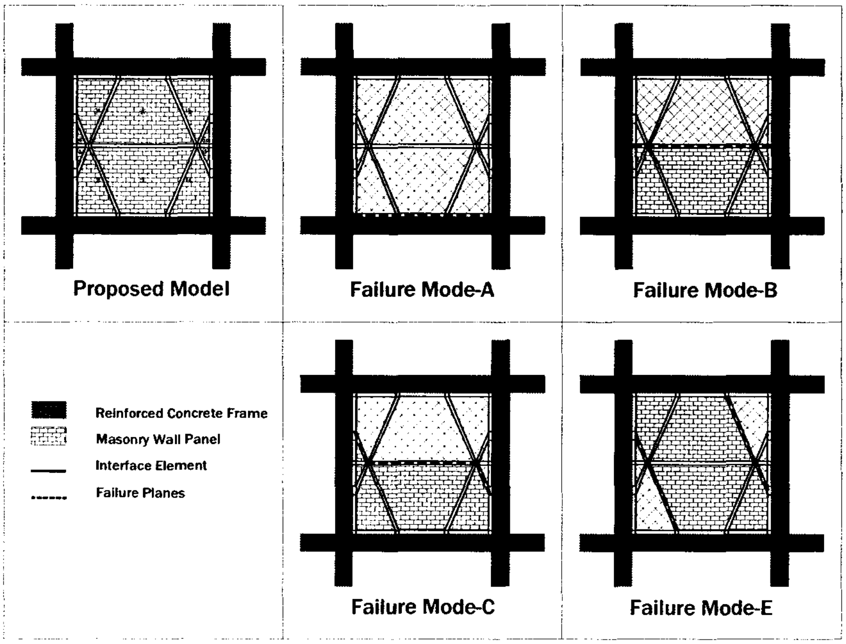

Fig. 2.2 Capability of proposed model to simulate various failure modes of masonry panel.

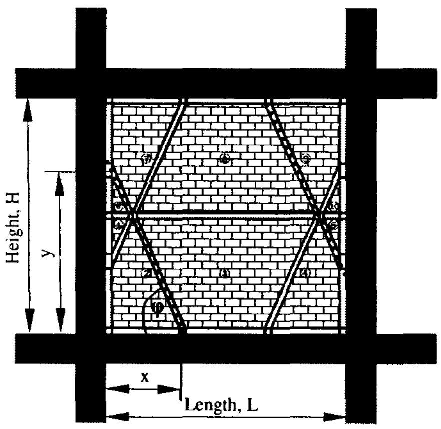

Fig. 2.3 Dimensions of the proposed model

Holmes (1961) proposed replacing the infill by equivalent pin-jointed diagonal strut of the same material with a width equal to one-third of the infill's diagonal length. He proposed that the effective width of an equivalent strut depends primarily on the thickness and the aspect ratio of the infill. Liauw and Kwan (1984) determined the width of the strut to be 0.707 L where L is the length of the infill panel. This is approximately equal to half of the diagonal dimension of the panel.

Figure 2.4 shows the separation coefficient results from a study by Singh et al. (1998). Separation coefficient was defined as the ratio of separation length to the dimension of the infill. The maximum value of separation coefficient on each side as estimated and those obtained experimentally by Choubey (1990) are shown in the figure. The strut width observed at the center was 0.627L. In the present model the width of the strut (i.e. the distance between the two inclined failure planes) was assumed to be 54% of the infill's diagonal length. However the proposed model is flexible enough to change the width and angle of inclination of the strut width.

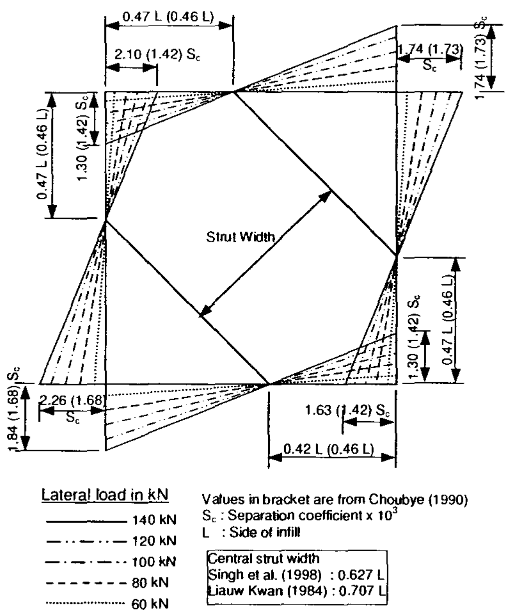

Fig. 2.4 Separation coefficients of frame with infill (Singh et al., 1998)

2.2.2 Computer Code

The Open System for Earthquake Engineering Simulation (OpenSees) code (OpenSees 2006) was chosen to verify the proposed model against numerical and experimental results for the following reasons:

1- The program and its development is a cooperative effort and is in the public domain.

2- The library of materials, elements and analysis commands makes OpenSees a powerful tool for numerical simulation of nonlinear structural and geotechnical systems.

3- The program library of components is ever-growing and at the leading edge of numerical simulation models.

4- The interface is based on a command-driven scripting language which enables the user to create more-versatile input files.

5- OpenSees is not a black box, making it a useful educational tool for numerical modeling.

6- New material, element or analysis tools can be created and easily incorporated into the OpenSees program.

7- Network for Earthquake engineering Simulation (NEES) is supporting integration of OpenSees as the simulation component of laboratory testing.

8- OpenSees includes linear, nonlinear structural and geotechnical models.

9- The computer code can simulate static push-over analyses, static reversed-cyclic analyses, dynamic time-series analyses, uniform-support excitation, and multi-support excitation.

2.3 MODELING OF RC FRAME

Different sections of RC frame members were modeled using Fiber Section object. A fiber section has a general geometric configuration formed by subregions of simpler, regular shapes called patches. Nonlinear Beam-Column element was used to model members of the RC frame. In addition, layers of reinforcement bars can be specified. The subcommands patch and layer (Circular Layer Command, Straight Layer Command) were used to define the discretization of the section into fibers. Individual fibers, however, can also be defined using the fiber command. Fiber objects are associated with *uniaxial-Material* objects Nonlinear Beam-Column command was used to model members of reinforced concrete frame as shown in figure 2.5.

Linear Transformation command was used to construct a linear coordinate transformation (LinearCrdTransf) object, which performed a linear geometric transformation of beam stiffness and resisting force from the basic system to the global-coordinate system for a two-dimensional problem, as shown in figure 2.5.

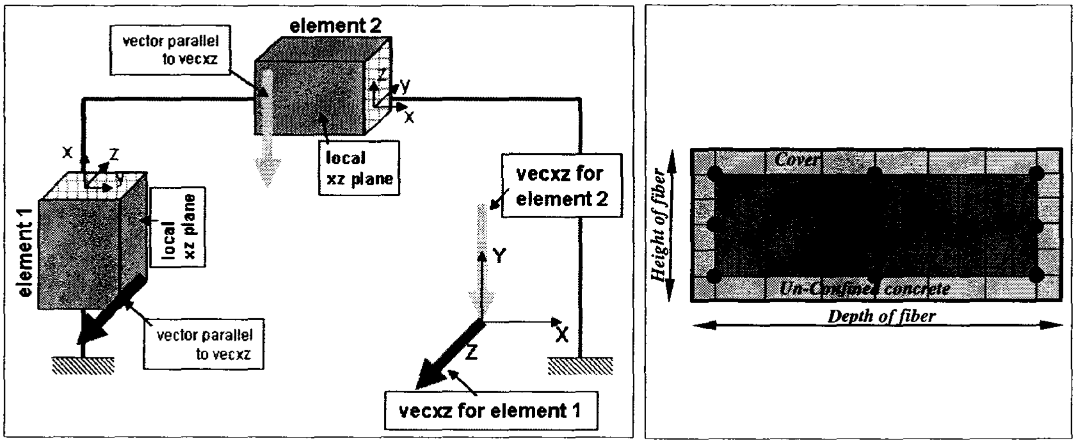

Fig. 2.5 Typical reinforced concrete frame and Fiber Section

2.3.1 Material model of concrete

Materials type Concrete01 was used to model confined and unconfined concrete in RC frame members. This command was used to construct a uniaxial Kent-Scott-Park concrete material object with degraded linear unloading/reloading stiffness according to the work of Karsan-Jirsa with no tensile strength.

The model contains a compressive strength of "fpc", a strain at the compressive strength of "epsc0", a crushing strength of "fpcu", and a strain at the crushing strength of "epscu". Compressive concrete parameters needed to be input as negative values for this model. Specification of minimum and maximum failure strains through the -min and -max switches are optional. Figures 2.6 illustrate material parameters of monotonic envelope and hysteretic behaviour of concrete materials.

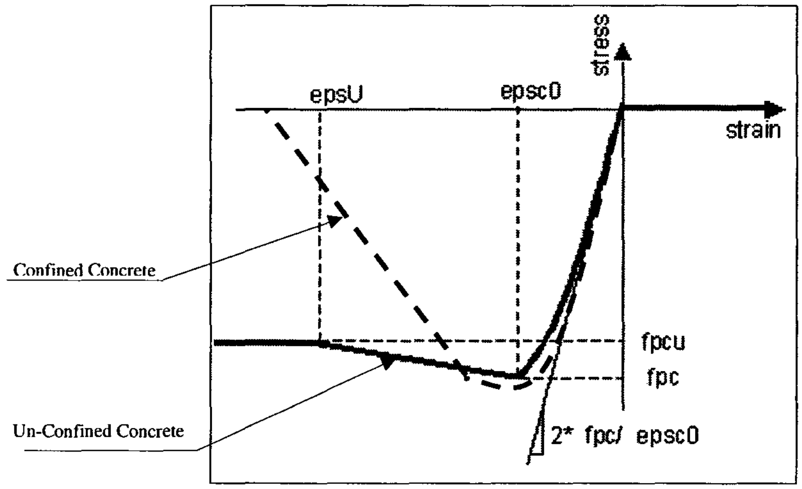

(a) Material parameters of monotonic envelope

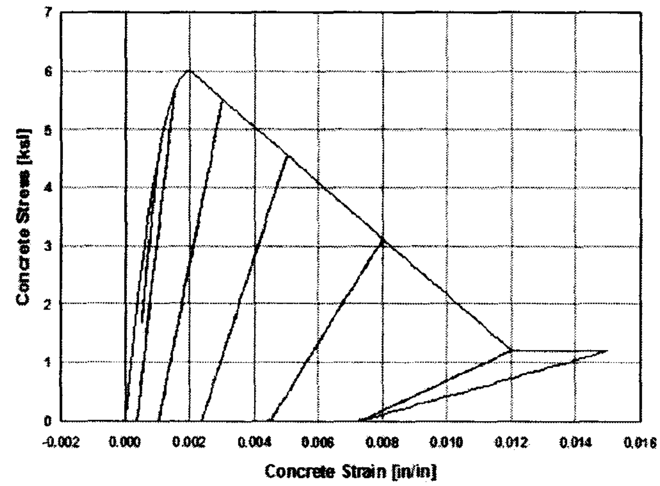

(b) Typical hysteretic stress-strain relation of concrete model

Fig. 2.6 Concrete material (OpenSees 2006).

The material was subjected to a series of ten uniaxial tension and compression strain cycles histories. Figure 2.6 is the response of this material to such strain excursions. The data shown are the normalized stresses versus strain. In the normalization process, the concrete stress was divided by the absolute value of compressive strength f_c to maintain positive tension and negative compression.

2.3.2 Material model of reinforcing steel

Materials type Steel01 was used to model reinforcing steel in RC frame members. This command was used to construct a uniaxial bilinear steel material object with kinematic hardening and optional isotropic hardening described by a non-linear evolution equation.

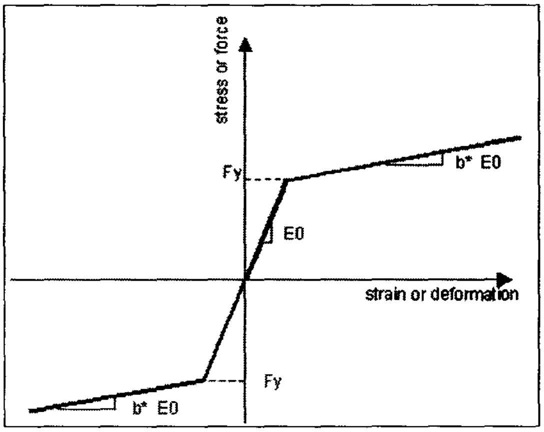

(a) Material parameters of monotonic envelope.

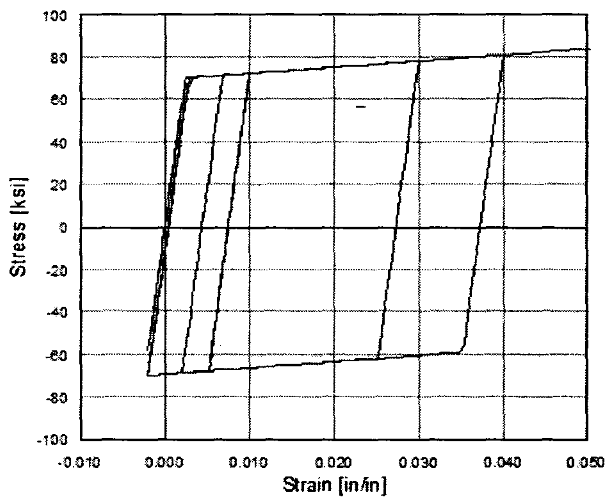

(b) Hysteretic of model without isotropic hardening.

Fig. 2.7 Steel material (OpenSees 2006).

The model contained yield strength of "fy", an initial elastic tangent of "E0", and a hardening ratio of "b". The optional parameters "a1, a2, a3, and a4" control the amount of isotropic hardening (default values are provided for no isotropic hardening). Specification of minimum and maximum failure strains through the -min and -max switches are optional and must appear after the specification of the isoptropic hardening parameters, if present. Figures 2.7 illustrate material parameters of monotonic envelope and hysteretic behaviour of steel materials.

The material was subjected to a series of ten uniaxial tension and compression strain cycles. Figure 2.7 is the response of this material to such strain excursions. The data shown are the normalized stresses versus strain. In the normalization, the steel stress was divided by the yield stress F_y.

2.3.3 Pinching Effect

Pinching4 material was used to include the pinching, stiffness degradation and strength deterioration effects to the behaviour of the moment resisting RC frame (as will be mentioned in the following section). This command was used to construct a uniaxial material that represented a 'pinched' load-deformation response and exhibited degradation under cyclic loading. Cyclic degradation of strength and stiffness occurs in three ways: unloading stiffness degradation, reloading stiffness degradation, strength degradation, as shown in figure 2.8.

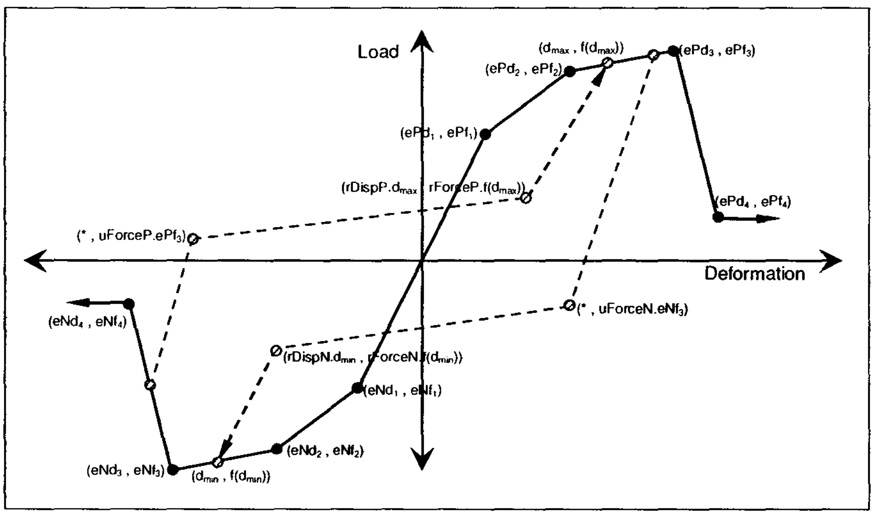

Fig. 2.8 Definition of Pinching4 uniaxial material model

2.3.4 Section Aggregator

This command was used to construct a Section Aggregator object which groups previously defined *UniaxialMaterial* objects into a single section force-deformation model. Section Aggregator command was used to group the Pinching4 material to a previously defined (existing) section. For example, create a new section with ID-tag "i", taking the existing material tag "γ" to represent shear and adding it to the existing section tag "k", which may be a fiber section where the interaction between axial force and flexure is already considered , as shown in figure 2.9.

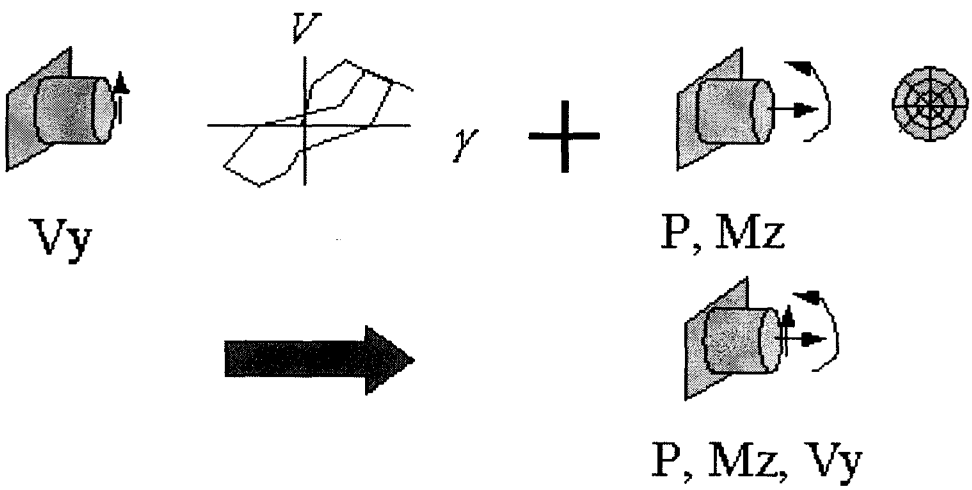

Fig. 2.9 Section Aggregator

2.4 MODELING OF MASONRY PANEL

2.4.1 Masonry Elements

Typical four-noded 2-D isoparametric elements (with two degrees of freedom per node) were used to model the infill panel, as shown in figure 2.10. These elements were connected together with a group of zero-length element.

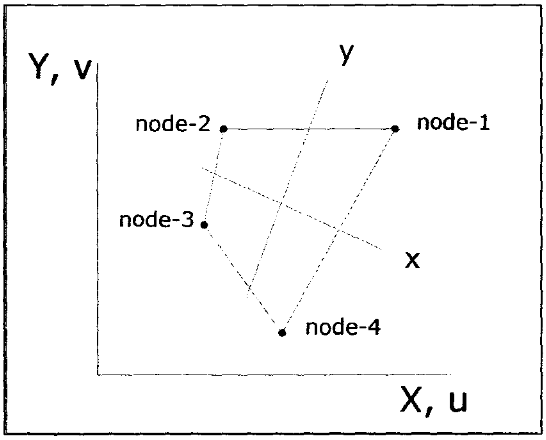

Fig. 2.10 Typical 4-node 2-D isoparametric element

2.4.2 Material model of Masonry

Unreinforced masonry is a composite material composed of units (e.g. clay bricks or concrete blocks) and mortar joints. It is recognized that the mortar joints, or more precisely the unit/mortar interfaces, often have a much lower strength than that of the intact unit or mortar. As such, the presence of these joints creates planes of weakness along which failures may initiate and propagate. This results in masonry displaying distinct directional properties. The overall behaviour of the masonry composite is determined by the properties of the intact materials (unit and mortar) and the strength and orientation of the unit/mortar interfaces (Stutcliffe et al, 2001).

Along with the presence of 'weak' joints, a large number of other factors may influence the strength and stiffness of the masonry composite. Such factors include anisotropy of the units, unit size and aspect ratio, joint dimensions, joint orientation, relative position of head and bed joints, properties of the units and mortar, properties of unit/mortar bond, and workmanship. The large numbers of variables make numerical simulation of masonry assemblages difficult.

Masonry units consist of coarse aggregate and a continuous matrix of mortar, which itself comprise a mixture of cement past and smaller aggregate particles. Its physical behaviour is complex, being largely determined by the structure of the composite material (i.e. water-cement ratio, cement-aggregate ratio, shape and size of aggregate, and the type of cement used). The structure of the material is ignored and a homogeneous continuum is assumed. Also the material is assumed to be initially isotropic.

A model for unreinforced masonry proposed by Kappos et al. (2002) is adopted in this research. The material constitutive law (Drucker-Prager model) used for masonry is shown in figure 2.11. The equivalent uniaxial stress-strain relationship is linear, with an elastic modulus coinciding with the value for elastic analysis, $E_{el} = 1000\ f_{cm}$ (CEN TC 250 1995), where f_{cm} is the compressive strength of the masonry wall, ultimate compressive strain $\varepsilon_u = 0.002$, and tensile strength $f_{tm} = 0.1\ f_{cm}$.

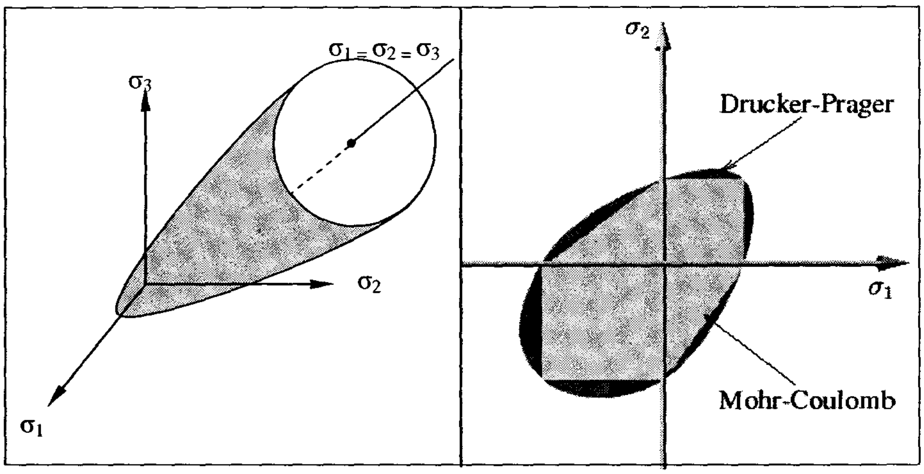

Fig. 2.11 Three-dimensional failure surface and corresponding biaxial strength envelope for unreinforced masonry

The biaxial strength envelope produced as a projection of the 3D failure surface, both shown in figure 2.11, is in good agreement with the one proposed on the basis of test results by Dhanasekar et al. (1985). After cracking, residual shear stiffness remains, equal to 60% of the un-cracked value. The use of a tensile strength equal to 10% of the compressive strength for unreinforced masonry, as well as the use of 60% of the uncracked shear stiffness after closing of a crack, were selected on the basis of a sensitivity analysis performed on a half-scale unreinforced masonry buildings tested at Istituto Sperimentale

Modelli e Strutture (ISMES) by Benedetti et al. (1998). Further information, especially regarding the tensile strength, can be found in the experimental work of Dhanasekar et al. (1985) and the analytical work of Ignatakis et al. (1989).

2.4.3 Plasticity Framework

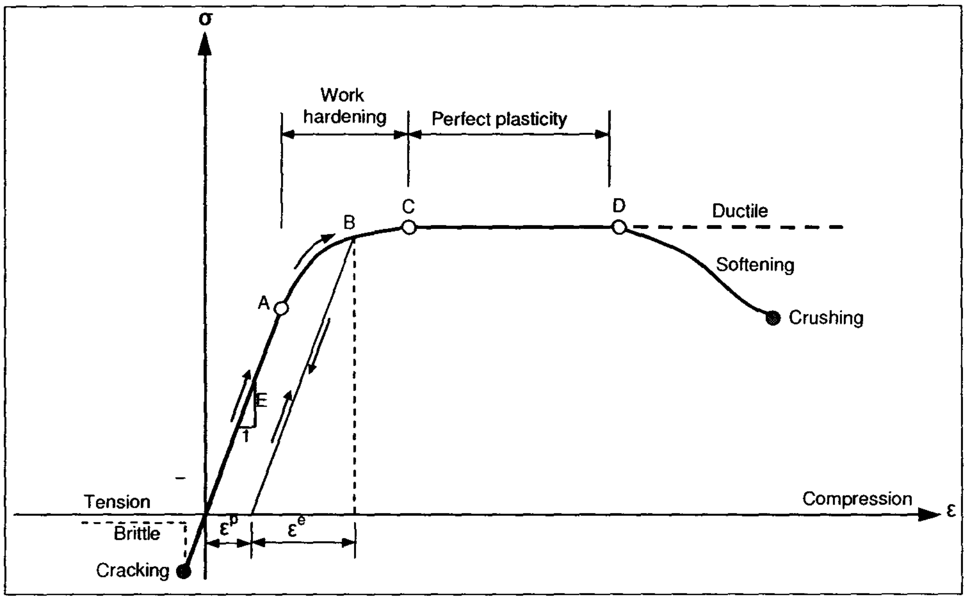

Fig. 2.12 Typical uniaxial stress-strain curve for masonry (pre- and post-failure regime)

Figure 2.12 shows a typical uniaxial stress-strain curve for masonry up to tensile and compressive failure. For tensile failure, the behaviour is essentially linearly elastic up to the failure load. For compressive failure, the material initially exhibits almost linear behaviour up to the proportional limit at point A, after which the material is progressively weakened by internal microcracking up to the end of the perfectly plastic flow region CD at point D. the nonlinear deformations are basically plastic, since upon unloading only the portion ε^e can be recovered from the total strain ε. The behaviour in the region AC and in the region CD corresponds to the behaviour of work-hardening elastoplastic and elastic perfectly plastic solid, respectively. As shown from figure 2.12, the total strain ε in a plastic material can be considered as the sum of reversible *elastic strain* ε^e and the permanent *plastic strain* ε^p. A material is defined as *perfectly plastic or work hardening* if it does or does not allow changes of permanent strain under constant stress (Chen, 1981).

The use of an elastic-work hardening plastic model to describe the stress-strain behaviour of masonry is attractive in view of the many apparent similarities between the behaviour of masonry materials in compression and of an idealized elastoplastic material with work hardening.

In developing constitutive equations for work-hardening material, two basic approaches may be used. The ***first approach*** to formulation is the *deformation theory* in the form of the total stress-strain relationship. This theory assumes that the state of stress determines the state of strain uniquely as long as the plastic deformation continues. The total stress-strain relationship based on deformation theory is only valid in the case of *proportional loading* as long as unloading does not occur.

The ***second approach*** to formulation is *the incremental theory* or *flow theory*. This type of formulation relates the increment of plastic strain components $d\varepsilon^p{}_{ij}$ to the state of stress, σ_{ij}, and the stress increment, $d\sigma_{ij}$. The fundamental difference is that the yield surface is now not fixed in stress space, but rather the stress point σ_{ij} is permitted to move outside the yield surface. The response of the material after initial yielding is described by specifying a new yield surfaces called the *subsequent yield surfaces*, and the rule that specifies this post-yield response is called the *hardening rule*.

From the above discussion, *the incremental theory* or *flow theory* seams to be the most appropriate plasticity framework to describe materials like plane concrete and masonry. In the following section, the key points of *the incremental theory* or *flow theory* are briefly discussed.

Key points of the incremental theory (flow theory)

The incremental theory of plasticity is based on three fundamental assumptions:

1- The *existence* of an *initial yield surface* which defines the elastic limit of the material in a multiaxial state of stress.

2- The *hardening rule* which describes the evolution of subsequent yield surfaces.

3- The *flow rule* which is related to a plastic potential function and defines the direction of the incremental plastic strain vector in strain space.

2.4.3.1 Loading Surfaces

Loading surface is the subsequent yield surface for an elastoplastically deformed material, which defines the boundary of the current elastic region. If a stress point lies within this region, no additional plastic deformation takes place. On the other hand, if the state of stress is on the boundary of the elastic region and tends to move out of the current loading surface, additional plastic deformations will occur, accompanied by a configuration change of the current loading surface. In other words, the current loading surface or the subsequent yield surface will change its current configuration when plastic deformation takes place. Thus, the loading surface may be generally expressed as a function of the current state of stress (or strain) and some hidden variables such that:

$$f(\sigma_{ij}, \varepsilon^{P}_{ij}, k)=0 \tag{2.4}$$

States for which $f=0$ represent yield states, while for $f<0$ elastic behaviour occurs. The so-called hidden variables are expressed in terms of the plastic strain ε^{P}_{ij} and a *hardening parameter k*.

Drucker-Prager yield function

Drucker-Prager criterion, formulated in 1952, is a simple modification of the Von Mises criterion, where the influence of a hydrostatic stress component on failure is introduced by inclusion of an additional term in the Von Mises expression to give:

$$f(I_1, J_2) = \alpha I_1 + \sqrt{J_2} - k = 0 \tag{2.5}$$

Where α and k are material constants. When α is zero equation (2.5) reduces to the Von Mises criterion, and;

$$I_1 = \sigma_1 + \sigma_2 + \sigma_3 \tag{2.6}$$

$$J_2 = \frac{1}{3}(I_1^{\,2} - 3I_2) \tag{2.7}$$

$$I_2 = \sigma_1\sigma_2 + \sigma_2\sigma_3 + \sigma_3\sigma_1 \tag{2.8}$$

The Mohr-Coulomb hexagonal failure surface is mathematically convenient only in problems where it is obvious which one of the six sides is to be used. If this information is not known in advance, the corner of the hexagonal can cause considerable difficulty and causes to complications in obtaining a numerical solution. The Drucker-Prager criterion, as a smooth approximation to the Mohr-Coulomb criterion, can be made to match the latter by adjusting the size of the cone. For example, if the Drucker-Prager circle is made to agree with the outer apices of the Mohr-Coulomb hexagon, where θ = 60, then the constants α and k in equation (2.5) are related to the constants c and φ by:

$$\alpha = \frac{2\sin\phi}{\sqrt{3}(3-\sin\phi)} \quad , \textit{and} \tag{2.9}$$

$$k = \frac{6c\cos\phi}{\sqrt{3}(3-\sin\phi)} \tag{2.10}$$

Where c is the cohesion and φ is the angle of internal friction; both are material constants determined by tests. Parameters c and φ can be expressed in terms of uniaxial tensile strength f_{tm} and uniaxial compressive strength f_{cm} of masonry material as:

$$\sin\phi = \frac{f_{cm} - f_{tm}}{f_{cm} + f_{tm}} \tag{2.11}$$

$$c = \frac{f_{cm} \cdot f_{tm}}{f_{cm} - f_{tm}} \tan\phi \tag{2.12}$$

The cone corresponding to the constants in equations (2.9) and (2.10) circumscribes the hexagonal pyramid and represents an outer bound on the Mohr-Coulomb failure surface as shown in figure 2.13 (Chen and Han, 1988).

The Drucker-Prager criterion for biaxial stress state is represented by the intersection of the circular cone with the coordinate plane of σ_3=0. Substituting σ_3=0 into equation (2.5) leads to:

$$\alpha(\sigma_1 + \sigma_2) + \sqrt{\frac{1}{3}\left(\sigma_1^2 - \sigma_1\sigma_2 + \sigma_2^2\right)} = k \tag{2.13}$$

Or rearranging

$$\left(1-3\alpha^2\right)\left(\sigma_1^2 + \sigma_2^2\right) - \left(1+6\alpha^2\right)\sigma_1\sigma_2 + 6k\alpha(\sigma_1 + \sigma_2) - 3k^2 = 0 \tag{2.14}$$

This is an equation of off-center ellipse as shown in figure 2.14.

Where $H_1 = \dfrac{\sqrt{3}k}{1-\sqrt{12}\alpha}$, $H_2 = \dfrac{\sqrt{3}k}{1+\sqrt{3}\alpha}$, $V_1 = \dfrac{\sqrt{3}k}{1+\sqrt{12}\alpha}$, $V_2 = \dfrac{\sqrt{3}k}{1-\sqrt{3}\alpha}$

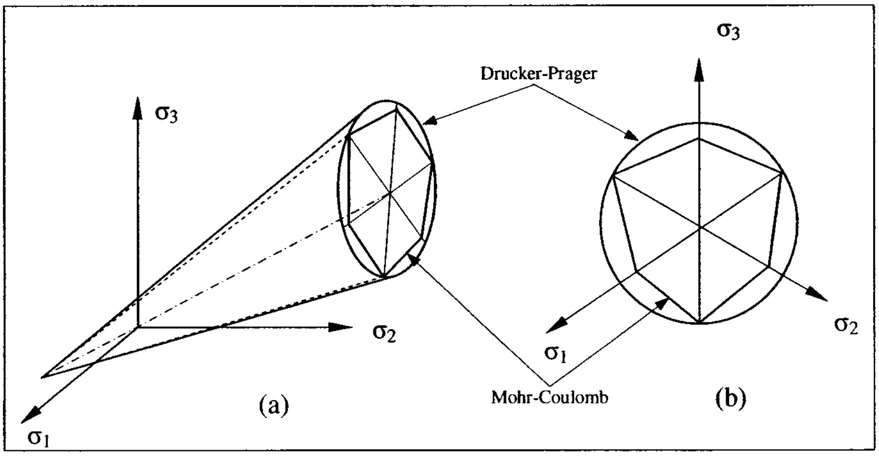

Fig. 2.13 Drucker-Prager and Mohr-Coulomb criteria matched along the compressive meridian (a) in principal stress space; (b) in the deviatoric plane.

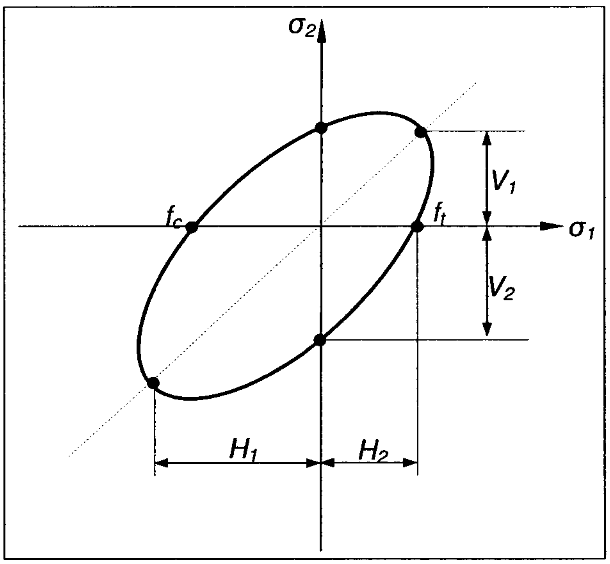

Fig. 2.14 Drucker-Prager criterion in the coordinate plane $\sigma_3 = 0$

2.4.3.2 Hardening Rule

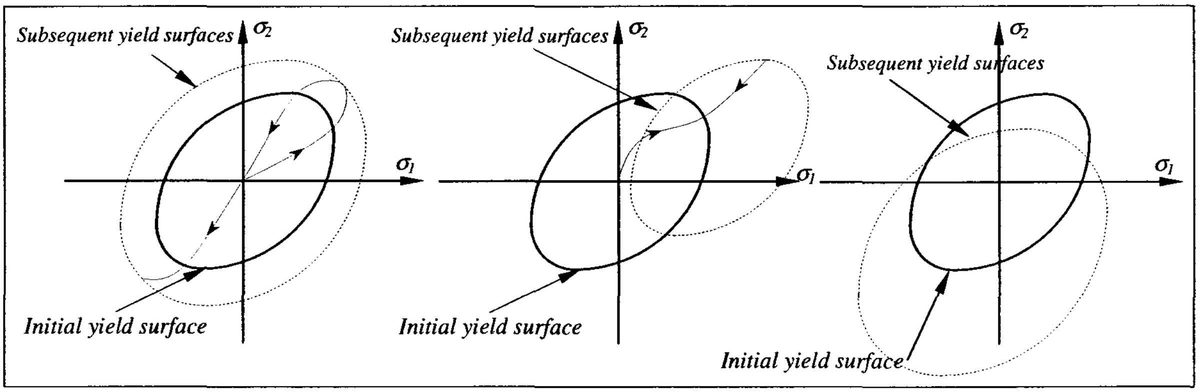

a-isotropic hardening **b-** kinematic hardening **c-** mixed hardening

Fig. 2.15 Isotropic hardening rules

The hardening rule defines the motion of the subsequent yield surfaces during plastic loading. A number of hardening rules have been proposed to describe the growth of subsequent yield surfaces for work-hardening materials. Three simple models will be briefly described: *isotropic hardening, kinematic hardening, and mixed hardening*. The isotropic model applies mainly to monotonic proportional loading; for cyclic and reversed types of loadings for materials with a pronounced *Bauschinger effect*, the kinematic hardening rule is more appropriate. Combinations of isotropic and kinematic hardening are called mixed hardening, which is more suitable for masonry material, as shown in figure 2.15. Mixed hardening rule is adopted in this research to simulate the behaviour of masonry material under biaxial stress state.

2.4.3.3 Flow Rule

So far, the loading surface alone has been considered, and the shape of the subsequent loading surface in a given loading program was determined by the choice of a specific hardening rule. The necessary connection between the loading function f and the stress-strain relation for a work-hardening material is governed by a flow rule (Chen, 1981).

When the current yield or loading surface f is reached, the material is in state of plastic flow upon further loading. If the load function and potential function are given by $f(\sigma_{ij}, \varepsilon^{p}_{ij}, k)$ and $g(\sigma_{ij}, \varepsilon^{p}_{ij}, k)$, respectively, the flow rule is termed associated if the plastic potential surface has the same shape as the current yield or loading surface [$g(\sigma_{ij}, \varepsilon^{p}_{ij}, k) = f(\sigma_{ij}, \varepsilon^{p}_{ij}, k)$], i.e., the plastic flow develops along the normal to the loading surface. Apart from its simplicity, this normality condition assures a unique solution for a given boundary value problem using any stress-strain relations developed on the basis of the equation:

$$d\varepsilon_{ij}^{p} = d\lambda \frac{\partial f}{\partial \sigma_{ij}} \tag{2.15}$$

Where dλ is a positive scalar factor of proportionality, which is nonzero only when plastic deformations occur. Relation (2.15) is called the associated flow rule because it is connected (associated) with the loading surface. The associated flow rule makes various generalizations of the constitutive equations possible by considering yield surfaces of more complex form.

Since there is little experimental evidence on subsequent loading surfaces, especially for masonry and concrete materials, the associate flow rule is applied predominantly for practical reasons.

Drucker-Prager failure criterion with mixed hardening rule and associated flow rule was used to simulate the behaviour of masonry. Tensile strength is assumed to be 10% of the compressive strength for un-reinforced masonry. "nDMaterial NewTemplate3Dep" command is used to construct the template elasto-plastic material object.

2.4.4 Contact Elements on Horizontal Planes

There are two different types of contact elements within the representation of infill panel. The first group of elements is the contact elements between masonry elements on horizontal failure plane, as shown in figure 2.16. The second group of elements models the contact elements between masonry elements on inclined failure plane. Both types of contact elements accept the specification of two different behaviours in any two different directions.

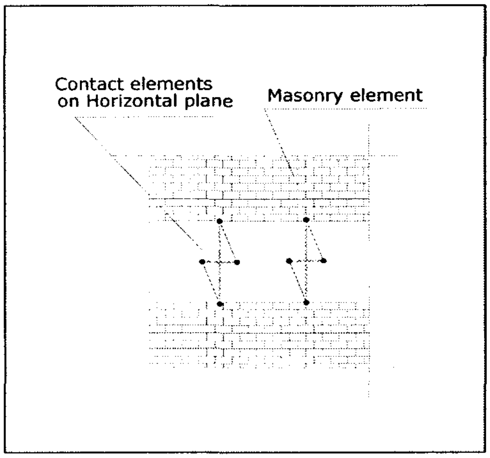

Fig. 2.16 Contact elements on horizontal failure planes

Material model of Mortar

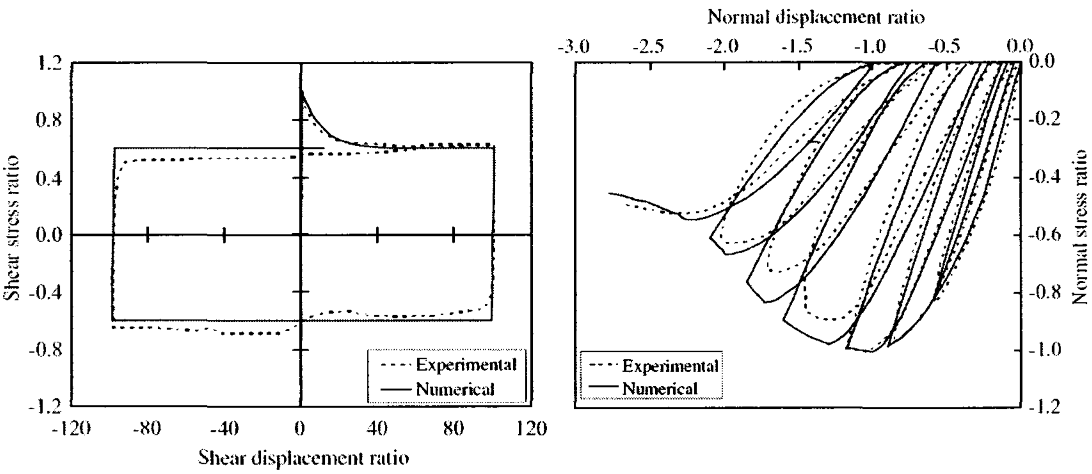

b- Direct shear test under cyclic loading

a- Uniaxial compressive test under cyclic loading

Fig. 2.17 Behaviour of mortar joint under uniaxial compression and direct shear (Oliveira et al. 2004).

Mortar joint elements are modeled using Zero-Length Element. ZeroLength element command is used to construct a ZeroLength element object, which is defined by two nodes at the same location. The nodes are connected by multiple UniaxialMaterial objects to represent the stress-strain (or force-deformation) relationship for the element. This element accepts the specification of two different material types (or relations) in any two arbitrary directions. First material type is used to describe the behaviour of mortar joint in normal direction. The second material type is used to describe behaviour of mortar joint in shear direction. Typical behaviour of mortar joint under both uniaxial compression cyclic loading and direct shear tests are shown in figure 2.17.

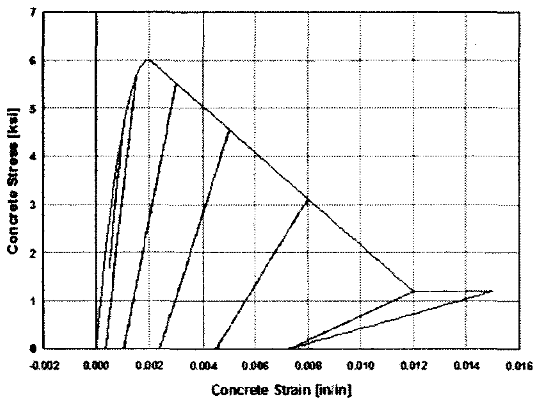

a- Hysteretic stress-strain relation of concrete01 model

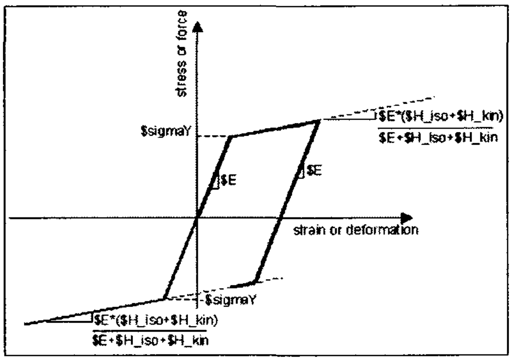

b- Hardening material

Fig. 2.18 Modelling of mortar joint in normal and shear directions (OpenSees Manual 2006)

Material type Concrete01 is used to simulate the behaviour of mortar joints under uniaxial compression and under cyclic loading. Hardening Material is used to model the behaviour of mortar joint under direct shear, as shown in figure 2.18.

2.4.5 Contact Elements on Inclined Planes

Figure 2.19 shows the contact elements on inclined failure planes of the proposed finite element model. Zero-length elements are used to simulate the behaviour of cracked masonry on inclined planes. Experimental observations show that diagonal cracks occur in masonry panels are usually saw-tooth cracks as shown in figure 2.20.

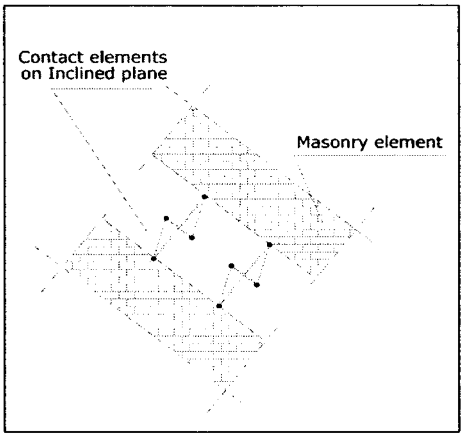

Fig. 2.19 Contact elements on inclined failure planes

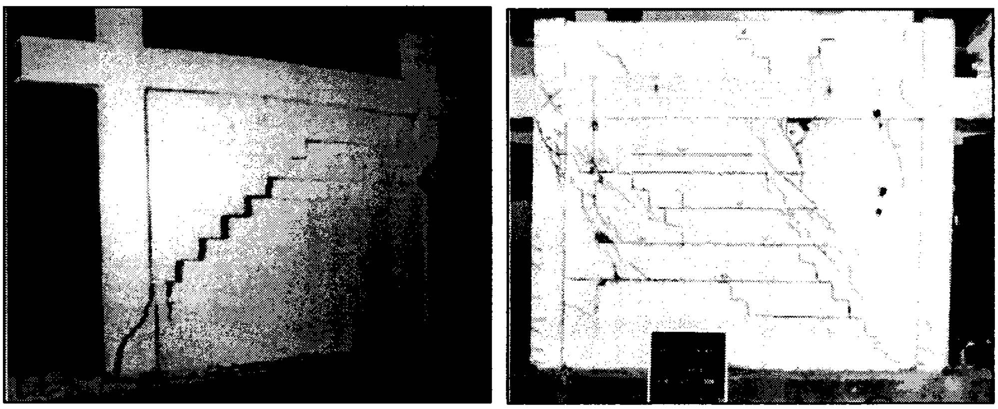

(François and Royer-Carfagni, 2005) (Shing and Mehrabi, 2002).

Fig. 2.20 Failure of masonry panel on inclined planes

Interface elements were initially employed in concrete by Ngo and Scordelis (1967), in rock mechanics by Goodman et al. (1968) and in masonry by Page (1978), being used since then in a variety of structural problems. The application of a micro-modelling strategy to the analysis of in-plane masonry structures using the finite element method requires the use of continuum elements and line interface elements. Usually, continuum elements are assumed to behave elastically whereas non-linear behaviour is concentrated in the interface elements. This approach to modelling is assumed applicable to structures where the interface appears well defined (as in masonry structures) and, therefore, the numerical simulation of the cyclic behaviour of interface elements is a key issue when dealing with micro-modelling (Oliveira et al., 2004).

Recent experimental work (Atkinson et al., 1989, and Lourenco and Ramos, 2004) carried out to investigate cyclic behaviour of interfaces has shown some important characteristics, such as:

- stiffness degrades in both tension and compression regimes;
- residual relative normal displacements at zero stress;
- absence of stiffness degradation in direct shear;
- complete crack closing under compressive loading.

Based on the available experimental results from the cyclic behaviour of interfaces, the following hypotheses will be adopted in the proposed model:

- elastic behaviour constitutes a satisfactory approach for shear unloading/reloading behaviour;
- elastic unloading/reloading is not an appropriate hypothesis for tensile and compressive loading since observed experimental behaviour cannot be simulated accurately, namely stiffness degradation and crack closing/reopening, which clearly exhibit nonlinear behaviour. Accordingly, non-linear constitutive material laws should be adopted (Oliveira et al., 2004).

Material model of diagonally cracked masonry

When quasi-brittle materials cracks such as concrete, ceramics or masonry, they exhibit considerable roughness, usually due to small-size heterogeneities. The roughness is the result of sand or stone aggregates in concrete. Roughness should not be neglected in any damage model for quasi-brittle materials. François and Royer-Carfagni (2005) presented an attempt to model the demand of a damage model involving rough fractures. The proposed approach is based on structured deformation theory and it is built within the irreversible process framework, following the generalized standard-material theory (Halphen and Nguyen 1975). The model structure assures easy numerical implementation and allows a straightforward extension to contemplate other approaches in the field of damage models (François and Royer-Carfagni 2005). Figure 2.21 shows Hysteretic loop in the (γ, τ) plane for compressed specimens with saw-tooth cracks.

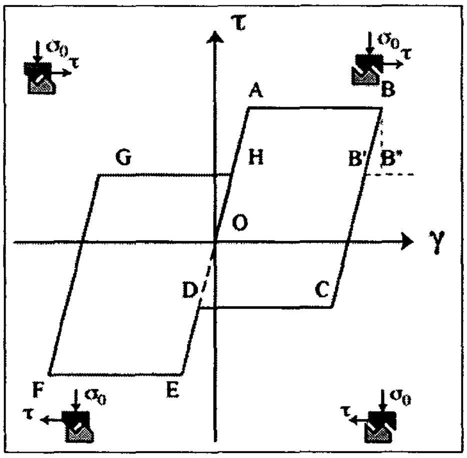

Fig. 2.21 Hysteretic loop in the (γ, τ) plane for compressed specimens with saw-tooth cracks (François and Royer-Carfagni 2005).

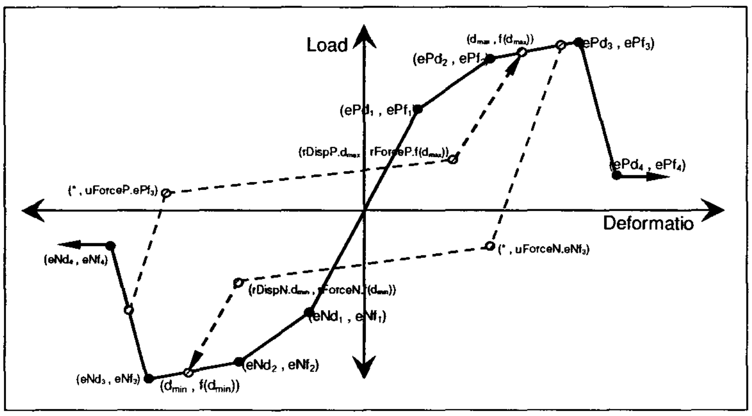

a- Pinching4 Material.

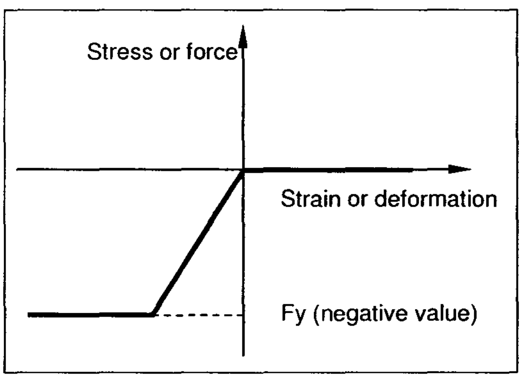

b- Elastic-Perfectly Plastic Gap Material.

Fig. 2.22 Modeling of inclined cracks of masonry panel in normal and shear directions (OpenSees 2006).

The use of 60% of the uncracked shear stiffness after closing of a crack, were decided on the basis of a sensitivity analysis performed for a half-scale unreinforced masonry building tested by Benedetti et al. (1998).

Material type "Pinching4" is used to simulate the behaviour of inclined cracks of masonry panels under direct cyclic shear load. While "Elastic-Perfectly Plastic Gap" Material is used to model the behaviour of inclined cracks of masonry panels under compression or tension load as shown in figure 2.22.

2.5 MODELING OF INTERFACE BETWEEN MASONRY PANEL AND RC FRAME

The interface between masonry panel and the boundary frame is mainly a mortar material. A number of horizontal and vertical zero-length elements is used to model this interaction. Figure 2.23 shows the interface elements between masonry and RC frame in different locations as per the proposed model.

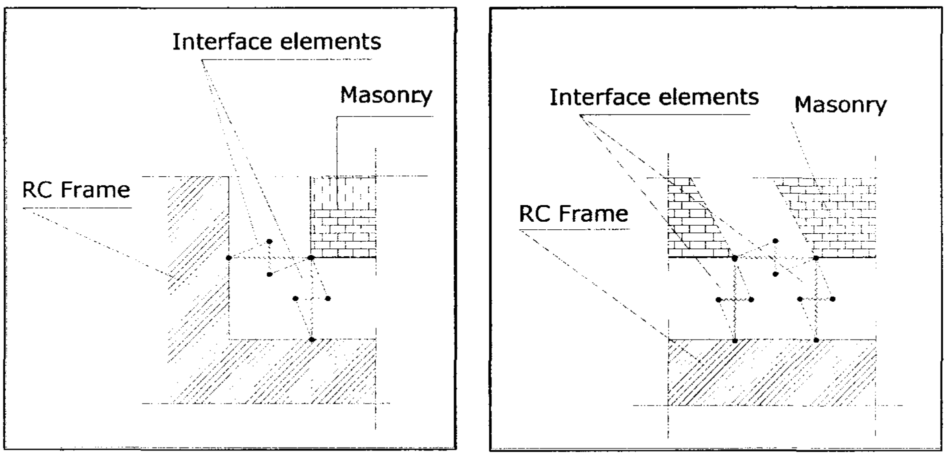

Fig, 2.23 Interface elements between RC frame and Masonry panel

Typical behaviour of mortar joint under both uniaxial compression cyclic loading and direct shear tests are shown in figure 2.24. As previously discussed in section 2.4.2, material type Concrete01 is used to simulate the behaviour of mortar joints under uniaxial compression and cyclic loading. Hardening Material is used to model the behaviour of mortar joint under direct shear, as shown in figure 2.25.

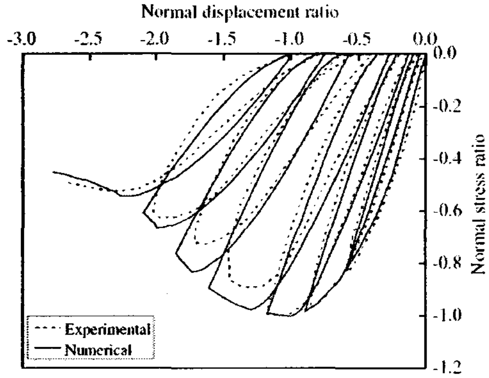

a- Uniaxial compressive test under cyclic loading

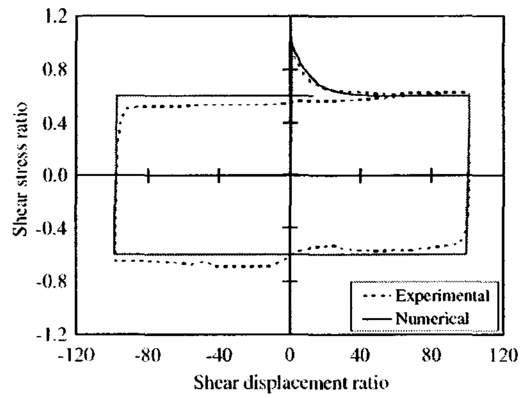

b- Direct shear test under cyclic loading

Fig. 2.24 Behaviour of mortar joint under uniaxial compression and direct shear (Oliveira et al. 2004).

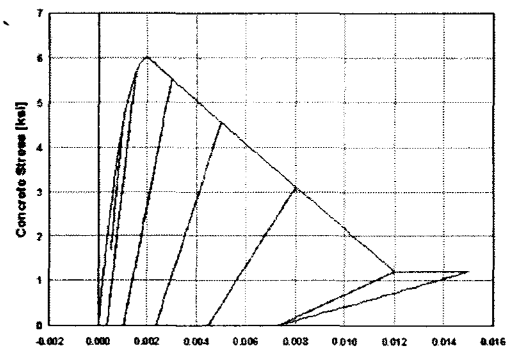

a- Hysteretic Stress-Strain Relation of Concrete01 Model

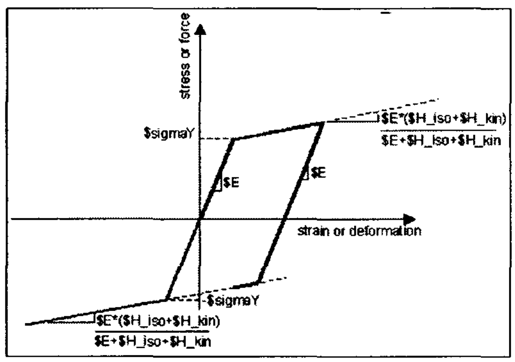

b- Hardening Material

Fig. 2.25 Modelling of mortar joint in normal and shear directions (OpenSees Manual 2006)

CHAPTER 3

MODEL VERIFICATION

3.1 INTRODUCTION

Model verification is an important phase of the theoretical investigation of the mechanical behaviour of materials and structures. Constitutive models for anisotropic materials, such as masonry, contain several material parameters that have to be quantified on the basis of tests. Nevertheless, these parameters cannot be determined explicitly from standard or sophisticated tests because of material heterogeneity and the simultaneous or sequential estimation through parameter identification method must be carried out. A parameter identification problem consists of the optimal estimate of the parameters through an inverse process in which the deviations between experimental and theoretical measurements are minimized. Several significant issues are identified in this type of process such as the optimal design of experiments, linear or non-linear programming and methods of error treatment in the optimization process or error estimate in the identified parameters (Bard, 1974; Sorenson, 1980; Luenberg, 1989; Federov and Hackl, 1997).

To verify the proposed model against experimental and analytical results, three applications will be presented in the following section. The comparisons will be in terms of overall load deflection relations, failure modes, and crack propagation.

3.2 APPLICATION -1: Single-story single-bay infilled RC frame

Choubey (1990) investigated experimentally a single story single bay reinforced concrete infilled frame. Configuration, dimensions, reinforcement details, and material properties of the investigated infilled RC frame are shown in figure 3.1.

Singh et al. (1998) presented an inelastic finite element model to simulate the behaviour of the same infilled reinforced concrete frames under static load condition. They considered that under load, the mortar may crack causing sliding and separation at the interface between the frame and the infill. Furthermore, the infill may be cracked and/or crushed which changes its structural behaviour and may render the infill ineffective, leaving the bare frame to take all the load which may lead to the failure of the framing system itself.

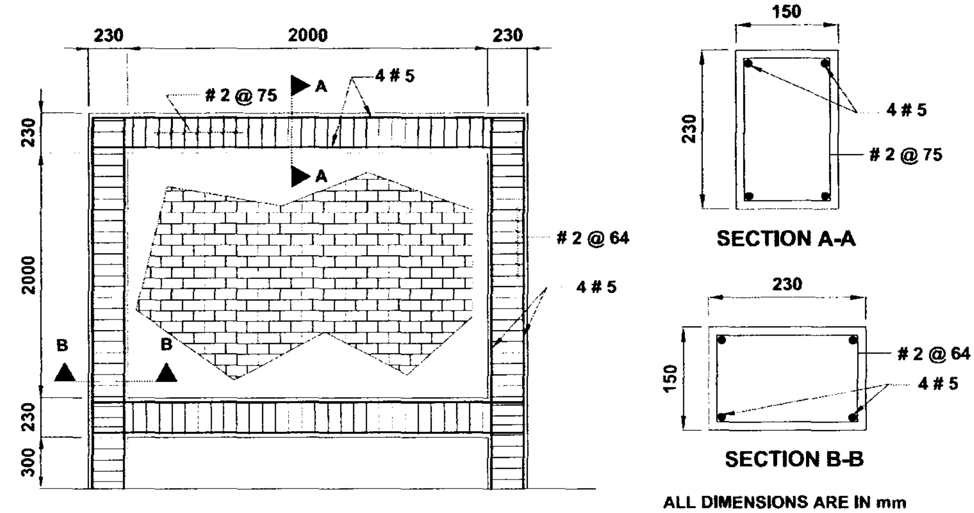

Concrete material	*Steel Material*	*Panel Material*
E_c = 10E3 MPa	E_s =200E3 MPa	E_m = 0.7E3 MPa
v_c = 0.2	v_s =0.3	v_m = 0.2
f_{cu} = 40 MPa	σ_{sy} =400 MPa	σ_u = 4.5 MPa

Fig. 3.1 Details of single story single bay infilled reinforced concrete frame

3.2.1 Modelling of infilled frame by Singh et al. (1998)

The reinforced concrete frame was modeled by 3-noded beam-column element. Inelastic behaviour of the element is governed by the interaction of the axial force, two flexural moments and a torsional moment.

Eight-noded isoparametric elements were used to model the brick masonry infill panel. The out-of-plane stiffness of the unreinforced masonry panels is very low as compared to its in-plane stiffness. In their study, only in-plane stiffness was taken into consideration. The material was assumed to be linearly elastic to failure. To predict the cracking and crushing type of failure, Von-Mises failure criterion with a tension cut off was adopted (Page and Ali, 1988). Upon crushing in compression, the stiffness and all stresses are reduced to zero. Upon cracking in tension, the stiffness normal to crack is reduced to zero but along the crack partial shear stiffness is maintained. The stress normal to the crack is reduced to zero;

however, a partial shear transfer due to interlocking between the particles is maintained. The normal stiffness and stresses along the crack are also maintained.

The behaviour of an infilled frame depends on the interaction between the infill and the frame. There can be separation, closing of gap and slipping between the frame and the infill. A six-nodded interface element was used, by Singh et al. (1998), to model this interaction behaviour between the frame element and the panel element. Two in-plane translational degrees of freedom per node were considered. The model presented by Singh et al., (1998) is shown in figure 3.2.

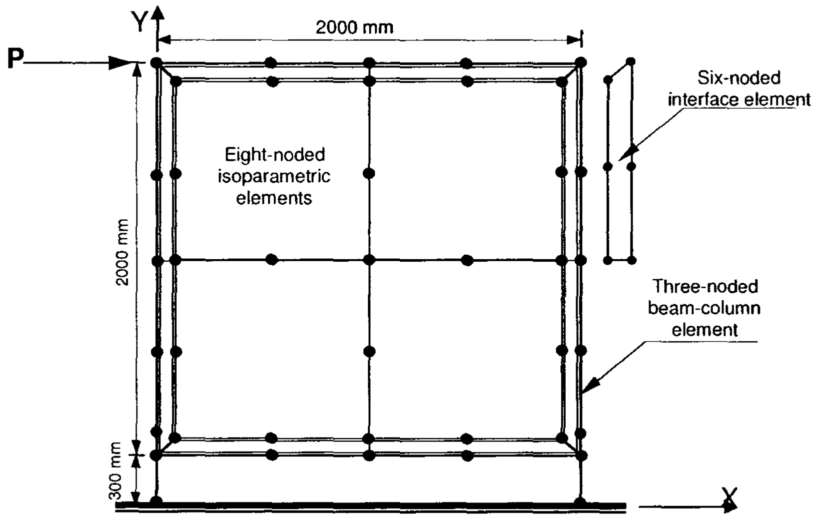

Fig. 3.2 The model presented by Singh et al., (1998)

3.2.2 Modelling of infilled frame using proposed model

The same infilled reinforced concrete frame was analyzed using the model developed in this study. Details of finite element model are shown in figure 3.3. In the figure, "M" identifies masonry elements. The material properties used are the same as shown in figure 3.1.

The load-deflection curve obtained using the proposed model was compared to that reported by Choubey (1990) and Singh et al. (1998) in figure 3.4. Good agreement with the experimental results was observed. The failure load of 170.68 kN as predicted by the proposed model is close to that obtained experimentally of 175.38 kN by Choubey (1990).

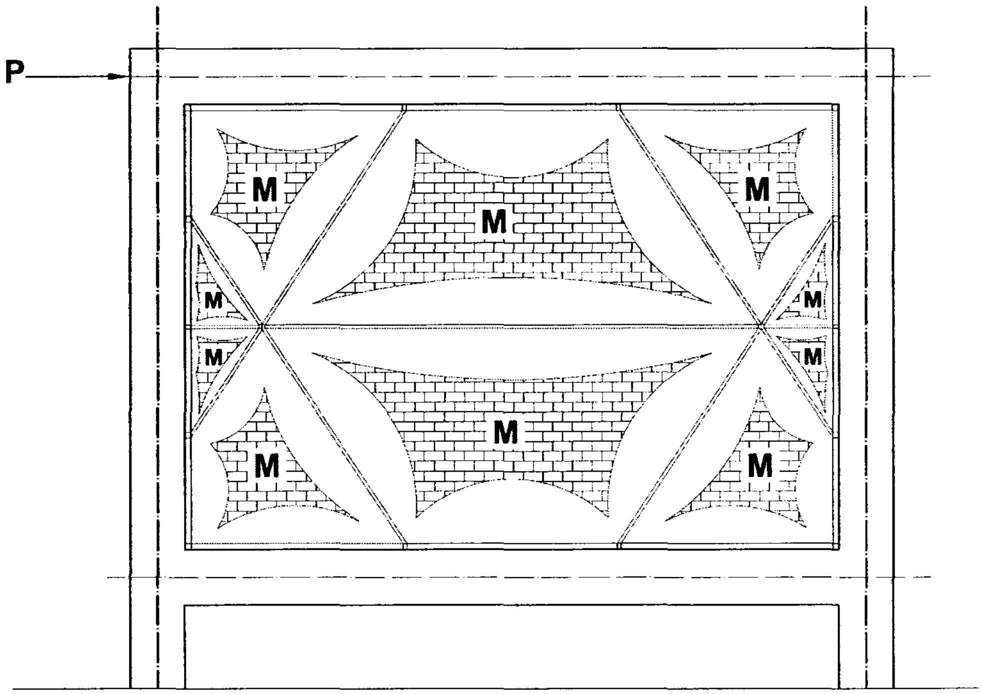

Fig. 3.3 Geometry and material properties of infilled RC frame.

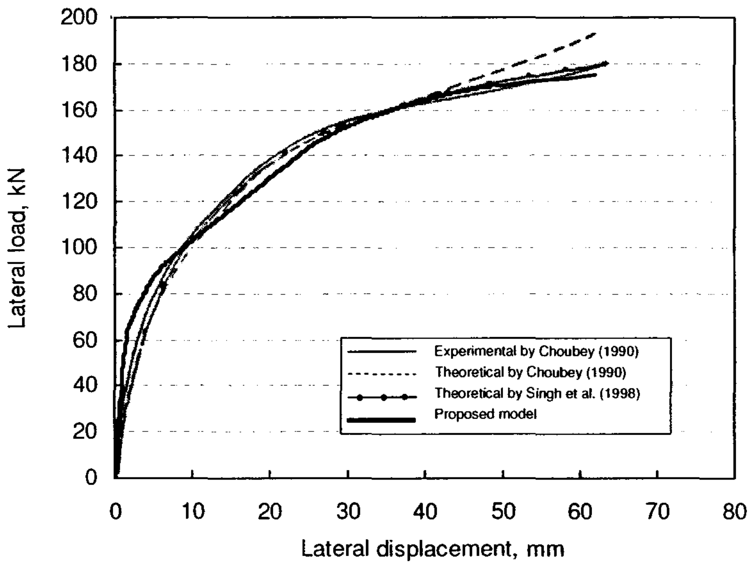

Fig. 3.4 Load-deflection behaviour of the infilled RC frame.

The crack patterns in the infill at failure predicted by the proposed model, as well as those obtained experimentally by Choubey (1990) and analytically by Singh et al. (1998) are presented in the figure 3.5. Reasonably good correlation exists between the predicted and the test results. The separation coefficients, defined as the ratio of separation length to the dimension of the infill, are plotted in figure 3.5c and 3.5d. The maximum value of the separation coefficient on each side as estimated and those obtained experimentally by Choubey (1990) are shown in the figure. The strut width observed at the center is 0.61L, while the strut width obtained analytically by Singh et al. (1998) is 0.627 L whereas that proposed by Liauw and Kwan (1984) is 0.707 L where L is the lateral dimension of the infill.

The location and direction of crack pattern obtained using the developed model is in good agreement with the crack pattern obtained from experimental test by Choubey (1990) and analytical study by Singh et al. (1998), as shown in figure 3.5a, 3.5b and 3.5c.

The location of plastic hinges in the columns of RC frame predicted by proposed model, as well as those obtained experimentally by Choubey (1990) and analytically by Singh et al. (1998) are in reasonable agreement.

The closeness between the experimental and analytical results by Choubey, 1990 and Singh et al., 1998 and the obtained results using the developed model in terms of; load-deflection behaviour, failure load, central strut width, location of hinges, crack pattern and mode of failure indicates the reliability of the proposed model to simulate the behaviour of the infilled RC frame.

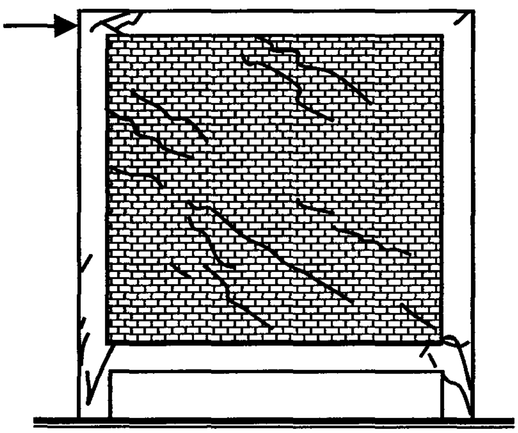

a- Crack pattern from test (Choubey, 1990)

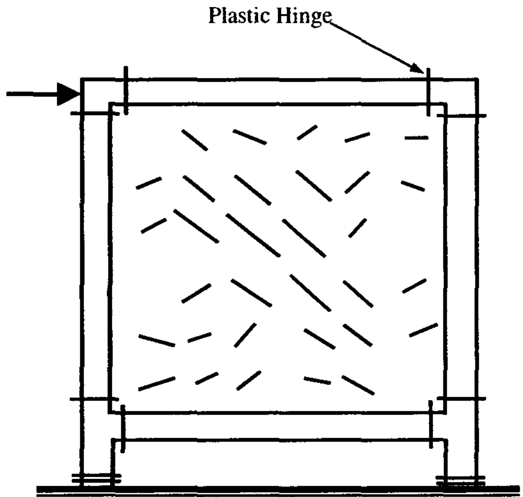

b- Analytical Crack pattern (Singh et al., 1998)

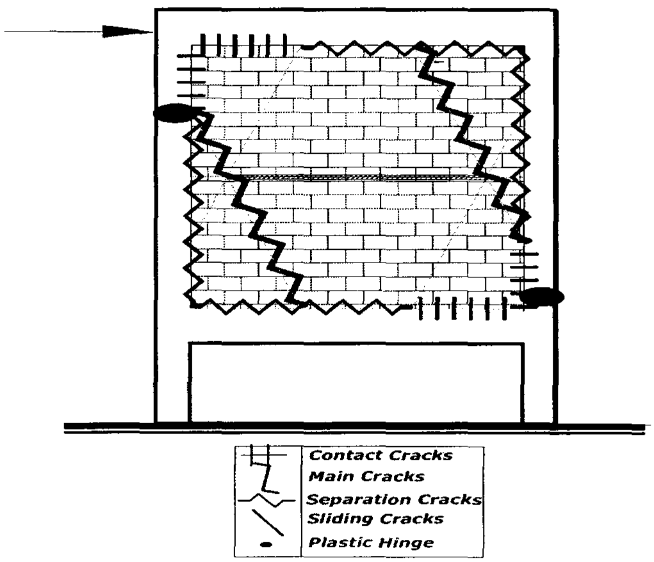

c- Crack pattern present study

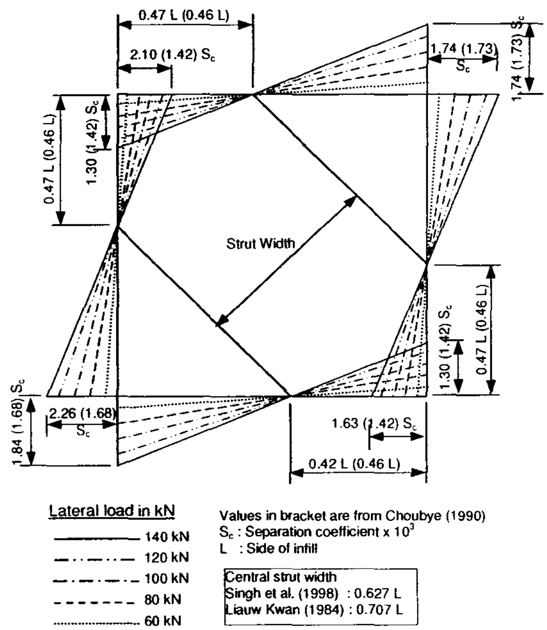

d- Separation of frame with infill using program NIFAP (Singh et al., 1998)

Fig. 3.5 Crack patterns and separation coefficients of the infilled RC frame

3.3 APPLICATION -2: Six-story three-bay infilled RC frame

Performance of masonry-infilled RC frames under in-plane lateral loading was investigated experimentally and analytically by Mehrabi et al. (1997). The prototype frame selected in this study was a six-story three-bay, moment resisting RC frame, with a 13.5 m by 4.5 m (45 ft by 15 ft) tributary floor area at each story. The design gravity loads were according to UBC (1991). Two types of frames were considered with respect to lateral loading. One was a "weak" frame design, which was based on a strong wind load. The second type was a "strong" frame design, which was based on the equivalent lateral static force for Seismic Zone 4 in the UBC. In the design of the frames, the contribution of infill panels to the lateral load resistance was not considered. The frames were designed in accordance with the provisions of ACI 318 (1989).

The test specimens were chosen to be 1/2-scale frame models representing the interior bay at the bottom story of the prototype frame. The design details for the weak and strong frames are shown in figure 3.6. For the infill panels, 92 x 92 x 194 mm (nominal 4 x 4 x 8 in) hollow and solid concrete masonry blocks, as shown in figure 3.6, were used in specimens to represent weak and strong infill panels, respectively.

Four different specimens were investigated in this study. The first specimen (specimen number 1) was weak bare frame. The other three specimens were infilled reinforced concrete frames. The second specimen, (specimen number 6), was strong frame with weak infill panel. The third specimen, (specimen number 8), was weak frame with weak infill panel. The fourth specimen, (specimen number 9), was weak frame with strong infill panel. All the specimens were monotonically loaded up to failure.

Material tests were conducted on the reinforcing steel, concrete and masonry samples for each infilled frame specimen. The material properties are summarized in Tables 3.1 and 3.2. The compressive strength of the hollow units given in column (10) was based on the net cross-sectional area, where as the compressive strength of the hollow prisms given in column (8) was based on the cross-sectional area of the face shell only.

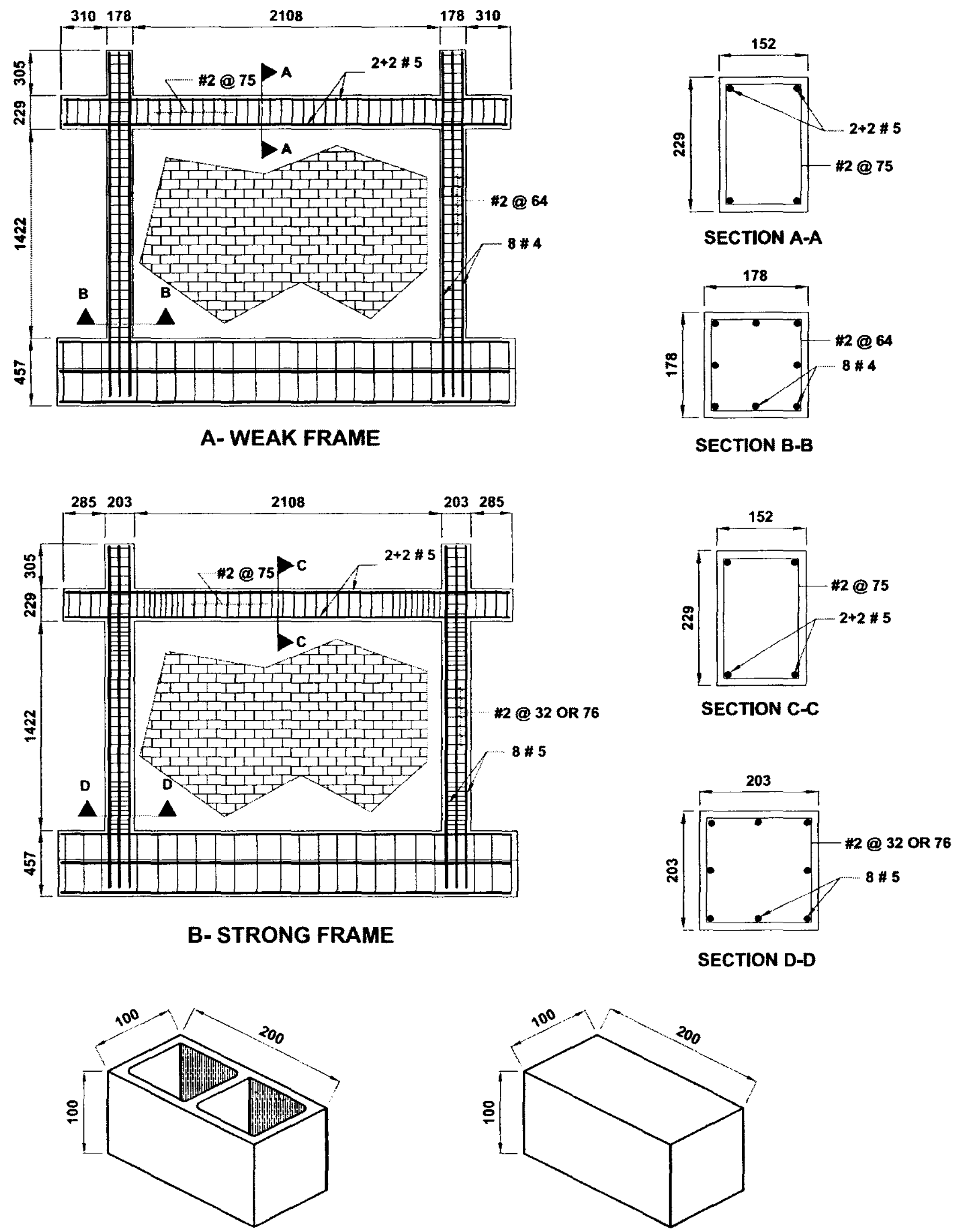

Fig. 3.6 Design details of test specimen (Mehrabi et al., 1997).

TABLE 3.1 Average Strength of Concrete and Masonry Material Mehrabi et al. (1997).

Specimen number	Frame Concrete					Three-Course Masonry Prisms			Compressive strength of masonry units (MPa)	Compressive strength of mortar cylinder (MPa)
	Secant modulus (MPa)	Compressive strength (MPa)	Strain at peak stress	Modulus of rupture (MPa)	Tensile strength (Mpa)	Secant modulus (MPa)	Compressive strength (MPa)	Strain at peak stress		
(1)	(2)	(3)	(4)	(5)	(6)	(7)	(8)	(9)	(10)	(11)
1	21,930	30.9	0.0018	6.76	3.29	--	--	--	--	--
6	19,960	25.9	0.0024	4.91	3.14	4,200	10.14	0.0032	16.48	16.76
8	17,240	26.8	0.0027	4.86	2.77	5,100	9.52	0.0027	16.48	15.52
9	17,240	26.8	0.0027	4.86	2.77	8,240	14.21	0.0026	15.59	12.48

TABLE 3.2 Average Tensile Strength of Reinforcing Steel

Bar size	Type of bar	Nominal diameter (mm)	Yield stress (MPa)	Ultimate stress (MPa)
(1)	(2)	(3)	(4)	(5)
no. 2	Plain	6.35	367.6	449.6
no. 4	Deformed	12.7	420.7	662.1
no. 5	Deformed	15.9	413.8	662.1

3.3.1 Modelling of infilled frame by Mehrabi et al. (1997)

The described group of frame specimens was analysed by Mehrabi et al. (1997). A smeared-crack finite element formulation developed previously by Lotfi and Shing (1991) was used by Mehrabi et al. (1997) to model concrete in RC frame and masonry units in the infill panels. In this formulation, a J_2-plasticity model with an isotropic strain-hardening/softening law was utilized to model the uncracked material. The plasticity model was combined with the Rankine tension cut-off criterion to signal the onset of cracking. After cracks have occurred, the material behaviour was modeled by nonlinear orthotropic model with a coaxial rotating crack formulation.

The concrete frame was modeled with nine-node quadrilateral smeared crack elements, and the shear reinforcement was smeared over concrete elements. The longitudinal bars in the frame were modeled with two-node elastic-hardening plastic bar elements. They were connected to the non-node concrete elements at the two external nodes. For masonry units, four- and nine-node smeared crack elements were used. The mortar joints in the masonry panels and along the interfaces between the infill and the frame were modeled by two-double-node interface elements. To model the possible shear failure of the columns, three-double-node interface elements were used at critical locations near the top and bottom sections of the columns.

3.3.2 Modelling of infilled frame using proposed model

The four specimens (specimens 1, 6, 8 and 9) were analyzed using the proposed finite element model. Details of finite element model and the material properties used are shown in figure 3.7. In the figure "M" identifies masonry elements.

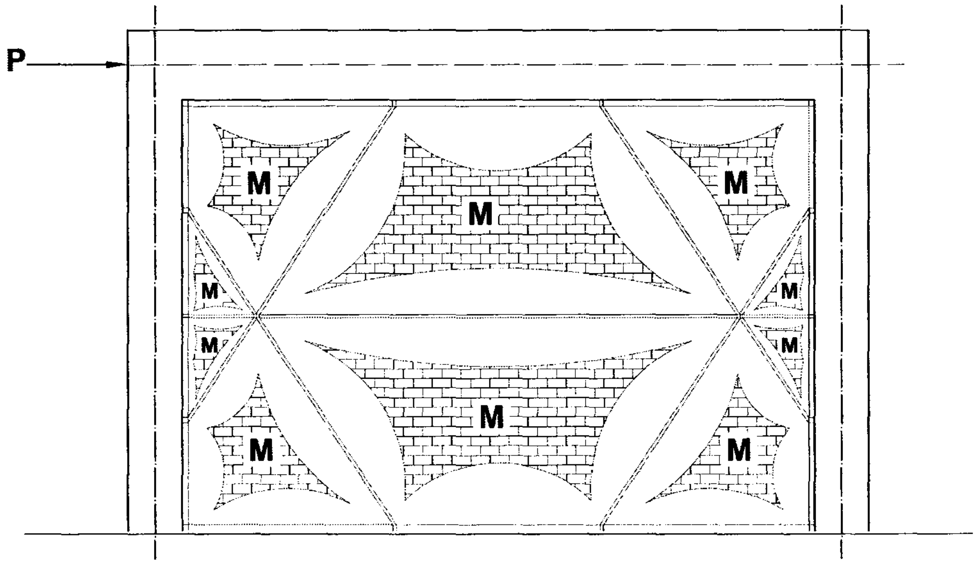

Fig. 3.7 Geometry and details of infilled RC frame.

A weak bare frame (specimen number 1) was subjected to a monotonically increasing lateral load up to failure. It exhibited a fairly flexible and ductile behaviour. The load-deflection curve obtained using the proposed model was compared to experimental and analytical results reported by Mehrabi and Shing (1997). Good agreements with the experimental and analytical results were obtained as shown in figures 3.8.

The load-deflection relationship for specimen number 6 (strong frame with weak infill panel) was compared to the experimental and analytical analysis reported by Mehrabi and Shing (1997) as shown in figure 3.9. Good agreement with the numerical results (with no bond-slip between steel reinforcing and concrete) is observed. The failure load of 240 kN as predicted by the proposed model is similar to that obtained numerically.

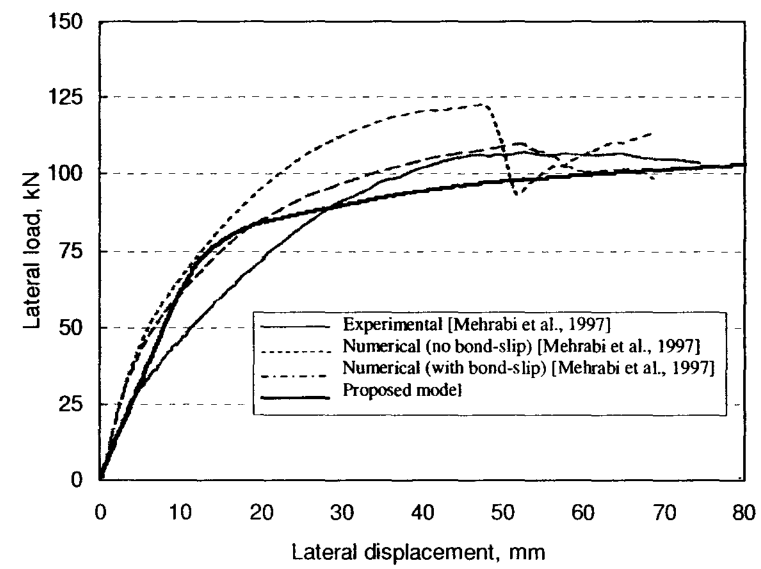

Fig. 3.8 Lateral load-Lateral displacement curve for specimen # 1

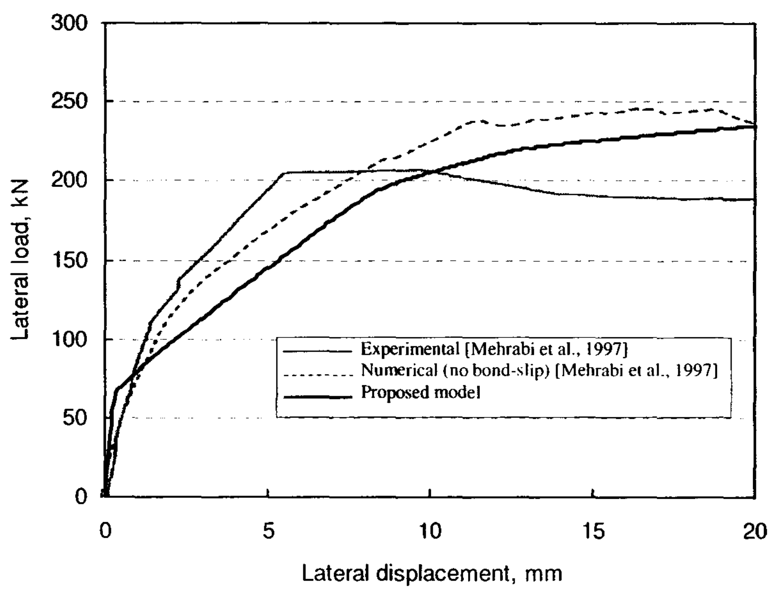

Fig. 3.9 Lateral load-Lateral displacement curve for specimen # 6

The load-deflection relationship obtained using the proposed model correlated well with load-deflection relationship obtained analytically by Mehrabi et al., 1997 (using no bond slip model), as shown in figure 3.9. The experimental load-deflection result of the same specimen is in good agreement with the analytical results of both Mehrabi et al. (1997) and the developed model up to the lateral load of approximately 200 kN. After this point, the infilled frame seams to lose part of its resistance to lateral load and the relation remain almost horizontal till failure. This behaviour was probably due to the failure of weak infill panel of the RC frame during the test.

Specimen 8 represented weak frame with a weak infill panel. The specimen was monotonically loaded up to failure. This specimen was previously investigated experimentally and analytically by Mehrabi and Shing (1997). Load-deflection relationship obtained using the proposed model was compared to relations obtained from experimental and finite element model by Mehrabi and Shing (1997), as shown in figure 3.10. Result of the developed model was again in close correlation with the analytical result of no bond slip model developed by Mehrabi et al. (1997). The experimental behaviour of specimen 8 showed increase in the lateral resistance of the infilled frame up to load of approximately 180 kN, followed by an almost flat curve. This behaviour of the test specimen was due to the failure of the weak infilled panel at load of approximately 180 kN.

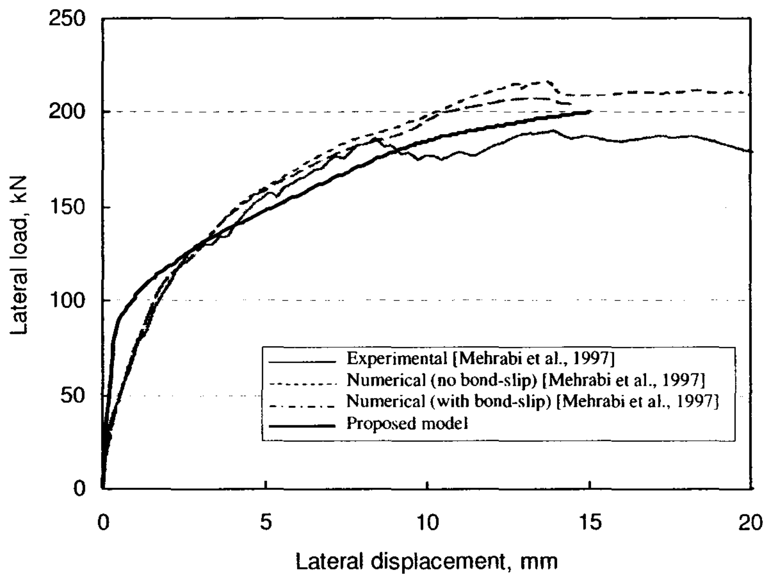

Fig. 3.10 Lateral load-Lateral displacement curve for specimen # 8

The location and direction of inclined cracks in the infill panel as well as the strut width can be observed from experimental results of specimen 8, as shown in figure 3.11(b). The direction of the diagonal cracks obtained using the developed model was in good correlation with results observed experimentally and analytically by Mehrabi et al., (1997). The locations of the plastic hinges formed during the test were near the top of the windward column and at the bottom of the lee word column, as shown in figure 3.11(b). The locations of the plastic hinges developed during the analysis using the proposed model were in the same location as obtained from the experimental results and analytical analysis by Mehrabi et al., (1997), as shown in figure 3.11(a, b, and c).

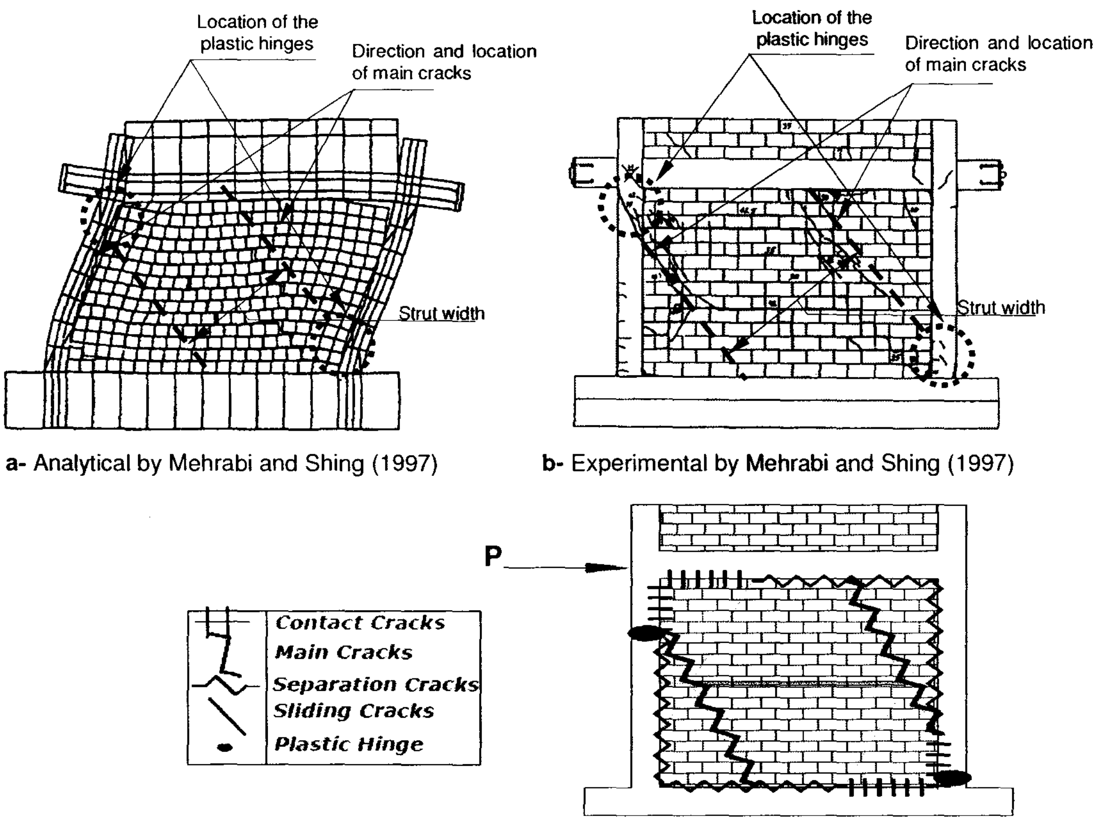

Fig. 3.11 Failure pattern for weak-frame with weak infill specimen # 8

Specimen 9 represented weak frame with a strong infill panel. The specimen was monotonically loaded up to failure. The same specimen was previously investigated experimentally and analytically by Mehrabi and Shing (1997). The behaviour of specimen 9 during the test showed increase in the lateral resistance up to a lateral load of approximately 260 kN, followed by a sudden drop in the resistance due to start of failure in the infill panel. The strong infill panel restored some of its resistance and started to show additional resistance to the infilled frame up to a load of approximately 290 kN. After this point, the infill panel lost its resistant and the only resisting element was the RC frame. Figure 3.12 shows the load-deflection relationship obtained using the proposed model as compared to the results obtained from experimental and finite element model by Mehrabi and Shing (1997).

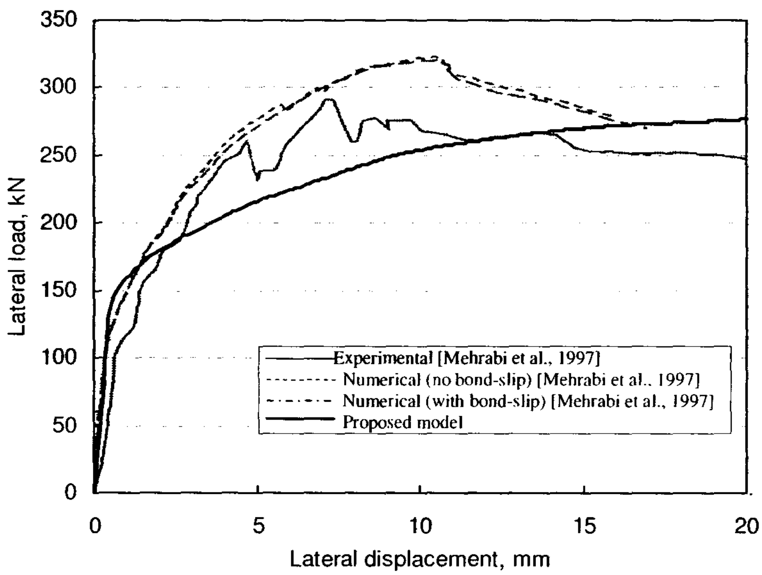

Fig. 3.12 Lateral load- Lateral displacement curve for specimen # 9

The crack pattern observed from the test and the analysis by Mehrabi and Shing (1997) correlated well with the crack pattern predicted using the developed model. It is important to observe that the location of the plastic hinges especially in the windward column of the RC frame was the same as that observed from the experimental results, as shown in figures 3.13b and 3.13c. These observations indicate that the developed model can predict the behaviour of the RC infilled frame in terms of main crack direction, crack locations, strut width, and most important, the location of plastic hinges in the RC boundary frame.

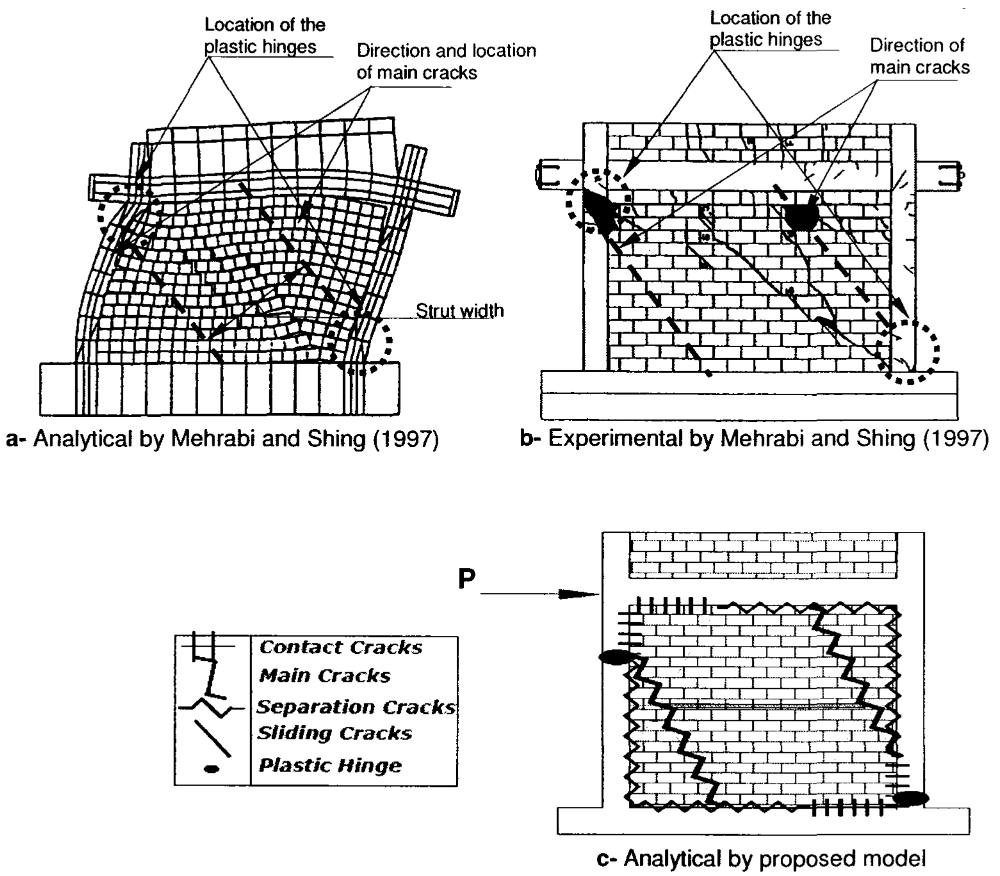

Fig. 3.13 Failure pattern for weak frame with strong infill for specimen # 9

For the case of infilled frame, infill panels increased the strength and stiffness of the RC frame by a substantial amount. In the infilled frame, significant nonlinear behaviour usually started with the cracking of the infill. Three types of failure mechanisms were observed. As shown in figure 3.11, a frame with a weak panel (specimen 8) had its lateral resistance governed by the sliding of the bed joints often occurring over the entire panel. In the case of a strong infill and a weak frame (specimen 9), the ultimate resistance and failure were dominated by diagonal and horizontal cracks in the Infill and the shear failure of the windward column, as shown in figure 3.13. In general, strong infill led to a higher lateral resistance and a better energy-dissipation capability. However, such an improvement was more pronounced in the strong frame than in the weak frame because of the brittle shear failure occurring in the columns of the boundary frame.

3.4 APPLICATION-3: Full-scale infilled RC frame

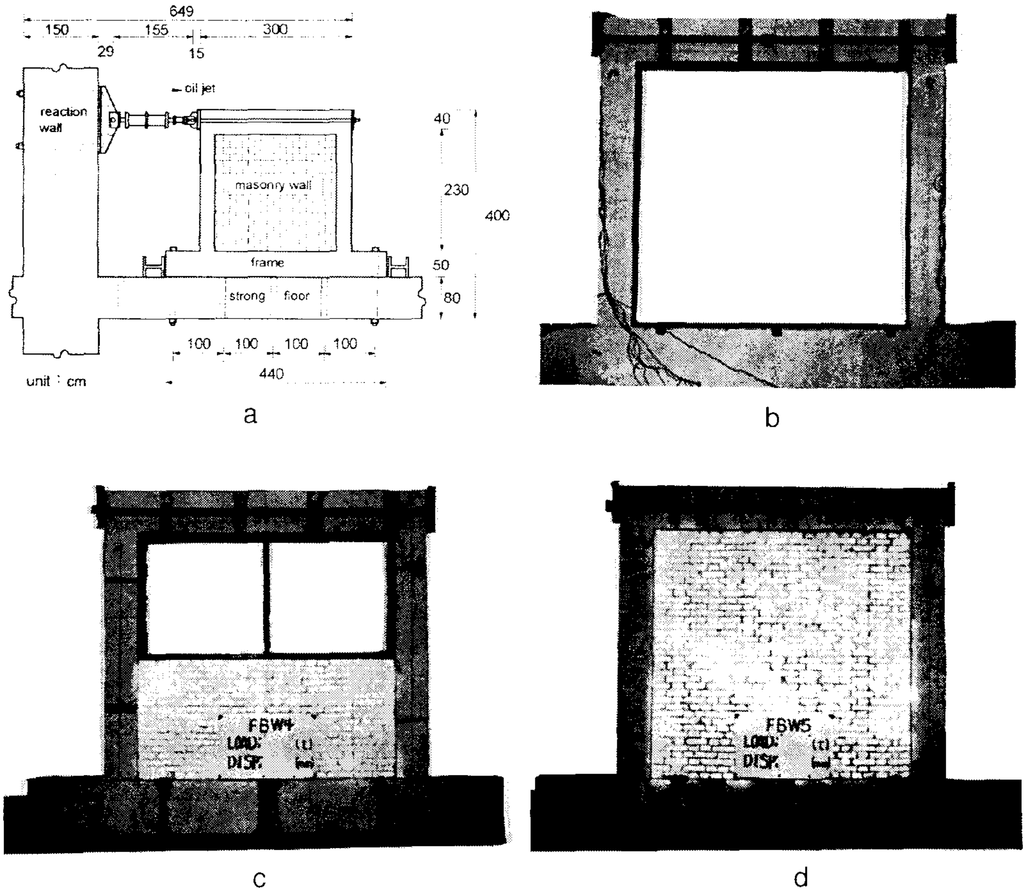

Fig. 3.14 Test Setup: (a) Experimental System; (b) RC Bare Frame; (c) RC Frame Partially Filled with Masonry Wall; (d) RC Frame Completely Filled with Masonry Wall

A full-scale test was conducted by Chiou et al. (1999) to study the behaviour of framed masonry walls and to verify the numerical solutions. The experimental system is shown in figure 3.14 a. The lateral force was applied by a jack, and the magnitude of force and lateral displacement were measured by the load cell and the clip-on gauge, respectively. Three specimens: (1) R.C. frame; (2) R.C. frame partially filled with masonry wall; and (3) R.C. frame completely filled with masonry wall as shown in figure 3.14 (b, c and d) were studied. The outside dimensions of the concrete frame were 320 × 300 cm. The cross sections of the beam and column elements were 35 × 40 cm and 30 × 35 cm, respectively.

The tension and compression reinforcements for beam and columns were taken as 4#7 bars. The diameter of the number 7 bar is 22.00 mm. The height of the masonry wall of the partially filled frame was 110 cm, and there was a wooden window in the opening area.

3.4.1 Modelling of framed masonry walls by Chiou et al. (1999)

Masonry walls were built using brittle bricks and mortar. Mortar is usually the weak plane of the masonry structure; therefore, cracking is frequently initiated in the mortar joints. The cracking of the mortar and separation of the bricks usually causes discontinuity and nonlinear behaviour.

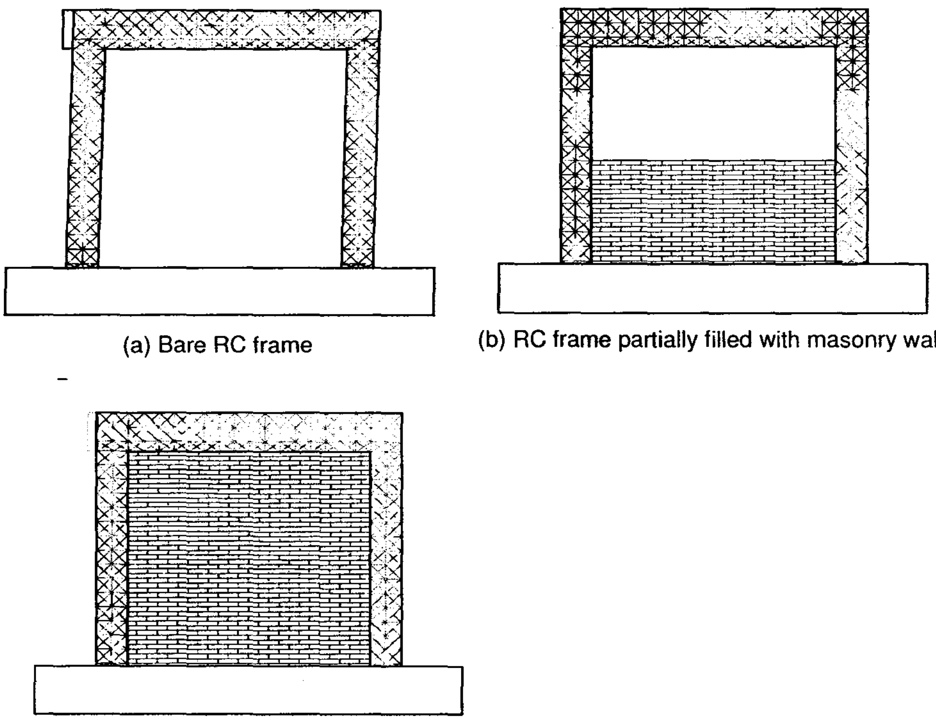

(a) Bare RC frame

(b) RC frame partially filled with masonry wall

(c) RC frame completely filled with masonry wall

Fig. 3.15 Element meshes of specimens

The failure modes of mortar are classified into two types: tensile failure and shear failure. The mixed mode failure of mortar was neglected in the study of Chiou et al. (1999). The masonry walls were divided into sub-blocks by artificial joints, which become with the same finite strength of mortar. The bricks were simulated by the sub-blocks and these sub-blocks were connected to one another by contact springs. The stiffness of the contact springs was proportional to the strength of mortar and had the dimension of force per length. The strength of mortar is represented by its resultant forces, which were determined by the effective length times either the tensile strength or the shear strength of the mortar. The contact conditions of blocks determine the contact length. The contact vertices share the contact length. The shared length is the effective length and is taken to be one-half of the contact length.

In the analysis of the framed masonry wall, the structure was divided into sub-blocks by the artificial joints. Each brick was simulated by a block, while the reinforced concrete frame was subdivided into triangular concrete sub-blocks and the reinforcements were modeled by the link elements. The wooden window in the partially filled masonry wall was neglected in the numerical model. The element meshes for the specimens: an RC frame, an RC frame partially filled with masonry wall, and an RC frame completely filled with masonry wall, are shown in figure 3.15. The RC frame was subdivided into 498 triangular concrete sub-blocks, the tension and compression reinforcements were modeled as 114 link elements, and the stirrups were modeled as 54 link elements. Because the specimens are over-reinforced, the effect of the stirrup spacing on the behaviour of RC frame is not significant. For simplicity, the stirrups modeled by the bolts were equally spaced.

The input material properties were the same as those of experimental specimens, which were determined by test. The elastic modulus of steel was $E_s = 1.96 \times 10^7$ N/cm^2 (1.96×10^5 MPa), and yield stress $f_{sy} = 3.74 \times 10^4$ N/cm^2 (374 MPa). The stress-strain relationship of the steel was assumed to be bilinear, and the plastic modulus of the steel is taken to be $E_p = 0.02E_s$. The compressive strength of the concrete was $f'_c = 26.66$ MPa, and the elastic modulus $E_c = 4696\sqrt{f'_c} = 2.4247 \times 10^6 \, N/cm^2$ (24,247 MPa). The tensile strength of the concrete was $f_t = 271$ N/cm^2 (2.71 MPa). The elastic modulus of the brick was $E_b = 2.087 \times 10^6$ N/cm^2 (2.087×10^4 MPa). The tensile strength of the interface mortar was 98 N/cm^2 (0.98 MPa), and its shear strength was

$$\tau_f = 3.64 + 0.75\,\sigma_n \text{ (kg/cm2)} \quad , \text{ or} \qquad \tau_f = 0.35672 + 0.0735\,\sigma_n \text{ (MPa)}$$

The stiffness of the contact springs was chosen to be $k_n = k_s = 1.96 \times 10^4$ N/mm.

3.4.2 Modelling of infilled frame using proposed model

The same three test frames were analysed using the proposed model. In modeling of RC frame partially filled with masonry wall, the elements used for modeling upper part of the wall were used with low material strength. Details and configuration of the proposed model are shown in figure 3.16.

The monotonic loading was adopted in this study and the load-deflection relationship of the RC bare frame, R.C. frame partially filled with masonry wall, and R.C. frame completely filled with masonry are presented in figure 3.17, 3.18 and 3.19 respectively. It was found that the proposed numerical solutions agree satisfactorily with the experimental and numerical results Chiou et al. (1999).

The failure configurations of the proposed model were compared to the experimental and numerical results of Chiou et al. (1999). Failure configurations for the RC bare frame, R.C. frame partially filled with masonry wall, and R.C. frame completely filled with masonry are presented in figure 3.20, 3.21 and 3.22 respectively.

Figure 3.20 illustrates the RC frame after yielding and failure. Figure 3.20(a) shows that the failure regions of the experimental specimen were concentrated at the top and bottom of the columns, the left and right ends of the beam, and the beam-column joints. As expected, most of the failures of columns and beam were flexural failure, while there were mixed failures at the joints of column and beam. It was found that there were many inclined cracks at the joints of the test specimen. The failure configuration predicted by numerical analysis by Chiou et al. (1999) is presented in figure 3.20(b). The solid lines indicate the failure surfaces. The failure regions predicted by Chiou et al. agree with those of the experimental results. However, because the specimen is divided by the artificial joints into triangular subblocks and its failure is assumed to be along the boundary of subblocks, the numerical solutions of Chiou et al. showed both flexural failure and shear failure in the columns and beam. This finding disagreed with the experimental results, in which the flexural failure is the dominant one except in the beam-column joints. Although the artificial joints need improving in that the failure direction is prescribed and they may create an additional failure mode, the numerical model eventually can predict the acceptable failure regions.

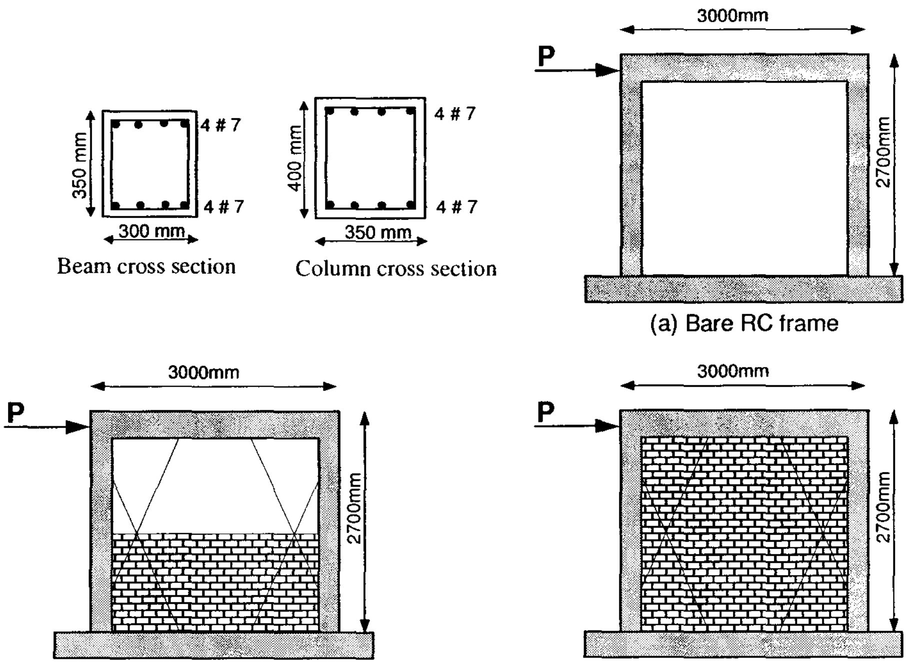

Fig. 3.16 Geometry and details of infilled RC frame.

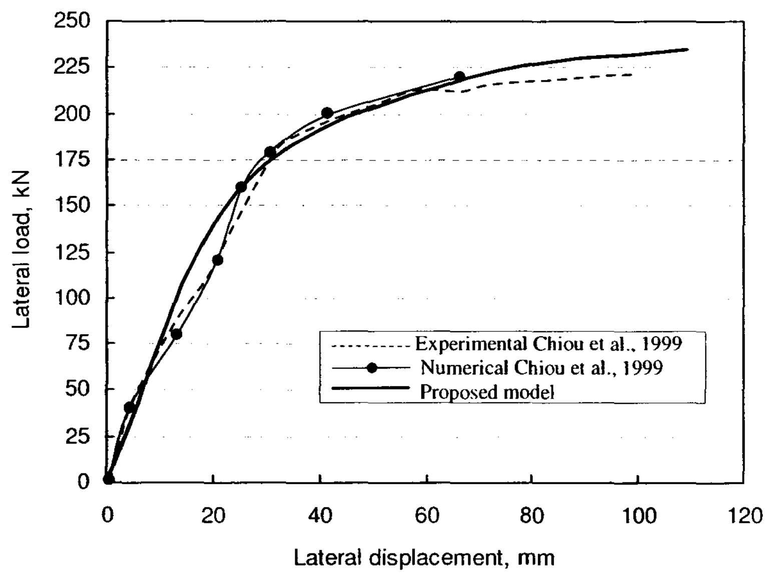

Fig. 3.17 Lateral load- Lateral displacement curve for specimen # 1

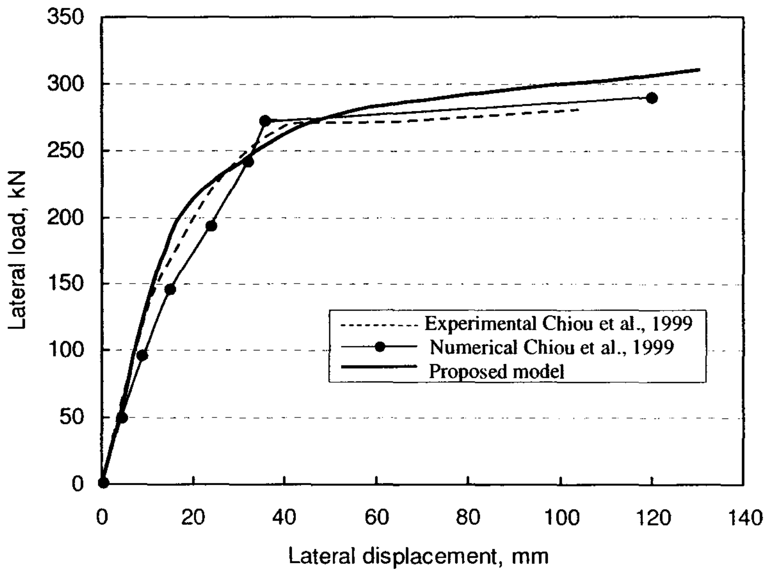

Fig. 3.18 Lateral load- Lateral displacement curve for specimen # 2

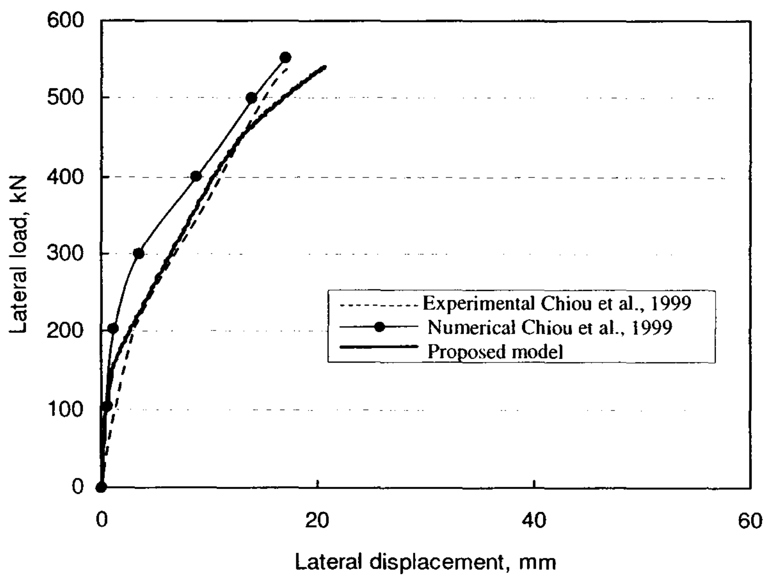

Fig. 3.19 Lateral load- Lateral displacement curve for specimen # 3

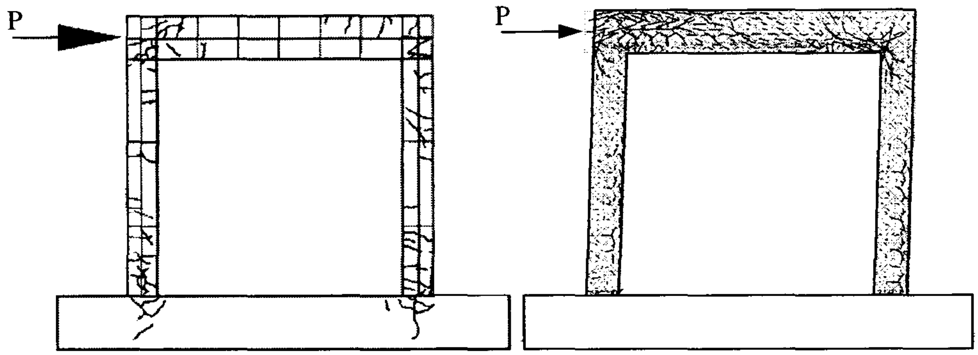

(a) Experimental result (Chiou et. al., 1999) (b) Analytical result (Chiou et. al., 1999)

Fig. 3.20 Failure configuration of bare RC frame.

Similar studies were made for the framed masonry wall. The load-deflection relationship of the RC frame partially filled with the masonry wall is presented in figure 3.18. It is found that the analytical result of the developed model agree with the experimental and analytical results by Chiou et al. (1999). However, because the wooden window is neglected in the numerical model, the predicted defections are larger than the experimental results. Figure 3.21 shows the failure of this framed wall after yielding of the structure. During the experiment, it was observed that the failures were concentrated in the RC frame, whereas there was no obvious crack found in the masonry wall. Many horizontal cracks were found to be concentrated in the center region of the left column around the left upper corner of the wall. Numerous cracks were also found at the top and bottom of the left column. The failure of the right column is found to be similar to that of the pure RC frame, while there are some cracks in the upper side of the beam. The reason for the different failure configuration of the left column is that the partially filled masonry wall caused the short column effect on the left column. Thus, failure of the left column was concentrated at the contact area of the column and the wall. The failure predicted analytically by Chiou et al. is presented in figure 3.21(b) and the solid lines indicate the failure surfaces. From the figure, the short column effect of the left column is clear. The failure regions of beam and columns predicted agree with those of the experimental results. However the failure region in the right columns, as shown in figure 3.21(b), was concentrated at the mid-height of the column which disagreed with the experimental observation. In addition, numerous failures were found in the masonry wall according to analytical results by Chiou et al. (1999). There are some reasons for the conflicting finding. First, the strength of mortar is much lower than that of concrete. Second, the wooden window frame is neglected in the numerical model and its effect on the column support was not included. Third, the rectangular brick block is not easily deformed. In addition, shear failure mode was also found in the columns and beam.

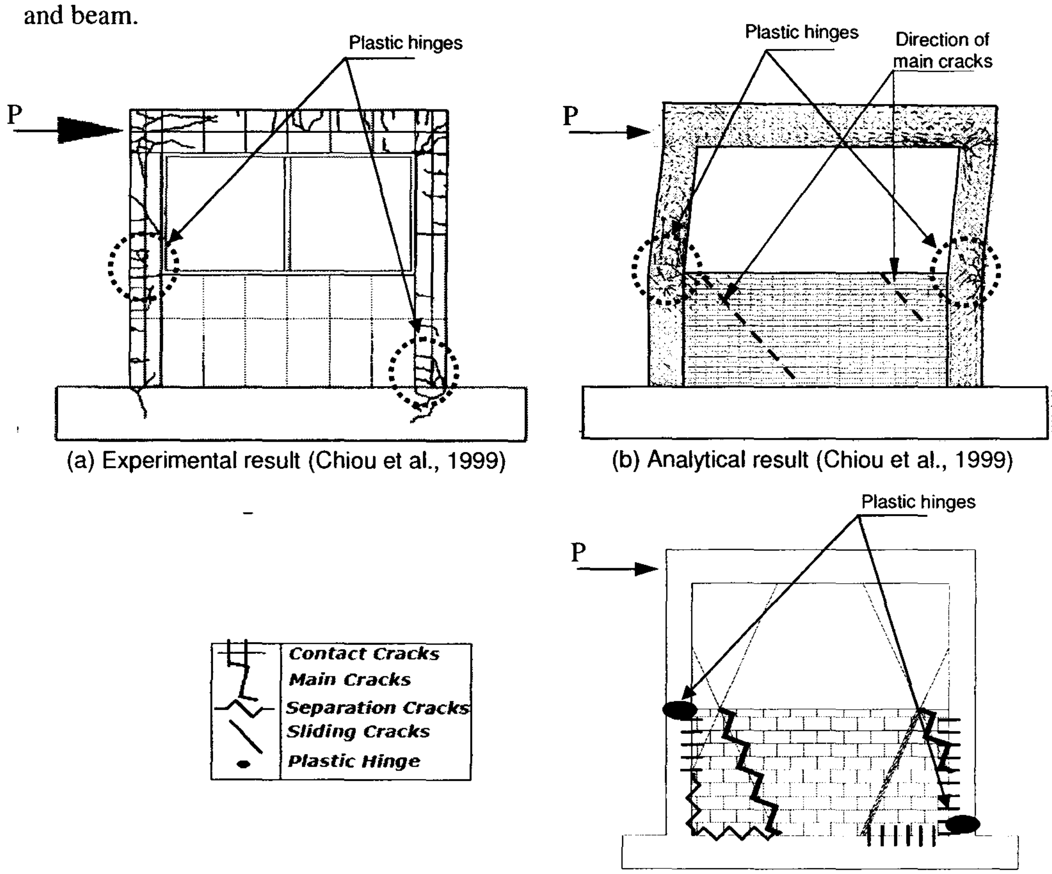

(a) Experimental result (Chiou et al., 1999)

(b) Analytical result (Chiou et al., 1999)

(c) Analytical model (developed model)

Fig. 3.21 Failure configuration of partially infilled RC frame.

The partially infilled RC frame was analyzed using the proposed model, and the failure configuration of the RC frame is shown in figure 3.21. Good agreement was found between the numerical results of the developed model and the experimental measurements by Chiou et al. (1999). The plastic hinges were located at mid height of the left column and at the bottom of the right column. This result is in good correlation with the experimental observation, as shown in figure 3.21a and 3.21c. However the results of the analytical model by Chiou et al. disagreed with experimental and results of proposed model especially in the case of the right column. It seams that there were constrains against lateral displacement in the region of masonry wall. These constrains made the behaviour of the right column similar to the behaviour of a short column. Short column failure mode may be expected in the case of the left column but not to the right column. There were no obvious cracks found in the masonry wall during the experiment. However, the cracks developed using the proposed model is in good agreement with the analytical solution by Chiou et al. (1999). Finally, it was found that most of the load was carried by the frame.

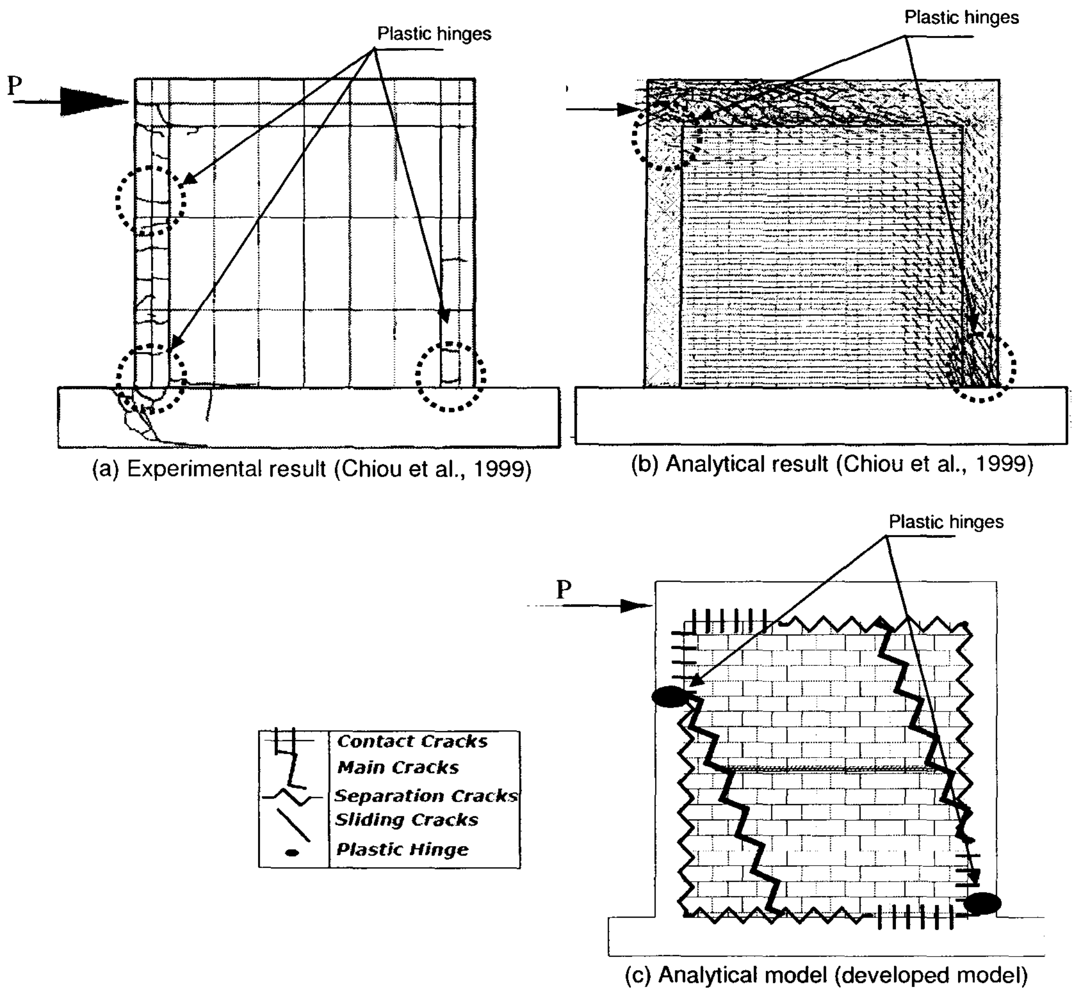

Fig. 3.22 Failure configuration of RC frame completely filled with masonry wall.

Figure 3.19 shows the load-deflection relationship of the RC frame completely filled with masonry wall. It was found that the solutions of the developed model agree with the experimental results. When the load is greater than 550 kN, the floor beam of the test specimen was found to have failed. Thus, the load-deflection relationship for a load greater than 550 kN is not presented in figure 3.19. The failure of this framed masonry wall after yielding of structure is shown in figure 3.22. Figure 3.22(a) shows that failures occurred in the columns, the left joint, and the masonry wall. There was no observable crack in the beam except at the left beam-column joint. The left column carried most of the load and there were a number of horizontal cracks in it. The failure configuration of this structure predicted by Chiou et al. (1999) is illustrated in figure 3.22(b). The failure regions of the developed model agreed with experimental results in terms of plastic hinges and direction of cracks in the wall, as shown in figure 3.22(a and c).

3.5 SUMMARY

The developed numerical model was verified by comparing the solutions with analytical solutions and experimental results by others. A satisfactory agreement was obtained. The model developed in this study was used to analyze eight different infilled RC frame specimens that were tested by three different researchers. The comparisons confirmed that the proposed model could predict the lateral load-deflection diagram fairly accurately. In addition, the model was capable of establishing the crack patterns and the failure modes of the tested RC frames with infills. The predetermined failure surfaces do not appear to represent significant limitation of the model. The number of elements used to model masonry panel is small when compared with traditional finite element meshes. This means that this model is efficient and can be applied for large scale structure. The proposed numerical model has showed capability of simulating the behaviour of masonry infilled RC frames subjected to in-plane monotonic loading and identifying the failure regions of the structure.

This page is intentionally left blank

CHAPTER 4

BEHAVIOUR OF FIRST FLOOR AND UPPER FLOORS OF INFILLED RC FRAME

4.1 INTRODUCTION

In this chapter, the behaviour of infilled RC frames of first story and the upper floors were investigated. Two different groups of frames were selected for this investigation. The first group of frames had the same dimensions and cross-section details similar to the RC infilled frame tested by Choubey (1990), as shown in figure 4.1(a). In this group, the lower beam was selected to be flexible with dimensions of 150 x 230 mm and the continuity of the RC frame was ignored. This frame configuration was chosen to study the effect of flexible beams in upper stories (rather than the first story) on the failure of infilled panel, which in return will affect the failure of the RC frame.

In the second group of frames, the lower beam was considered rigid and had relatively large inertia with respect to the cross section dimensions of the RC frame (figure 4.1(b)). This configuration was chosen to represent the behaviour of infilled RC frames in the first story, where the inertia of foundation of the building is large relative to the dimensions of the upper frame. In addition, to the large inertia of the lower beam in the second group of frames, the continuity of the infilled panel and the surrounding frame in the upper story was considered, as shown in figure 4.1(b). Dimensions and configurations of the second group of frames were selected to be similar to the dimensions and configuration of the specimen tested by Mehrabi et al. (1997).

In both groups of frames, the cross-section dimensions and details will remain unchanged throughout the analysis. Dimensions of the infill panel will be varied throughout the investigation to study the effect of variation of aspect ratio of infill panel on the behaviour and failure mechanisms of the two groups of frames.

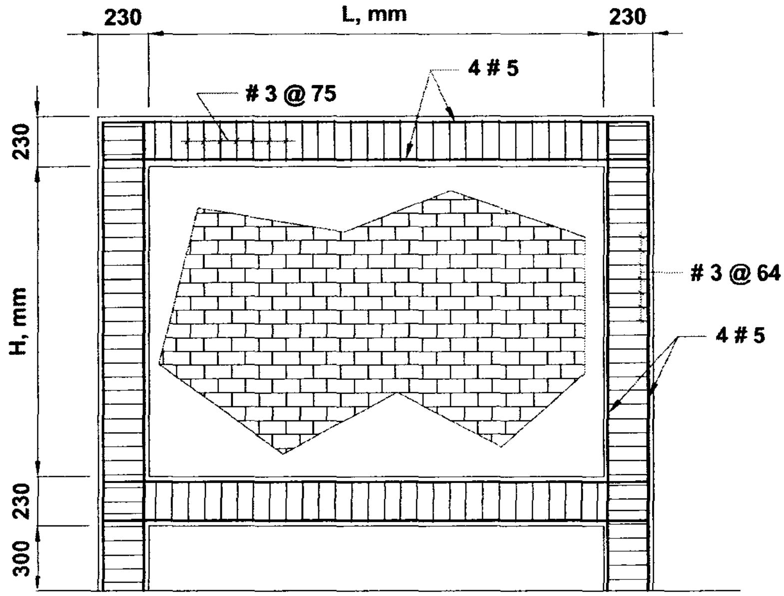

(a)

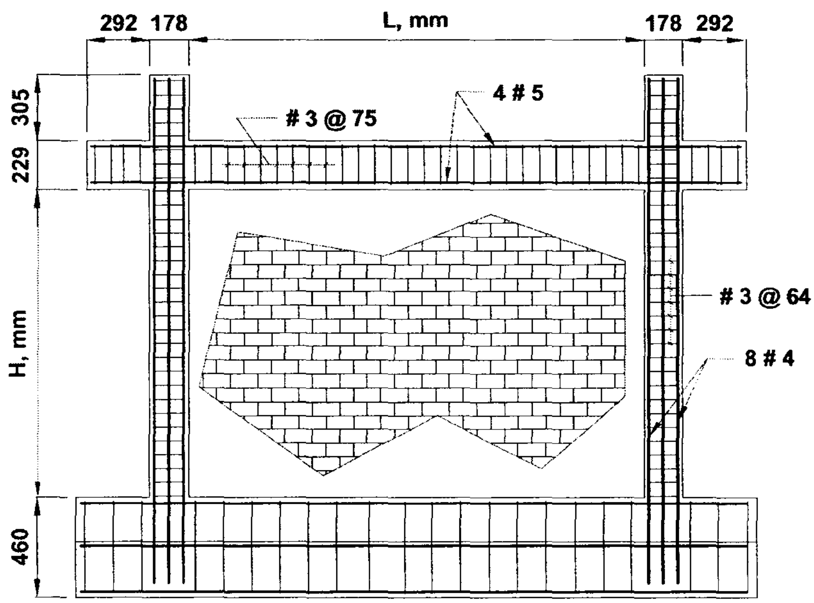

(b) **ALL DIMENSIONS ARE IN mm**

Fig. 4.1 Configurations of the two frame groups. a) frame with flexible lower beam, b) frame with rigid lower beam and upper frame continuity.

4.2 INFILLED FRAME-1

In this section, the effect of aspect ratio on the behaviour of infilled RC frames with flexible lower beam is presented. This frame was previously analysed by Choubey (1990). The frame height is H and the bay width is L. The column cross section was 230 × 150 mm. The main reinforcement was 4 # 5 bars of nominal diameter of 15.9 mm of total area of steel of 804 mm^2. The dimensions of upper and lower beams were 150 × 230 mm with main reinforcement of 4 # 5 bars of nominal diameter of 15.9 mm of total area of steel of 804 mm^2. The cross section dimensions and reinforcement of the columns and beams remained unchanged throughout this study. Material properties of concrete, reinforcing steel and masonry panel are listed in Table 4-1. The configuration, cross sections details of the RC infilled frame are shown in figure 4.2.

TABLE 4-1 Material properties of RC infilled frame.

Concrete material		*Steel Material*		*Panel Material*	
E_c =	10,000 MPa	E_s =	200 GPa	E_m =	700 MPa
ν_c =	0.2	ν_s =	0.3	ν_m =	0.2
f_{cu} =	40 MPa	σ_{sy} =	400 MPa	σ_u =	4.5 MPa

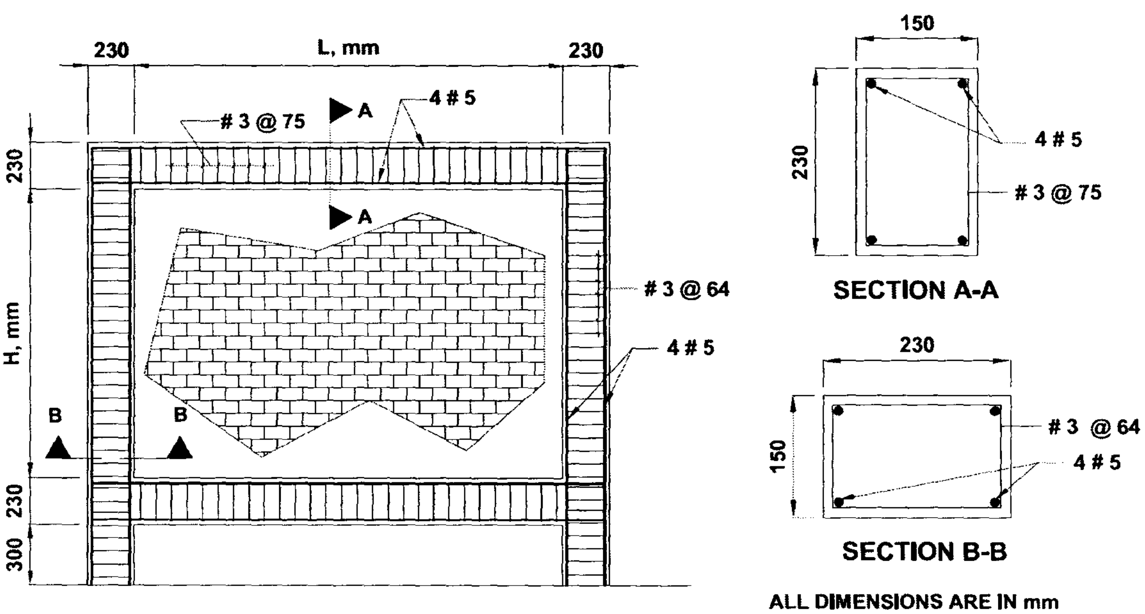

Fig. 4.2 Configuration and details of Frame-1.

In this study three groups of frames were investigated. The first group of frames (Group-B) represented frames of height H = 3 m. In this group, the length of the frame was varied from 3 to 6 m with a step of 0.5 m. The second group of frames (Group-C) represented frames of constant height of H = 3.5 m. The length of the frame in this group was varied from 3 to 7 m with a step of 0.5 m. The last group of frames (Group-D) represented frames of height H = 4.0 m. The length of the last group of frames was varied from 3 to 8 m with a step of 0.5 m. This combination of height and length dimensions was selected to cover most of the practical aspect ratios available. The aspect ratio was defined by the height divided by the length of the frame (i.e. aspect ratio = H/L). The dimensions and aspect ratios of the three groups of frames are listed in Table 4-2. The three groups were monotonically loaded up to failure. A single increasing horizontal force was applied at the center of the upper beam.

TABLE 4-2 Dimensions and aspect ratio of different frame groups.

Group-B				Group-C				Group-D			
Frame	Height m	Length m	Aspect Ratio	Frame	Height m	Length m	Aspect Ratio	Frame	Height m	Length m	Aspect Ratio
B1	3.00	3.00	1.00	C1	3.50	3.00	1.17	D1	4.00	3.00	1.33
B2	3.00	3.50	0.86	C2	3.50	3.50	1.00	D2	4.00	3.50	1.14
B3	3.00	4.00	0.75	C3	3.50	4.00	0.88	D3	4.00	4.00	1.00
B4	3.00	4.50	0.67	C4	3.50	4.50	0.78	D4	4.00	4.50	0.89
B5	3.00	5.00	0.60	C5	3.50	5.00	0.70	D5	4.00	5.00	0.80
B6	3.00	5.50	0.55	C6	3.50	5.50	0.64	D6	4.00	5.50	0.73
B7	3.00	6.00	0.50	C7	3.50	6.00	0.58	D7	4.00	6.00	0.67
				C8	3.50	6.50	0.54	D8	4.00	6.50	0.62
				C9	3.50	7.00	0.50	D9	4.00	7.00	0.57
								D10	4.00	7.50	0.53
								D11	4.00	8.00	0.50

The three groups of frames were analyzed using the developed model and the OpenSees code. The load-deflection relationships for frame groups B, C and D are plotted in figures 4.3, 4.4 and 4.5 respectively. The load-deflection relationships of frames of Group-B showed that frame B2 of aspect ratio of 0.86 had the maximum drift of 144.1 mm at lateral load of 156.1 kN. Frame B7 with aspect ratio of 0.50 had the maximum lateral load carrying capacity of 163.2 kN at lateral displacement of 40.7 mm, as shown in figure 4.3. Results of frames Group-C show that the frame C3 of aspect ratio of 0.88 had the maximum lateral displacement of 194.6 mm at lateral load of 143.7 kN. The maximum load capacity of 158 kN was carried by the frame C9 of aspect ratio 0.50. Results of frames Group-D showed that the maximum drift of 255.4 mm was obtained from frame D3 of aspect ratio of 1.0 at lateral force of 126.5 kN, and the maximum lateral load capacity of 155.0 kN was obtained from frame D11 of aspect ratio 0.50.

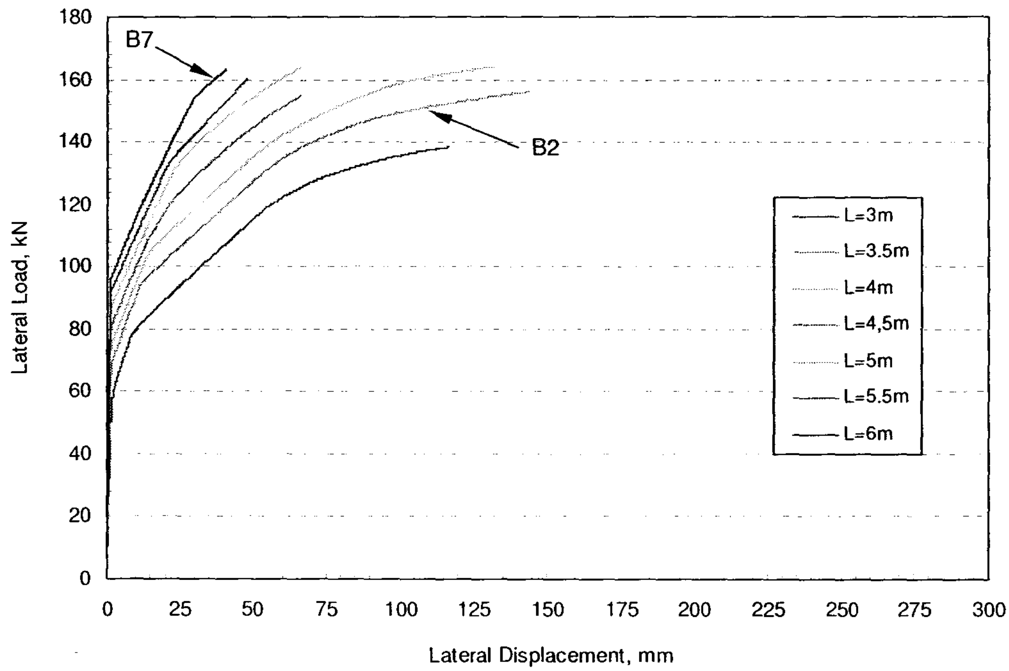

Fig. 4.3 Load-deflection relationships for Group-B frames (height=3.00 m)

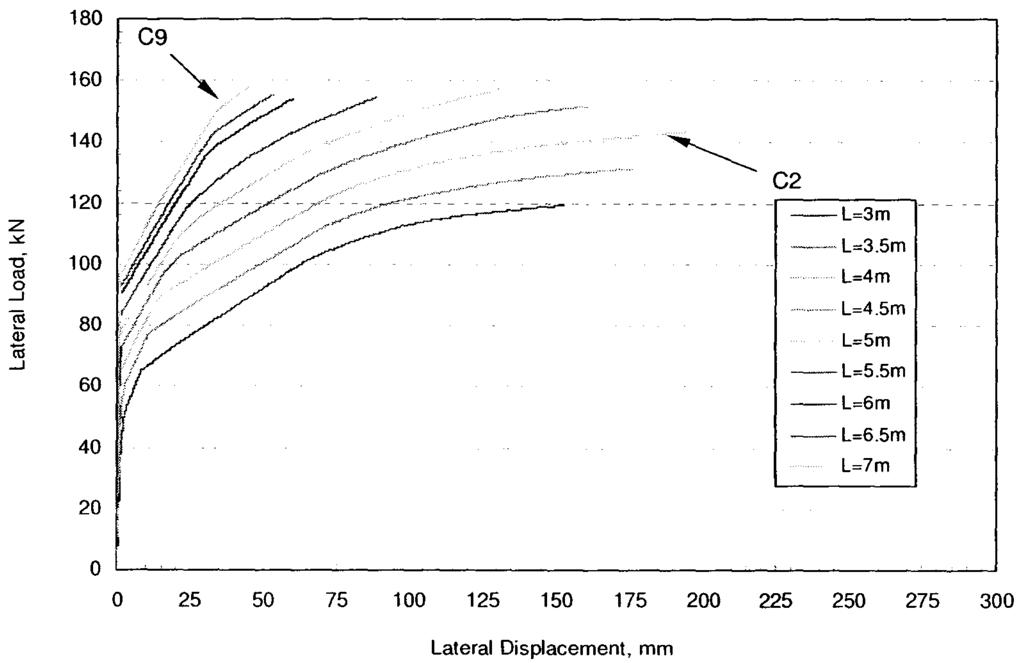

Fig. 4.4 Load-deflection relationships for Group-C frames (height=3.50 m)

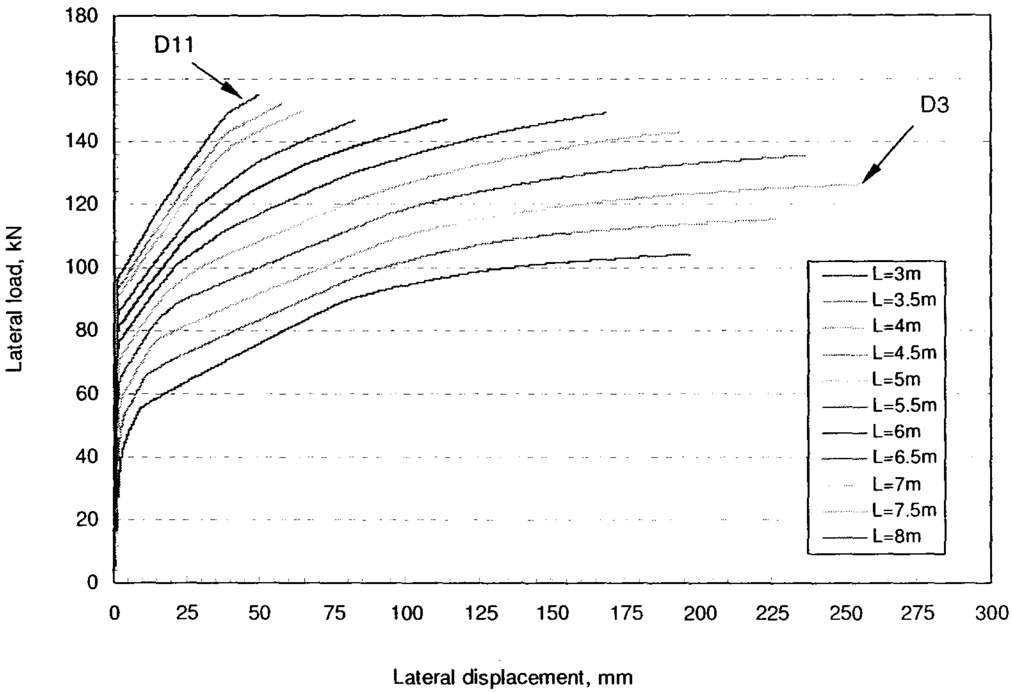

Fig. 4.5 Load-deflection relationships for Group-D frames (height=4.00 m)

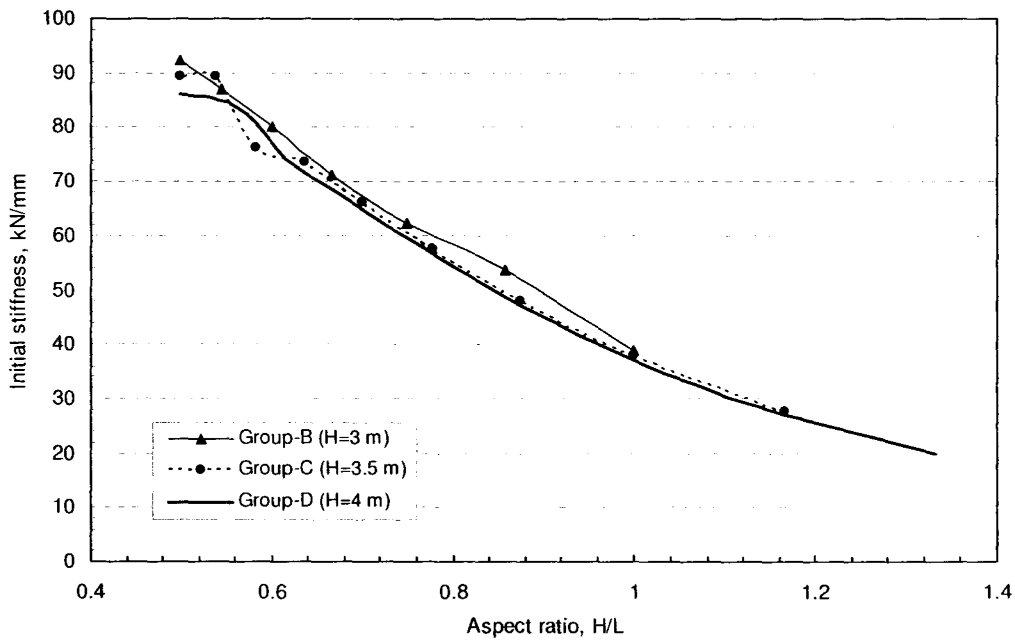

Fig. 4.6 Variation of the initial stiffness with the aspect ratio

The three figures 4.3, 4.4 and 4.5 showed that the decrease of aspect ratio to 0.5 in all cases increase the resistance of the infilled RC frame to lateral load. This result may be due to the increase the area of infill panel in the infilled RC frame. However, the infilled RC frame tends to behave in a brittle way. This observation may be due to the fact that masonry panel has a brittle characteristics.

Comparing the frames with maximum displacement in the three groups (i.e. frames B2, C2 and D3) showed that increasing the height of the RC infilled frame was accompanied by increased drift that can be reached by this frame. However, the increase of the drift is accompanied by decrease in the lateral load resistance.

Relationship between aspect ratio and initial stiffness of the three groups are shown in figure 4.6. The relationship is almost linear for the three groups. The initial stiffness of frames of Group-B were higher than Group-C and Group-D at all points of the same aspect ratio. Frames with lower aspect ratio showed higher initial stiffness in each group of frames.

The variation of the maximum displacement with the aspect ratio for all frames in the three groups is shown in figure 4.7. The relationship remained almost linear up to an aspect ratio of approximately 0.7 with the change in the height of the frames having no effect on the displacement result. For aspect ratio higher than 0.7 the change in the frame height started to show an effect. The aspect ratios corresponding to maximum displacements for frames with heights of 3.0, 3.5, and 4.0 metre were 0.82, 0.88 and 0.98, respectively. The variation of the maximum displacement/elastic displacement with the aspect ratio is shown in figure 4.8. Ductility of the three groups of frames remained almost the same up to aspect ratio of 0.7, after this point the heights of different frames started to have an effect on the ductility of the frames. The maximum ductility occurred at aspect ratios of 0.82, 0.87 and 0.91 for frames of heights 3.0, 3.5 and 4.0 metre, respectively. The behaviour in figures 4.7 and 4.8 are fairly similar because the elastic displacement varies in a small range between 1.08 mm and 2.03 mm.

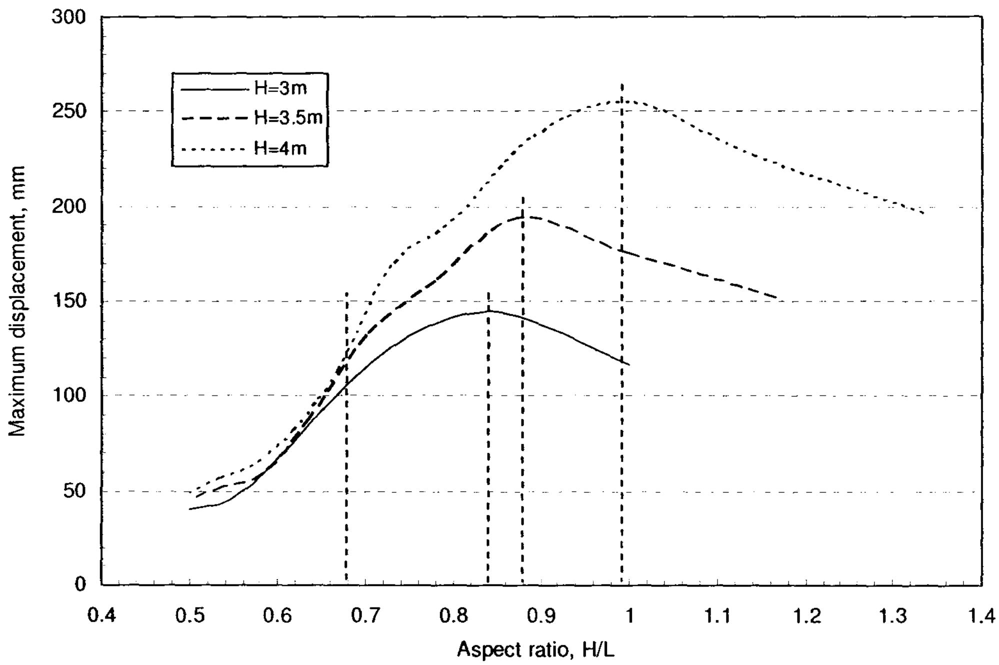

Fig. 4.7 Variation of the maximum displacement with the aspect ratios

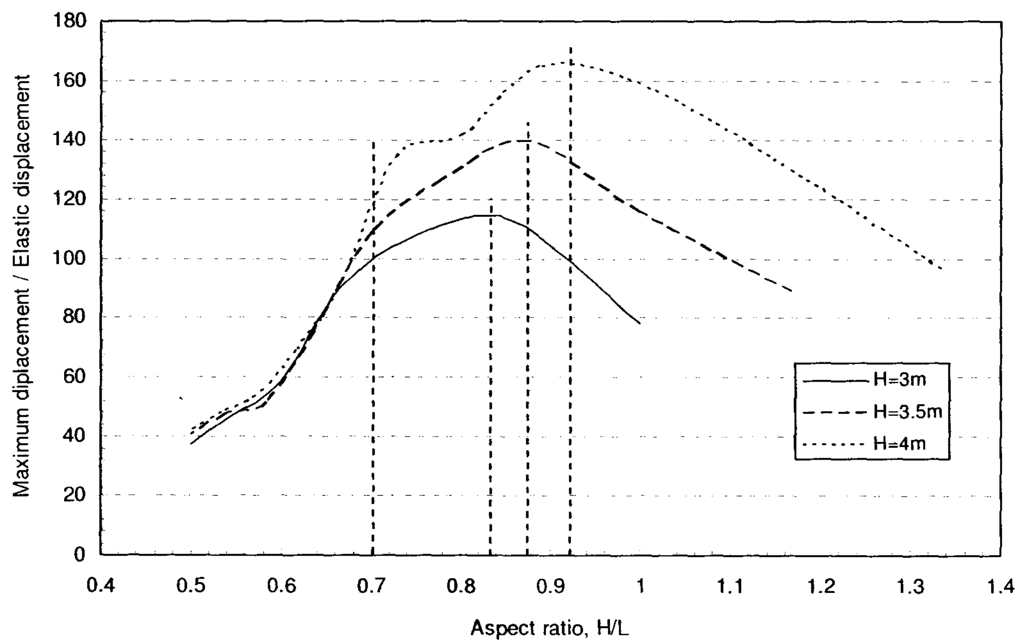

Fig. 4.8 Aspect ratio-maximum/elastic displacements relationship

The relationship between the aspect ratio and the maximum load is shown in figure 4.9. The maximum load, calculated using the proposed model was obtained when the results of two consecutive iterations failed to converge. To insure that the results of the maximum load are not due to numerical instability, every problem was analysed using two different displacement steps, since the runs are displacement control. As shown in figure 4.9, the maximum load is almost constant up to aspect ratio of 0.75, and then it decreases linearly with the increase of aspect ratio.

At low aspect ratio (less than 0.7) the area of infill panel is relatively large and its percentage of lateral load resistance is relatively high. With the increase of aspect ratio, the area of infill panel decreases and its resistance to lateral load decreases too. However, the RC frame strength could cover this decrease in the resistance of the infill panel up to an aspect ratio of 0.7. After aspect ratio of 0.7, the RC frame reached its maximum lateral load resistance, and the overall resistance of the infilled frame started to decrease. This aspect ratio level marks a change in the failure mode of the infilled frame.

The relationship between the aspect ratio and maximum/elastic load ratio is shown in figure 4.10. The relationship was approximately of constant slope for the three groups of frames.

From the behaviour given by figures 4.3 to 4.10 for infilled frames with lower flexible beam it is concluded that:

1. increasing the height or aspect ratio of frames caused decrease of the initial stiffness.
2. the effect of the frame height on the maximum displacement was negligible for various frames up to aspect ratio of 0.7.
3. frames of aspect ratio between 0.82 and 0.91 had the maximum ductility.
4. aspect ratios less than or equal to 0.75 had no effect on the maximum load carrying capacity of frames with the constant height.
5. increasing the aspect ratio to more than 0.75 decreased the lateral load capacity of the frame.

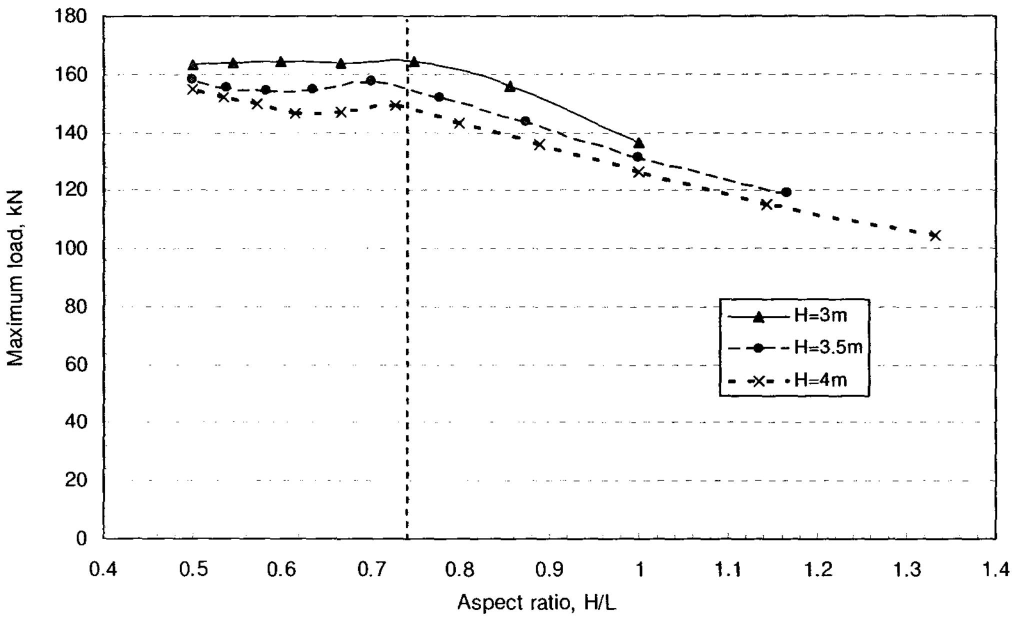

Fig. 4.9 Aspect ratio-the maximum load relationship

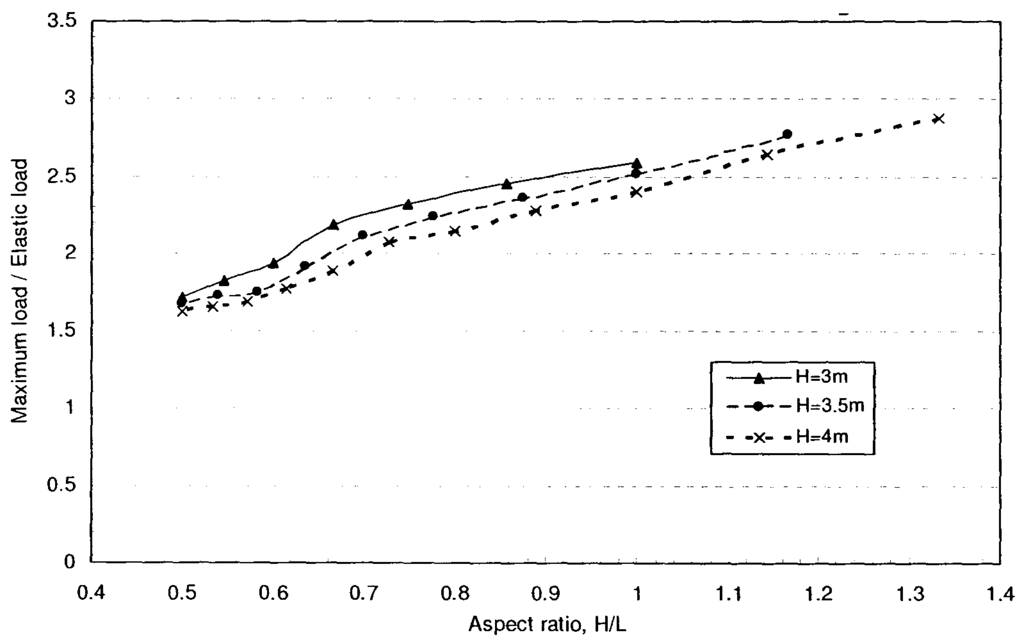

Fig. 4.10 Aspect ratio-maximum/elastic loads relationship

The failure mechanism of the frames with different heights and different spans are shown in figure 4.11. There were two different types of failure mechanism. First type of failure mechanism was Mode-E. This mode was characterized with two distinct parallel cracks in addition to sliding crack at mid-height of the masonry panel. In this mode two locations of plastic hinges in the RC frames were observed in the figures. The first location was at the beginning of the diagonal crack at the upper corner of the left column. The second location of plastic hinge was at the bottom corner of right column. Failure mechanism, Mode-E, takes place when the aspect ratio (H/L) was more than or equals to 0.75, 0.77 and 0.8 for frames with height of 3, 3.5 and 4, respectively. Theses aspect ratios were approximately the same as the aspect ratios corresponding to the change in slopes in the maximum load-aspect ratio relationships as shown in figure 4.8. Referring to figures 4.6 and 4.7, the peak points in the relationships occurred at aspect ratios between 0.8 and 1.0 for the frames.

The second type of failure was Mode-C. Diagonal cracks propagated from the loaded corner to mid-height of the panel; this crack was joined by the horizontal crack at mid-height of the infill panel. In this study, Mode-C takes place when the aspect ratio (H/L) < 0.75. In this mode three different locations of plastic hinges in the RC frames were as shown in the figures. The first location was at mid-height of the left column. The second location was at mid-height of the right column. The third location of plastic hinge is at the bottom corner of right column, since the load was applied at the top left point of the frame.

The change in failure mode from Mode-E to Mode-C in the three frames occurred at aspect ratio of 0.75. In all three cases the failure changes from diagonal crack to horizontal crack with an additional plastic hinge at the middle of the right columns. This explains the significance of aspect ratio of 0.75.

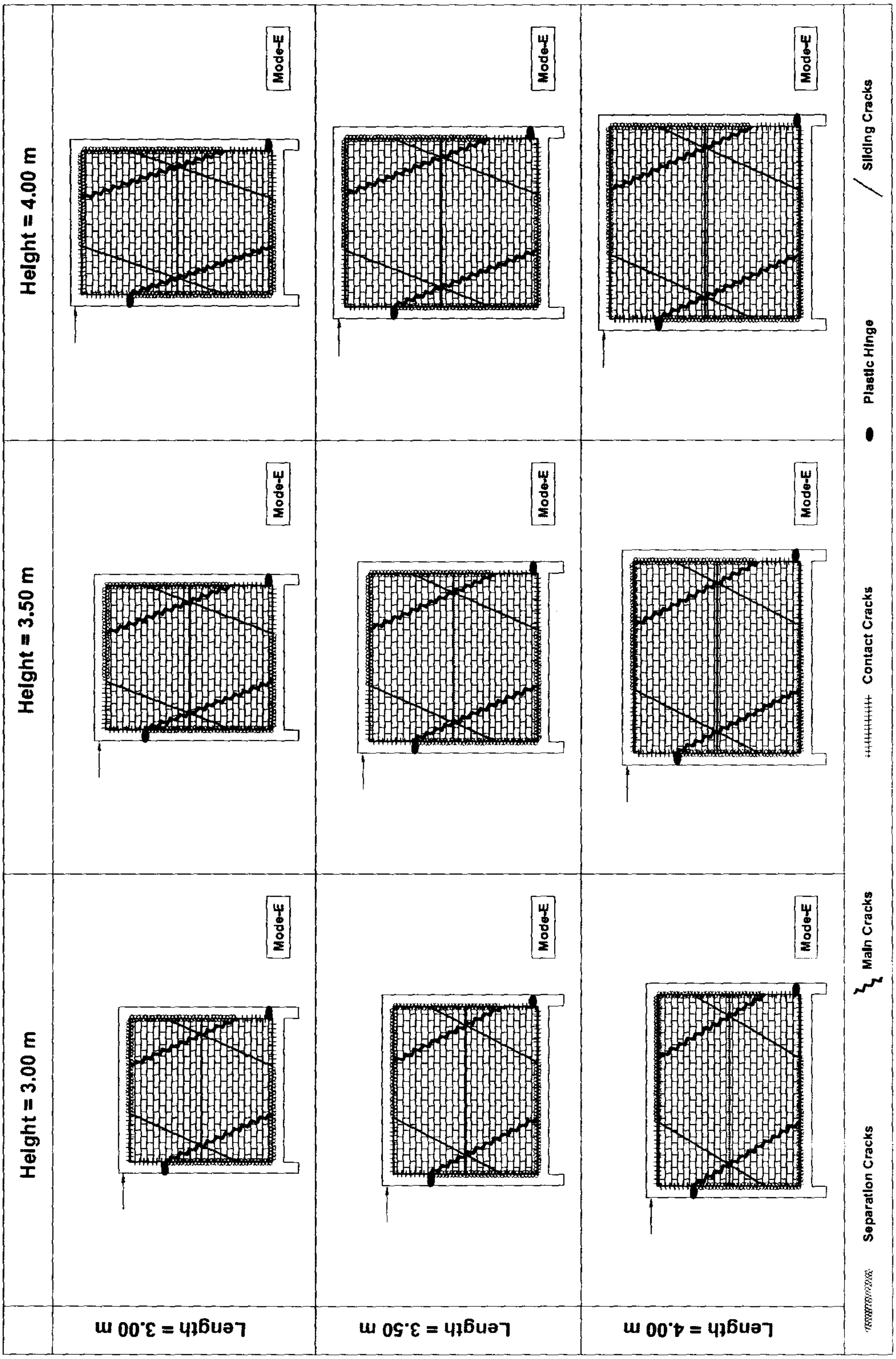

Fig. 4.11 Failure mechanisms for infilled frames-1

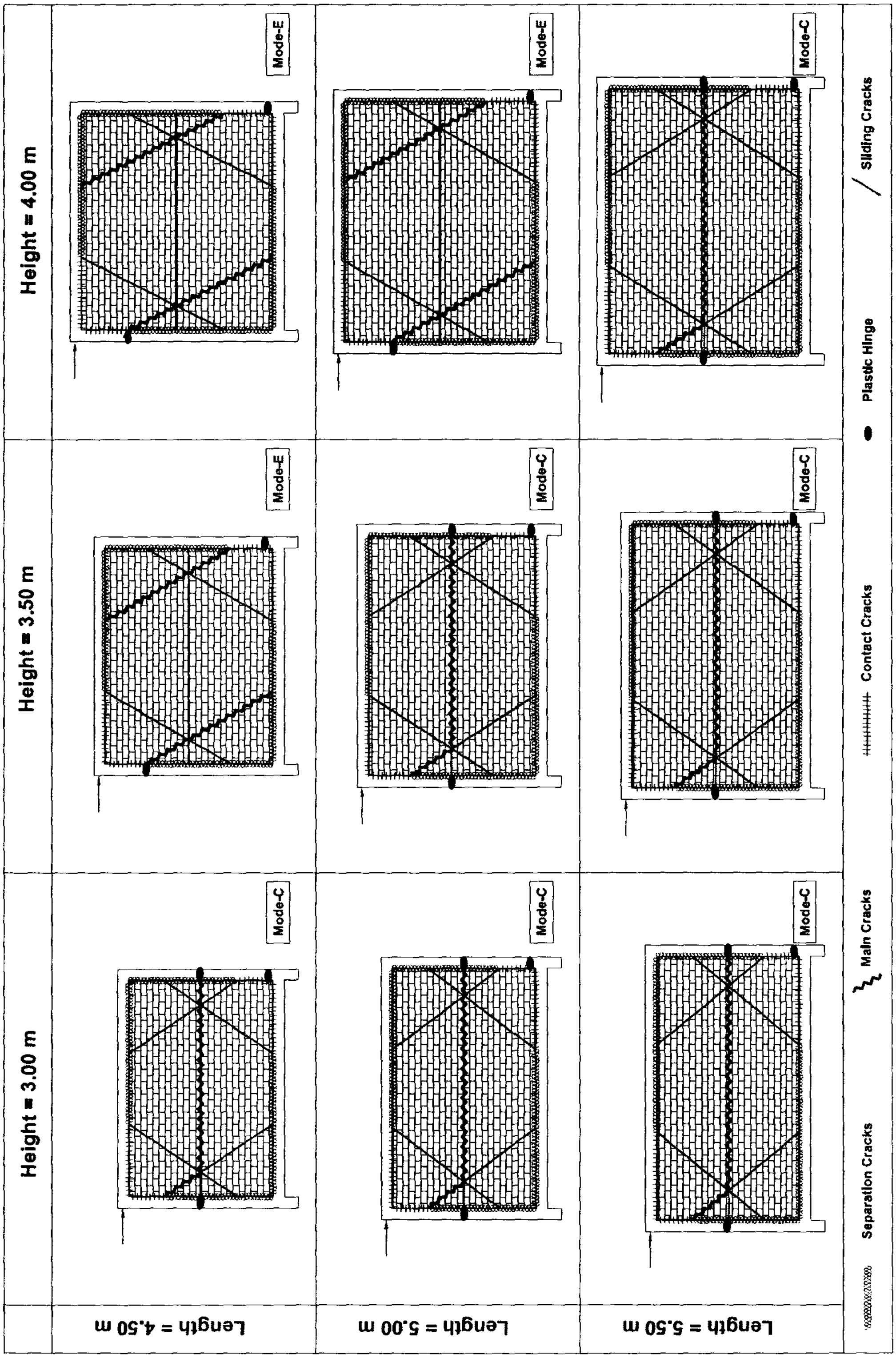

Fig. 4.11 Failure mechanisms for infilled frames-1 (Cont...)

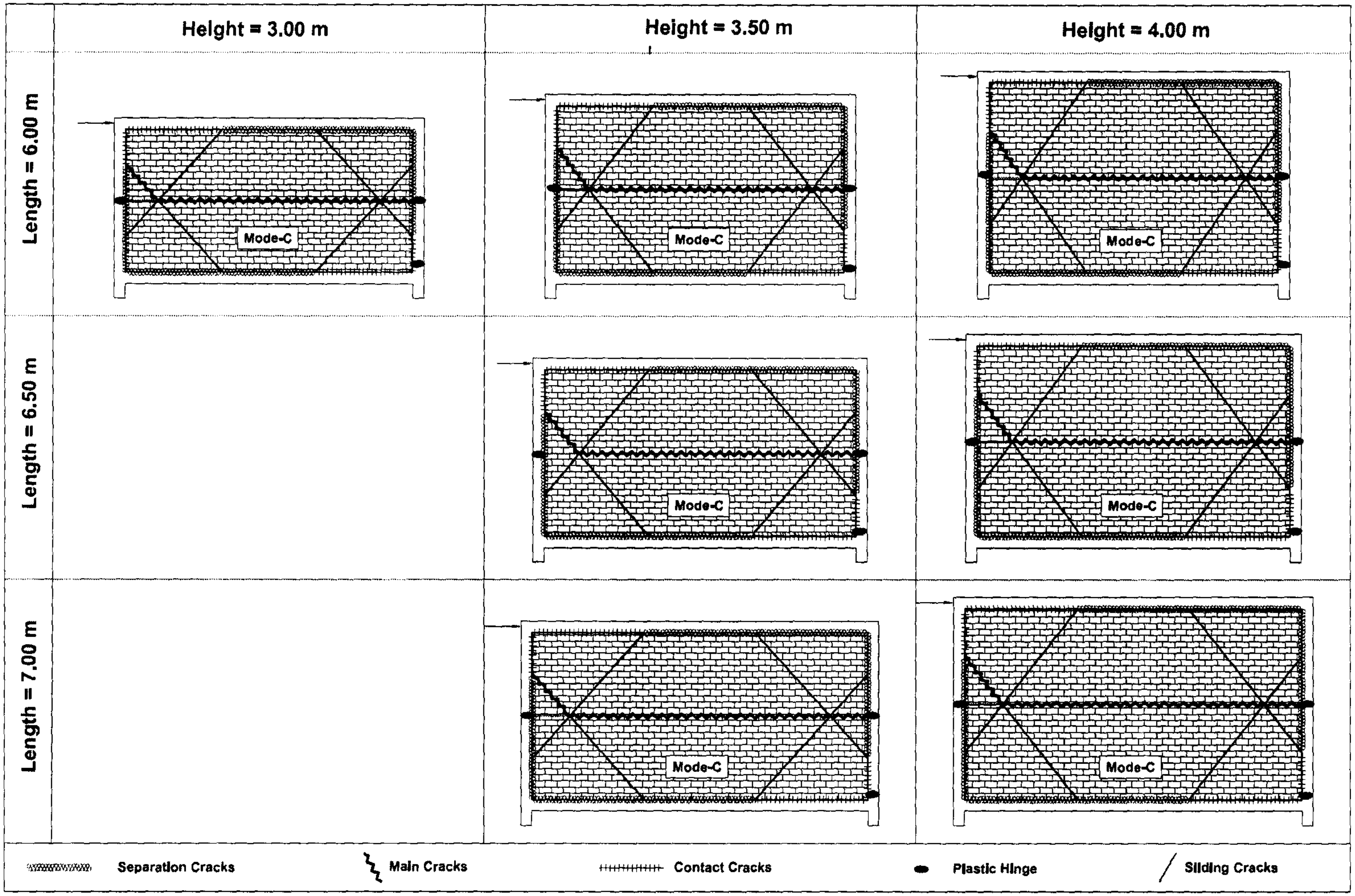

Fig. 4.11 Failure mechanisms for infilled frames-1 (Cont…)

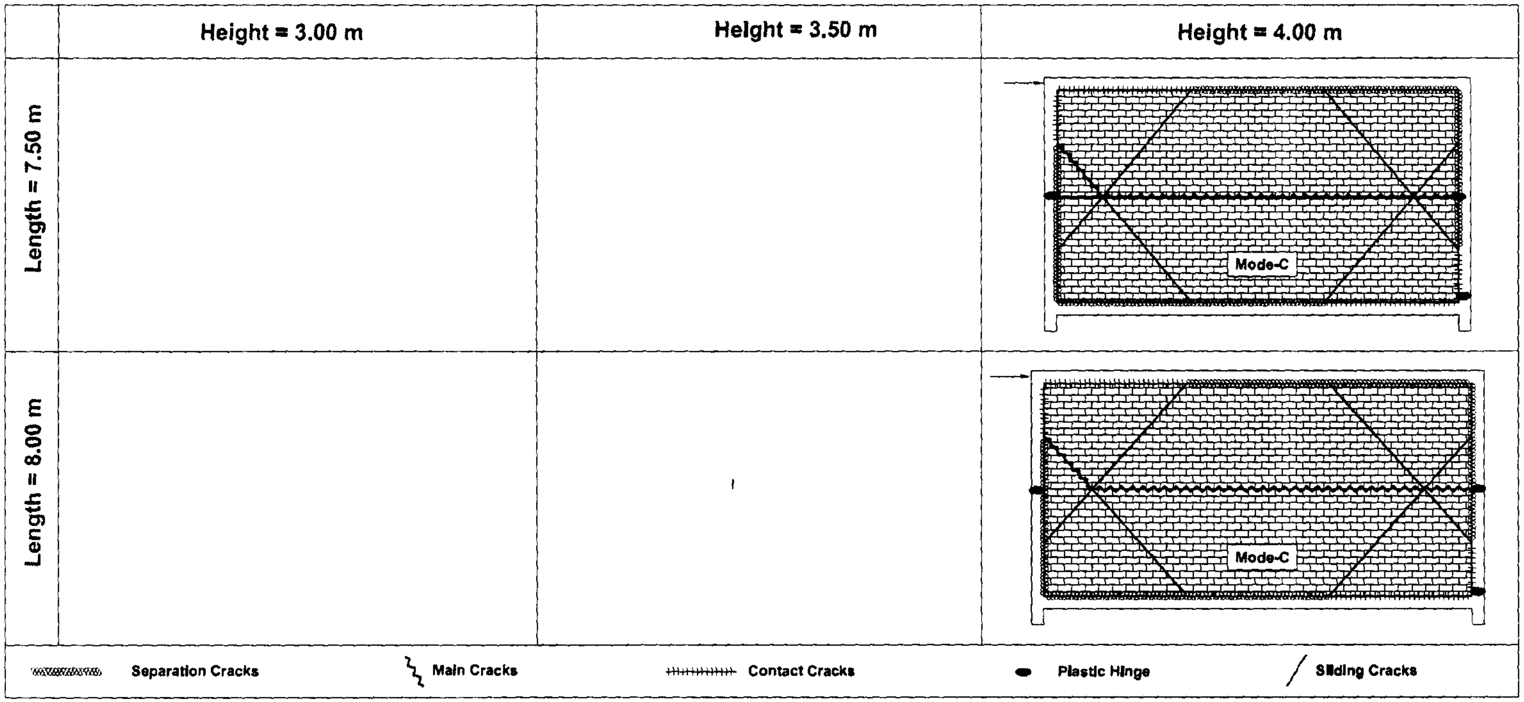

Fig. 4.11 Failure mechanisms for infilled frames-1 (Cont…)

4.3 INFILLED FRAME-2

In this section, the behaviour of a group of frames with a rigid lower beam is presented. The lower beam was considered rigid since it has a relatively large inertia with respect to the dimensions of the RC frame. The inertia of foundation of the building was considered to be relatively large in comparison to the dimensions of the upper frame. In addition to the large inertia of the lower beam in this group of frames, the continuity of the infilled panel and the surrounding frame in the upper story was considered. This configuration was selected to investigate the behaviour of first story infilled RC frames. Continuity of the RC frame was considered to study the effect of the continuity of columns and infill panel on the failure mechanism of the infilled RC frame. Configuration details and dimensions of the frame are shown in figure 4.12. The height and length were taken as H and L, respectively. The column cross sections were 178 x 178 mm with main reinforcement of 8 # 4 bars of nominal diameter of 12.7 mm for total area of steel of 1062 mm^2. The dimensions of upper beam were 152 x 229 mm with main reinforcement of 4 # 5 bars of nominal diameter of 15.9 mm for total area of steel of 804 mm^2. The dimensions of lower beam are 200 x 460 mm and with a main reinforcement of 8 # 6 bars of nominal diameter of 19.1 mm of total area of steel of 2513 mm^2. The cross section dimensions and reinforcement of the columns and beams remained unchanged through out this study.

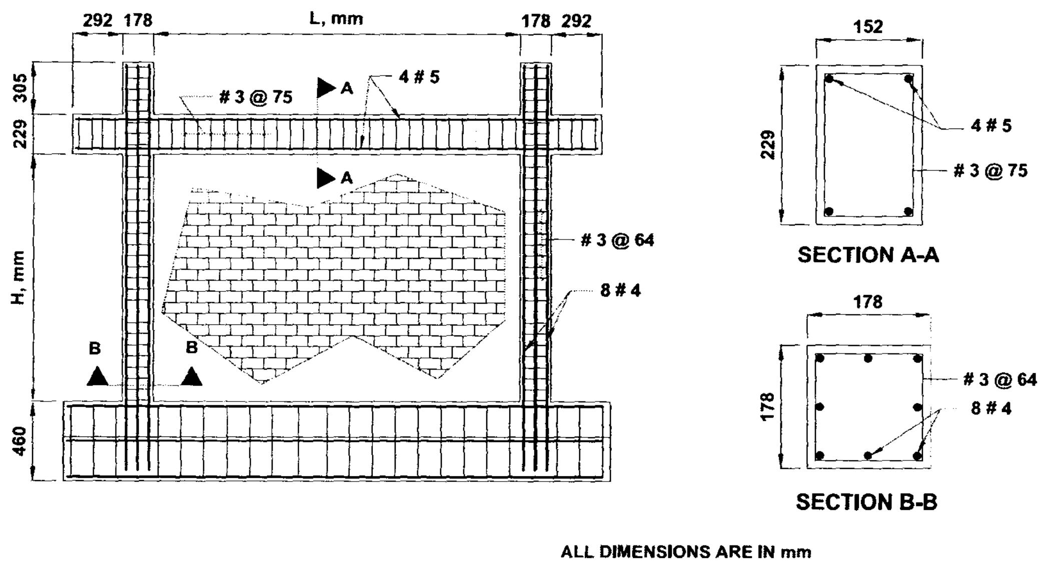

Fig. 4.12 Details of single story single bay infilled reinforced concrete frame

In this study, three groups of frames were investigated. The first group of frames (Group-E) represented frames of height H = 3 m. In this group, the length of the frame was varied from 3 to 6 m with a step of 0.5 m. The second group of frames (Group-F) represented frames of constant height of H = 3.5 m. The length in this group was varied from 3 to 7 m with a step of 0.5 m. the last group of frames (Group-G) represented frames of height H = 4.0 m. the length of the last group of frames was varied from 3 to 8 m with a step of 0.5 m. the height and length combinations were selected to cove most of the practical aspect ratios. The aspect ratio was defined as the height divided by the length of the frame. The dimensions and aspect ratio of all the frames are listed in Table 4-3. The frames were monotonically loaded up to failure. A single increasing horizontal force was applied at the center of the upper beam.

TABLE 4-3 Dimensions and aspect ratio of different frame groups.

Group-E				Group-F				Group-G			
Frame	Height m	Length m	Aspect Ratio	Frame	Height m	Length m	Aspect Ratio	Frame	Height m	Length m	Aspect Ratio
E1	3.00	3.00	1.00	F1	3.50	3.00	1.17	G1	4.00	3.00	1.33
E2	3.00	3.50	0.86	F2	3.50	3.50	1.00	G2	4.00	3.50	1.14
E3	3.00	4.00	0.75	F3	3.50	4.00	0.88	G3	4.00	4.00	1.00
E4	3.00	4.50	0.67	F4	3.50	4.50	0.78	G4	4.00	4.50	0.89
E5	3.00	5.00	0.6.0	F5	3.50	5.00	0.70	G5	4.00	5.00	0.80
E6	3.00	5.50	0.55	F6	3.50	5.50	0.64	G6	4.00	5.50	0.73
E7	3.00	6.00	0.50	F7	3.50	6.00	0.58	G7	4.00	6.00	0.67
				F8	3.50	6.50	0.54	G8	4.00	6.50	0.62
				F9	3.50	7.00	0.50	G9	4.00	7.00	0.57
								G10	4.00	7.50	0.53
								G11	4.00	8.00	0.50

The three groups of frames were analyzed using the developed model and the OpenSees code. The load-deflection relationships of each group of frames were plotted together for comparison, as shown in figures 4.13, 4.14 and 4.15. The load-deflection relationships of frames of Group-E showed that frame E3 of aspect ratio of 0.75 had the maximum lateral displacement of 104.6 mm (at lateral load level of 160 kN), and frame E7 with aspect ratio of 0.50 had the maximum lateral load carrying capacity of 184.9 kN (at lateral displacement of 36 mm), as shown in figure 4.13. Results of frames Group-F showed that the frame F4 of aspect ratio of 0.78 had the maximum drift of 164 mm at load level of 154.4 kN and the maximum lateral load capacity (183.4 kN) is carried by the frame F9 of aspect ratio 0.50

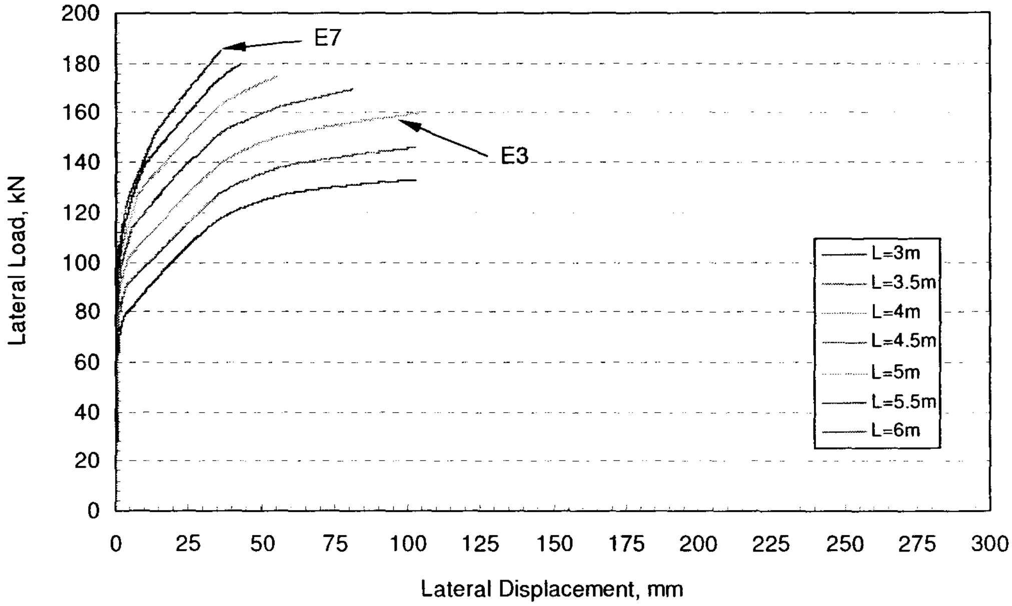

Fig. 4.13 Load-deflection relationships for Group-E frames (height=3 m)

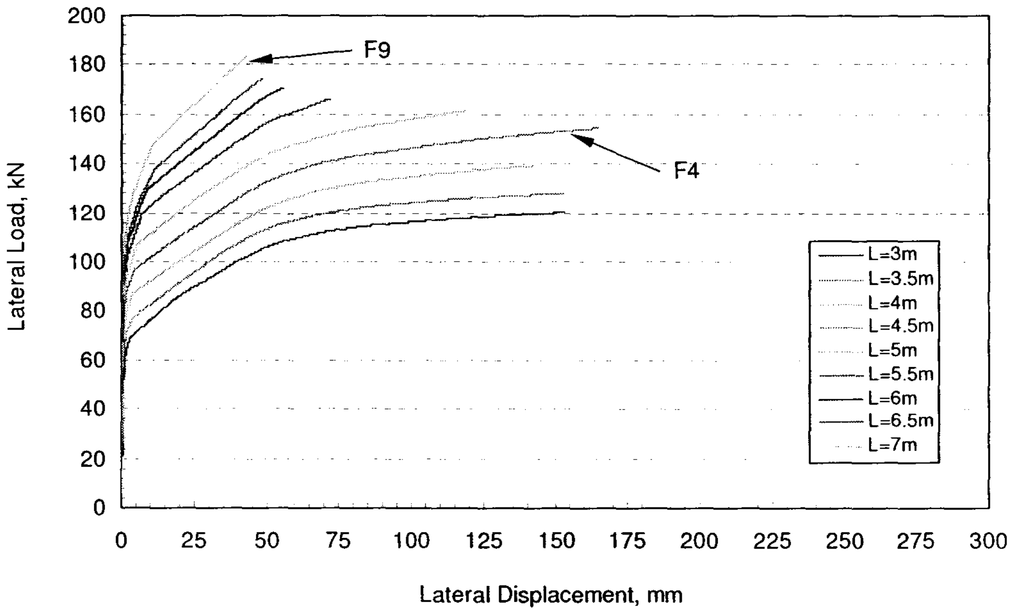

Fig. 4.14 Load-deflection relationships for Group-F frames (height=3.5 m)

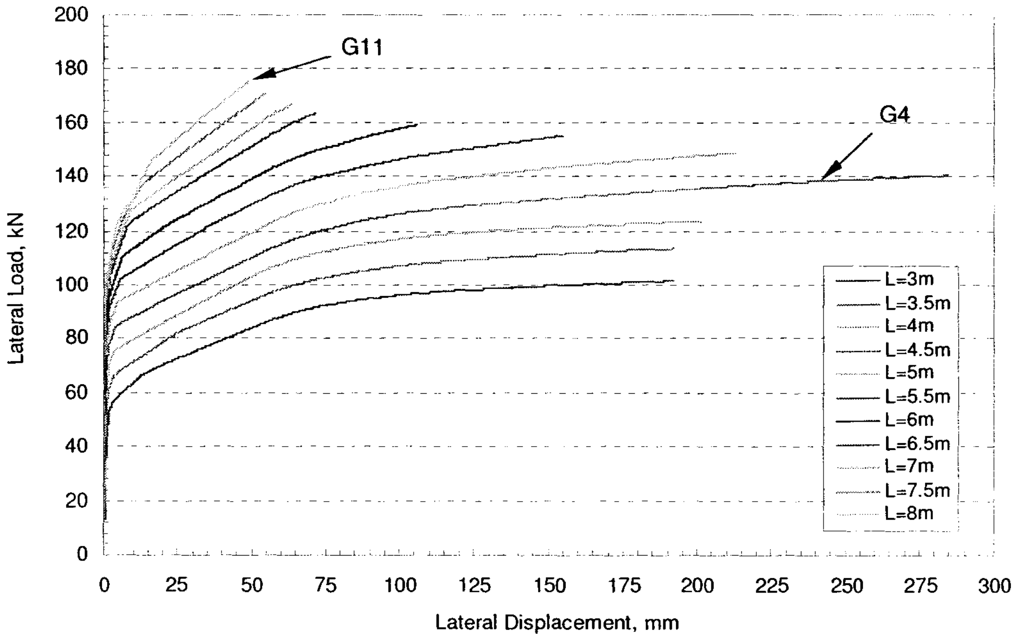

Fig. 4.15 Load-deflection relationships for Group-G frames (height=4.0 m)

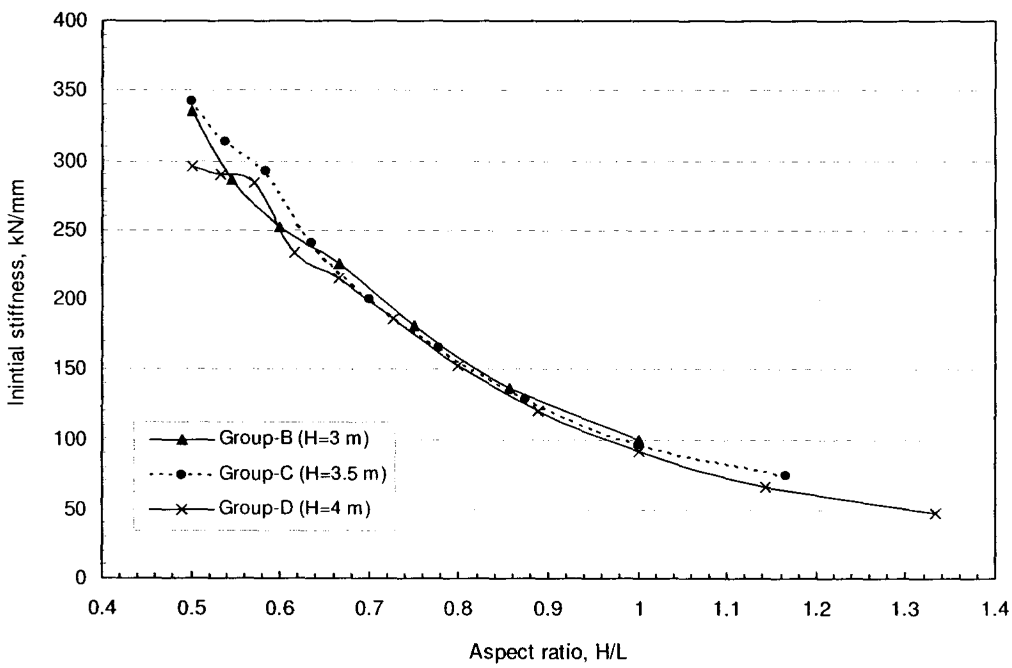

Fig. 4.16 Variation of the initial stiffness with the aspect ratio

corresponding to lateral displacement of 43 mm. Results of frames Group-G showed that the maximum drift (285 mm) was obtained from frame G4 of aspect ratio of 0.89, and the maximum lateral load capacity of 174.4 kN was obtained from frame G11 of aspect ratio 0.50.

Relationship between aspect ratio and initial stiffness of the three groups are shown in figure 4.16. The figure showed that increase in the height or aspect ratio of the frame corresponded to decrease of the initial stiffness.

The variation of the maximum displacement with the aspect ratio for all frames in the three groups is shown in figure 4.17. The relationship remained almost linear up to an aspect ratio of 0.65 and the change in height of the frames had little effect on the displacement results. For aspect ratios higher than 0.65 the change in the frame height started to show an effect. The aspect ratios corresponding to maximum displacements for frames with heights of 3, 3.5, and 4 metre were 0.75, 0.77 and 0.89, respectively. After reaching the peak values, a decrease in the maximum displacement with the increase in the aspect ratio occurred. After aspect ratios of 0.8, 0.9 and 1.05 (for frames with heights of 3, 3.5 and 4, respectively) the relationships remain constant.

The variation of the maximum displacement/elastic displacement with the aspect ratio is shown in figure 4.18. The maximum ductility occurred at aspect ratios of 0.75, 0.77 and 0.89 for frames of heights 3, 3.5 and 4, respectively. The behaviours shown in figures 4.17 and 4.18 were fairly similar because the elastic displacement varied in a small range between 0.3 mm and 1.05 mm.

The relationship between aspect ratio and maximum load is shown in figure 4.19. The relationships showed constant decrease in the lateral load capacity with the increase in the aspect ratio. This observation means that for frame with constant height, the increase in the length of the frame is accompanied with increase in the capacity of the frame to carry more lateral load. The relationship between the aspect ratio and maximum/elastic load is shown in figure 4.20. The relationship showed approximately constant slope for the three frames.

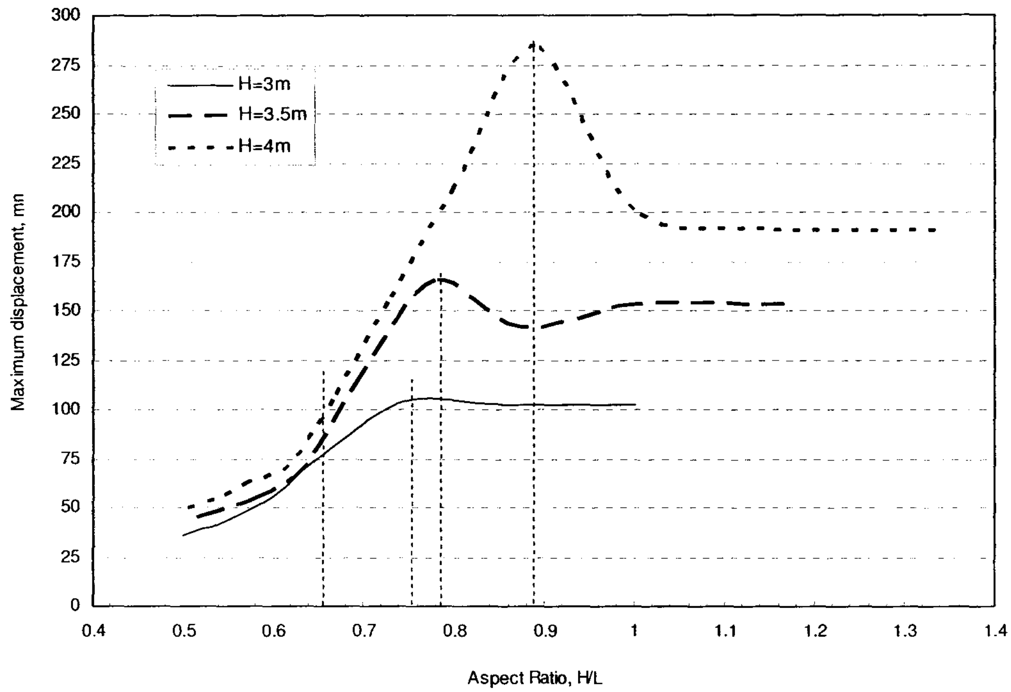

Fig. 4.17 Aspect ratio-maximum displacement relationship

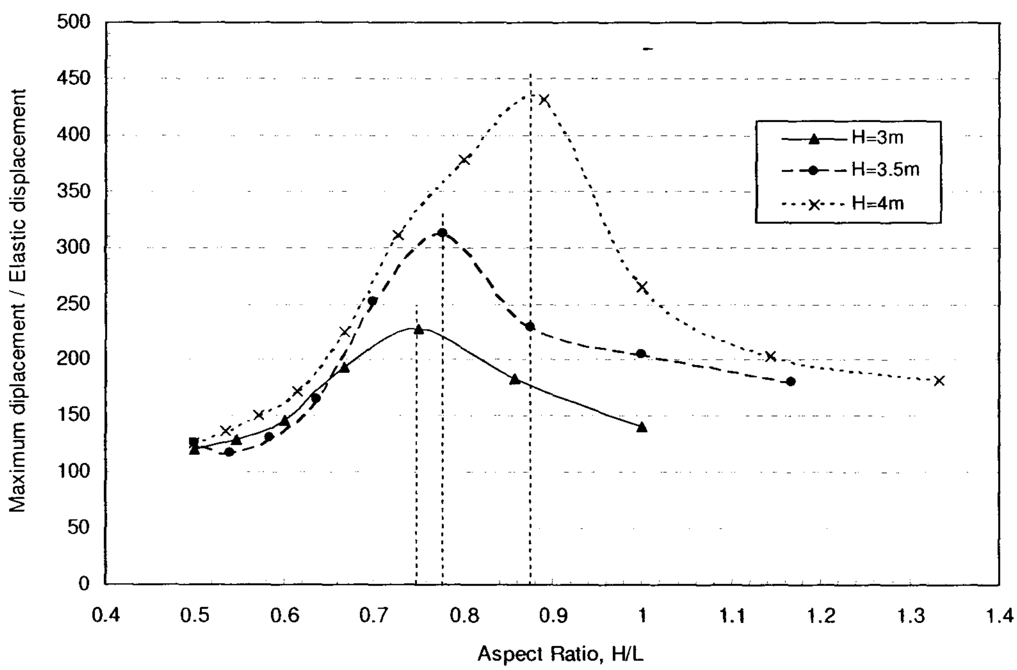

Fig. 4.18 Aspect ratio-maximum/elastic displacements relationship

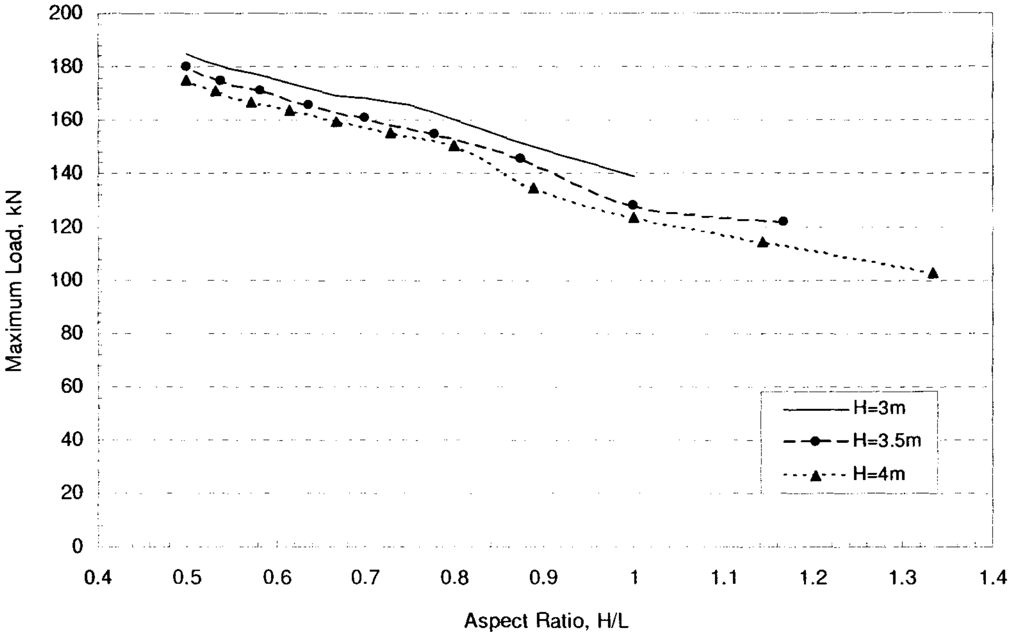

Fig. 4.19 Aspect ratio-maximum load relationship

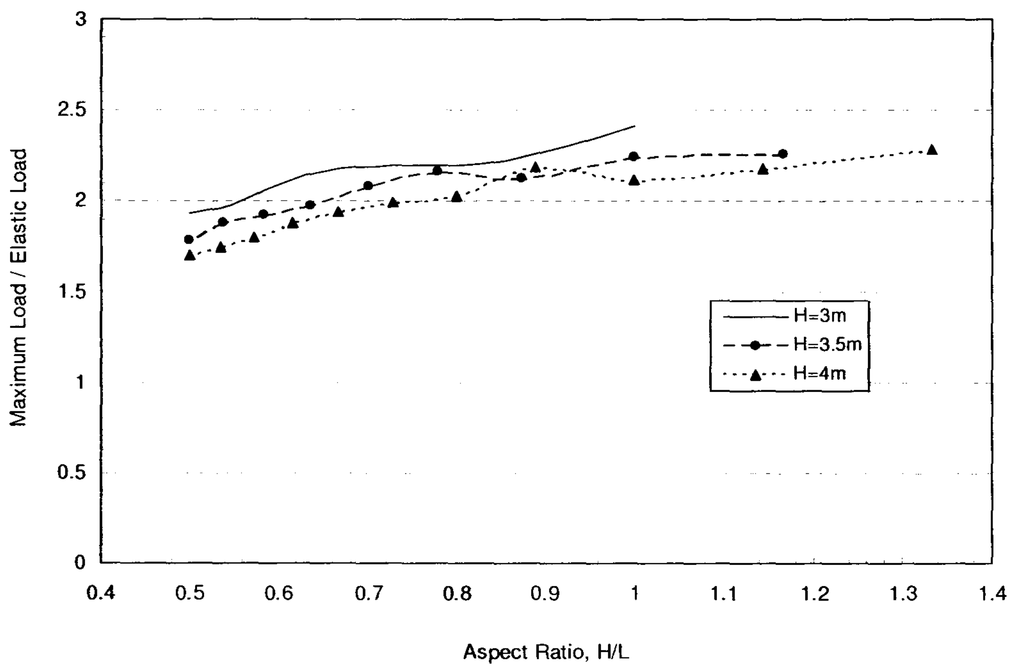

Fig. 4.20 Aspect ratio-maximum/elastic loads relationship

The failure mechanism of the frames with different heights and different lengths are shown in figure 4.21. All frames are laterally loaded with a point load at the top left corner in left-right direction. There were two different types of failure mechanism. First type of failure mechanism was Mode-E. This mode was characterized with two distinct parallel cracks in addition to sliding crack at mid-height of the masonry panel. In this mode two locations of plastic hinges in the RC frames were identified in the figures. The first location was at the beginning of the diagonal crack at the upper corner of the left column. The second location of plastic hinge was at the bottom corner of right column. Failure mechanism, Mode-E, occurred when the aspect ratio (H/L) was more than or equal to 0.75, 0.77 and 0.8 for frames with height of 3, 3.5 and 4, respectively. Theses aspect ratios were approximately the same as those at the peak points in figure 4.17 and 4.18. The same failure mechanism was observed by Al-Chaar et. al. (2002) for an infilled RC Frame with aspect ratio of 0.7, as shown in figure 4.22.

The second type of failure was Mode-C. Diagonal cracks propagated from loaded corner to the mid-height of the panel; this crack was jointed by the horizontal crack at mid-height of the infill panel. In this study, Mode-C occurred when the aspect ratio (H/L) < 0.75, 0.77 and 0.8 for frames of 3, 3.5 and 4 m height respectively. In this mode three different locations of plastic hinges in the RC frames were observed in the figures. The first location was at mid-height of the left column. The second location was at mid-height of the right column. The third location of plastic hinge was at the bottom corner of right column, since the load was applied at the top left point of the frame. This failure mode was observed in a study presented by Colangelo (2005) in his study for a frame with low aspect ratio of 0.57, as shown in figure 4.23.

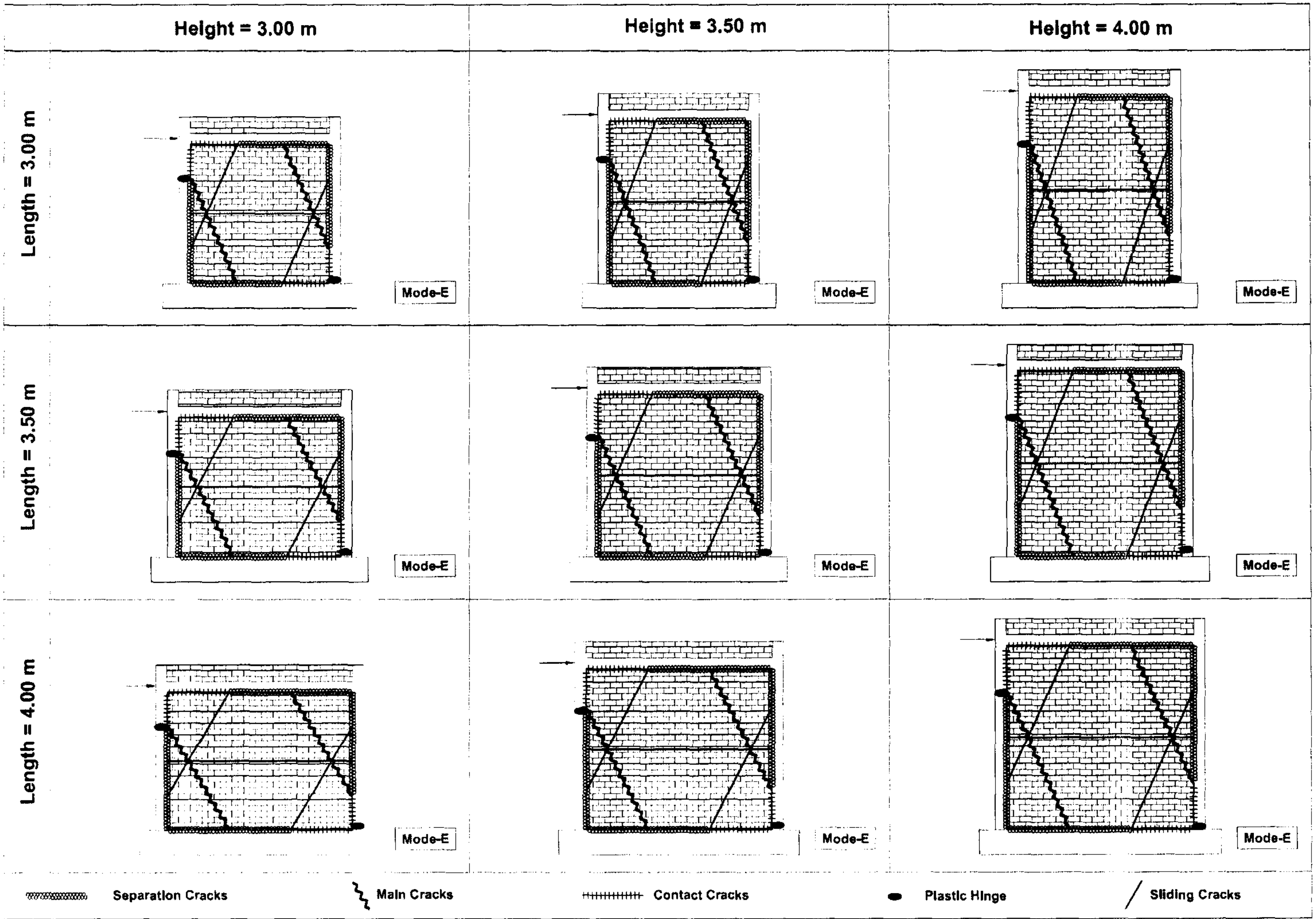

Fig. 4.21 Failure mechanisms of infilled frame-2

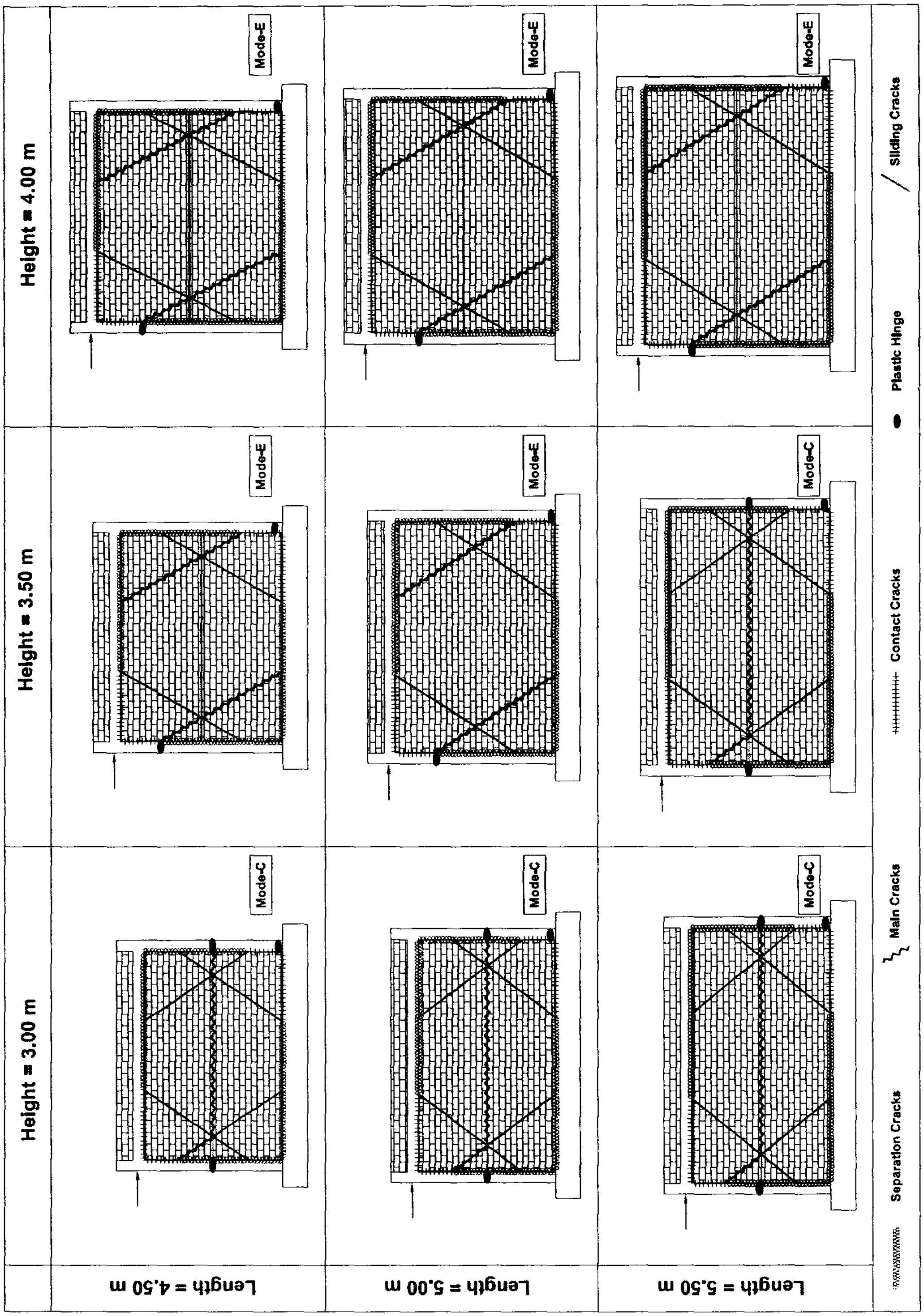

Fig. 4.21 Failure mechanisms of infilled frame-2 (Cont...)

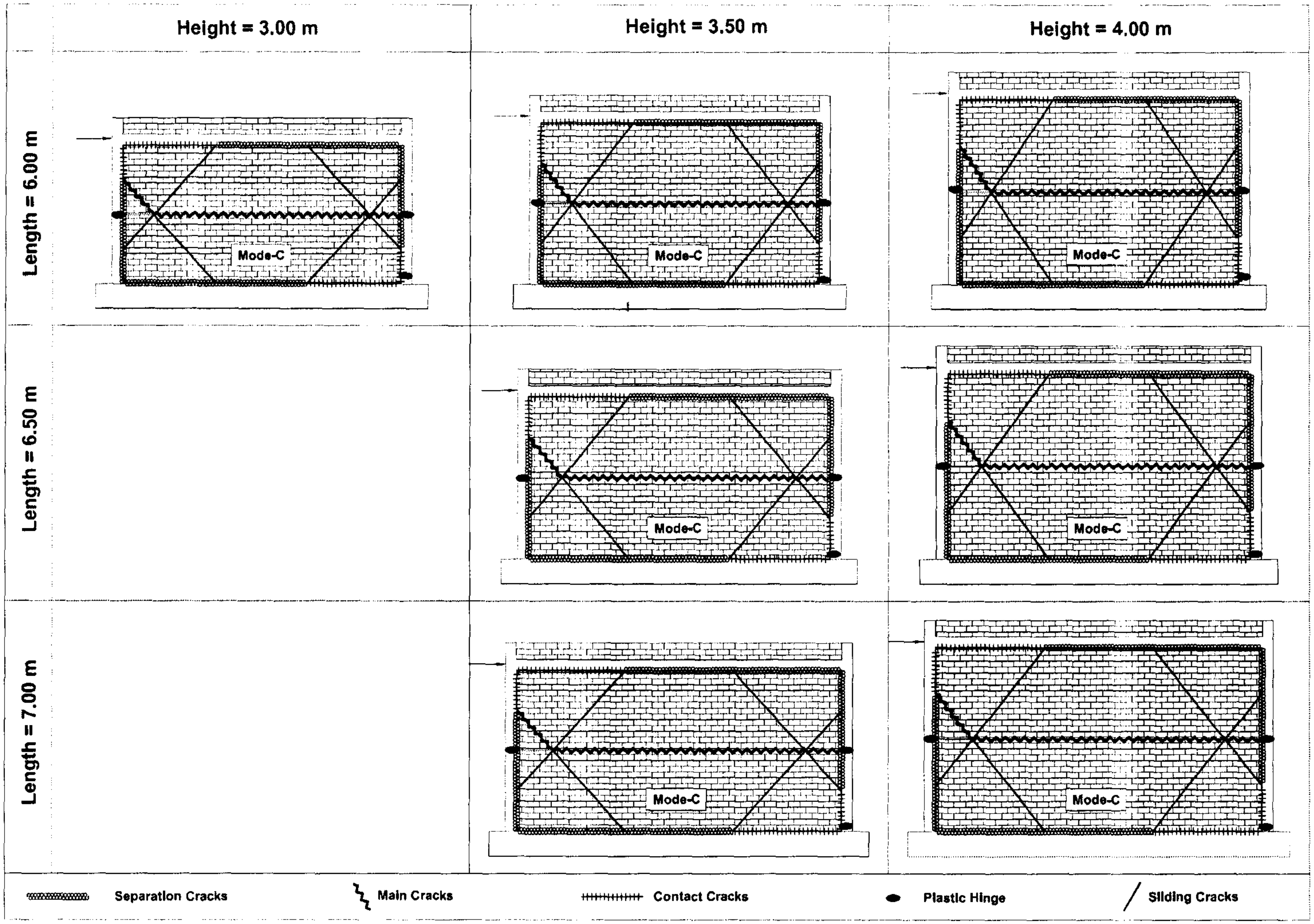

Fig. 4.21 Failure mechanisms of infilled frame-2 (Cont…)

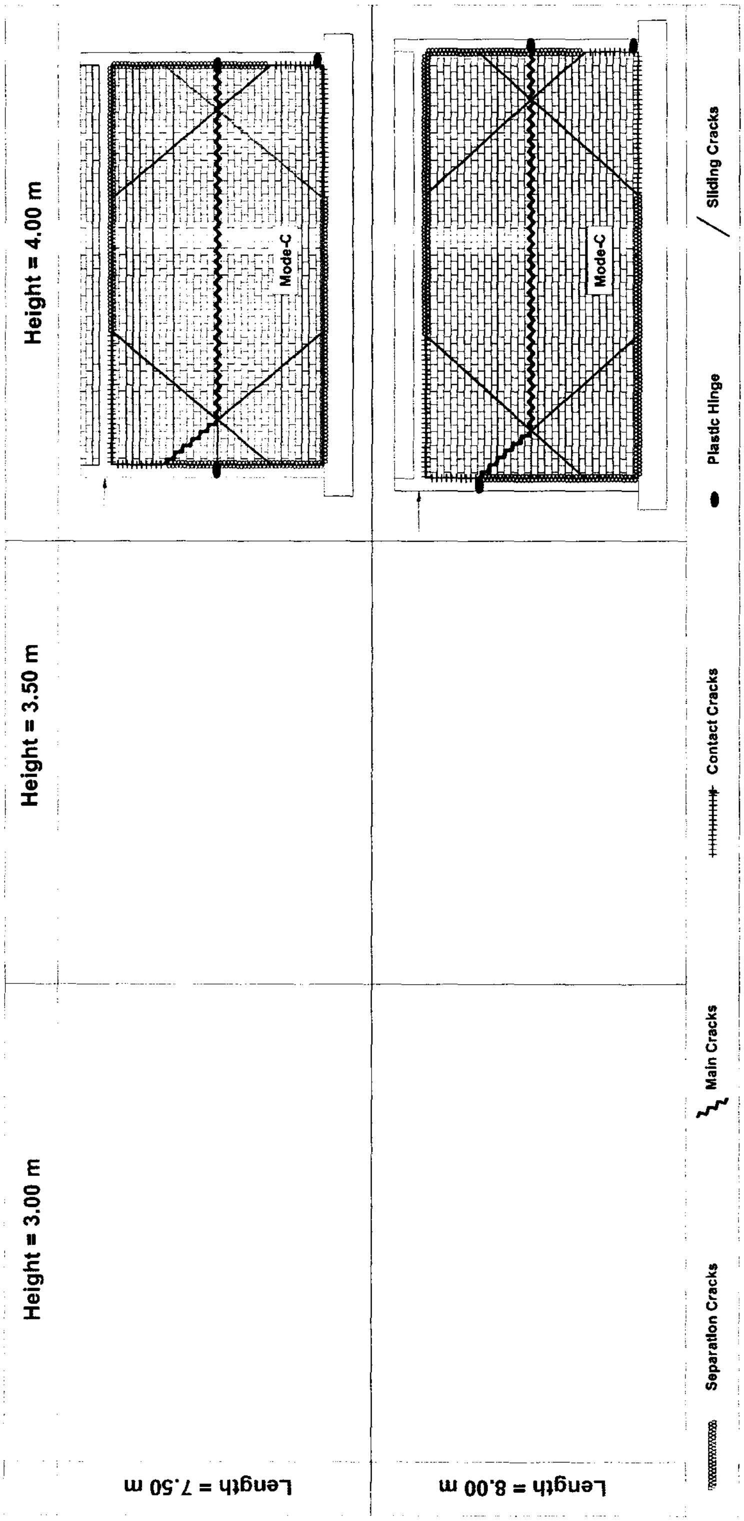

Fig. 4.21 Failure mechanisms of infilled frame-2 (Cont...)

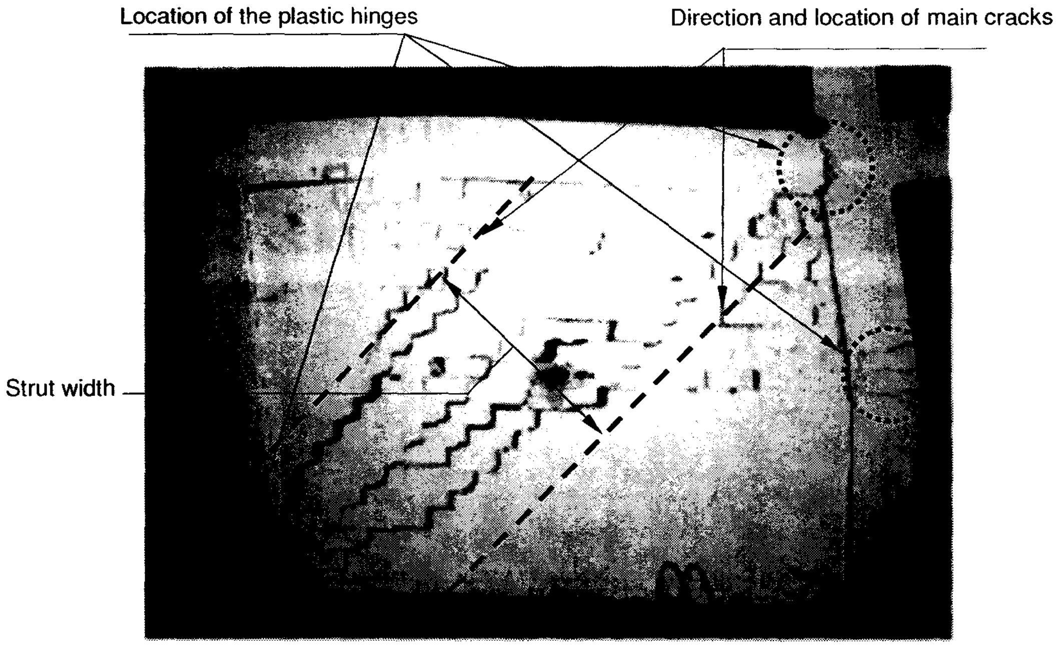

Fig. 4.22 Failure mechanism, Mode-E, for infilled RC frame with aspect ratio of 0.7 (Al-Chaar et. al. 2002).

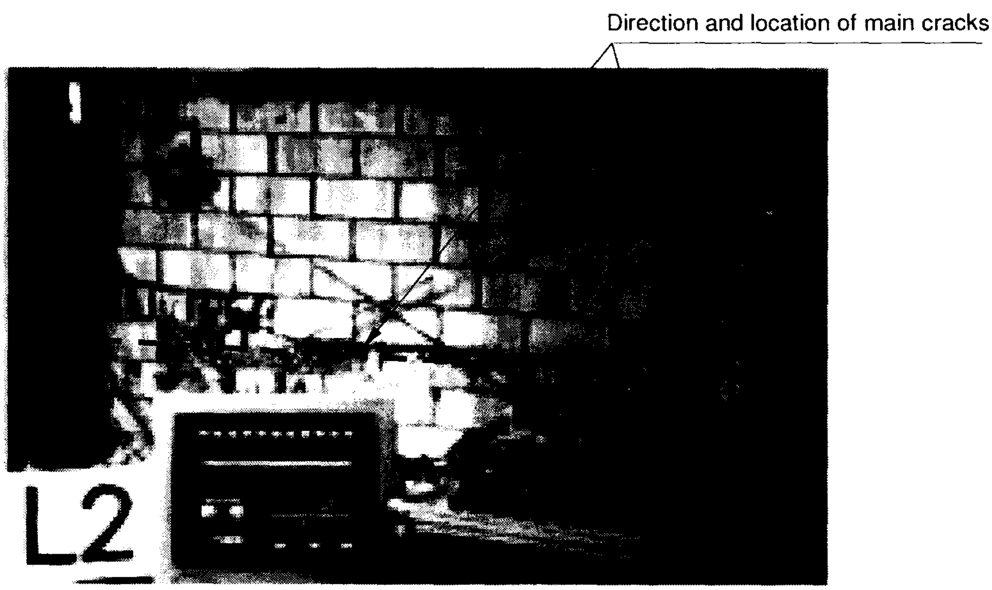

Fig. 4.23 Failure mechanism, Mode-C, for infilled RC frame with aspect ratio of 0.57 (Colangelo 2005).

4.4 SUMMARY

In this chapter two different frames were investigated. The first frame was an infilled frame with lower flexible beam to represent the behaviour of a typical floor in an infilled moment resisting frame. The second frame was an infilled frame with relatively rigid lower beam and continuity of the upper floors to represent the first floor in an infilled moment resisting frame. Different heights and aspect ratios were considered for each frame. Both frames showed change in the failure mechanism at aspect ratio of approximately 0.75. The change in the failure mechanism was observed at aspect ratios close to the points of peak displacements in the maximum displacement-aspect ratio relationships.

In the following discussion, "first group of frames" refers to frames with lower flexible beams and "second group of frames" refers to frames with rigid foundation beam. Comparing the results of first and second group of frames showed that:

1- Increase in the height or aspect ratio of frames of both groups was accompanied by decrease in the initial stiffness.
2- Elastic load of second group was higher, for all aspect ratios, than elastic loads of first group of frames. This means that the first group of frames reached the yield point at lower load level than the second group of frames.
3- Although frames of first group had less reinforcement than frames of second group, frames of first group dissipate more energy than the frames of the second group for the same aspect ratios.
4- Ductility level at failure of second group of frames was higher, for all aspect ratios, than the ductility level of the first group of frames.
5- Resistance of the second group of frames to the lateral load was higher than the resistance of first group of frames for all aspect ratios.
6- Loss of strength of frames of the second group of frames was faster than the loss of strength of the first group of frames.
7- The variation of yield displacement with aspect ratio and the variation of the average yield displacements with the height of the frame for first and second group of frames are shown in figures 4.24 and 4.25, respectively. It is observed that the average yield displacement varies almost linearly with height for both frames.

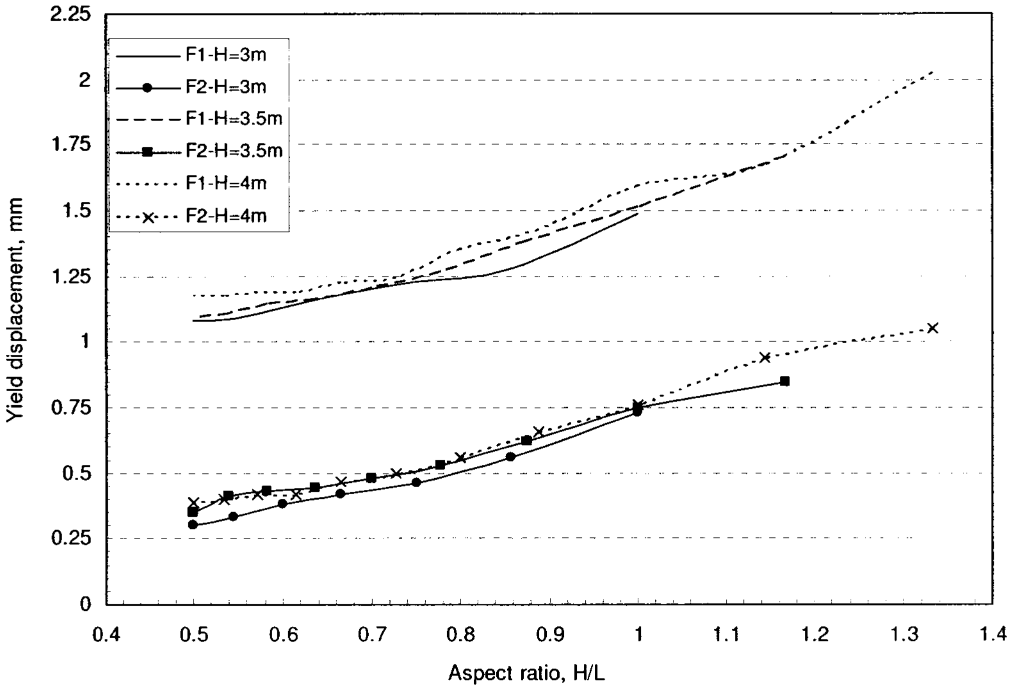

Fig. 4.24 Variation of the yield displacement with the aspect ratio of the frames

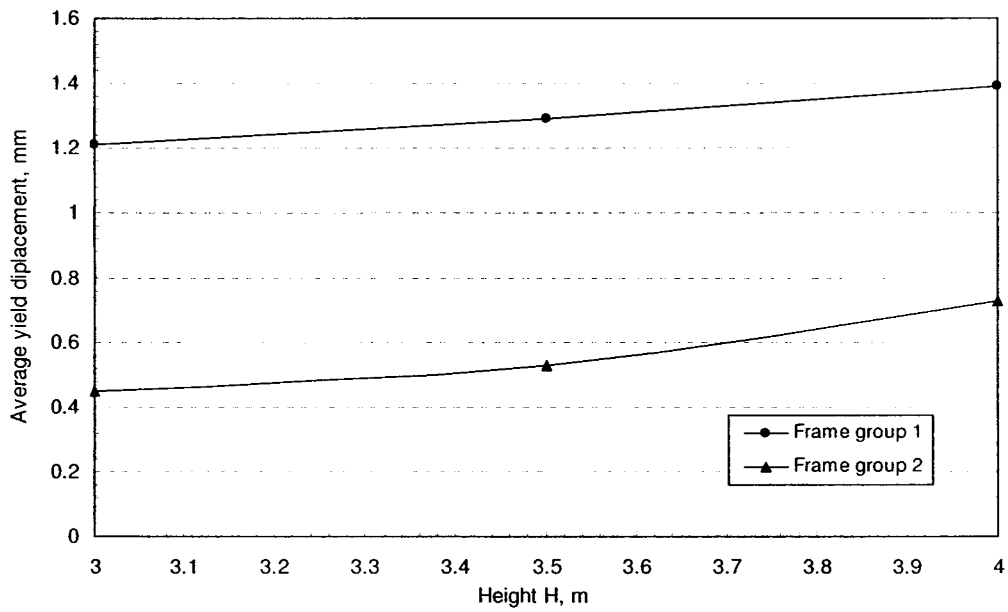

Fig. 4.25 Variation of the average yield displacement with the height of the frame

First group of frames showed higher yield displacement at all points, than the second group of frames. This means that frames of the first group showed displacement values between 3 an 1.8 times the displacement of the second group at yield points at the same height. This is due to the increased fixity at the bottom of the second group of frames.

Summary of the failure mechanism of the two groups of frames with different aspect ratios are illustrated in Table 4-4. There were two different types of failure mechanism. Failure mechanism Mode-E occurred for frames with flexible beam at aspect ratio H/L ≥ 0.75; and for frames with rigid beam at aspect ratio H/L ≥ 0.7. However, failure mechanism Mode-C occurred for frames with flexible beam at aspect ratio H/L < 0.73; and for frames with rigid beam at aspect ratio H/L < 0.67.

TABLE 4-4 Failure mechanism corresponding to aspect ratio

Frame with flexible beam			Frame with rigid beam			Failure mechanism
Aspect ratio			Aspect ratio			
Height 3.0 m	Height 3.5 m	Height 4.0 m	Height 3.0 m	Height 3.5 m	Height 4.0 m	
1.00	1.17	1.33	1.00	1.17	1.33	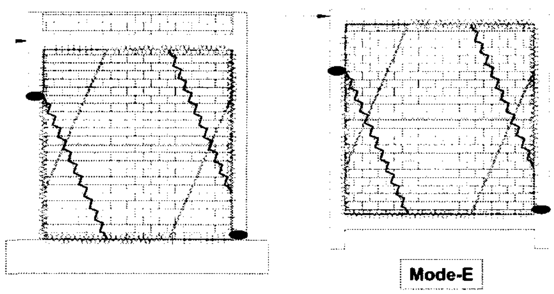
0.86	1.00	1.14	0.86	1.00	1.14	
0.75	0.88	1.00	0.75	0.88	1.00	
	0.78	0.89		0.78	0.89	
		0.8		0.7	0.8	
					0.73	
0.67	0.7	0.73	0.67	0.64	0.67	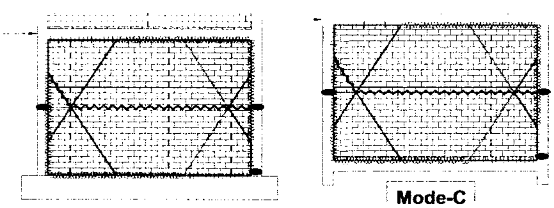
0.6	0.64	0.67	0.60	0.58	0.62	
0.55	0.58	0.62	0.55	0.54	0.57	
0.5	0.54	0.57	0.5	0.5	0.53	
	0.5	0.53			0.5	
		0.5				

The maximum load carrying capacity of both group of frames occurred at aspect ratio of 0.5 for different frame height. Comparing every two frames with similar aspect ratio, it was found that the load resistance of frames with rigid beam were higher than the capacity of frames with flexible beam at all cases. The increase in load resistance was ranging between 12.6% and 16.1%. From these results, we can conclude that there is no significant difference between the first and the upper floor of infilled RC fame in term of lateral load capacity.

However, since the applied seismic loads are higher at the first floor level, failure of the first story is expected before failure of the higher floors. This conclusion agrees with observed failure of infilled frame structures following earthquake events.

This page is intentionally left blank

CHAPTER 5

BEHAVIOUR OF STRONG AND WEAK INFILL RC FRAMES

5.1 INTRODUCTION

In this chapter, effect of masonry/concrete relative strength on the behaviour and failure mechanism of a strong infilled frame was investigated. The masonry compressive strength and concrete compressive strength were varied. The frame dimensions, reinforcement and details remained constant throughout the analysis. Concrete and masonry strength values were selected to cover the practical range.

The behaviour of two types of frames of different aspect ratios were investigated. The first group of frames were strong frames with columns dimensions of 300 × 300 mm and beam dimensions of 300 × 400 mm. The second group of frames were weak frames with columns dimensions of 250 × 250 mm and beam dimensions of 250 × 400 mm. Strong masonry infill was used throughout the analysis process of the two groups of frames to investigate the effect of frame strength. The aspect ratio of the frames and infill panel of both groups ranged between 2.33 and 0.5. The selected frame dimensions and parameters were the same as those tested by Chiou et al. (1999). The experimental observation and data reported by Chiou et al were used to support the analysis results.

The objective of the analysis is to investigate the limits of applicability of the proposed finite element model. Moreover, an attempt was made to define the upper and lower limits of parameters affecting the type of resulting failure mechanism and the effect of aspect ratio and type of frame on this limit.

5.2 CONCRETE/MASONRY RELATIVE STRENGTH

The aim of this analysis was to investigate the influence of the relative compressive strength of masonry infill with respect to compressive strength of concrete of the surrounding frame on the overall behaviour and failure mechanism of the boundary RC frame. In this study, two cases of frames were analyzed. The first case consisted of four infilled RC frames with strong infill. The second case consisted of four infilled RC frames with weak infills. Infill compressive strength of f_{cm} = 14 MPa was used in the first case to represent strong infill and infill compressive strength of 6 MPa was used to represent weak infill in the second group. The frame had clear span of 4,000 mm and clear height of 3,000 mm. The column and beam dimensions were 300 x 300 mm and 300 x 400 mm, respectively. The main reinforcement of the columns was 6 # 5 bars of nominal diameter of 15.9 mm and the main reinforcement of the beam was 6 # 5 bars of nominal diameter of 15.9 mm. The dimensions and details of the frame are shown in figure 5.1. In every case, four different concrete compressive strength of f_{cu} =20, 30, 40 and 50 MPa were considered in the analysis.

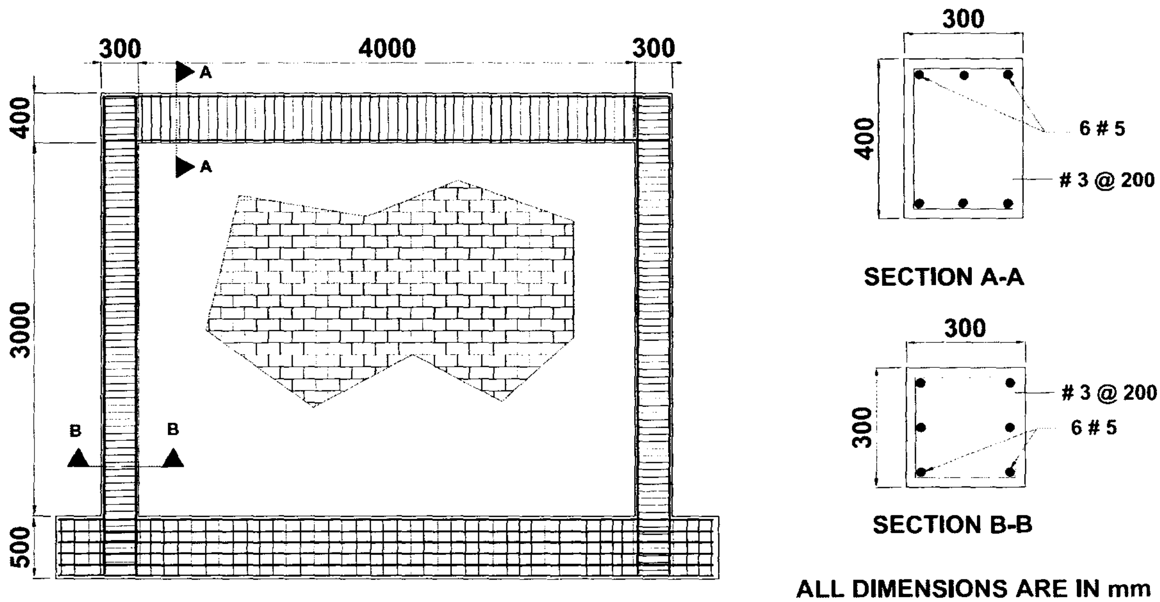

Fig. 5.1 Reinforcement details and dimensions of RC frame.

The load-deflection relationships for RC frames with strong and weak infills are shown in figure 5.2 and 5.3. The graphs representing different frames concrete strength almost coincide. However, the curves end at different displacements.

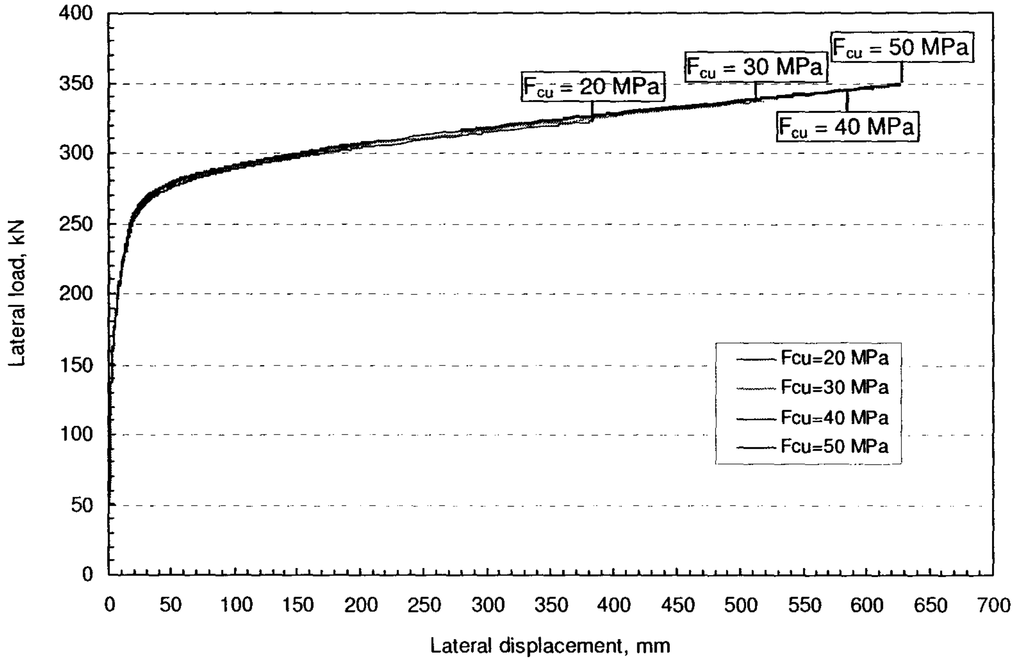

Fig. 5.2 Load-deflection relationship for frames with strong infill.

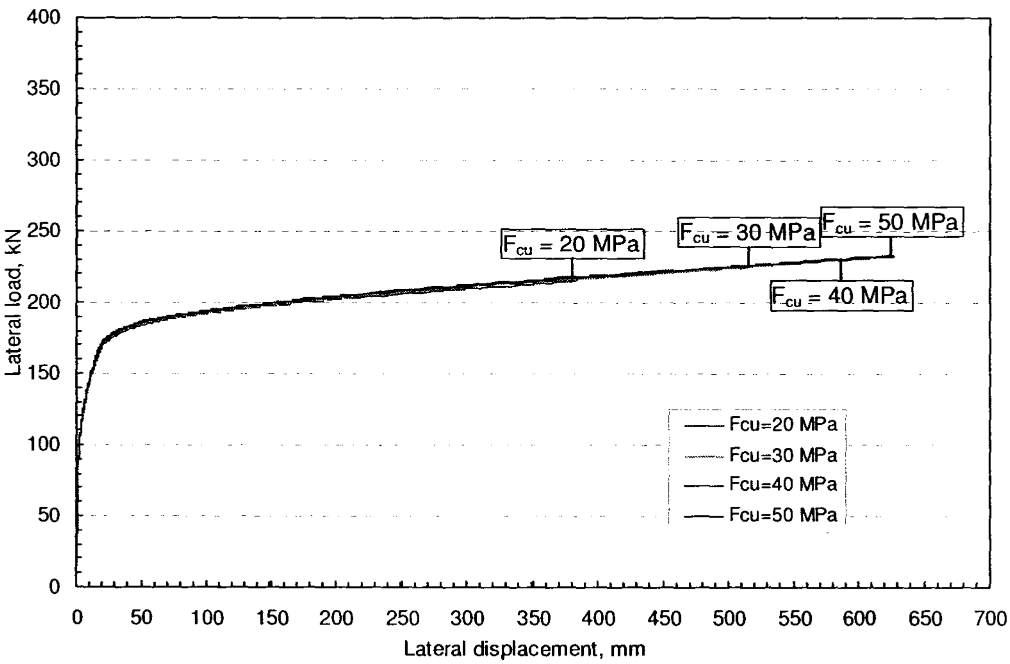

Fig. 5.3 Load-deflection relationship for frames with weak infill.

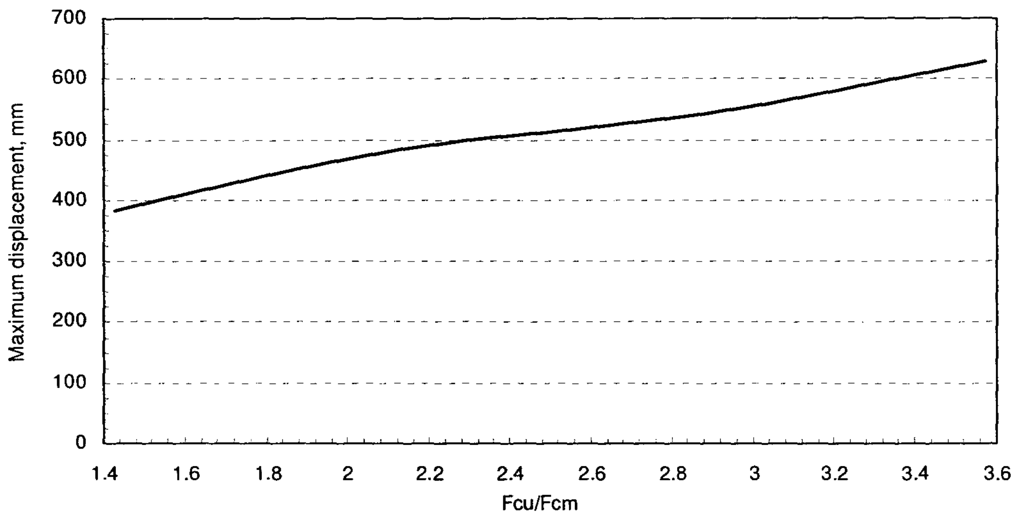

(a) Effect of concrete/masonry strength ratio on maximum displacement.

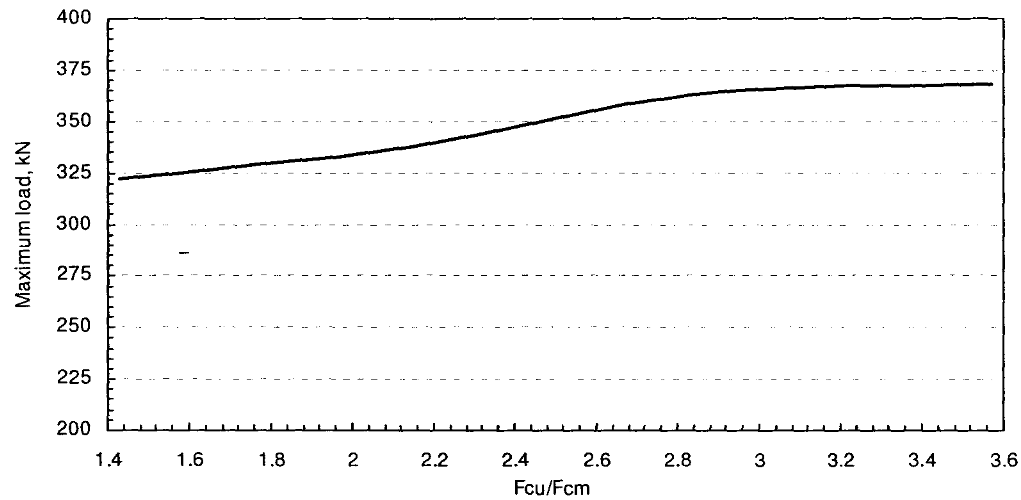

(b) Effect of concrete/masonry strength ratio on maximum load.

Fig. 5.4 Frames with strong infill

The change in the compressive strength of concrete affected the maximum displacement without significant effect on the ultimate strength of different frames. On the other hand, comparing figures 5.2 and 5.3 showed that the ultimate strength of the RC frames with strong infill was approximately 1.5 times that of an RC frames with weak infills without much effect on the ultimate displacement. This indicates that most of the lateral resistance of the infilled RC frames depends on the strength of the infill. After failure of the infill, the RC frame started to resist the lateral force alone. This may explain the reason for having approximately the same maximum displacement in both frames with weak and strong infills.

The relationship between relative concrete/masonry strength and maximum displacement and maximum load of the frames with strong infill are shown in figure 5.4. The relation was almost linear in the case of infilled frames with strong infill. The relationships show approximately constant slope for all concrete/masonry strength ratios.

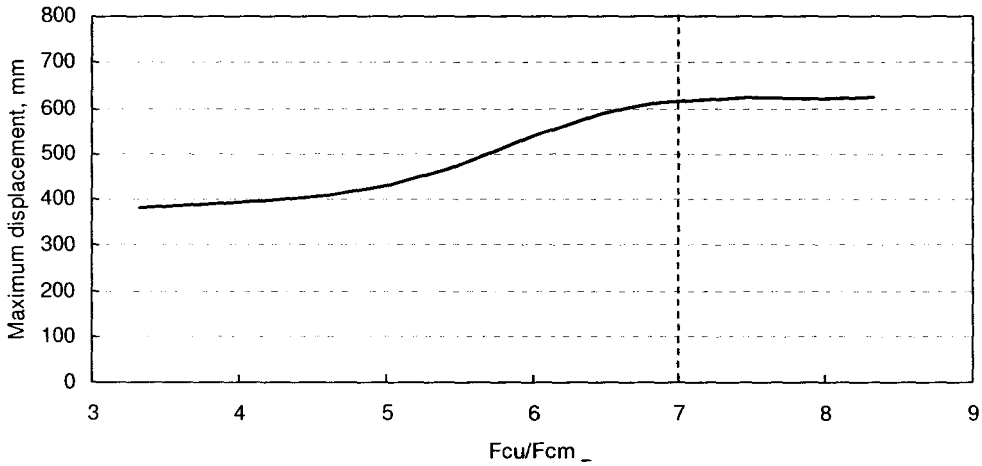

(a) Effect of concrete/masonry strength ratio on maximum displacement.

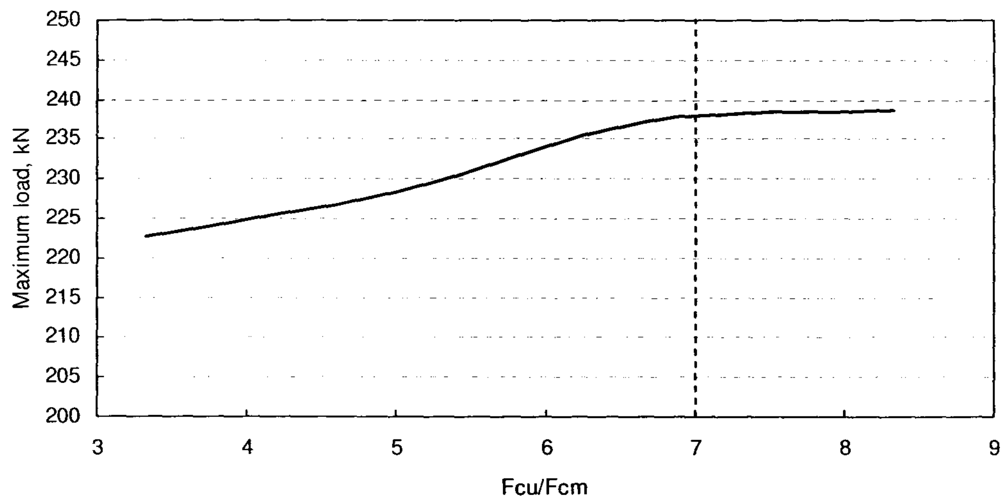

(b) Effect of concrete/masonry strength ratio on maximum load.

Fig. 5.5 Frames with weak infill

The relationship between relative concrete/masonry strength and maximum displacement and maximum load of RC frames with weak infill are shown in figure 5.5. The relationships showed approximately constant slope up to relative concrete/masonry strength ratio of 7, and then the slope of curve becomes almost horizontal. The horizontal part of the curve indicates that after a relative concrete/masonry strength ratio of approximately 7, in RC frames with weak masonry infill, the increase in the strength of concrete with respect to strength of masonry had no effect on the maximum displacement or the maximum load. Most likely, this behaviour occurs because masonry panel is very weak and already failed and what is left is the resistance of the bare RC frame, where the increase in concrete compressive strength "f'_c" increases slightly the load resistance of the infilled frame.

The analysis was conducted for a single frame of aspect ratio of 0.75. The failure mechanisms of frames with strong and weak infills are shown in figure 5.6. The figure shows that the failure mechanism is the same for all cases. This means that the type of infill (strong/weak) or strength of concrete material have limited effect on the failure mechanism of the infilled frame.

The failure mechanism of all infilled frames is Mode-E. This mode is characterized by two distinct parallel cracks in addition to a sliding crack at mid-height of the masonry panel. In this mode two locations of plastic hinges in the RC frames are indicated in the figures. The first location was in the left column at the start of the diagonal crack. The second location of plastic hinge was at the bottom of the right column.

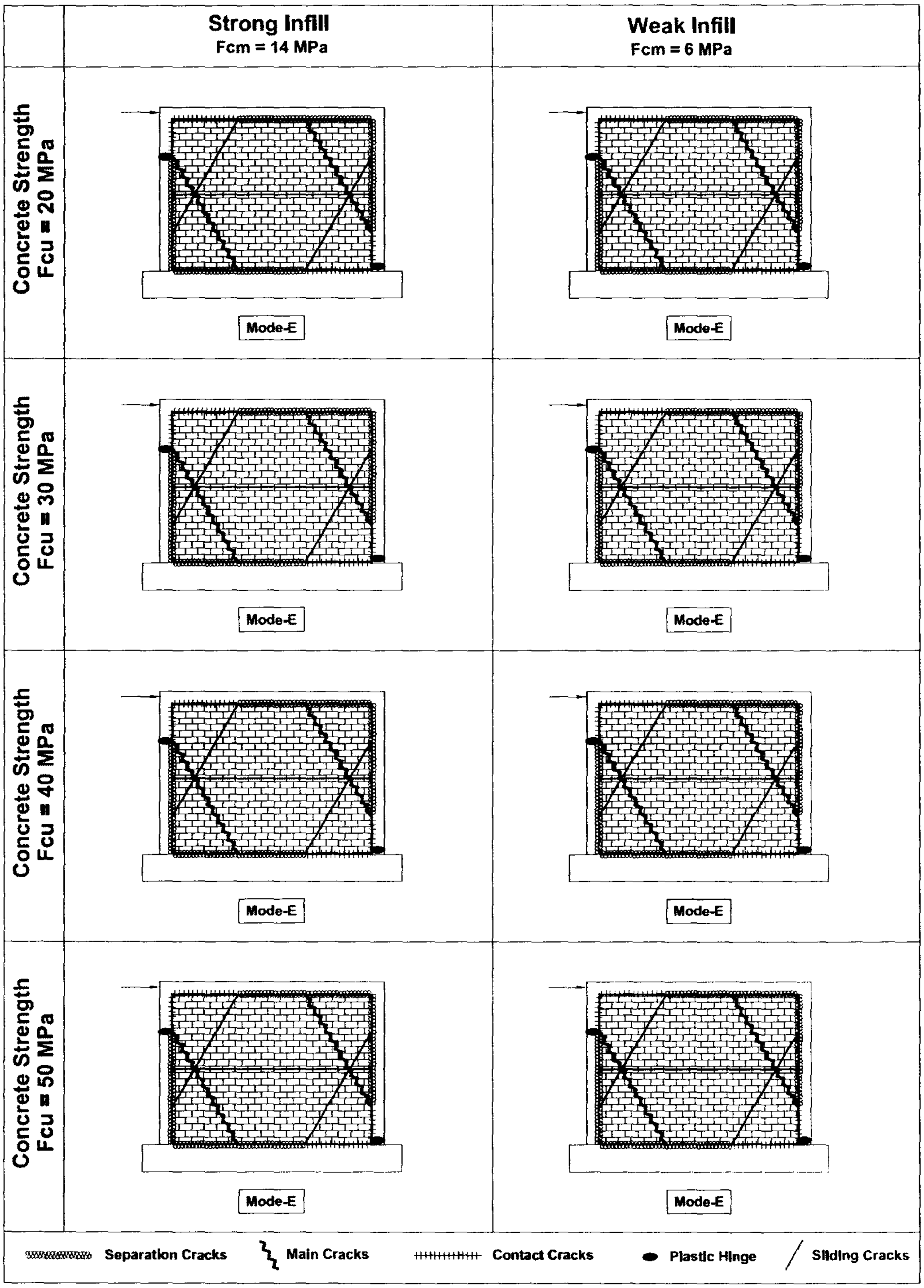

Fig. 5.6 Failure mechanisms

5.3 ASPECT RATIO EFFECT ON THE BEHAVIOUR OF INFILLED RC FRAME

5.3.1 Strong RC Frames

In this section the effect of aspect ratio variation on the behaviour and failure mechanism of strong infilled frames were investigated. The strong RC frames had columns and beam dimensions of 300 x 300 mm and 300 x 400 mm, respectively and main reinforcement of 6 # 5 bars of nominal diameter of 15.9 mm in both the beam and columns. The Details, configuration and dimension of the frame are shown in figure 5.7. The lower beam is a rigid beam to represent a frame at the first story in a moment resisting frame. The continuity of the upper floors was neglected throughout this investigation. Different aspect ratios were considered for this group of frames, starting from aspect ratio of 0.5 up to aspect ratio of 2.33. The dimensions and reinforcement of different cross sections of the frames remained unchanged throughout the analysis.

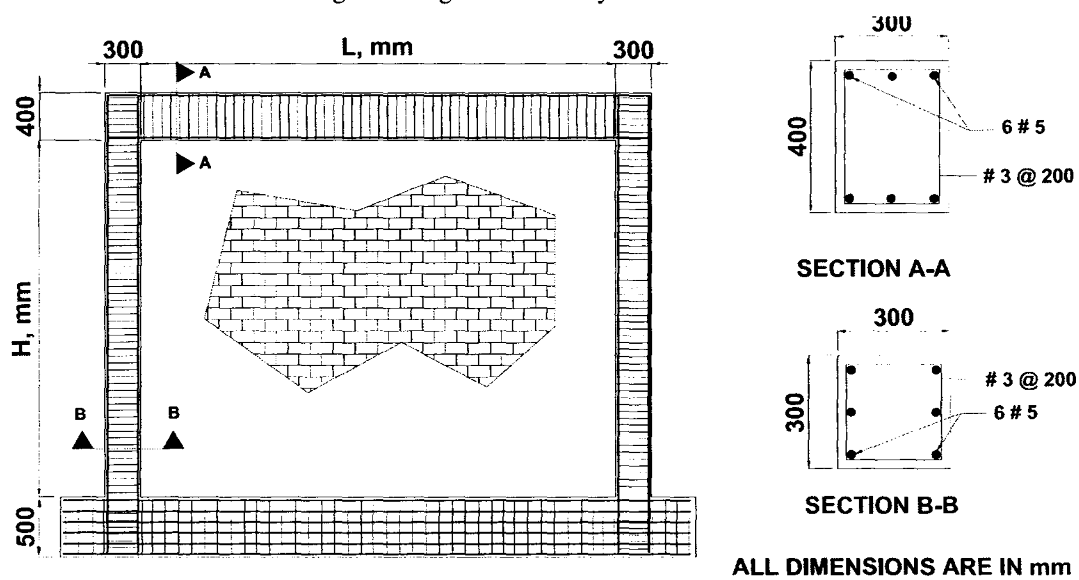

Fig. 5.7 Reinforcing details and dimensions of strong infilled RC frame.

In this section six different groups of frames were investigated. The first group of frames (Group-H) was assigned for frames with height of H = 3.00 m. The length of frame was varied from 3.00 to 6.00 m with 0.5 m step. The second group (Group-J) represented frames of constant height of H = 3.50 m. The length of frames varies between 3.00 to 7.00 m with a step of 0.50 m. The third group (Group-K) had a constant height of H = 4.00 m and variable length between 3.00 and 8.00 m with a step of 0.50 m. the last three groups (Groups L, M and N) represented frames of heights of 5.00, 6.00 and 7.00 m respectively. The length of the three groups varied from 3.00 to 7.00 m with a step of 1.00 m. the dimensions and aspect ratios of the different groups of frames are listed in Table 5-1.

TABLE 5-1 Dimensions and aspect ratios of different frame groups.

Group-H				Group-J				Group-K			
Frame	Height m	Length m	Aspect Ratio	Frame	Height m	Length m	Aspect Ratio	Frame	Height m	Length m	Aspect Ratio
H1	3.00	3.00	1.00	J1	3.50	3.00	1.17	K1	4.00	3.00	1.33
H2	3.00	3.50	0.86	J2	3.50	3.50	1.00	K2	4.00	3.50	1.14
H3	3.00	4.00	0.75	J3	3.50	4.00	0.88	K3	4.00	4.00	1.00
H4	3.00	4.50	0.67	J4	3.50	4.50	0.78	K4	4.00	4.50	0.89
H5	3.00	5.00	0.60	J5	3.50	5.00	0.70	K5	4.00	5.00	0.80
H6	3.00	5.50	0.55	J6	3.50	5.50	0.64	K6	4.00	5.50	0.73
H7	3.00	6.00	0.50	J7	3.50	6.00	0.58	K7	4.00	6.00	0.67
				J8	3.50	6.50	0.54	K8	4.00	6.50	0.62
				J9	3.50	7.00	0.50	K9	4.00	7.00	0.57
								K10	4.00	7.50	0.53
								K11	4.00	8.00	0.50

Group-L				Group-M				Group-N			
Frame	Height m	Length m	Aspect Ratio	Frame	Height m	Length m	Aspect Ratio	Frame	Height m	Length m	Aspect Ratio
L1	5.00	3.00	1.67	M1	6.00	3.00	2.00	N1	7.00	3.00	2.33
L2	5.00	4.00	1.25	M2	6.00	4.00	1.50	N2	7.00	4.00	1.75
L3	5.00	5.00	1.00	M3	6.00	5.00	1.20	N3	7.00	5.00	1.40
L4	5.00	6.00	0.83	M4	6.00	6.00	1.00	N4	7.00	6.00	1.17
L5	5.00	7.00	0.71	M5	6.00	7.00	0.86	N5	7.00	7.00	1.00

Different groups of frames were analyzed using the proposed model and the OpenSees computer code. The average load-deflection relationships for frames groups H, J, K and L are plotted in figure 5.8.

The average load-deflection relationships of frames showed that frames of Group-M with heights of 6.00 m had the maximum drift of 490 mm at lateral load of 290.1 kN. Frames Group-H with heights of 3.00 m had the maximum lateral load carrying capacity of 381.4

kN at lateral displacement of 188.7 mm, as shown in figure 5.8. Results of frames Group-J show that the frames with heights 3.50 m had average lateral displacement of 266.6 mm at lateral load of 365.4 kN. The maximum load capacity of 328.7 kN was carried by the frames of Group-K of height 4.00 m. Results of frames Group-L showed that the maximum drift of 465.4 mm was obtained from frames with heights 5.00 m at lateral force of 314.7 kN. The minimum lateral load capacity of 234.5 kN was obtained from frames Group-N of heights 7.00 m at lateral displacement of 142.4 mm. With in each group (Groups-H though –N), the variation of maximum displacement between different frames in the same group ranged between 10.5% and 17.4%. Moreover, the variation of lateral load capacity between different frames in the same group ranged between 5.4% and 11.1%. However, the effect of maximum lateral displacement at failure is not large for different lengths.

For frames with height more than 7.00 m, the proposed model failed to solve the problem. This may be, due to one of the following reasons; 1) the relatively large size of the masonry element; 2) The small dimension of the column and beam sections with respect to the over all dimensions of the infilled frames; or 3) The large aspect ratio of the infilled frame especially at spans with small values.

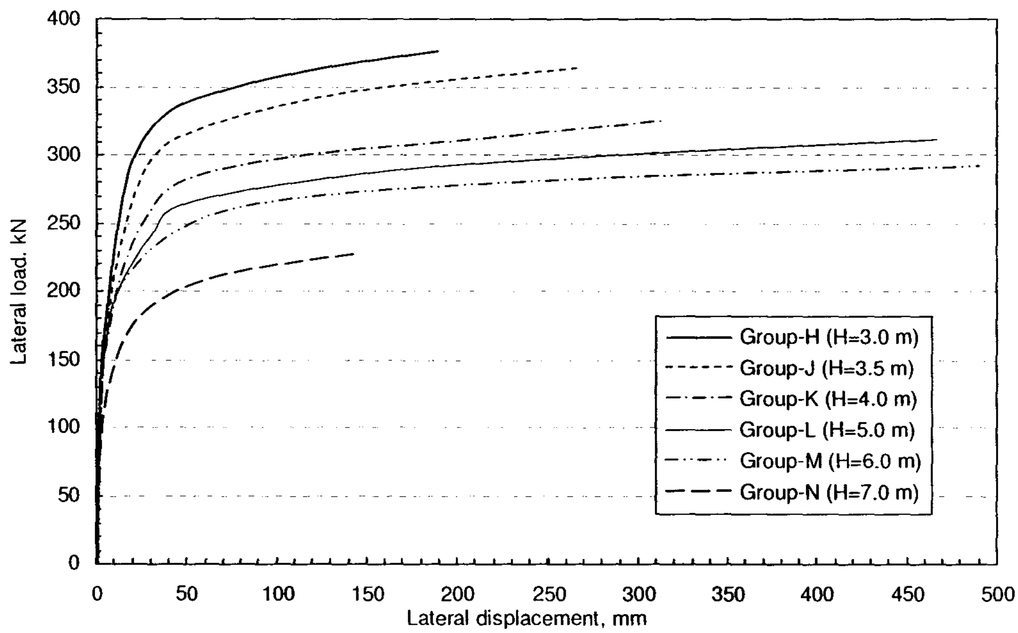

Fig. 5.8 Average load-deflection relationships for Groups-H, -J, -K, -L, -M and -N

The variation of the maximum displacement with the aspect ratio for all frames in the six groups is shown in figure 5.9. The figure shows that the relationship remained almost linear up to an aspect ratio of approximately 0.55 with the change in the height of the frames having no effect on the displacement result. For aspect ratio higher than 0.55 the change in the frame height started to influence the maximum displacements. The aspect ratios corresponding to maximum displacements for frames with heights of 3, 3.5, 4, 5, 6 and 7 meter were 0.60, 0.64, 0.68, 0.79, 0.84 and 0.93, respectively. After the peak value the relation in the three curves (frames groups of heights 3.0, 3.5 and 4.0 m) decreased with a relatively flat slope. The behaviour of the second three groups (frames group-L, -M and –N) is similar to the behaviour of the first three groups (frames group-H, -J and –K), the only difference is that the plot of second three groups started after the peak points. The behaviour of the other three curves of frames (frame groups of heights 5.0, 6.0 and 7.0) was expected since the aspect ratios at start points were after the peak values shown in figure 5.12.

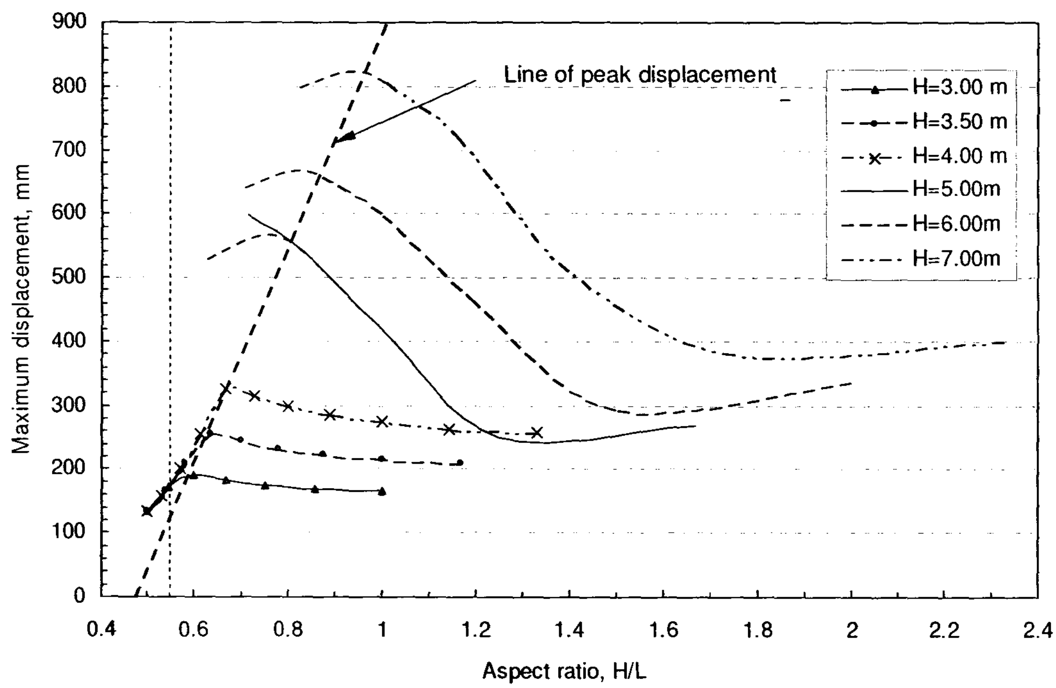

Fig. 5.9 Variation of the maximum displacement with the aspect ratios

Figure 5.9 shows that the combined resistance of both frame and infill increases until the peak points, after that the increase in the aspect ratios causes a decrease in the maximum displacement of the infilled frame. The decrease in the displacement of infilled frame continues until aspect ratios of 1.35, 1.55 and 1.84 for frames of heights of 5.00, 6.00 and 7.00 m respectively. After that the relationship remained almost flat. This means that the increase of aspect ratios beyond these points resulted in no change in the maximum displacement.

The peak displacements of various curves appear to lie on a straight line as shown in figure 5.9. This line we represents the behaviour of frames with different aspect ratios and heights between 3.0 and 7.0 m. This line may be useful in displacement-base design application.

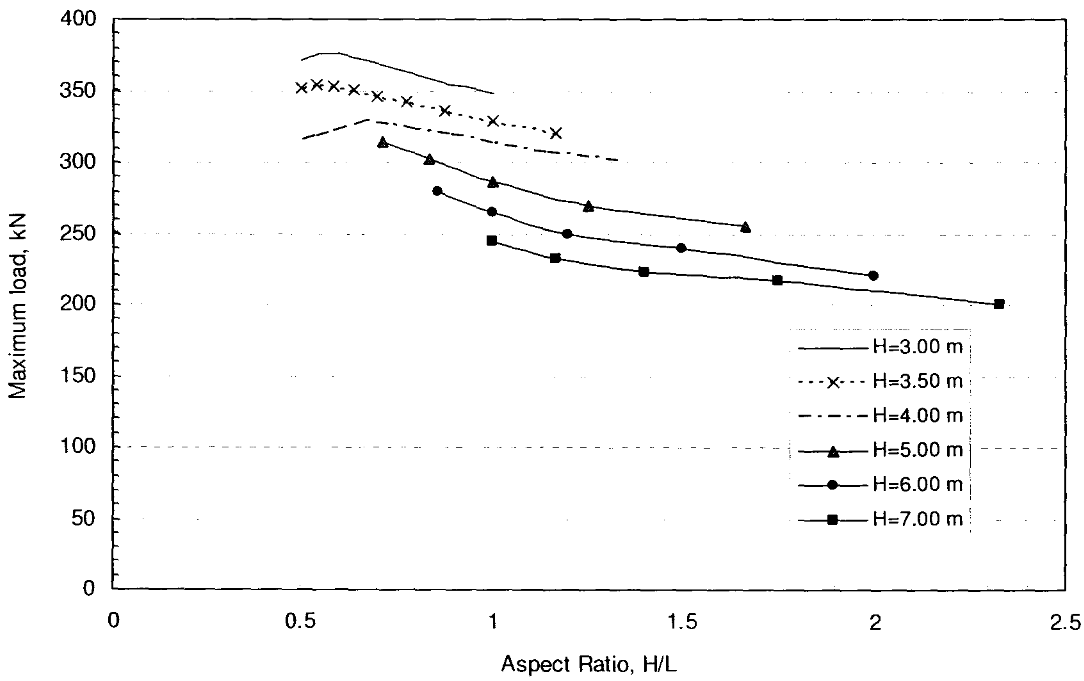

Fig. 5.10 Variation of maximum load with frame aspect ratio.

The relationship between the aspect ratio and the maximum load is shown in figure 5.10. The maximum load calculated using the proposed model was obtained when the results of two consecutive iterations failed to converge. To insure that the results of the maximum loads are not due to numerical instability, every problem was analysed using two different displacement steps, since the runs are displacement control. Figure 5.10 shows that the maximum lateral load resistance of frames group-H (height = 3.0 m) is the highest at the same aspect ratio. The maximum lateral load resistance decreases with the increase of frames height at all aspect ratios. This observation is true for all groups.

The failure mechanism of the frames with different heights and different spans are shown in figure 5.11. There were three different types of failure mechanism. Failure mechanisms corresponding to different aspect ratios are summarized in Table 5-2.

For tall panels with high aspect ratio, the failure mode was Mode-A. This mode was a purely flexural mode in which the frame and the infill act as an integral flexural element. This behaviour occurs at a low load level, where the separation of the frame and the infill has not occurred. The behaviour rarely evolves into a primary failure mechanism, except for the case of tall slender frames with low flexural reinforcement in the columns. A relatively low reinforcement ratio causes the early yielding of the flexural steel in the windward column when it is subjected to tension. In most cases, infill panels tend to partially separate from the bounding frame at a moderate load level, if the two are not securely tied. Mode-A, occurs when the aspect ratio (H/L) was higher than or equals to 1.67, as shown in Table 5-2.

For intermediate aspect ratios, the type of failure mechanism was Mode-E. This mode was characterized by two distinct parallel cracks in addition to sliding crack at mid-height of the masonry panel. In this mode two plastic hinges were formed in the RC frames. The first location was at the start of the diagonal crack near the upper corner of the left column. The second location of plastic hinge was at the bottom corner of right column. Failure mechanism, Mode-E, takes place when the aspect ratio (H/L) was more than or equals to 0.67 but less than 1.50.

For short panels with low aspect ratios, failure was Mode-C. Diagonal cracks propagated from the loaded corner to mid-height of the panel; this crack was jointed by the horizontal crack at mid-height of the infill panel. Mode-C, in this study, takes place when the aspect ratio (H/L) < 0.71. In this mode plastic hinges formed at three different locations in the RC frames. The first location was at mid-height of the left column. The second location was at mid-height of the right column. The third location of plastic hinge was at the bottom corner of right column, since the load was applied at the top left point of the frame.

TABLE 5-2 Failure mechanism corresponding to various aspect ratios.

Aspect Ratio						Failure Mechanism
H = 3.0 m	H = 3.5 m	H = 4.0 m	H = 5.0 m	H = 6.0 m	H = 7.0 m	
---	---	---	1.67	2.00	2.33	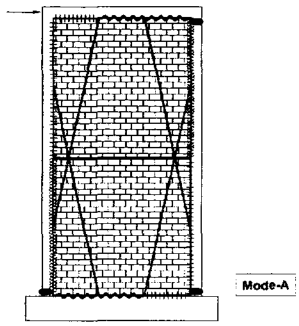
---	---	---	---	---	1.75	
---	---	---	---	---	---	
---	---	---	---	---	---	
---	---	---	---	---	---	
---	---	---	---	---	---	
1.00	1.17	1.33	1.25	1.50	1.40	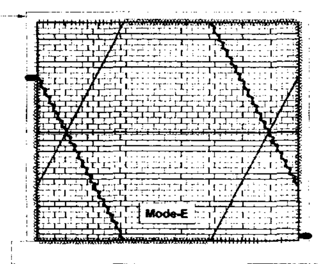
0.86	1.00	1.14	1.00	1.20	1.16	
0.75	0.88	1.00	0.83	1.00	1.00	
0.67	0.78	0.89	---	0.85	---	
---	0.70	0.80	---	---	---	
---	---	0.72	---	---	---	
0.60	0.63	0.67	0.71	---	---	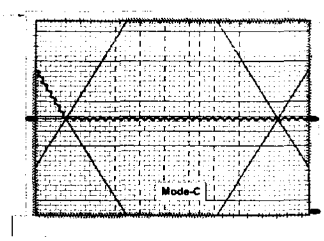
0.55	0.58	0.62	---	---	---	
0.50	0.54	0.57	---	---	---	
---	0.50	0.5	---	---	---	
---	---	---	---	---	---	
---	---	---	---	---	---	

Failure mechanism corresponding to various heights and lengths in matrix form is shown in table 5-3. According to tables 5-2 and 5-3, failure mechanism Mode-A occurs at aspect ratios higher than 1.67; failure mechanism Mode-E occurs at aspect ratio between 0.67 and 1.50; and failure Mode-C occurs at aspect ratio less than 0.67.

TABLE 5-3 Failure mechanism corresponding to various heights and lengths.

Height, H / Length, L	3.00 m	3.50 m	4.00 m	5.00 m	6.00 m	7.00 m
3.00 m	E	E	E	A	A	A
3.50 m	E	E	E	---	---	---
4.00 m	E	E	E	E	E	A
4.50 m	C	E	E	---	---	---
5.00 m	C	E	E	E	E	E
5.50 m	C	C	E	---	---	---
6.00 m	C	C	C	E	E	E
6.50 m	---	C	C	---	---	---
7.00 m	---	C	C	C	E	E
7.50 m	---	---	C	---	---	---
8.00 m	---	---	C	---	---	---

Details of failure mechanisms, location of main cracks, location of sliding cracks and location of the plastic hinges for all aspect ratios for the six groups of frames are shown in figure 5.11.

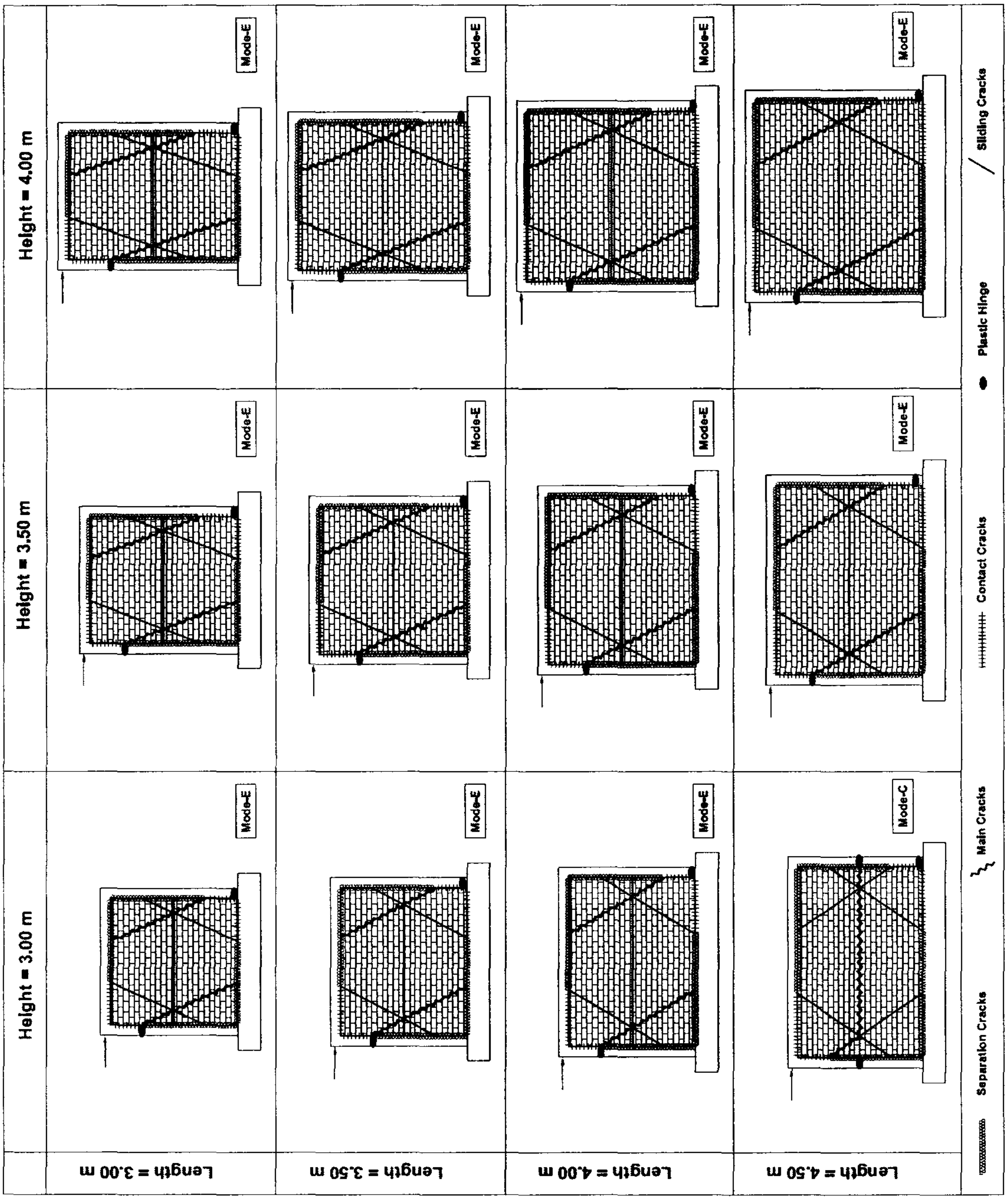

Fig. 5.11 Failure mechanisms for strong RC frames

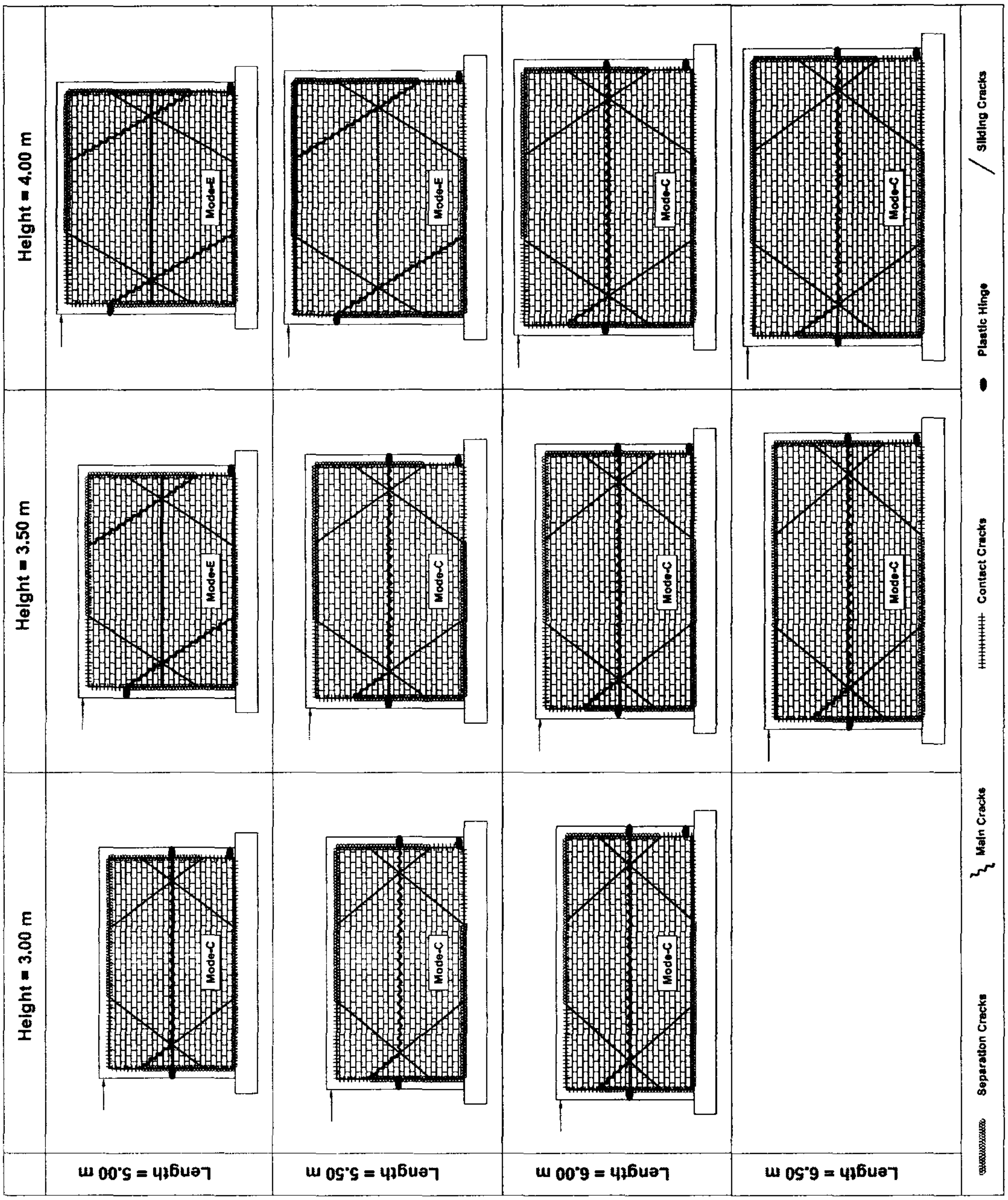

Fig. 5.11 Failure mechanisms for strong RC frames (Cont…)

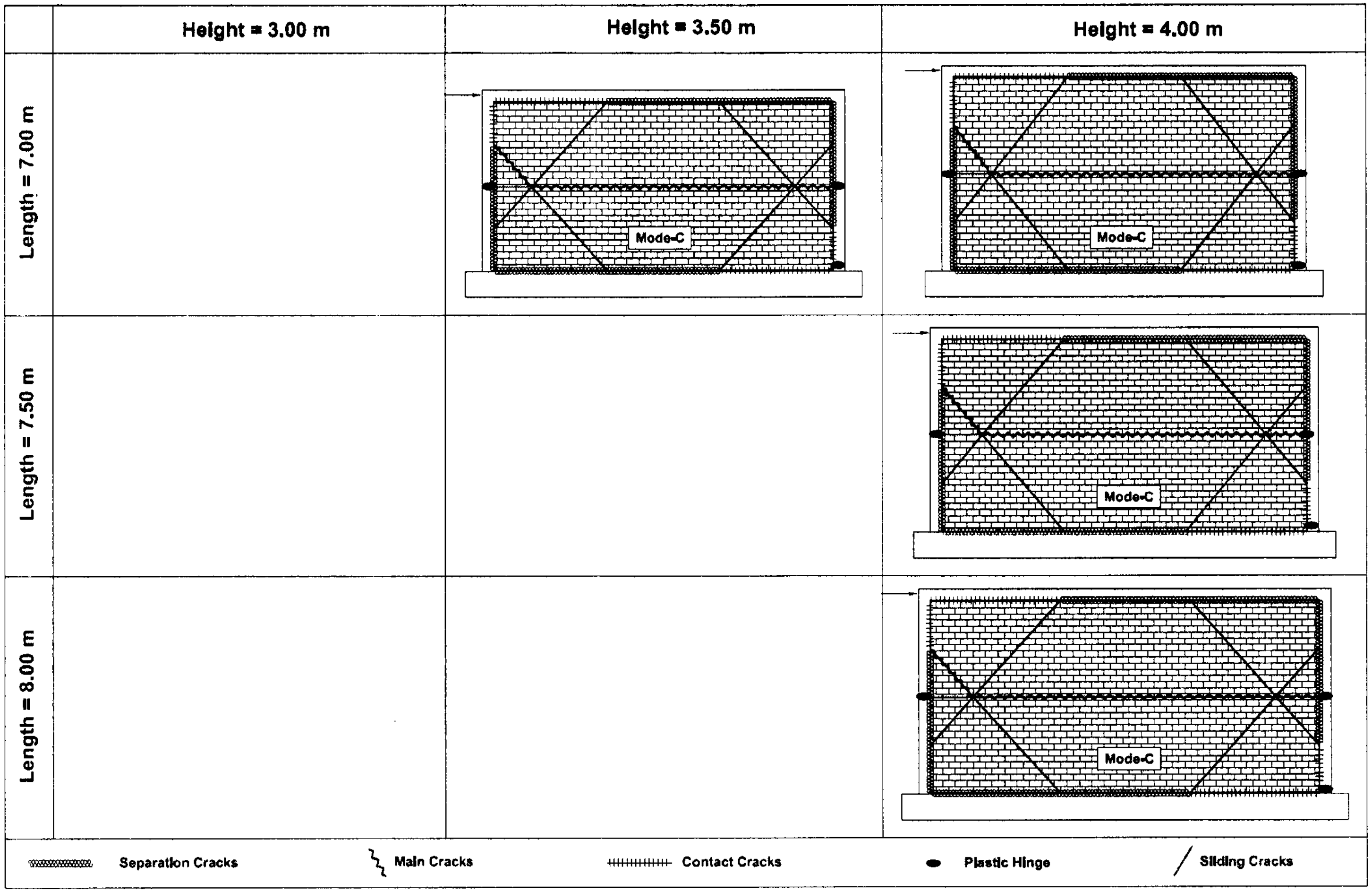

Fig. 5.11 Failure mechanisms for strong RC frames (Cont…)

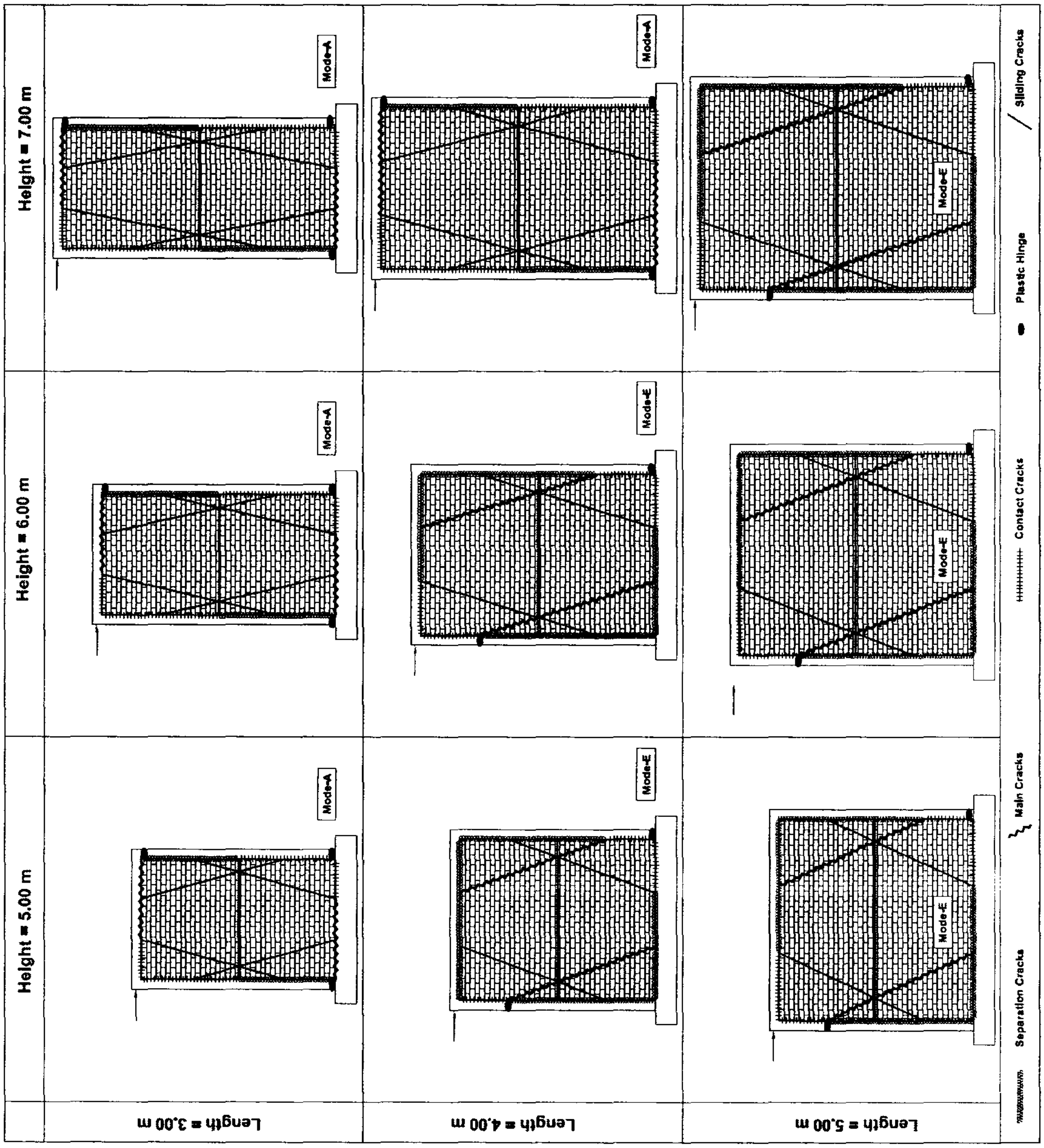

Fig. 5.11 Failure mechanisms for strong RC frame (Cont…)

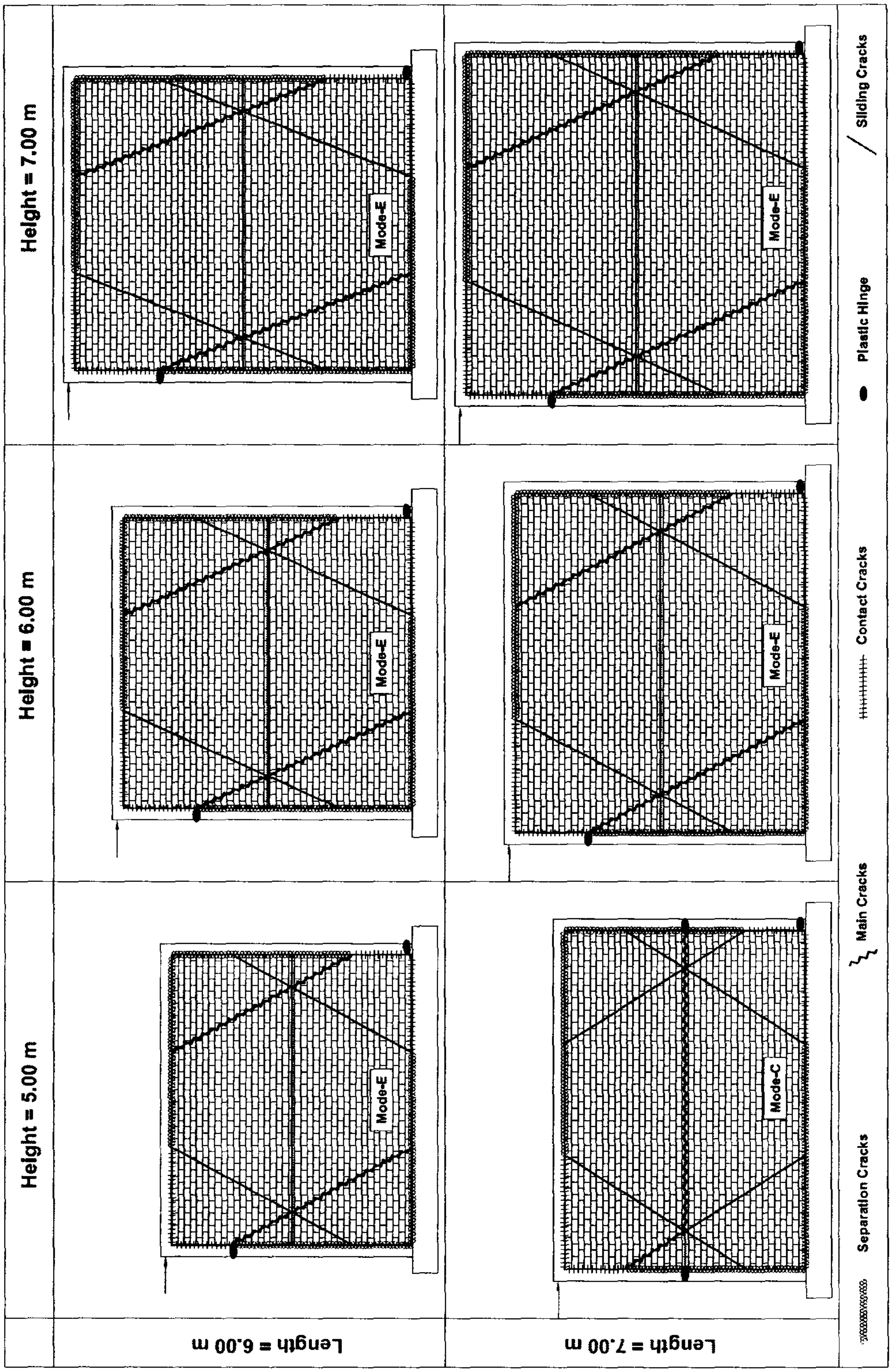

Fig. 5.11 Failure mechanisms for strong RC frames (Cont…)

5.3.2 Weak RC Frames

In the following section the effect of the aspect ratio variation on the behaviour and failure mechanism of weak infilled frames was investigated. The weak infilled RC frames had columns and beam dimensions of 250 x 250 mm and 250 x 400 mm, respectively, and main reinforcement of 6 # 4 bars of nominal diameter of 12.7 mm in both beam and columns. Detail, configuration and dimensions of the frame are shown in figure 5.12. The lower beam is a rigid beam to represent a frame at the first story in a moment resistance frame. Different aspect ratios were considered for this group of frames, starting from aspect ratio of 0.5 up to aspect ratio of 2.33. Aspect ratios and variation of length and height were selected to be the same as in the case of strong infilled frames, to investigate the effect of strength of the RC frame on the behaviour of infilled frame. The dimensions and reinforcement of different cross sections of the frames remained constant for all cases analyzed.

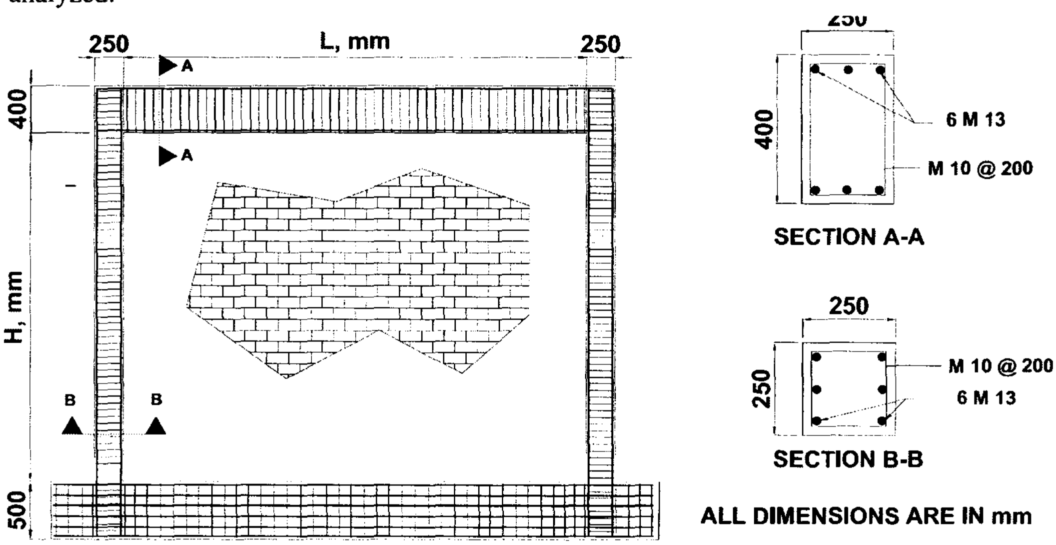

Fig. 5.12 Reinforcing details and dimensions of weak infilled RC frame.

Six different groups of frames were investigated. The same aspect ratios were used again in the case of weak infilled RC frames. The first group of frames (Group-P) was assigned for frames with height of H = 3.00 m. The length of frame was varied from 3.00 to 6.00 m with 0.5 m step. The second group (Group-Q) represented frames of constant height of H = 3.50 m. The length of frames varied between 3.00 to 7.00 m with a step of 0.50 m. The third group (Group-R) had a constant height of H = 4.00 m and variable length between 3.00 and 8.00 m with a step of 0.50 m. The last three groups (Groups S, T and X) represented frames of heights of 5.00, 6.00 and 7.00 m, respectively. The length of the three groups varied from 3.00 to 7.00 m with a step of 1.00 m. The dimensions and aspect ratio of different groups of frames are listed in Table 5-4.

TABLE 5-4 Dimensions and aspect ratio of different weak RC frame groups.

Group-P				Group-Q				Group-R			
Frame	Height m	Length m	Aspect Ratio	Frame	Height m	Length m	Aspect Ratio	Frame	Height m	Length m	Aspect Ratio
P1	3.00	3.00	1.00	Q1	3.50	3.00	1.17	R1	4.00	3.00	1.33
P2	3.00	3.50	0.86	Q2	3.50	3.50	1.00	R2	4.00	3.50	1.14
P3	3.00	4.00	0.75	Q3	3.50	4.00	0.88	R3	4.00	4.00	1.00
P4	3.00	4.50	0.67	Q4	3.50	4.50	0.78	R4	4.00	4.50	0.89
P5	3.00	5.00	0.60	Q5	3.50	5.00	0.70	R5	4.00	5.00	0.80
P6	3.00	5.50	0.55	Q6	3.50	5.50	0.64	R6	4.00	5.50	0.73
P7	3.00	6.00	0.50	Q7	3.50	6.00	0.58	R7	4.00	6.00	0.67
				Q8	3.50	6.50	0.54	R8	4.00	6.50	0.62
				Q9	3.50	7.00	0.50	R9	4.00	7.00	0.57
								R10	4.00	7.50	0.53
								R11	4.00	8.00	0.50

Group-S				Group-T				Group-X			
Frame	Height m	Length m	Aspect Ratio	Frame	Height m	Length m	Aspect Ratio	Frame	Height m	Length m	Aspect Ratio
S1	5.00	3.00	1.67	T1	6.00	3.00	2.00	X1	7.00	3.00	2.33
S2	5.00	4.00	1.25	T2	6.00	4.00	1.50	X2	7.00	4.00	1.75
S3	5.00	5.00	1.00	T3	6.00	5.00	1.20	X3	7.00	5.00	1.40
S4	5.00	6.00	0.83	T4	6.00	6.00	1.00	X4	7.00	6.00	1.17
S5	5.00	7.00	0.71	T5	6.00	7.00	0.86	X5	7.00	7.00	1.00

Different groups of frames were analyzed using the proposed model and the OpenSees code. Load-deflection relationships for frames groups P, Q, R, S, T and X are plotted in figures 5.13.

The average load-deflection relationships of frames showed that frames of Group-R with heights of 4.00 m had the maximum drift of 504 mm at lateral load of 270.1 kN. Frames Group-P with heights of 3.00 m had the maximum lateral load carrying capacity of 297.4 kN at lateral displacement of 271.4 mm, as shown in figure 5.13. Results of frames Group-

Q show that the frames with heights 3.50 m had average lateral displacement of 378.3 mm at lateral load of 280.3 kN. The maximum load capacity of 239.6 kN was carried by the frames of Group-S of height 5.00 m at lateral displacement of 327.4 mm. Results of frames Group-T showed that the maximum drift of 327.8 mm was obtained from frames of 6.00 m height at lateral force of 219.2 kN. The minimum lateral load capacity of 192.4 kN was obtained from frames Group-X of heights 7.00 m at lateral displacement of 174.8 mm. Within each group (Groups-P though -X), the variation of maximum displacement between different frames in the same group ranged between 13.7% and 18.3%. Moreover, the variation of lateral load capacity between different frames in the same group ranged between 6.9% and 8.2%. However, the effect of maximum lateral displacement at failure is not large for different lengths. For frames with height more than 7.00 mm, the proposed model failed to solve the problem due to numerical instability for the possible reasons discussed in section 5.3.1.

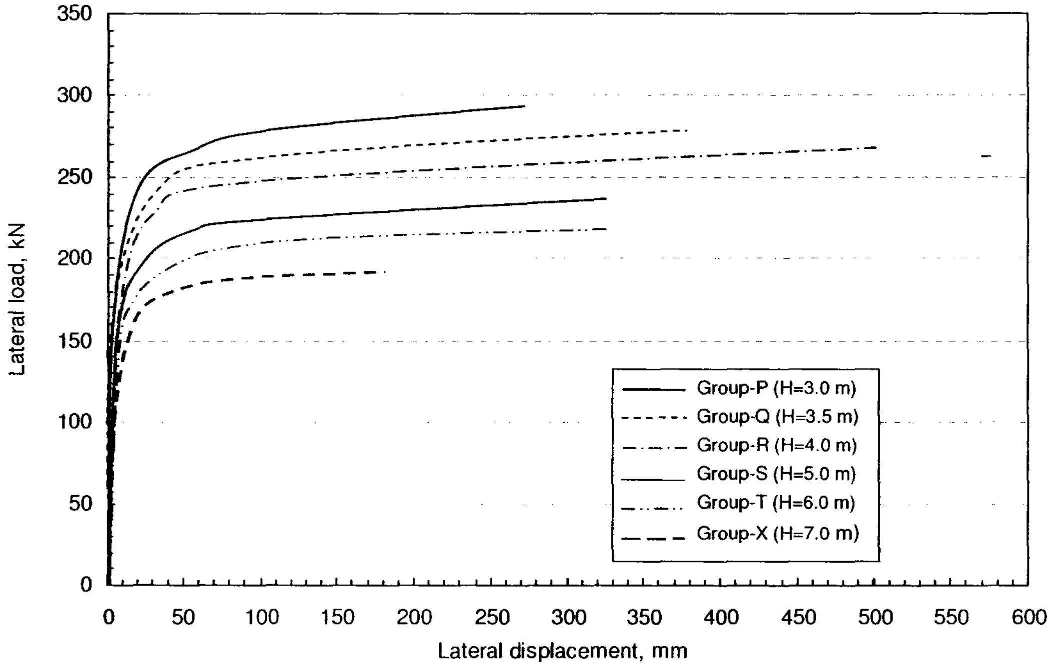

Fig. 5.13 Average load-deflection relationships for Groups-P, -Q, -R, -S, -T and -X

The variation of the maximum displacement with the aspect ratio for all frames in the six groups is shown in figure 5.14. The relationships in figure 5.14 for the first three groups remained almost linear up to an aspect ratio of approximately 0.55 and the change in the height of the frames had no effect on the displacement result. For aspect ratios higher than 0.55 the change in the frame height started to show an effect. This aspect ratio corresponded to the start of failure mechanism Mode-C. The aspect ratios corresponding to maximum displacements for frames with heights of 3, 3.5, and 4 meter were 0.58, 0.64 and 0.68, respectively. After the peak value the calculated maximum displacement decreased up to aspect ratios between 0.9 and 1.0 for the three curves. This behaviour did not appear in the strong infilled frames. As shown in figure 5.14, the variation of maximum displacement with aspect ratio for the next three groups of frames showed similar behaviour. The maximum displacement started to decrease from the maximum point, then the frames restored some of their resistance with the increase of the aspect ratios. The start points for the last three groups were after the peak values of the three curves, that was the reason for this behaviour.

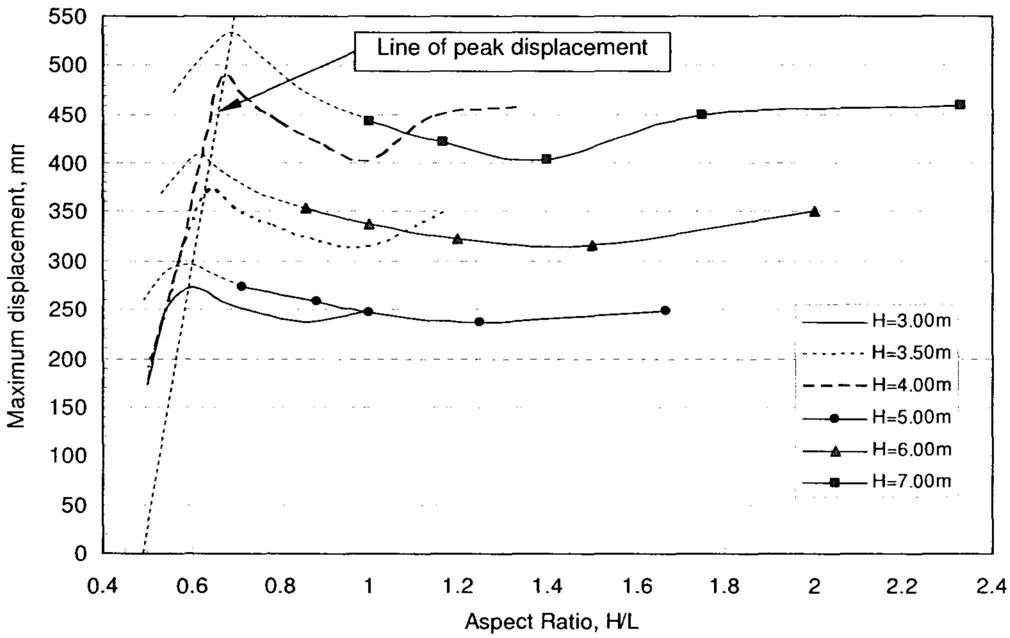

Fig. 5.14 Variation of the maximum displacement with the aspect ratios

The peak maximum displacement of the six groups appears to lie on a straight line s shown in figure 5.14. This line may be useful in design applications giving the expected peak displacement for frames of different aspect ratios.

The relationship between the aspect ratio and the maximum load is shown in figure 5.15. From figure 5.15, the maximum load decreases linearly with the increase of aspect ratio. In figure 5.15, the relationship between maximum loads and aspect ratios decreases linearly.

Figure 5.15 shows that the maximum lateral load resistance of frames Group-P (height = 3.0 m) is the highest for the aspect ratios up to 0.8. The maximum lateral load resistance decreased with the increase of frame height at the same aspect ratio. This observation holds true for all groups.

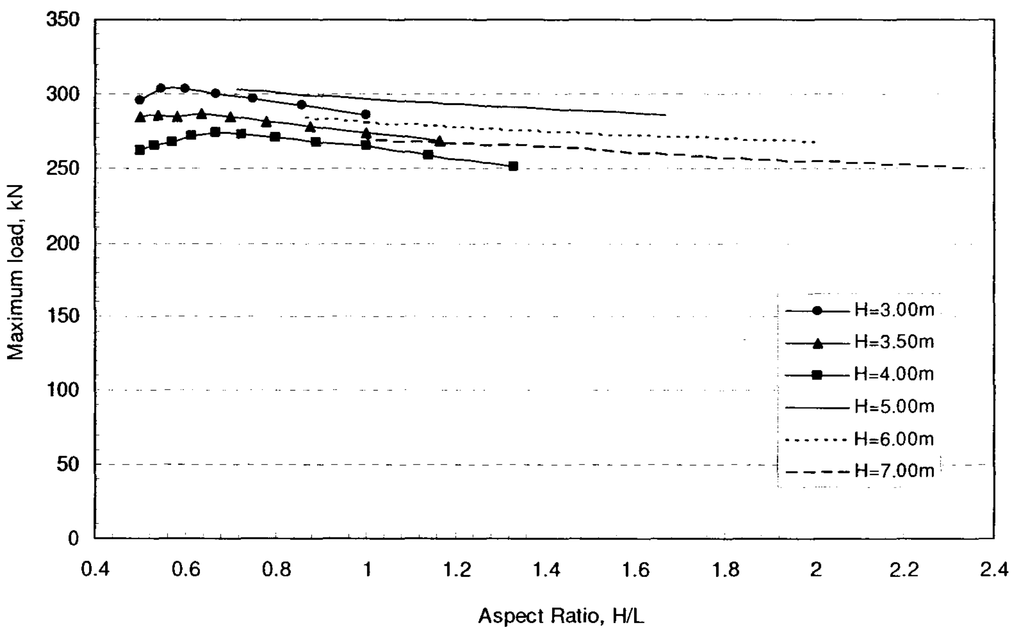

Fig. 5.15 Variation of maximum load with frame aspect ratio.

The failure mechanism of the frames with different heights and different spans are shown in figure 5.16. There were three different types of failure mechanisms. Failure mechanisms corresponding to different aspect ratio is summarized in Table 5-5.

The first failure mode was Mode-A. This mode was a purely flexural mode in which the frame and the infill act as an integral flexural element. This behaviour may occur at low load level, where the separation of the frame and the infill has not occurred. This behaviour rarely evolves into a primary failure mechanism, except for the case of tall slender frames with low flexural reinforcement in the columns. A relatively low reinforcement ratio causes the early yielding of the flexural steel in the left column when it is subjected to tension. In most cases, infill panels tend to partially separate from the bounding frame at a moderate load level if the two are not securely tied. Mode-A, happened when the aspect ratio (H/L) was higher than or equals to 1.50 in the case of weak infilled frames, as shown in Table 5-5.

TABLE 5-5 Failure mechanism corresponding to aspect ratio.

Aspect Ratio						Failure Mechanism
H = 3.0 m	H = 3.5 m	H = 4.0 m	H = 5.0 m	H = 6.0 m	H = 7.0 m	
---	---	---	1.67	2.00	2.33	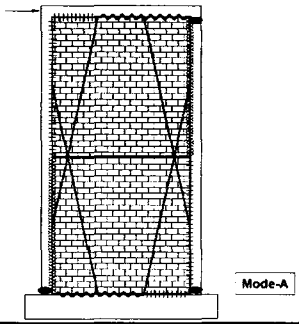
---	---	---	---	1.50	1.75	
---	---	---	---	---	---	
---	---	---	---	---	---	
---	---	---	---	---	---	
---	---	---	---	---	---	
1.00	1.17	1.33	1.25	1.20	1.40	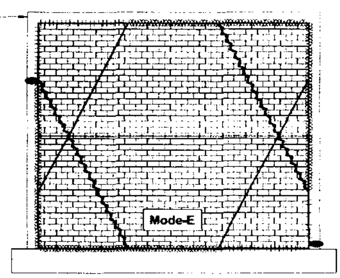
0.86	1.00	1.14	1.00	1.00	1.16	
0.75	0.88	1.00	0.83	0.85	1.00	
0.67	0.78	0.89	---	---	---	
---	---	0.80	---	---	---	
---	---	---	---	---	---	
0.60	0.7	0.72	0.71	---	---	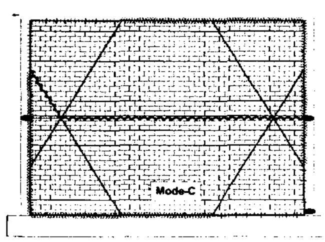
0.55	0.63	0.67	---	---	---	
0.50	0.58	0.62	---	---	---	
---	0.54	0.57	---	---	---	
---	0.50	0.5	---	---	---	
---	---	---	---	---	---	

The second type of failure mechanism was Mode-E. This mode was characterized by two distinct parallel cracks in addition to sliding crack at mid-height of the masonry panel. In this mode, plastic hinges occur at two locations in the RC frames. The first location was at the beginning of the diagonal crack near the upper part of the left column. The second location of plastic hinge was at the bottom of the right column. Failure mechanism, Mode-E, takes place when the aspect ratio (H/L) was more than or equals to 0.67 but less than 1.4.

The third type of failure was Mode-C. Diagonal cracks propagated from the loaded corner to mid-height of the panel; this crack was joined by the horizontal crack at mid-height of the infill panel. In this study, Mode-C occurs when the aspect ratio (H/L) < 0.72. In this mode plastic hinges occur at three locations in the RC frames. The first location was at the mid-height of the left column. The second location was at the mid-height of the right column. The third location of plastic hinge was at the bottom of right column, since the load was applied at the top left point of the frame.

Failure mechanisms corresponding to various heights and lengths in matrix form are shown in Table 5-6. According to Tables 5-5 and 5-6, failure mechanism Mode-A occurs at aspect ratios higher than 1.67; failure mechanism Mode-E occurs at aspect ratio between 0.67 and 1.50; and failure Mode-C occurs at aspect ratio less than 0.67. This the same observation as in the case of strong frames with some changes within these groups, as shown in Table 5-6.

TABLE 5-6 Failure mechanism corresponding to various heights and lengths.

Height, H / Length, L	3.00 m	3.50 m	4.00 m	5.00 m	6.00 m	7.00 m
3.00 m	E	E	E	A	A	A
3.50 m	E	E	E	---	---	---
4.00 m	E	E	E	E	A	A
4.50 m	C	E	E	---	---	---
5.00 m	C	C	E	E	E	E
5.50 m	C	C	C	---	---	---
6.00 m	C	C	C	E	E	E
6.50 m	---	C	C	---	---	---
7.00 m	---	C	C	C	E	E
7.50 m	---	---	C	---	---	---
8.00 m	---	---	C	---	---	---

Details of failure mechanisms, location of main cracks, location of sliding cracks and plastic hinges for different aspect ratios for the six groups of frames are shown in figure 5.16.

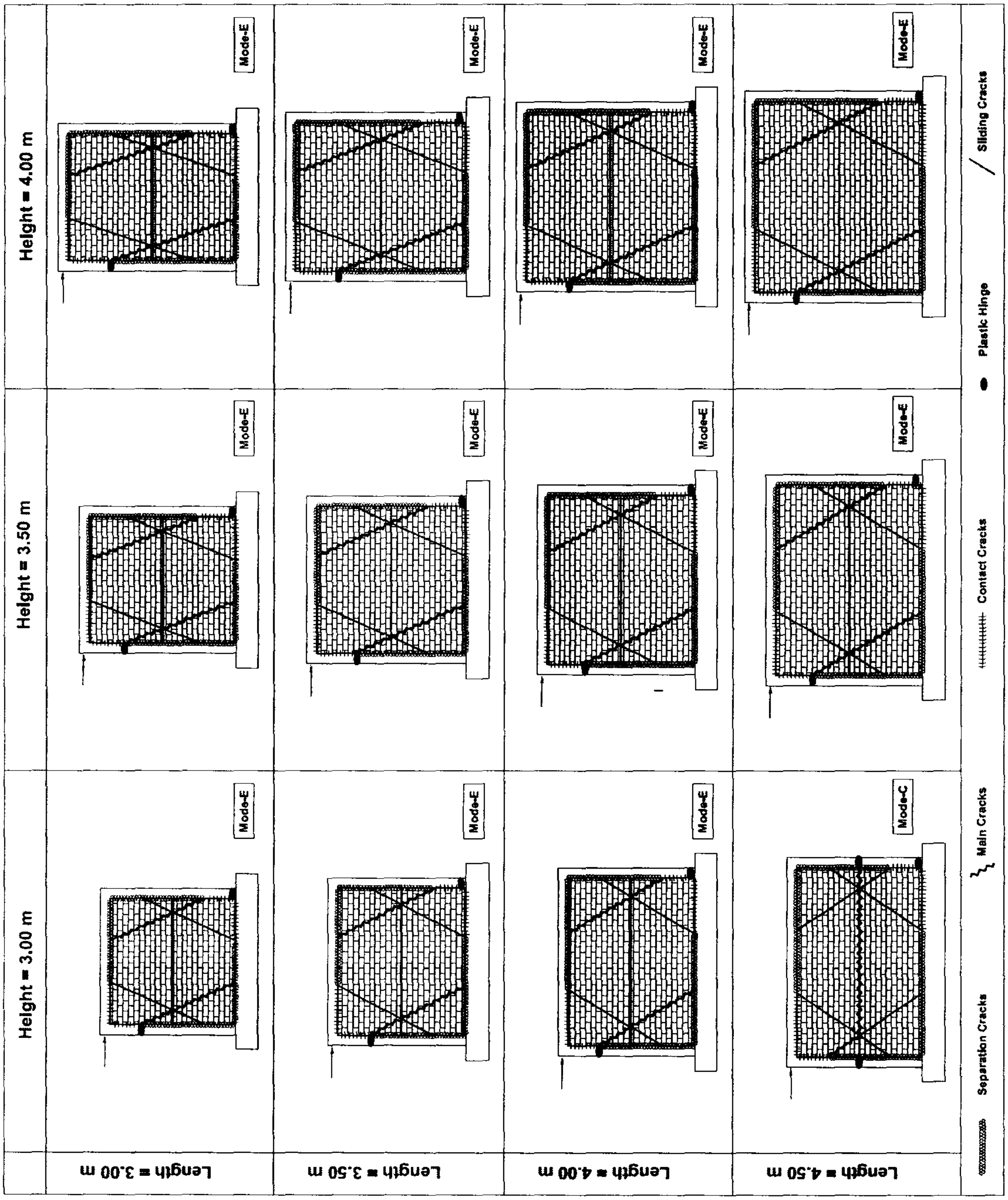

Fig. 5.16 Failure mechanisms for weak RC frames

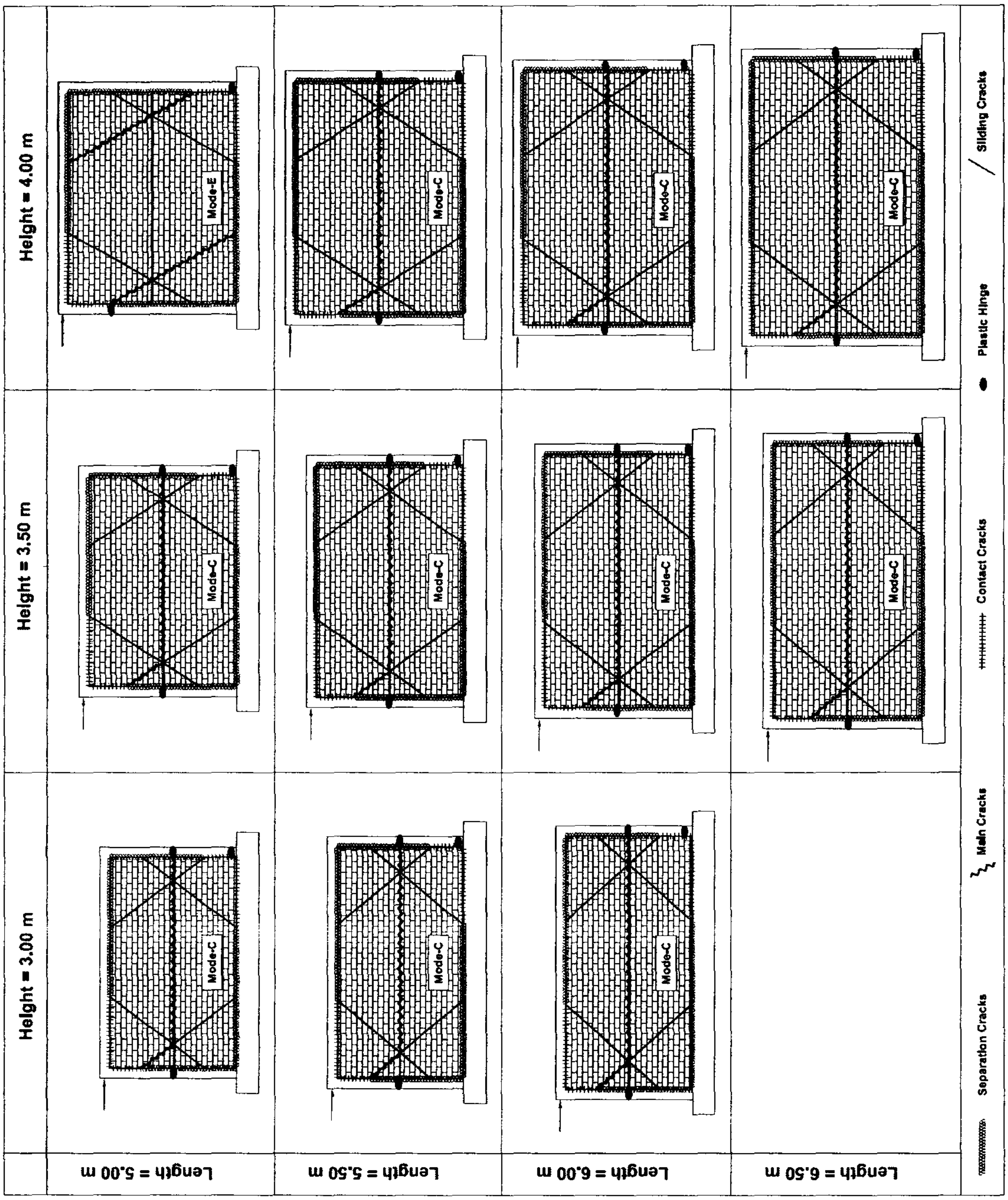

Fig. 5.16 Failure mechanisms for weak RC frames (Cont…)

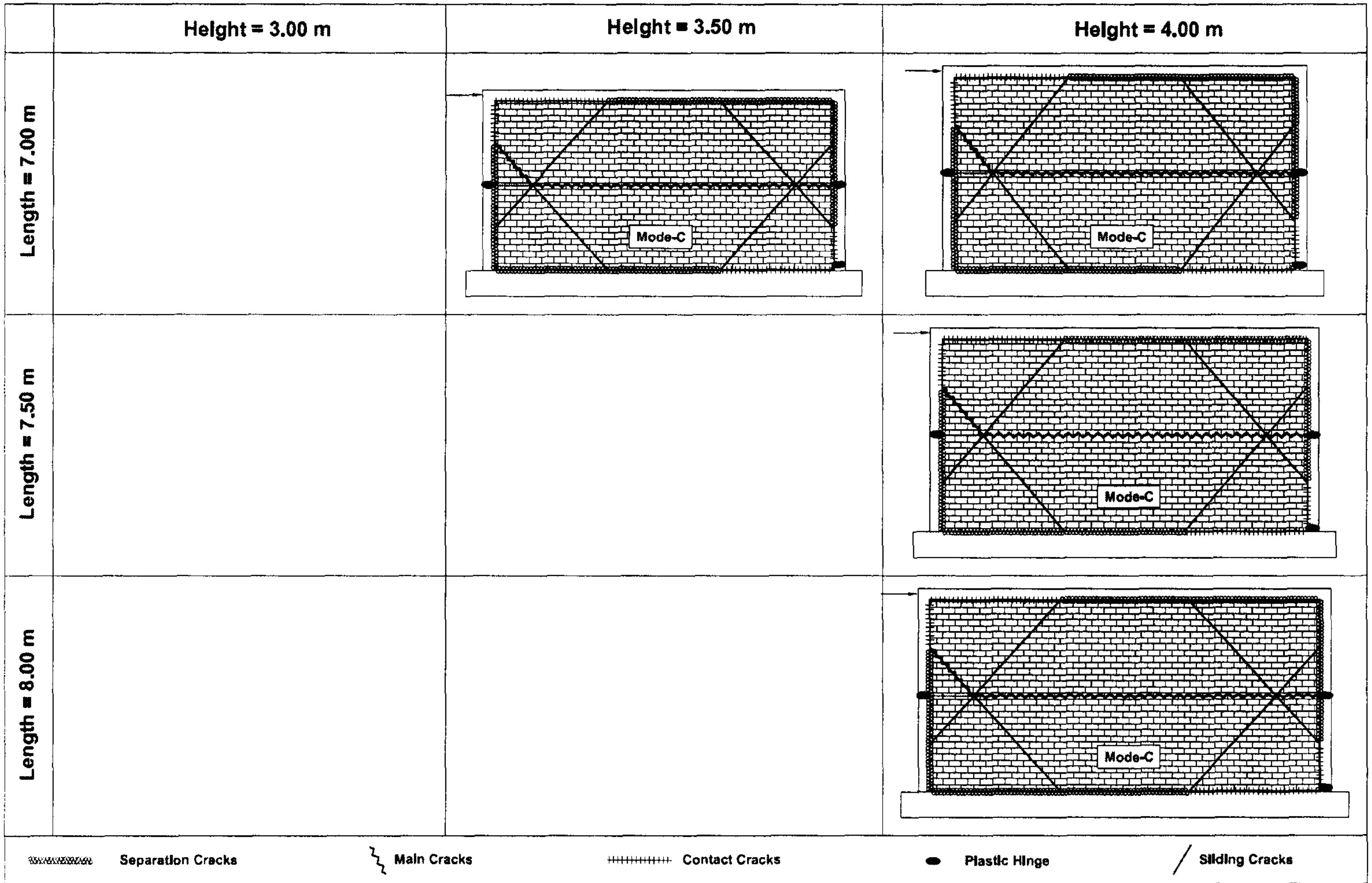

Fig. 5.16 Failure mechanisms for weak RC frames (Cont…)

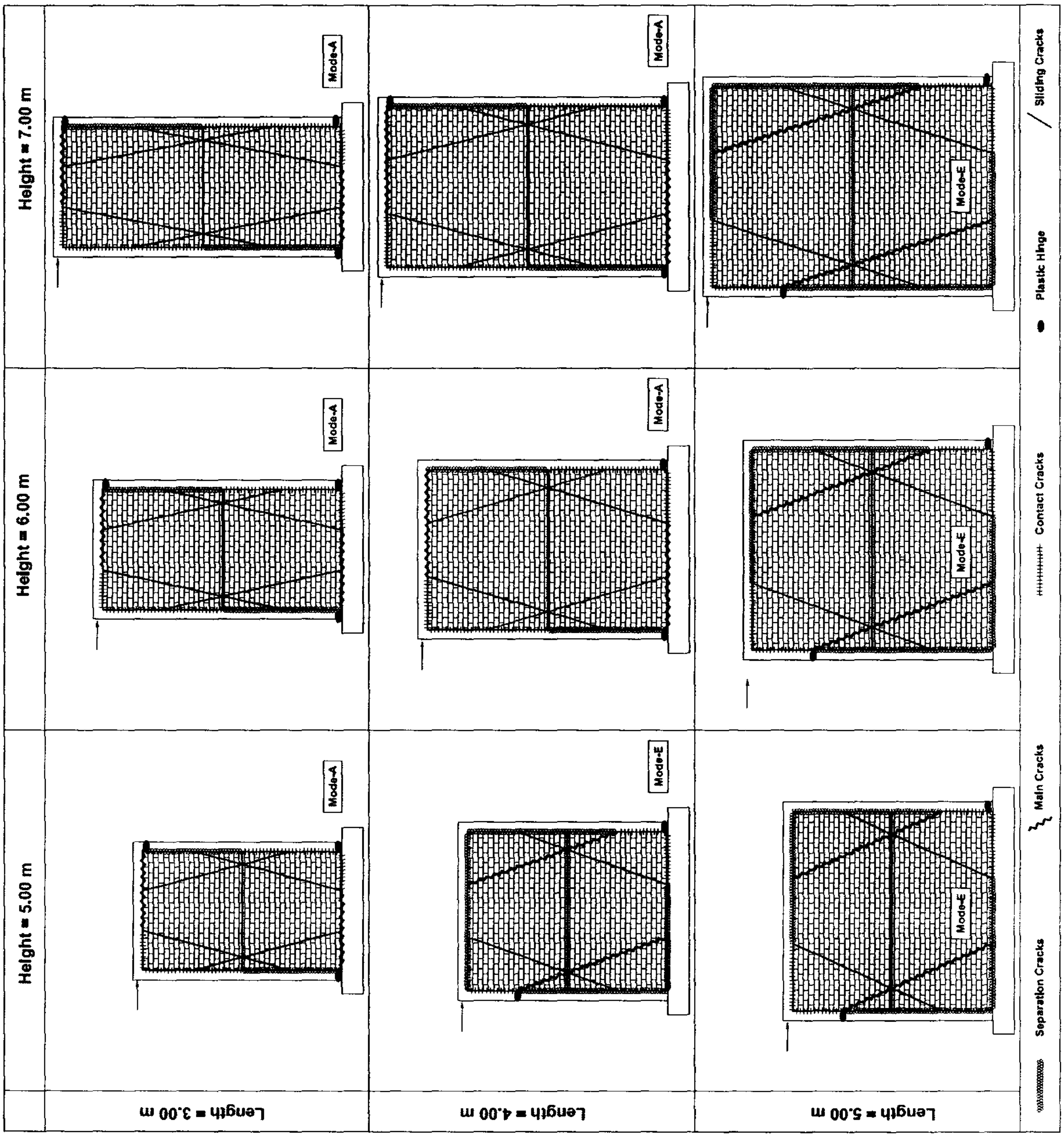

Fig. 5.16 Failure mechanisms for weak RC frames (Cont...)

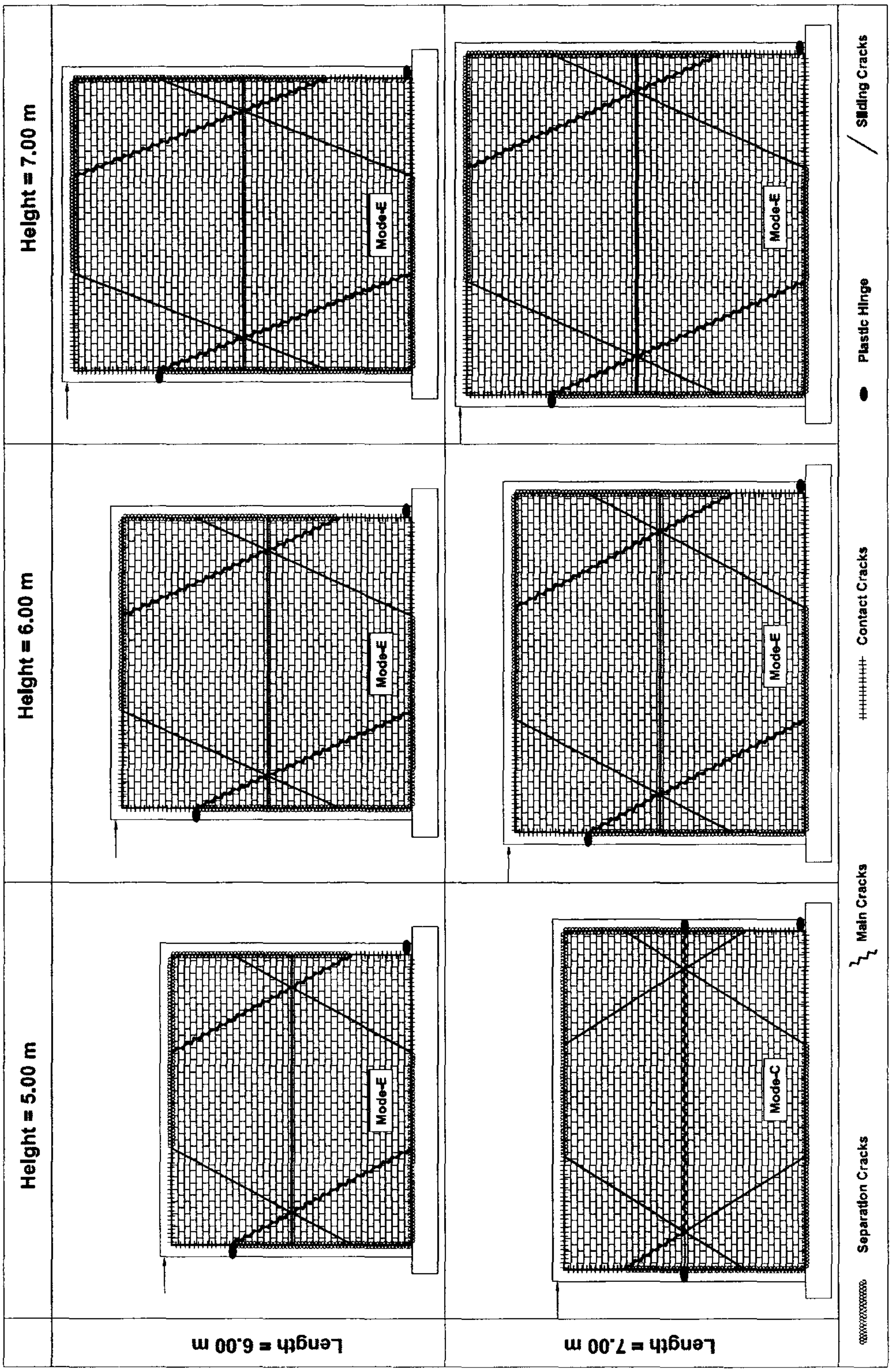

Fig. 5.16 Failure mechanisms for weak RC frames (Cont...)

5.4 DISCUSSION

The lateral load resistance of a strong frame is relatively higher than the capacity of the weak frame with the same infill type. The increase in the strength of strong relative to weak frames ranged between 17.9% for frames Group-N and –S (frames with height of H=7.00 m) and 22.3% for frames Group-H and –P (frames with height of H=3.00 m). The increase in displacements at failure of weak frame with respect to strong frames ranged between 2.8% for frames of maximum lateral displacements (Group-R for weak frames and Group-m for strong frame) and 18.4% for frames with minimum lateral displacement (Group-N and –X for strong and weak frames, respectively).

Ductility of all weak infilled frames shows higher values than the strong infilled frames. Comparing weak and strong frames in the case of maximum displacements, the ductility level of weak and strong frames are 29.65 and 24.5, respectively. For frames with maximum lateral load resistance, the ductility level of weak and strong frames are 13.5 and 12.4, respectively.

The results show that, strong infilled frames have significant lateral load resistance relative to the weak infilled frames. However, the variations in the ductility level between weak and strong frames are relatively low.

For both weak and strong frames, the peak displacements of all groups are lie on a straight line. This line can be used to predict the behaviour of infilled RC frames with different aspect ratios and heights between 3.0 and 7.0 m.

Failure modes of both infilled weak and strong frame are one of three failure modes (Mode-A, -C or –E) depending on the aspect ratio and strength of the RC frame.

There was numerical instability when analyzing frames with height more than 7.00 m, and the proposed model did not converge. This may be, due to one of the following reasons; 1) the relatively large size of the masonry element; 2) the small dimension of the columns and beams sections with respect to the over all dimensions of the infilled frames; 3) the high aspect ratio of the infilled frame especially for small spans.

Dynamic or cyclic loading are not considered in this analysis or results. However, some verifications and analysis will be conducted in the next chapter to study the capability of the proposed model to simulate cyclic behaviours of infilled frames.

5.5 SUMMARY

From the investigation conducted in this chapter the following points can be summarized:

- Type of infill, strong or weak, has strong effect on the capacity of the infilled frames.
- The most important factor that affects the failure mechanism of infilled RC frames is the aspect ratio of the infill panel.
- Type of RC frame, strong or weak, has small effect on the failure mechanism of the infilled frame.
- Type of RC frame has effect of approximately 25% on the overall strength of the infilled frame.

CHAPTER 6

CYCLIC LOAD ANALYSIS

6.1 INTRODUCTION

The objective of this chapter is to verify results of the developed finite element model for infilled RC frames under cyclic loading. Different aspect ratios, frame types (strong and weak), different loading conditions and different infill types are considered throughout the verification process. This chapter is divided into two sections.

In the first section, the influence of masonry infill panels on the seismic performance of RC frames that were designed in accordance with 1991 UBC provisions were investigated using the developed finite element model. These infilled RC frames were tested by Mehrabi et al. (1996). Two types of frames were considered. One frame was designed for wind loads and the other for strong earthquake forces. Six-½ scale, single-story, single-bay, frame specimens were tested. The parameters investigated include the strength of infill panels with respect to that of the boundary frame, the panel aspect ratio, the distribution of vertical loads, and the lateral-load history.

In the second section of this chapter, the influence of masonry infills on the seismic performance of RC frames designed to modern code provisions was investigated. Two types of masonry infills were considered that had different compressive strength but almost identical shear strength. Infills were designed so that the lateral cracking load of the solid infill was less than the available column shear resistance. Seven 1/3-scale, single-story, single-bay frame specimens were tested, by Kakaletsis and Karayannis (2008), under cyclic horizontal loading up to a drift level of 28%. The parameter investigated was the infill compressive strength. The assessment of the behaviour of the frames is presented in terms of failure modes, strength deterioration and stiffness degradation. The same infilled RC frames were analyzed using the proposed finite element model. A comparison between the analytical and experimental results in terms of failure mechanism, hysteresis behaviour, initial secant stiffness, and energy dissipation was carried out.

6.2 APPLICATION ONE

6.2.1 Test Frames

Performance of masonry-infilled RC frames under in-plane lateral cyclic loading was investigated experimentally and analytically by Mehrabi et al. (1996). The prototype frame selected in this study was a six-story three-bay, moment resisting RC frame, with a 13.5 m by 4.5 m (45 ft by 15 ft) tributary floor area at each story. The height/length (H/L) ratio for each bay was selected to be 1/1.5 (0.67). The design gravity loads were according to UBC (1991). The service live load was taken to be 2.39 kPa (50 psf), and the dead load was estimated to be 6.21 kPa (130 psf). Two types of frames were designed with respect to lateral loading. One was a "weak" frame, which was designed for lateral wind pressure of 1.24 kPa (26 psf), corresponding to basic wind speed of 160 km/h (100 mph). The second frame was a "strong" frame, which was designed for a set of equivalent static force according to Seismic Zone 4 in the UBC (1991). The former type of frame represented existing RC frames that do not meet the detailing requirements of the current seismic design provisions. The frames were designed in accordance with the provisions of ACI 318 (1989). In the design of the frames, the contribution of infill panels to the lateral load resistance was not considered.

The test specimens were chosen to be 1/2-scale frame models representing the interior bay at the bottom story of the prototype frame. The design details for the weak and strong frames are shown in figure 6.1. The design of the weak frame is shown in figure 6.1(a), which had weak columns and strong beams. The strong frame is shown in figure 6.1(b). The columns were larger than the columns of weak frame with closely spaced ties near the ends. The beam design in the strong frame was identical to that in the weak frame, except that the former had more shear reinforcement in critical regions. Although the strong frame had height/length ratio of about 1/1.5, two H/L ratios were considered for the weak frame, which were approximately 0.67 and 0.48. A frame with the lower H/L ratio is shown with a masonry infill in figure 6.1(c). The beam and column cross sections for strong and weak frames are shown in figure 6.1. For infill panels, 0.1 × 0.1 × 0.2 m (4 × 4 × 8 in) hollow and solid concrete masonry blocks were used in test specimens to represent weak and strong infill respectively.

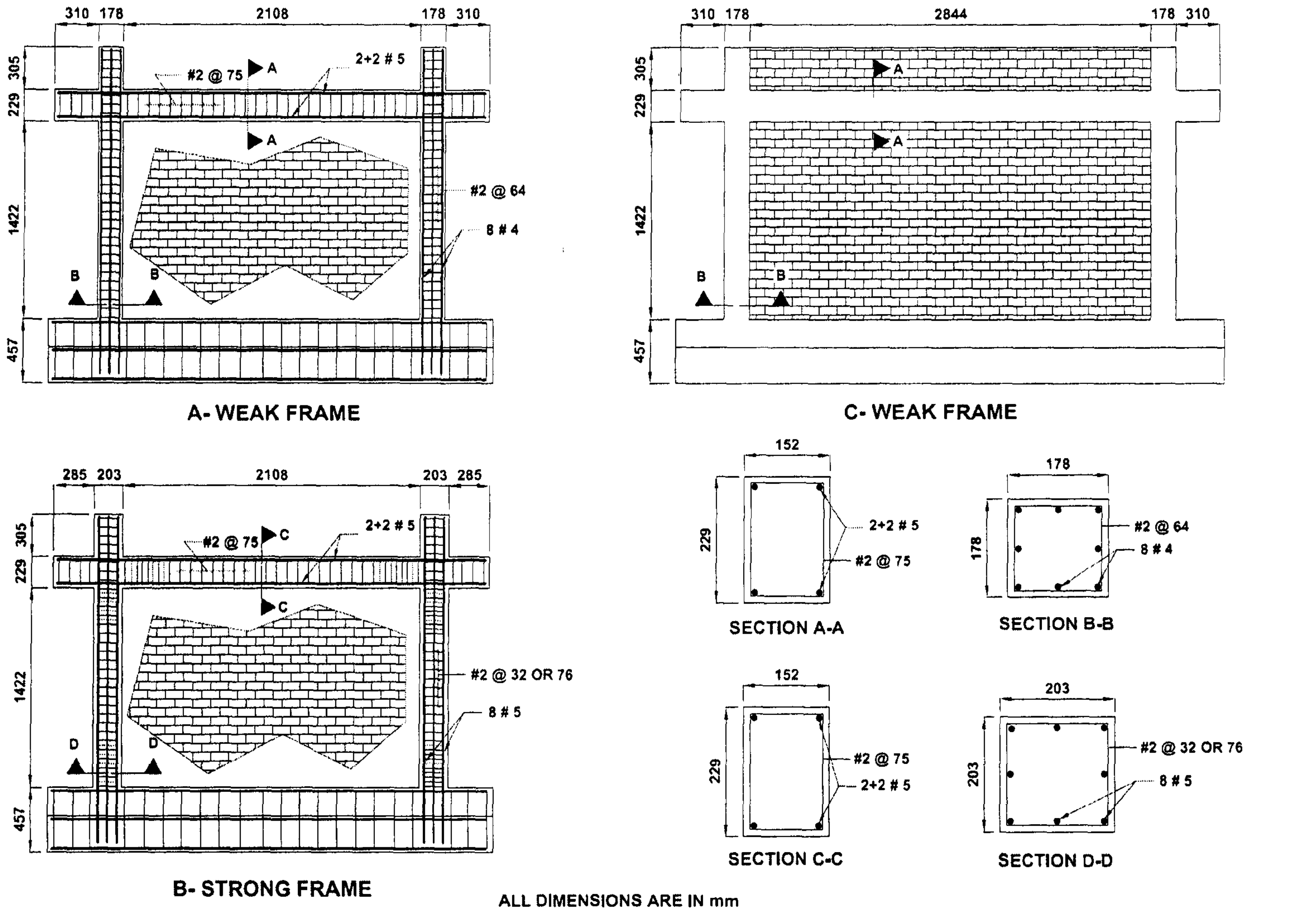

Fig. 6.1 Design test specimen: A- Weak frame (H/L = 0.67); B- Strong frame (H/L = 0.67); C- Weak frame (H/L = 0.48)

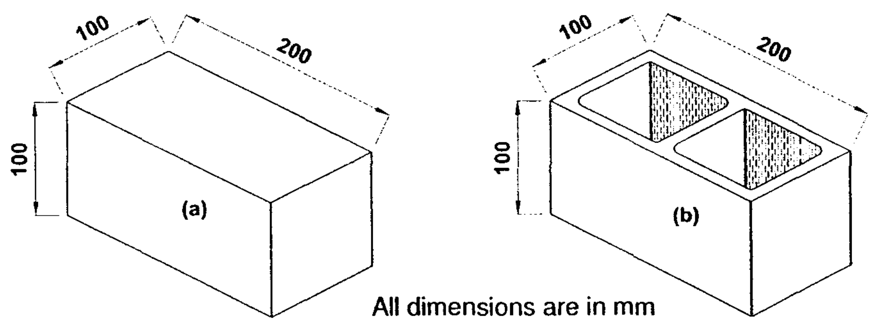

Fig. 6.2 Masonry units: (a) Solid; (b) Hollow.

Six specimens were tested under cyclic lateral load. For each specimen distributed load and concentrated loads were applied to the top beam and the two columns respectively to represent the loads from upper stories. The specimens were subjected to different combinations of vertical and lateral loads. The vertical load applied onto the specimen was maintained constant during each test. Two different vertical load distributions were employed: one with vertical loads applied onto the beam only, and the other with 1/3 of total vertical load applied onto the beam and 2/3 onto the columns. Details of the applied load to each specimen are shown in Table 6-1.

TABLE 6.1 Test specimens under cyclic lateral loads. Mehrabi et al. (1996).

Specimen number (1)	Type of frame (2)	Type of masonry units (3)	Panel aspect ratio (H/L) (4)	Lateral load (5)	Vertical load distribution (kN) Columns (6)	Beams (7)
4	Weak	Hollow	0.67	Cyclic	196	98
5	Weak	Solid	0.67	Cyclic	196	98
6	Strong	Hollow	0.67	Cyclic	196	98
7	Strong	Solid	0.67	Cyclic	196	98
11	Weak	Solid	0.48	Cyclic	196	98
12	Weak	Solid	0.48	Cyclic	294	147

6.2.2 Material Properties

Material tests were conducted on the reinforcing steel, concrete and masonry samples for each infilled frame specimen. The material properties are summarized in Tables 6-2 and 6-3. The compressive strength of the hollow units given in column (10) was based on the net cross-sectional area, where as the compressive strength of the hollow prisms given in column (8) was based on the cross-sectional area of the face shell only.

TABLE 6-2 Average strength of concrete and masonry material Mehrabi et al. (1996).

Specimen number	Frame Concrete					Three-Course Masonry Prisms			Compressive strength of masonry units (MPa)	Compressive strength of mortar cylinder (MPa)
	Secant modulus (MPa)	Compressive strength (MPa)	Strain at peak stress	Modulus of rupture (MPa)	Tensile strength (MPa)	Secant modulus (MPa)	Compressive strength (MPa)	Strain at peak stress		
(1)	(2)	(3)	(4)	(5)	(6)	(7)	(8)	(9)	(10)	(11)
4	17,237	26.8	0.0027	4.86	2.77	4,600	10.62	0.0030	16.48	11.17
5	18,065	22.8	0.0026	4.38	1.82	8,950	13.86	0.0023	15.59	13.38
6	19,858	25.9	0.0024	4.91	3.14	4,200	10.14	0.0032	16.48	16.76
7	18,617	33.4	0.0030	5.13	2.26	9,080	13.59	0.0026	15.59	15.52
11	18,134	25.7	0.0028	4.25	3.09	9,610	11.45	0.0025	15.58	13.03
12	20,134	26.9	0.0021	4.75	2.98	7,340	13.29	0.0029	15.58	17.86

TABLE 6-3 Average tensile strength of reinforcing steel

Bar size (1)	Type of bar (2)	Nominal diameter (mm) (3)	Yield stress (MPa) (4)	Ultimate stress (MPa) (5)
no. 2	Plain	6.35	367.6	449.6
no. 4	Deformed	12.7	420.7	662.1
no. 5	Deformed	15.9	413.8	662.1

6.2.3 Loading Routine

The cyclic load tests started with five cycles of load control, in which the amplitude of the load was increased gradually until the lateral load was slightly lower than the load at which a major crack was expected to occur in the infill. The cracking load for the infill was estimated from the analysis of specimens subjected to monotonically increasing lateral loads. The displacement controlled cycles started from amplitude of 3.8 mm, which was increased in increments of 3.8 mm. Each specimen was subjected to three fully reversed displacement cycles at each amplitude level. The 3.8 mm displacement was the level about which a major crack was expected to initiate in an infill panel. For each specimen the lateral load-displacement hysteresis curve and the crack pattern were plotted.

6.2.4 Analysis

All specimens were reanalyzed using the proposed model. Each specimen was subjected to one fully reversed displacement cycles at each amplitude level. The amplitude level used was 3.8 mm, similar to that used through the experimental program. To verify the numerical results, all specimens were reanalyzed using IDARC-2D (Version 6.1, 2006) software. In the developed model, the masonry wall was modeled using 10 quadrilateral isoparametric elements connected on the prescribed failure planes with contact zero-length elements. In the IDARC-2D model, the masonry wall was modeled using one rectangular element connected to the surrounding frames at the corner points only. Modeling of the RC frame using the developed model and IDARC-2D model are presented in figure 6.3. In the figure W is the uniformly distributed load, P is the concentrated vertical load, C is the lateral cyclic load and M is the masonry elements.

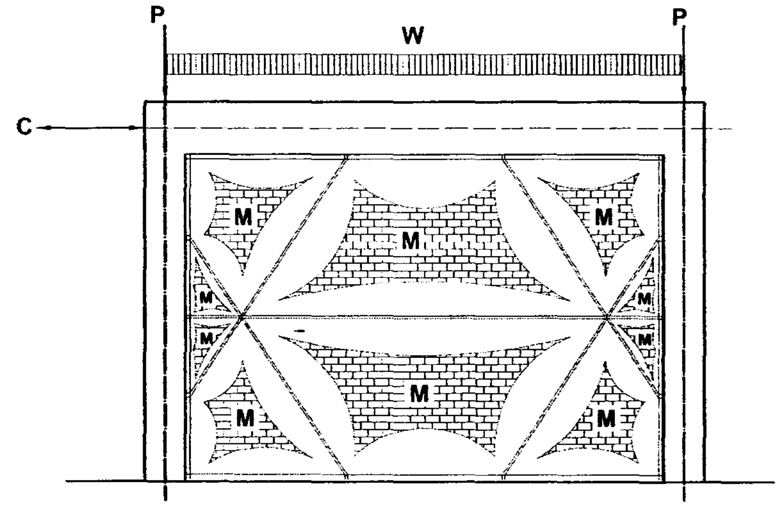

(a)

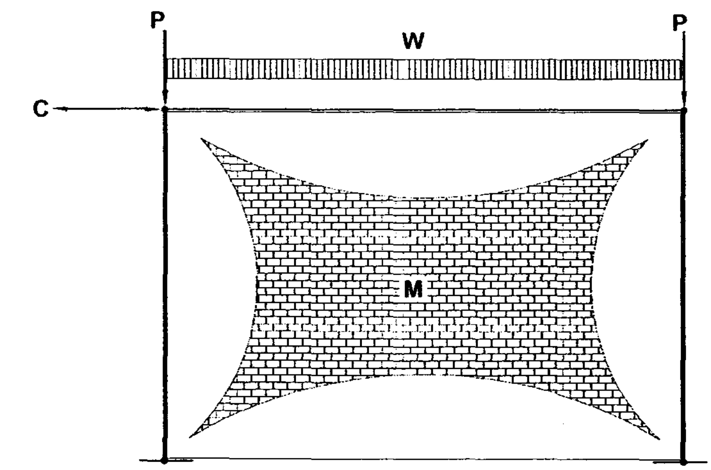

(b)

Fig. 6.3 Infilled RC model: (a) proposed model; (b) IDARC-2D model.

6.2.5 Results

The lateral load-displacement hysteretic curve and the failure mechanism of the experimental, proposed model and IDARC-2D model for each specimen are plotted in figures 6.4 through 6.33. The envelope curves of the experimental and analytical results are also plotted for each specimen.

6.2.5.1 Weak frame (aspect ratio 0.67)

Mehrabi et al. (1996) conducted a test on a weak frame without infill panel. The lateral load resistance of the bare weak frame was 106.3 kN and the maximum lateral displacement was 65.28 mm. The bare frame test is labelled specimen # 1W. For the case of cyclic loading, the secant stiffness is the slope of the line connecting the extreme points of a small amplitude displacement cycle. The secant stiffness, relative secant stiffness, maximum lateral load, relative maximum load, displacement at maximum load and relative maximum displacement for specimens 1w, 4 and 5 are summarized in Table 6-4.

TABLE 6-4 Results of weak bare and infilled frames with aspect ratio of 0.67 (specimens # 1W, 4 and 5)

Spec. # (1)	Case (2)	Secant stiffness (kN/mm) (3)	Relative secant stiffness Infilled/bare frame (4)	Max. lateral load (kN) (5)	Relative max. load Infilled/bare frame (6)	Displacement at max. load (mm) (7)	Relative max. displacement Infilled/bare frame (8)
1W	Experimental	4.2	---	106.23	---	65.28	---
	Proposed model	---	---	---	---	---	---
	IDARC-2D	---	---	---	---	---	---
4	Experimental	75.3	17.93	-153 , +162	-1.44 , +1.53	-7.1 , +11.9	-0.11 , +0.18
	Proposed model	84.4	20.10	-182, +182	-1.77 , +1.77	-10.1 , +10.1	-0.15 , +0.15
	IDARC-2D	78.6	18.71	-196 , +196	-1.85 , +1.85	-11.9 , +11.9	-0.18 , +0.18
5	Experimental	224.2	53.37	-232 , +267	-2.18 , +2.52	-15.2 , +9.14	-0.23 , +0.14
	Proposed model	235.5	56.1	-263 , +263	-2.48 , +2,48	-13.8 , +13.8	-0.21 , +0.21
	IDARC-2D	176.6	42.05	-224 , +224	-2.11 , +2.11	-12.0 , +12.0	-0.18 , +0.18

As shown by specimens 1, 4 and 5, the stiffness of a weak frame-weak panel specimen was about 18 times that of a bare frame, while that of a weak frame-strong panel was approximately 50 times. The maximum load resistance of a weak frame-weak panel specimen was approximately 1.5 times that of a bare frame, while the resistance of a weak frame-strong panel specimen was approximately 2.3 times.

A- Infilled frame test 4

Specimen number 4 was a weak frame with weak infill panel with an aspect ratio of 0.67. The hysteresis curves resulting from experimental program by Mehrabi et. al. (1996), the proposed model and the IDARC-2D model are shown in figures 6.4, 6.5 and 6.6, respectively. The load-displacement envelops for the three results are shown in figure 6.7. Both OpenSees model and IDARC-2D model give good simulation of the experimental behaviour.

The failure patterns for the experimental, proposed model and IDARC-2D model were presented in figure 6.8. The experimental results showed that, the first major damage observed in specimen number 4 was a diagonal/sliding crack in the infill, which coincided with the maximum lateral loads. As the amplitude of displacement cycles increased, large slips occurred along the bed joints, which resulted in the crushing and degradation of mortar joints. The yielding of the longitudinal reinforcement was first detected in the columns. At higher displacement amplitudes, crushing occurred in the infills at the corners and inside the panel.

According to the proposed model, the cracks in the infill panel started as a diagonal crack near the corner of the loaded point in direction of mid-height of the panel. This diagonal crack was followed by a sliding crack at the mid-height failure surface, and then followed by another diagonal crack in the opposite direction of the loaded point. Plastic hinges in the RC frame were located near the upper end of the column (near to beam-column connection) and at the bottom of the columns (just above the support point). These locations are compatible with the locations observed during the test.

In the IDARC-2D model, no cracks are shown in the infill panel because IDARC-2D uses one element to model the infill panel. The locations of plastic hinges were at the top beam (near to the beam-column connection). No plastic hinges were shown at the upper end of columns. However, two plastic hinges were located at the bottom of the both columns just above the support point. Some cracks at the top of columns were observed. Most likely, this behaviour occurred because the infill panel was modeled in the IDARC-2D as one rectangular 4 node element connecter with the surrounding frame at its four corners.

Figures 6.4 to 6.8, show that the proposed model is capable of simulating the overall behaviour of both infill panel and the surrounding RC frame. The model can also predict the location of cracks of the infill panel and location of plastic hinges/shear cracks and failure mode of the RC frame. However, the IDARC-2D model can produce the overall cyclic behaviour of the infilled frame, but it can not predict the failure mechanism of the RC frame correctly. This is because the infill panel was considered as one element in the IDARC-2D model.

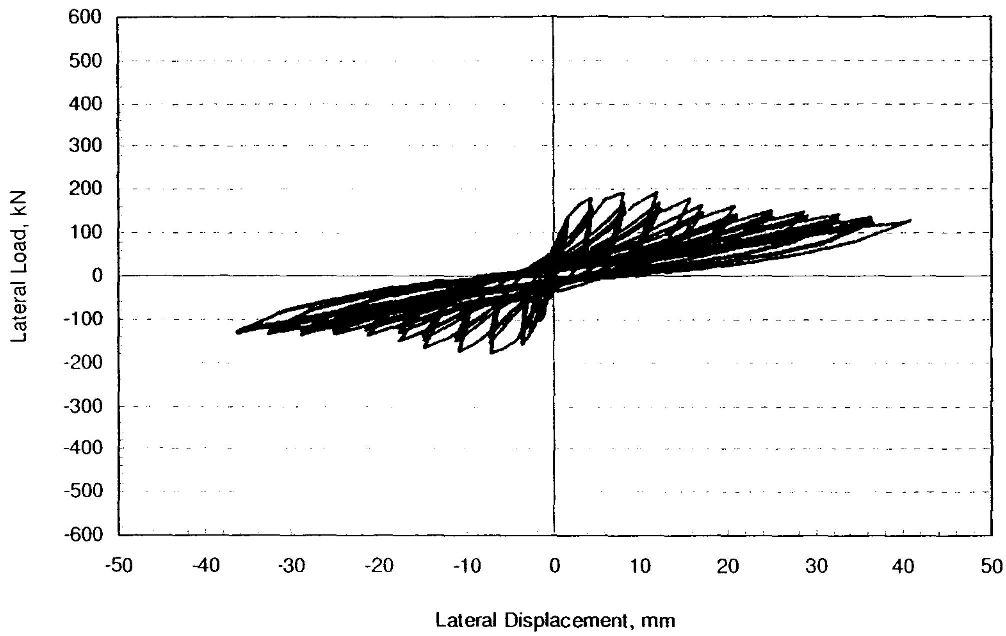

Fig. 6.4 Experimental lateral load-displacement hysteresis curves for specimen # 4 (Mehrabi et al., 1996)

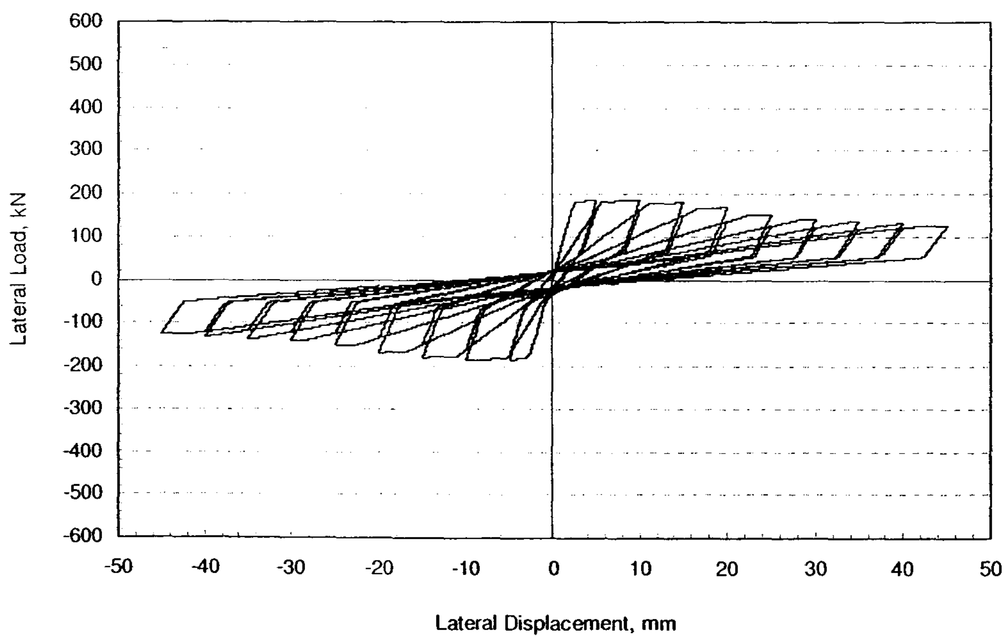

Fig. 6.5 Lateral load-displacement hysteresis curves for specimen # 4 (Proposed model-OpenSees)

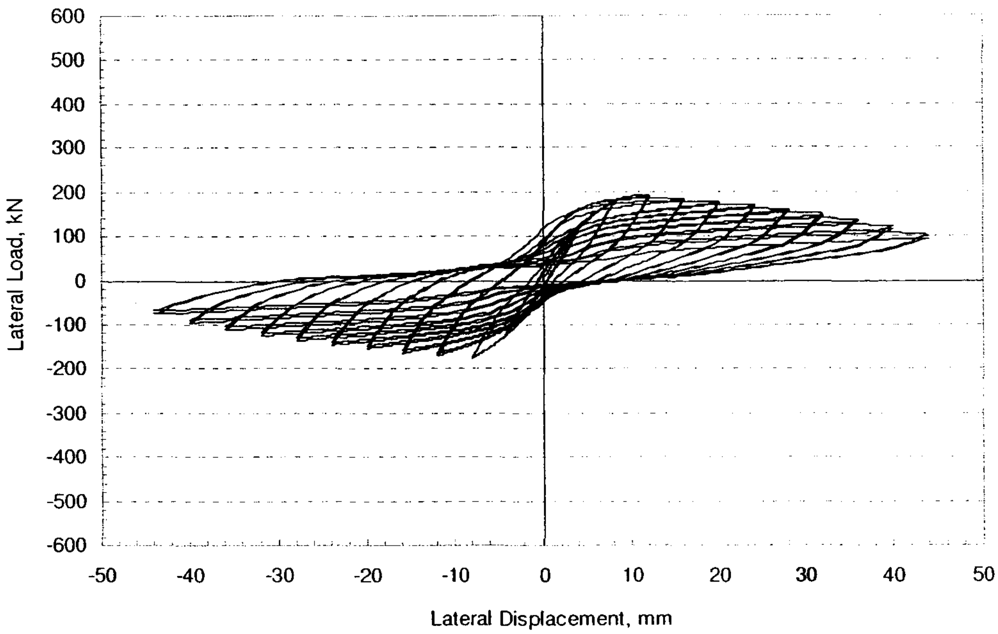

Fig. 6.6 Lateral load-displacement hysteresis curves for specimen # 4 (IDARC 2D-V6.1, 2006)

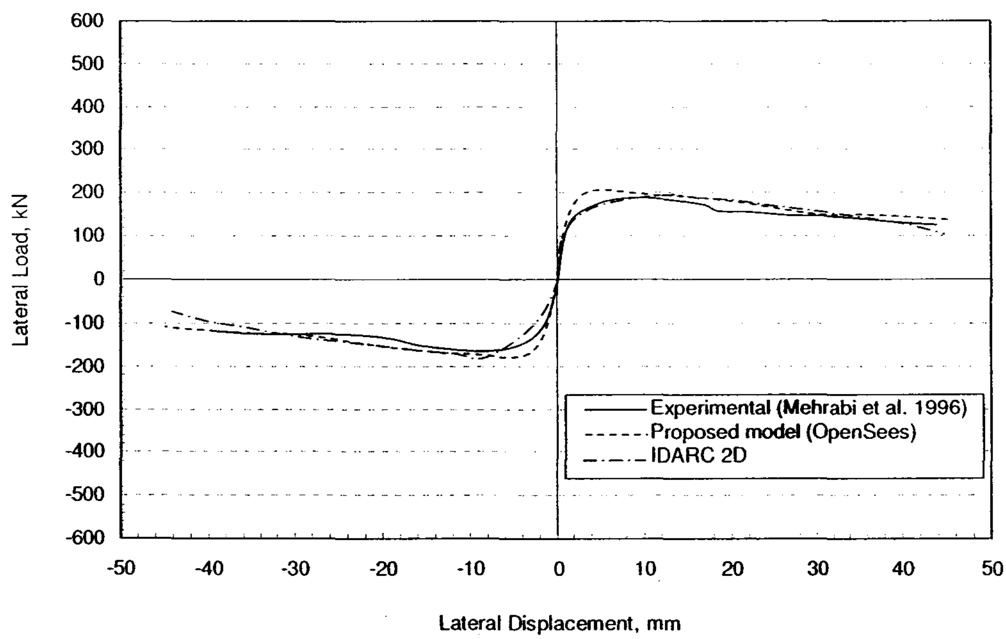

Fig. 6.7 Lateral load-displacement envelopes for specimen # 4

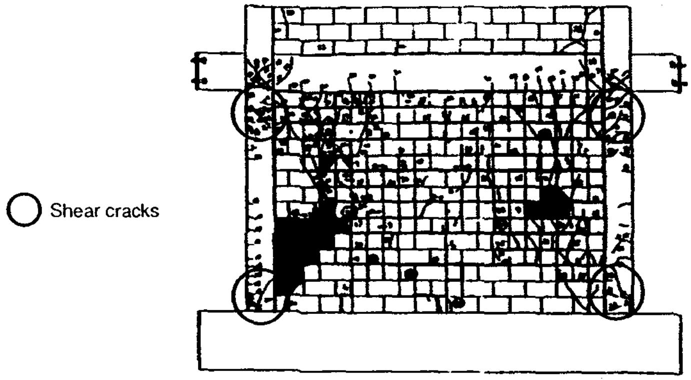

a- Mehrabi et al. (1996).

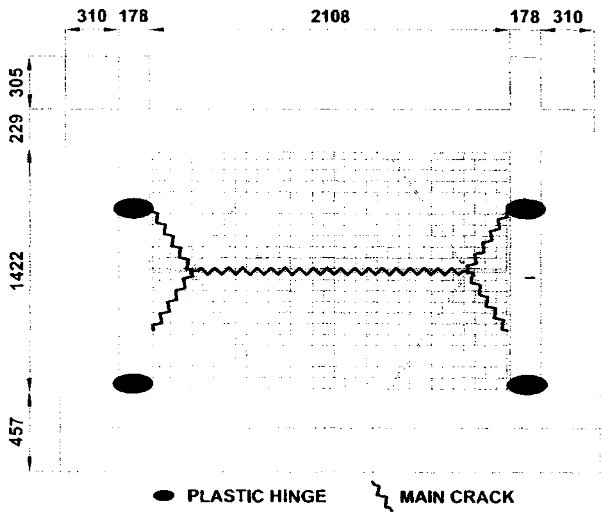

b- Proposed model (OpenSees)

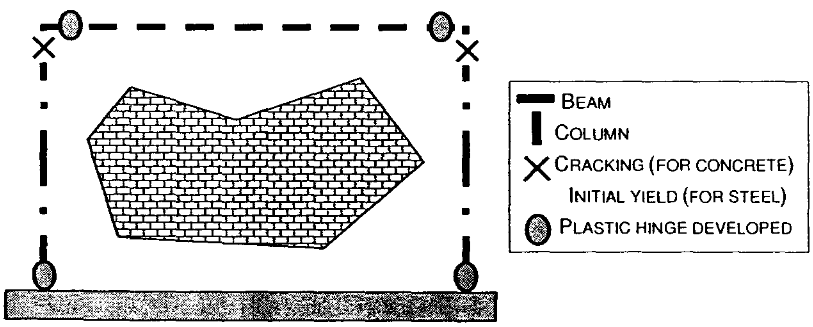

c- IDARC 2D (Versions 6.1, 2006)

Fig. 6-8 Failure mechanism of specimen # 4

B- Infilled frame test 5

Specimen number 5 was a weak frame with strong infill panel and had an aspect ratio of 0.67. The hysteresis curves resulting from the experimental program by Mehrabi et. al. (1996), the proposed model and the IDARC-2D model are shown in figures 6.9, 6.10 and 6.11, respectively. The load-displacement envelopes for the experimental and analysis results are shown in figure 6.12.

The hysteretic curve envelops of the experimental, proposed model and IDARC-2D model (figure 6.12), shows that the hysteretic behaviour of proposed model is closer to the experimental results than the IDARC-2D model. However, the proposed model slightly over estimates experimental results while the IDARC-2D model grossly under estimate the experimental results. The proposed model is capable of producing approximately the same secant stiffness as the experimental results.

The failure mechanism of the experimental, proposed model and IDARC-2D model were shown in figure 6.13. As shown by the hysteresis curves, the maximum load was higher while the strength deterioration in this specimen was faster than that in specimen 4, which had weak panel. However, in spite of the shear failure of columns, the energy dissipation of this specimen appears to be higher than the case of specimen 4 (Mehrabi et al., 1996). The diagonal/sliding cracks in the infills were first observed, by Mehrabi et al. (1996), at the maximum lateral loads. They were followed immediately by shear cracks in the columns. As the amplitude of displacement cycles increased, crushing developed in the infill.

As shown in figure 6.13(b), the failure mechanism according to the proposed model, cracks in the infill panel started as a diagonal crack near the corner of the loaded point in direction of mid-height of the panel. This diagonal crack was followed by a sliding crack at the mid-height failure surface, and then followed by another diagonal crack in the opposite direction of the loaded point. Plastic hinges in the RC frame are located at the top end of columns, near to beam-column connection and at the bottom of the columns (just above the support point). These locations are approximately the same locations that were observed during the test.

The IDARC-2D model, could not predict the cracking in the infill panel, since the model considers the infill panel as one rectangular element. The locations of plastic hinges are in the top beam close to the beam-column connection. No plastic hinges were formed in the upper end of columns. However, two plastic hinges are located at the bottom of the both columns just above the support point. Some cracks at the top of columns occurred. Most likely, this behaviour of the infilled frame occurred due to considering the whole infill panel as one rectangular element.

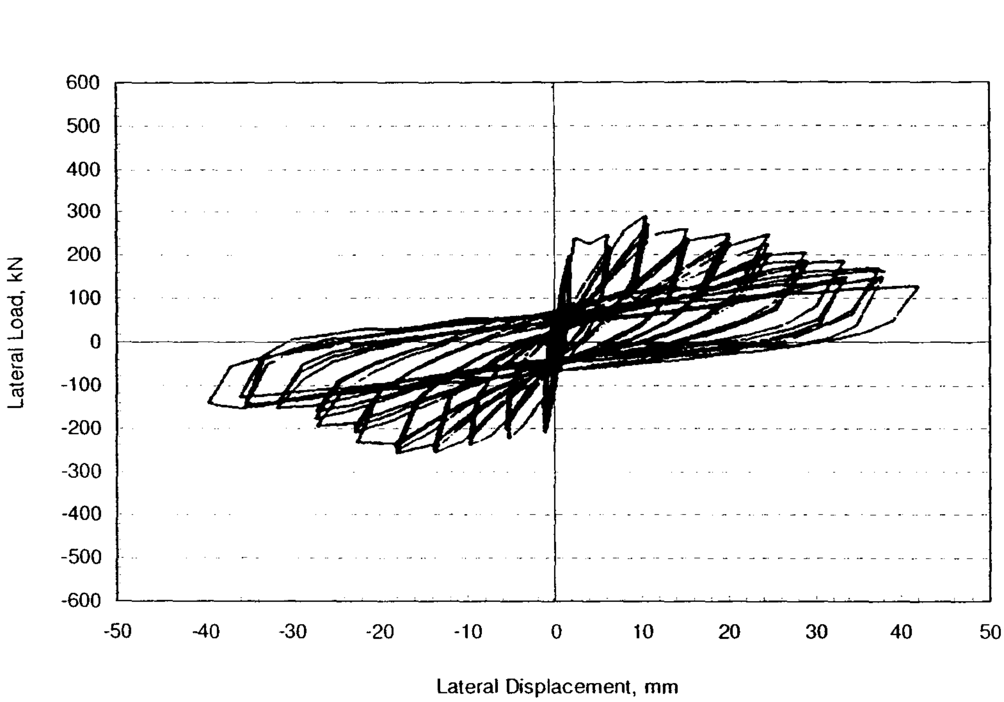

Fig. 6.9 Experimental lateral load-displacement hysteresis curves for specimen # 5 (Mehrabi et al., 1996)

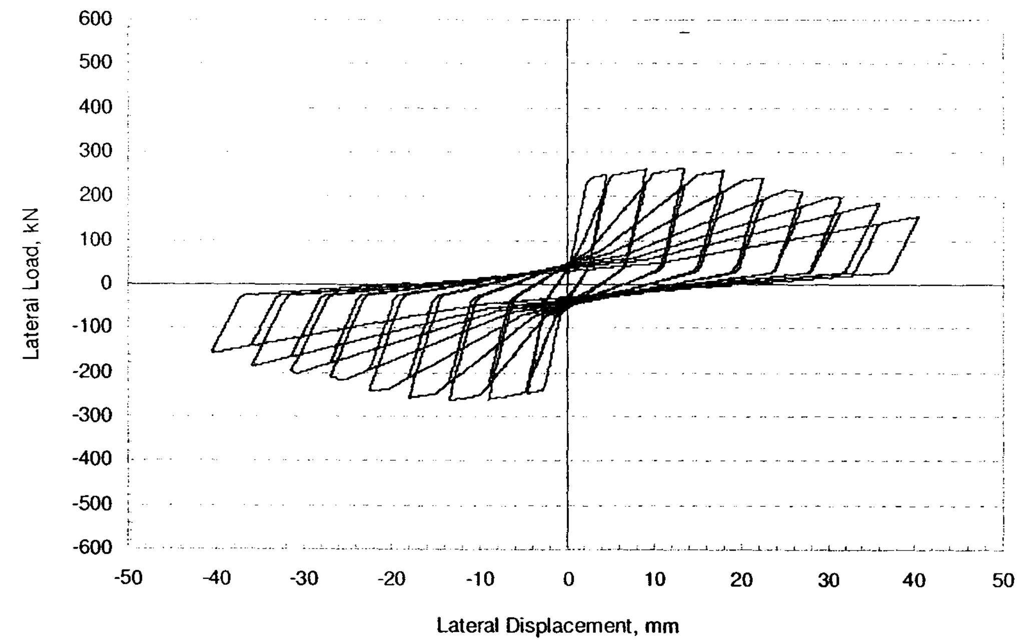

Fig. 6.10 Lateral load-displacement hysteresis curves for specimen # 5 (Proposed model-OpenSees)

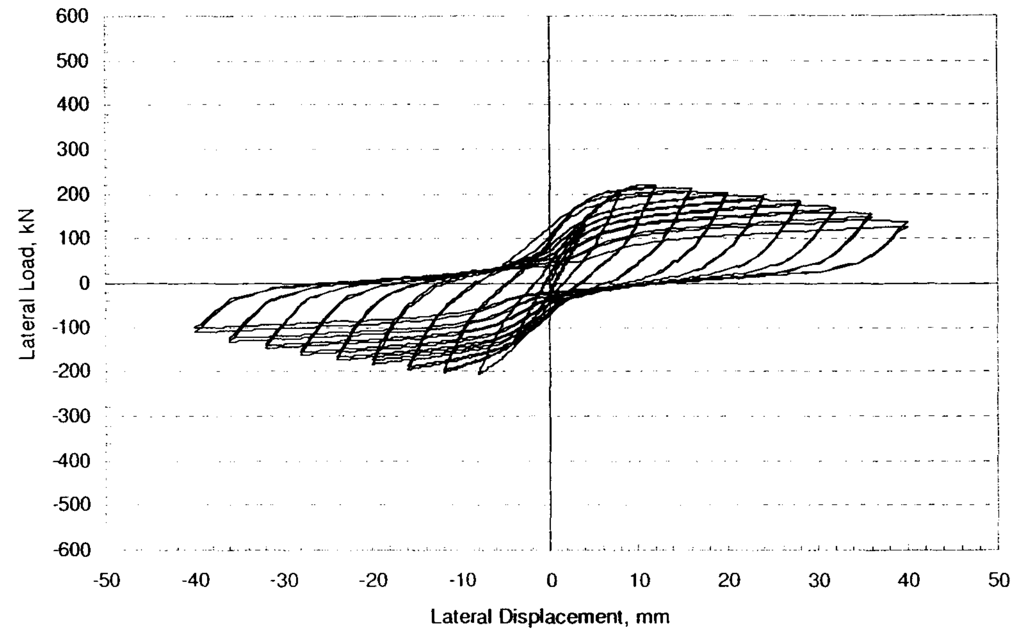

Fig. 6.11 Lateral load-displacement hysteresis curves for specimen # 5 (IDARC 2D-V6.1, 2006)

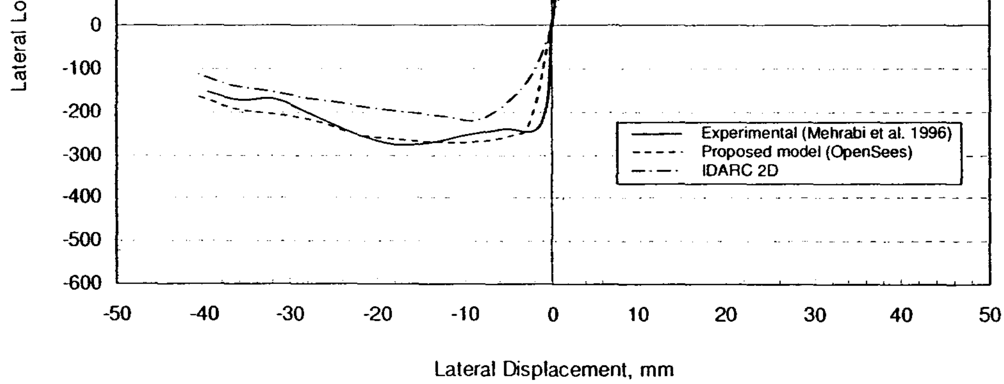

Fig. 6.12 Lateral load-displacement envelopes for specimen # 5

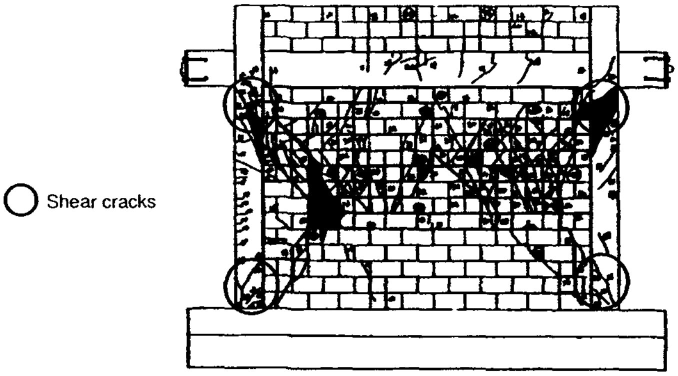

a- Mehrabi et al. (1996).

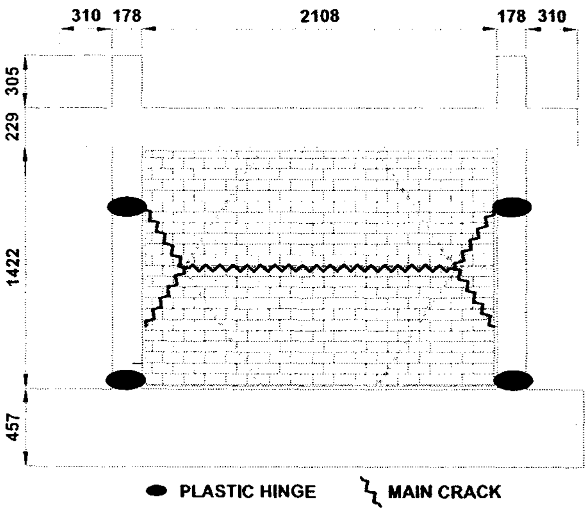

b- Proposed model (OpenSees)

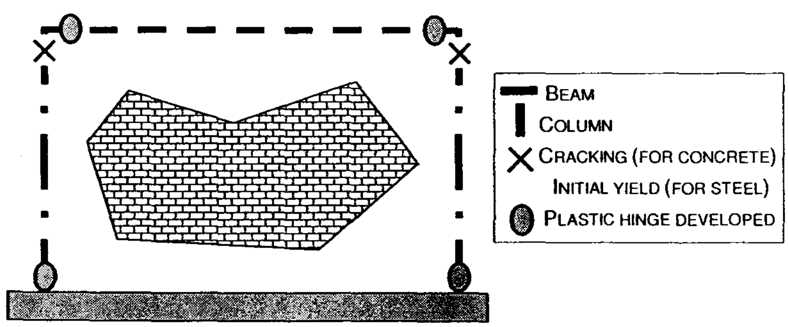

c- IDARC 2D (Versions 6.1, 2006)

Fig. 6.13 Failure mechanism of specimen # 5

6.2.5.2 Strong frame (aspect ratio 0.67)

No test was conducted on a strong frame without infill panel. However, the lateral resistance of the strong frame was estimated by Mehrabi et al. (1996) to be 145 kN, which had been computed theoretically but with a 15% increase to account for possible discrepancy between the actual and theoretical values. The maximum lateral displacement was 32.46 mm. The secant stiffness, relative secant stiffness, maximum lateral load, relative maximum load, displacement at maximum load and relative maximum displacement for specimens 1S, 6 and 7 are summarized in Table 6-5

TABLE 6-5 Results of strong bare and infilled frames with aspect ratio of 0.67 (specimens # 1S, 6 and 7)

Spec. # (1)	Case (2)	Secant stiffness (kN/mm) (3)	Relative secant stiffness Infilled/bare frame (4)	Max. lateral load (kN) (5)	Relative max. load Infilled/bare frame (6)	Displacement at max. load (mm) (7)	Relative max. displacement Infilled/bare frame (8)
1S	Mehrabi et al.	8.4	---	145.00	---	32.46	---
	Proposed model	---	---	---	---	---	---
	IDARC-2D	---	---	---	---	---	---
6	Mehrabi et al.	84.06	10.00	-188 , +207	-1.30 , +1.43	-8.9 , +9.7	-0.27 , +0.30
	Proposed model	97.4	11.60	-213, +213	-1.47 , +1.47	-13.1 , +13.1	-0.41 , +0.41
	IDARC-2D	75.6	9.00	-222 , +222	-1.53 , +1.53	-12 , +12	-0.38 , +0.38
7	Mehrabi et al.	255.7	30.44	-489 , +445	-3.37 , +3.07	-11.4 , +10.2	-0.35 , +0.31
	Proposed model	266.5	31.73	-460 , +460	-3.17 , +3.17	-12.1 , +12.1	-0.37 , +0.37
	IDARC-2D	242.6	28.89	-453 , +453	-3.15 , +3.15	-9.2 , +9.2	-0.28 , +0.28

Where " + " represent push and " - " represent pull.

Comparing the lateral resistance of strong bare frame to the strength developed by specimens 6 and 7 indicated that the maximum resistance of the strong frame were increased due to the weak and strong infills by factors of 1.4 and 3.2, respectively. Furthermore, frame with strong panels exhibited much better hysteretic energy dissipation than that of a frame with weak panel, regardless of the frame design.

As shown by specimens 1S, 6 and 7, the stiffness of a strong frame-weak panel specimen was about 10 times as higher than that of a bare frame, while that of a strong frame-strong panel was about 30 times.

The proposed model estimated maximum lateral load better than IDARC-2D model except for the positive load cycle of specimen # 7 (column (5) Table 6-5). The proposed model overestimated the displacement at maximum load, while the IDARC model underestimated the displacement at maximum load (column (7) of Table 6-5). The reason behind this behaviour was because the proposed analysis models the masonry panel using 10 2-D finite elements in addition to a number of contact elements which allow for more lateral displacements. The IDARC-2D model, masonry panel was represented by one element connected with the surrounding frame at corners.

A- Infilled frame test 6

Specimen number 6 was a strong frame with weak infill panel and had an aspect ratio of 0.67. The hysteresis curves resulting from the experimental program by Mehrabi et. al. (1996), the proposed model and the IDARC-2D model are shown in figures 6.14, 6.15 and 6.16, respectively. The load-displacement envelops for the three curves are shown in figure 6.17. The figure indicates that the behaviour of proposed model and IDARC-2D model were similar to the test. However, the proposed model overestimated the experimental results, while the IDARC-2D model underestimated the test results.

The behaviour of specimen number 6 was quite similar to that of specimen number 4, but its lateral strength was 28% higher than that of specimen 4. Unlike specimen 4, slip was first observed in specimen 6 along the bed joint at the beam-to-wall interface, and the yielding of longitudinal reinforcement in the beam occurred prior to that in the columns.

No failure pattern was provided by Mehrabi et al. (1996) for specimen number 6. However, the failure patterns for specimen number 6 given by proposed model and IDARC-2D model are shown in figure 6.18. According to the proposed model, the cracks in the infill panel started as a diagonal crack near the corner of the loaded point in direction of mid-height of the panel. This diagonal crack is followed by a sliding crack at the mid-height failure surface, and then followed by another diagonal crack in the opposite direction of the loaded point. Plastic hinges in the RC frame are located near the upper end of the column (near to beam-column connection) and at the bottom of the columns (just above the support point). These locations are compatible with the locations observed during the test by Mehrabi et al. (1996).

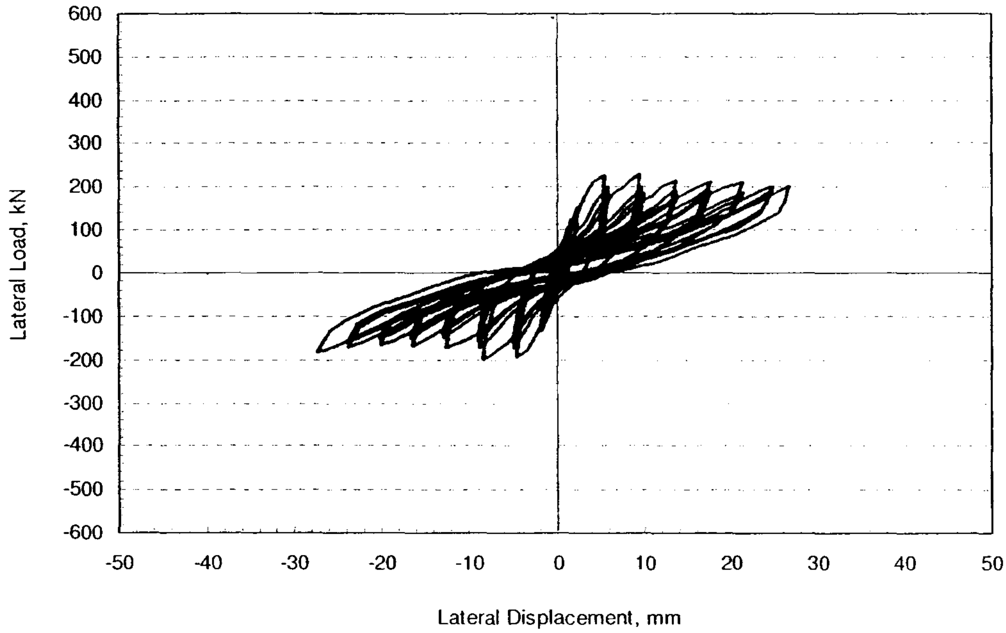

Fig. 6.14 Experimental lateral load-displacement hysteresis curves for specimen # 6 (Mehrabi et al., 1996)

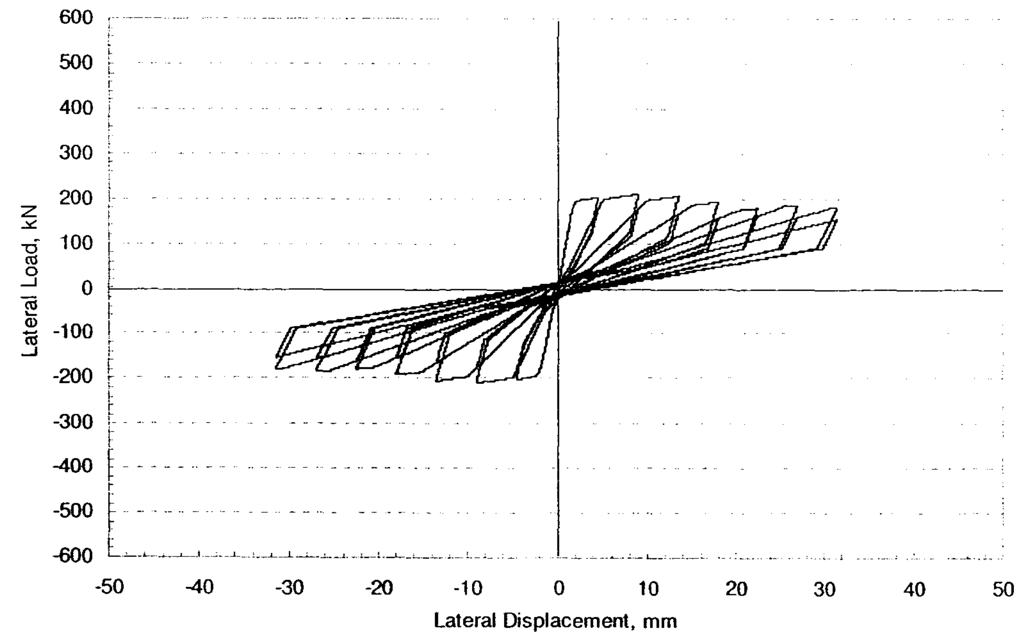

Fig. 6.15 Lateral load-displacement hysteresis curves for specimen # 6 (Proposed model-OpenSees)

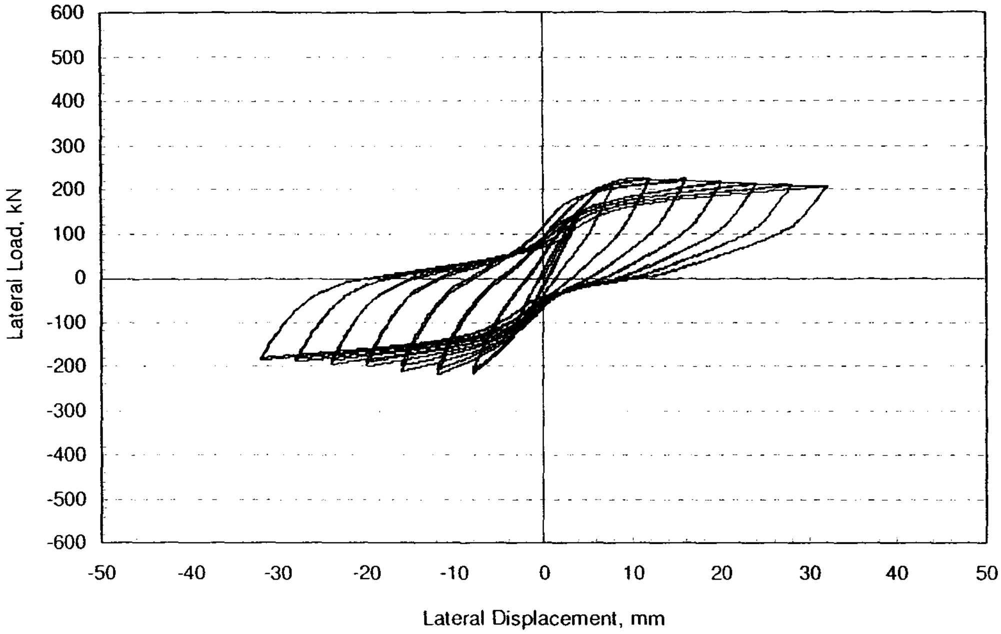

Fig. 6.16 Lateral load-displacement hysteresis curves for specimen # 6 (IDARC 2D-V6.1, 2006)

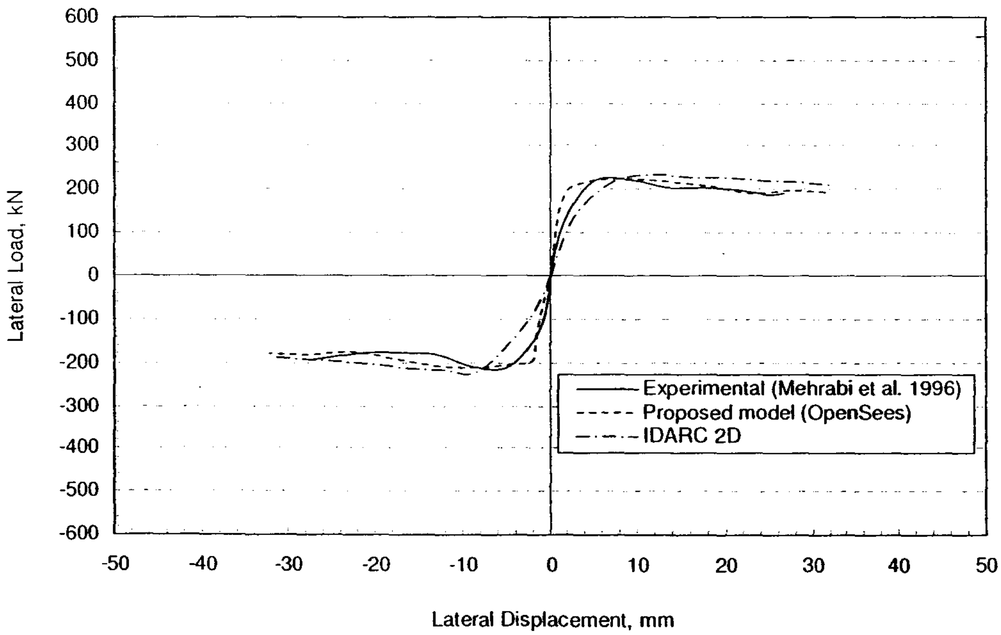

Fig. 6.17 Lateral load-displacement envelopes for specimen # 6

In the IDARC-2D model, no cracks are shown in the infill panel. The locations of plastic hinges were in the top beam (near to the beam-column connection). No plastic hinges were shown in the upper end of columns. However, two plastic hinges were located at the bottom of the both columns just above the support points. Some cracks at the top of columns were observed. This behaviour is quite similar to the behaviour obtained throughout the analysis of specimen # 4.

Failure mechanism obtained from the proposed model was similar to the experimental observations by Mehrabi et al. (1996), except that no plastic hinges were formed in the top beam in the proposed model. However in the IDARC-2D model plastic hinges were formed in the top beam and no plastic hinges were formed in the columns.

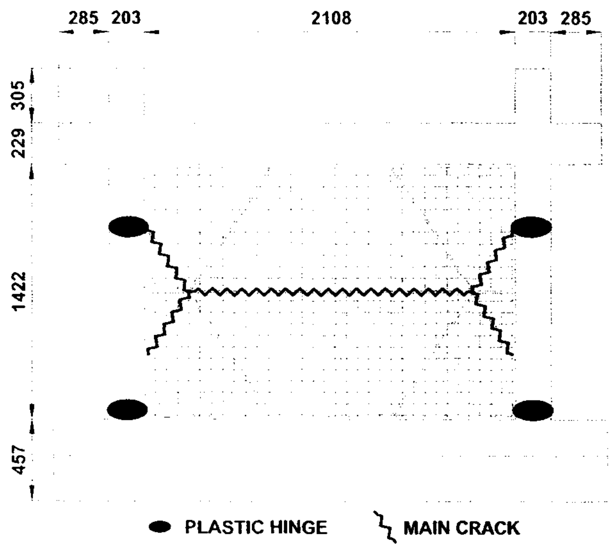

a- Proposed model (OpenSees)

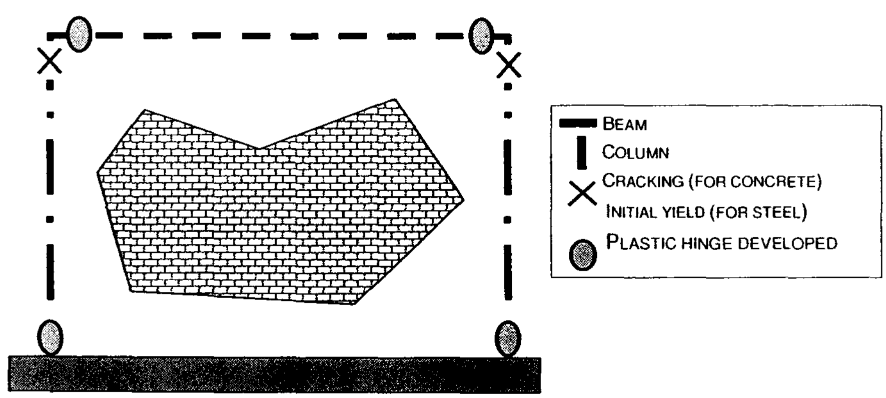

b- IDARC 2D (Versions 6.1, 2006)

Fig. 6.18 Failure mechanism of specimen # 6

B- Infilled frame test 7

Specimen # 7 was a strong frame with strong panel and had an aspect ratio of 0.67. The hysteresis curves resulting from the experimental program by Mehrabi et. al. (1996), the proposed model and the IDARC-2D model are shown in figures 6.19, 6.20 and 6.21, respectively. The load-displacement envelops for the three curves are shown in figure 6.22.

The behaviour of specimen # 7 was quite similar to that of specimen # 5, but its lateral strength was 28% higher than that of specimen 5. Unlike specimen 5, slip was first observed in specimen 7 along the bed joint at the beam-to-wall interface, and the yielding of longitudinal reinforcement in the beam occurred prior to that in the columns.

As shown in lateral load-displacement envelops (figure 6.22), the proposed model behaviour follows the experimental behaviour, by Mehrabi et al. (1996), to failure point far closer than the IDARC-2D model results.

The failure patterns for specimen # 7 obtained from the test by Mehrabi et al. (1996), proposed model and IDARC-2D model are shown in figure 6.23. Mehrabi et al. observed that the first crack in the infill developed along the bed joint at the beam-to-wall interface, which did not affect the response considerably. The lateral resistance dropped when the diagonal/sliding crack developed in the infill. This was followed immediately by shear cracks at the top of the columns. However, the lateral load increased again gradually with increasing displacement amplitude. The maximum lateral resistance was reached when the crushing of the infill occurred at the corners. Its maximum resistance was about 88% higher than that of specimen that had weak frame and a strong panel.

According to the proposed model, two parallel diagonal cracks in the infill panel formed diagonal strut mechanism. These diagonal cracks were followed by a sliding crack at the mid-height failure surface. Plastic hinges in the RC frame were located near the upper end of the column (near to beam-column connection) and at the bottom of the columns (just above the support point).

In the IDARC-2D model, no cracks are shown in the infill panel. The locations of plastic hinges are at the top beam (near to the beam-column connection). No plastic hinges were formed in the upper end of columns. However, two plastic hinges were located at the bottom of the both columns just above the support point. Some cracks at the top of columns were observed.

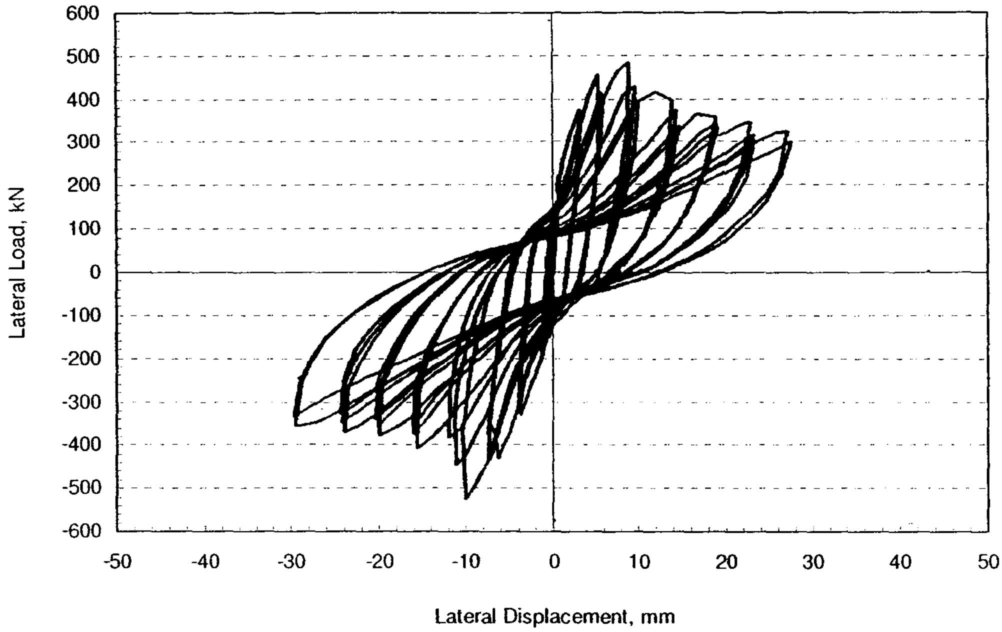

Fig. 6.19 Experimental lateral load-displacement hysteresis curves for specimen # 7 (Mehrabi et al., 1996)

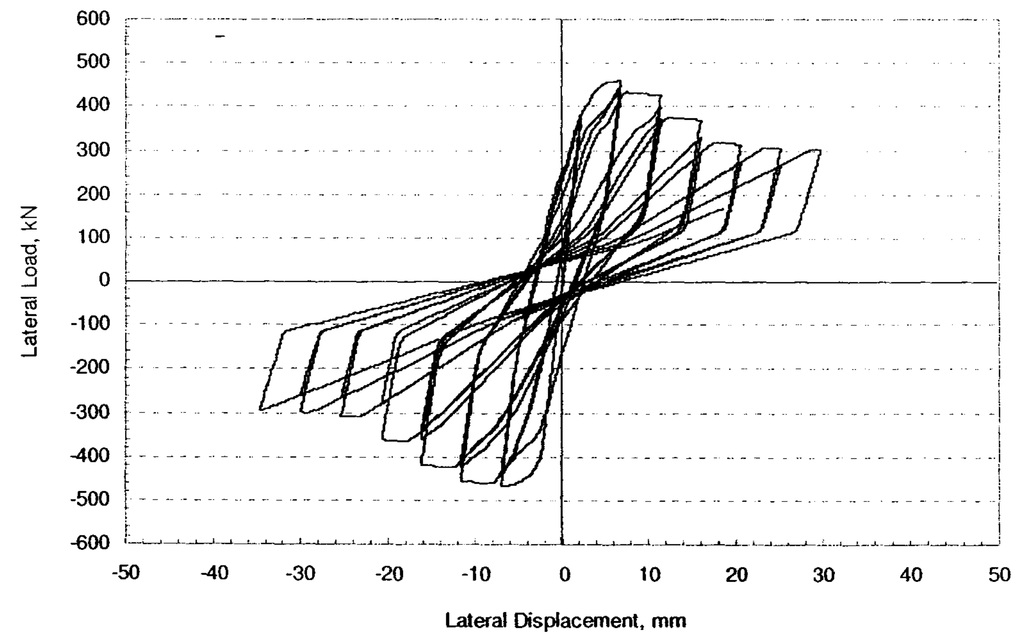

Fig. 6.20 Lateral load-displacement hysteresis curves for specimen # 7 (Proposed model-OpenSees)

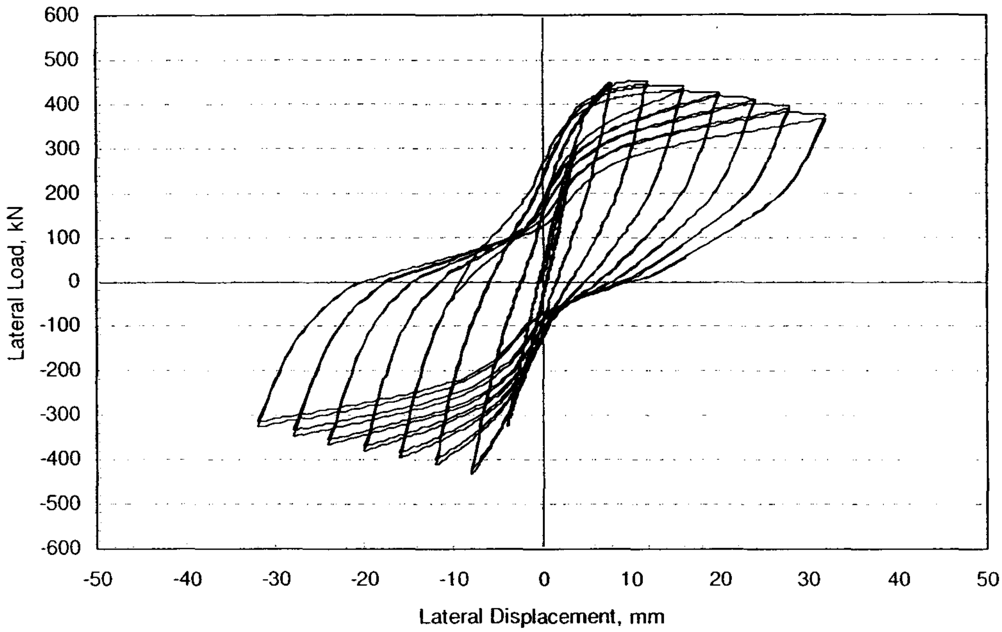

Fig. 6.21 Lateral load-displacement hysteresis curves for specimen # 7 (IDARC 2D-V6.1, 2006)

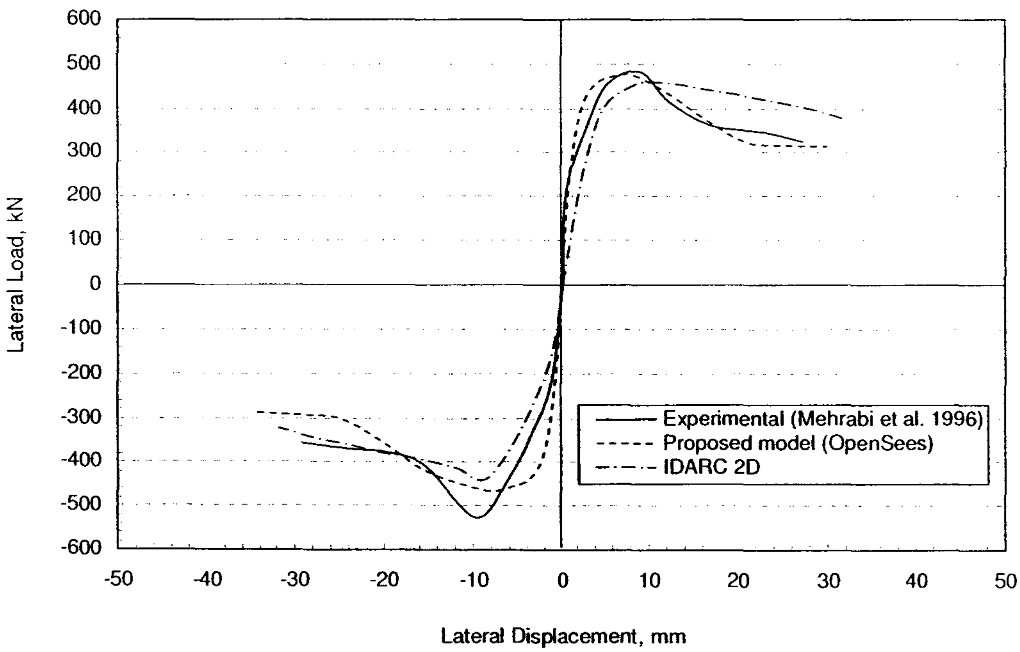

Fig. 6.22 Lateral load-displacement envelopes for specimen # 7

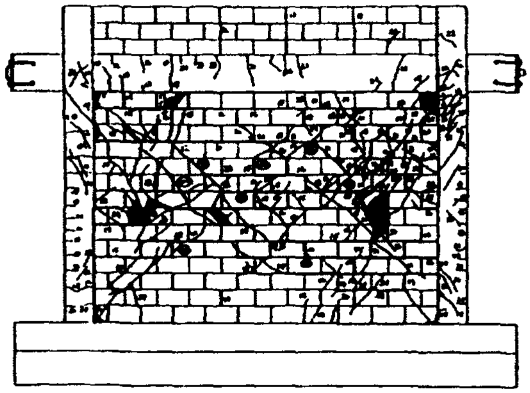

a- Mehrabi et al. (1996).

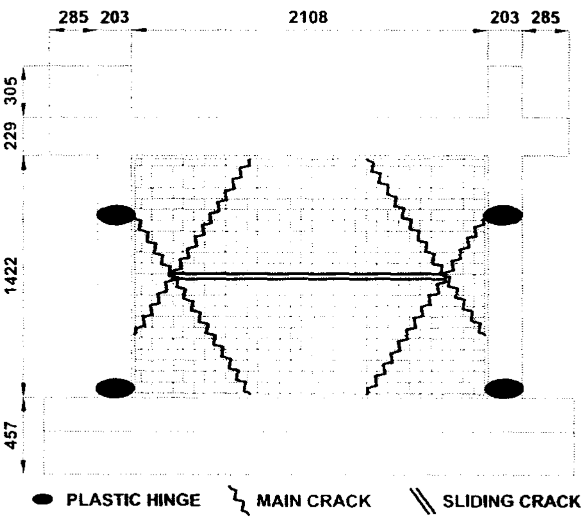

b- Proposed model (OpenSees)

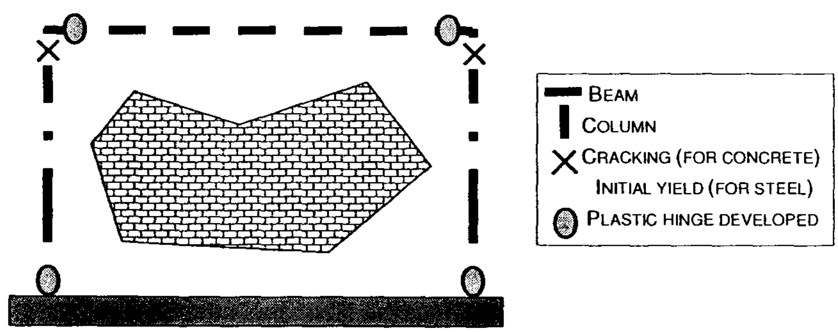

c- IDARC 2D (Versions 6.1, 2006)

Fig. 6.23 Failure mechanism of specimen # 7

6.2.5.3 Weak frame (aspect ratio 0.48)

Specimen 5, 11 and 12 were of weak frames and strong infills, the aspect ratio (H/L) of specimen 5 was 0.67, and that of specimens 11 and 12 was 0.48. Specimen 12 was subjected to a 50% higher vertical load than specimens 5 and 11. The hysteresis curves resulting from experimental program by Mehrabi et. al. (1996), the proposed model and the IDARC-2D model are shown in figures 6.24, 6.25 and 6.26, respectively for specimen 11 and in figures 6.29, 6.30 and 6.31, respectively for specimen 12. The load-displacement envelopes for the three curves for specimens 11 and 12 are shown in figure 6.27 and 6.32, respectively. As shown by hysteresis curves, the strength deterioration in these specimens was faster than that in specimen 4, which had weak panel but higher aspect ratio.

As shown in lateral load-displacement envelopes (figures 6.27 and 6.32), the proposed model behaviour follows the experimental behaviour, by Mehrabi et al. (1996), to failure point closer than the IDARC-2D model results.

The failure mechanism of specimens 5, 11 and 12 are shown in figure 6.13, 6.28 and 6.33, respectively. The behaviour and failure patterns for these specimens were very similar. However, in spite of the shear failure of columns, the energy dissipation of these specimens appears to be better than that of specimen 4 (Mehrabi et al., 1996). They noted that the diagonal/sliding cracks in the infills were first observed at the maximum lateral loads. They were followed immediately by shear cracks in the columns. As the amplitude of displacement cycles increased, crushing developed in the infill. The maximum lateral resistance of specimen 11 was 10% higher than that of specimen 5 and 25% lower than that of specimen 12.

No failure pattern was provided by Mehrabi et al. (1996) for specimens 11 and 12. However, the failure patterns for specimens 11 and 12 obtained by proposed model and IDARC-2D model are shown in figure 6.28 and 6.33, respectively. According to the proposed model, the cracks in the infill panel started as a diagonal crack near the corner of the loaded point in direction of mid-height of the panel. This diagonal crack was followed by a sliding crack at the mid-height failure surface, and then followed by another diagonal crack in the opposite direction of the loaded point. Plastic hinges in the RC frame are located near the upper end of the column (close to beam-column connection) and at the bottom of the columns (just above the support point). These locations are compatible with the locations observed during the test. This behaviour is quite similar to the behaviour of specimen # 4.

In the IDARC-2D model, no cracks are shown in the infill panel. The locations of plastic hinges were in the top beam (near the beam-column connection). No plastic hinges were shown at the upper end of columns. However, two plastic hinges were located at the bottom of the both columns just above the support point. Some cracks at the top of columns were observed.

The analytical results from the proposed model are in a good agreement with the experimental results by Mehrabi et. al. (1996) in terms of initial stiffness, maximum load resistance, displacement at maximum load, and maximum displacement. In addition, the failure mechanism results from the proposed model were in a good agreement with that obtained by the experimental program. The location of plastic hinges in the RC frame and the direction and location of cracks in the infill panel were similar to the experimental results. The IDARC-2D model could capture the overall behaviour of the infilled frame but it failed to identify the failure mechanism of the RC frame similar to that obtained by the experimental program. This may be due to the fact that the infill panel was modeled as one rectangular element.

Mehrabi et al. (1996), concluded that, the failure mechanism of an infilled frame depends very much on the strengths of the frame and the infill. In general, a frame with weak (hollow) panel had its lateral resistance governed by the sliding of the panel along its bed joints, as shown by specimen # 4. In such a case, the resistance of the panel does not seem to be influenced by the frame-panel interaction, and the total strength of the specimen is equal to flexural resistance of a bare frame plus the sliding shear strength of the panel. In the case of a strong infill and weak frame, the ultimate resistance and failure were very much dominated by the diagonal/sliding crack and the shear failure of the windward column, as shown by specimen # 5. In the case of strong infill and a strong frame, as shown by specimen # 7, the ultimate resistance was governed by the corner crushing in the infill. In this case, the diagonal compression strut mechanism was fully developed, and the infill was effective in enhancing the lateral resistance of the frame. Such mechanism is very much influenced by the frame-panel interaction.

Fig. 6.24 Experimental lateral load-displacement hysteresis curves for specimen # 11 (Mehrabi et al., 1996)

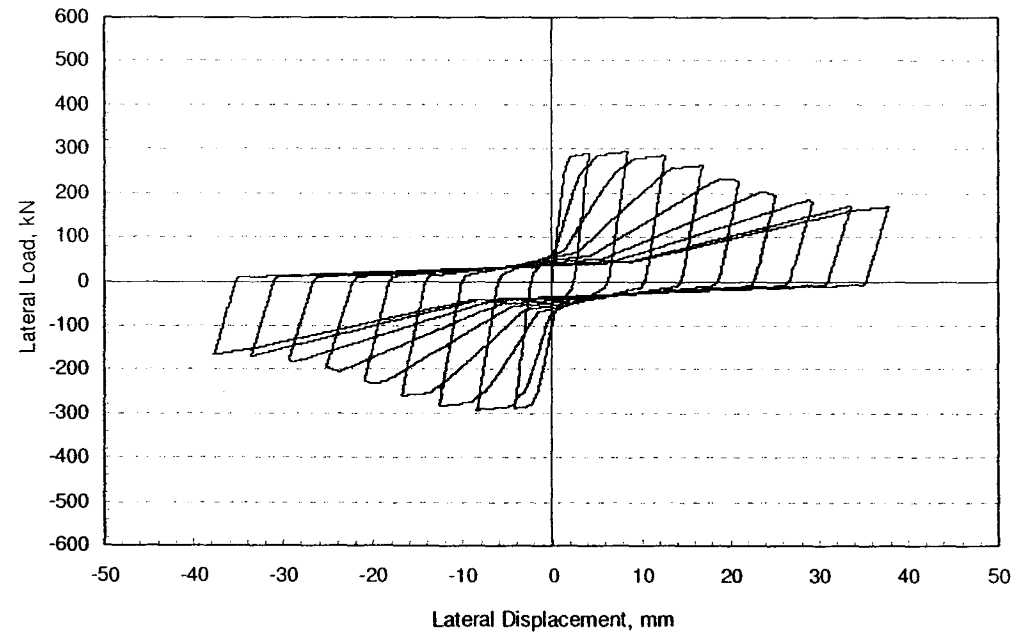

Fig. 6.25 Lateral load-displacement hysteresis curves for specimen # 11 (Proposed model-OpenSees)

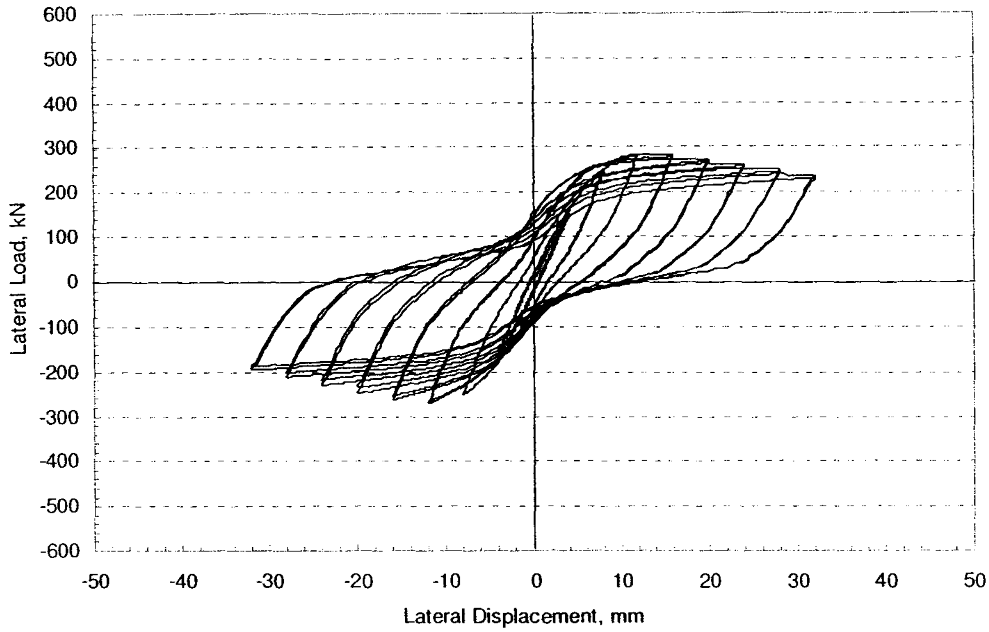

Fig. 6.26 Lateral load-displacement hysteresis curves for specimen # 11 (IDARC 2D-V6.1, 2006)

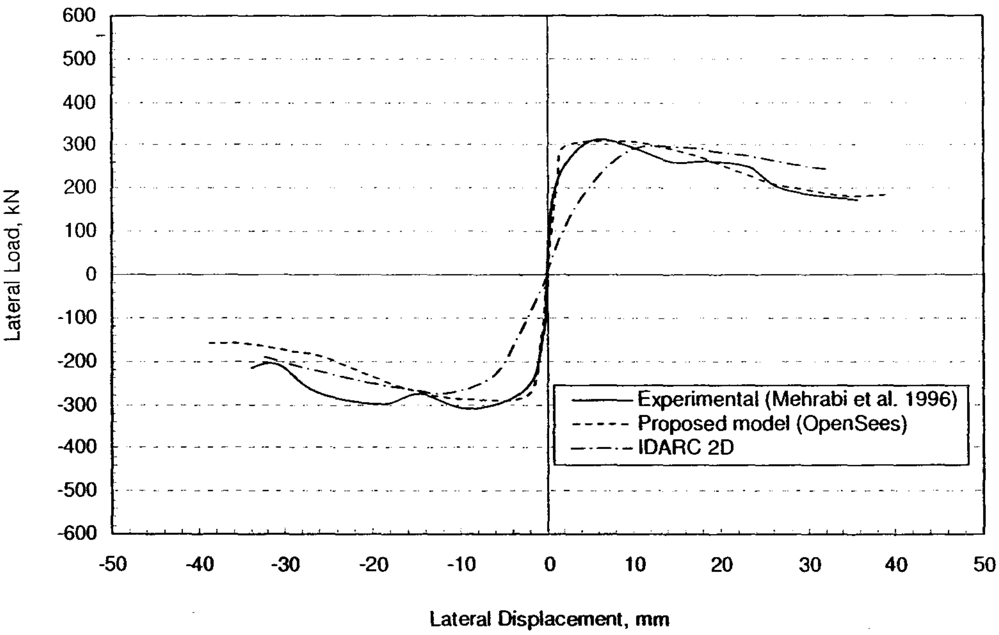

Fig. 6.27 Lateral load-displacement envelopes for specimen # 11

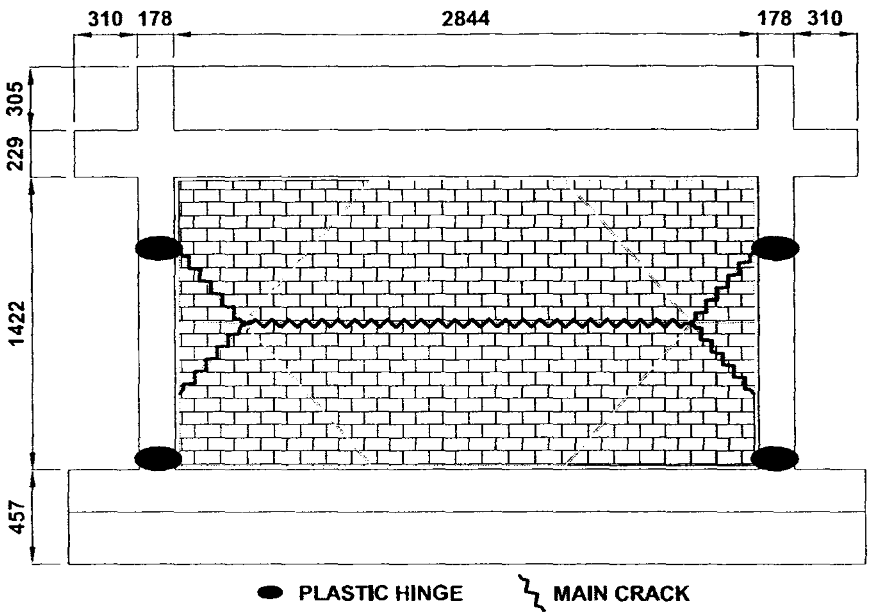

a- Proposed model (OpenSees)

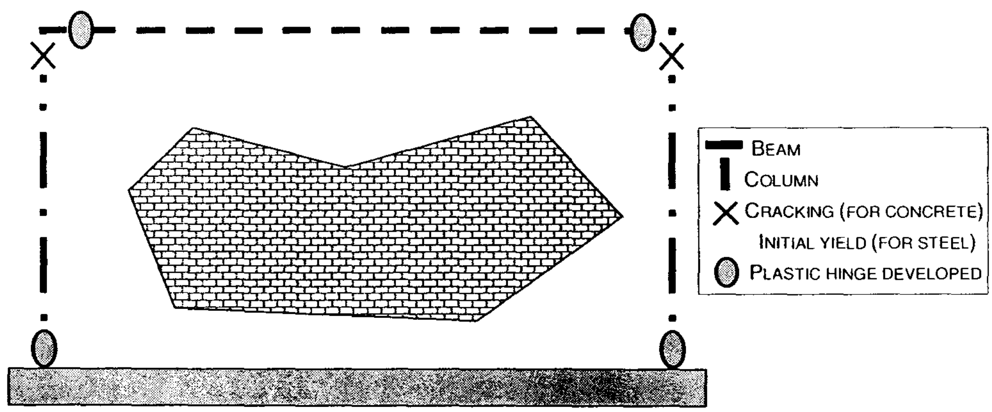

b- IDARC 2D (Versions 6.1, 2006)

Fig. 6.28 Failure mechanism of specimen # 11

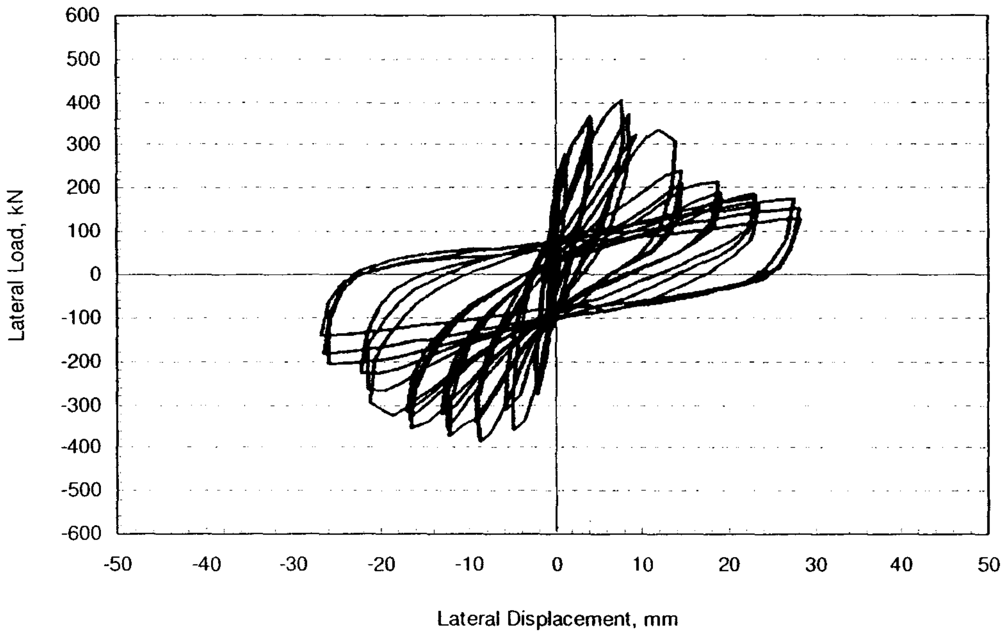

Fig. 6.29 Experimental lateral load-displacement hysteresis curves for specimen # 12 (Mehrabi et al., 1996)

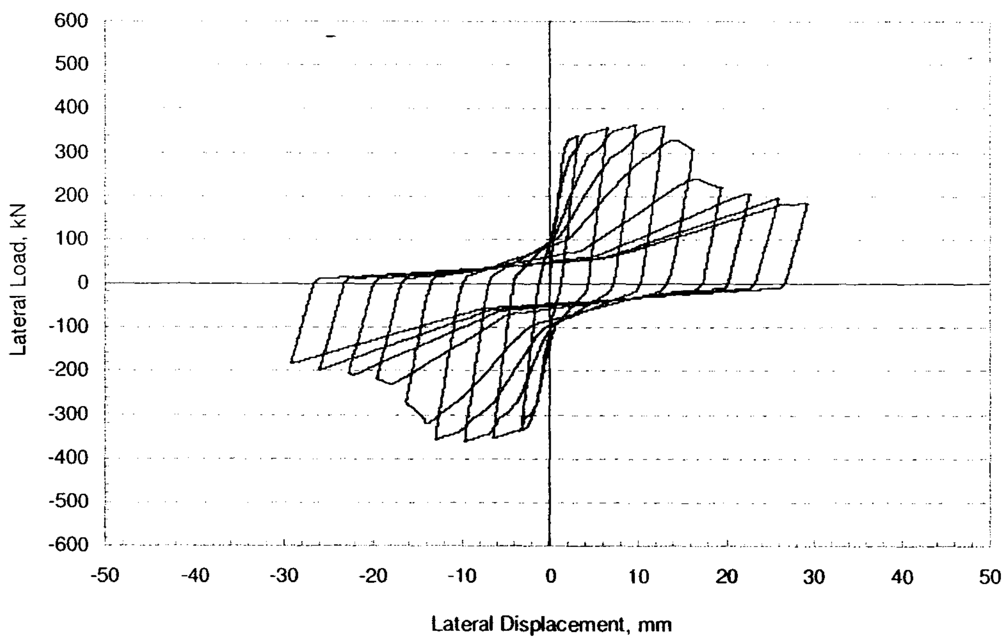

Fig. 6.30 Lateral load-displacement hysteresis curves for specimen # 12 (Proposed model-OpenSees)

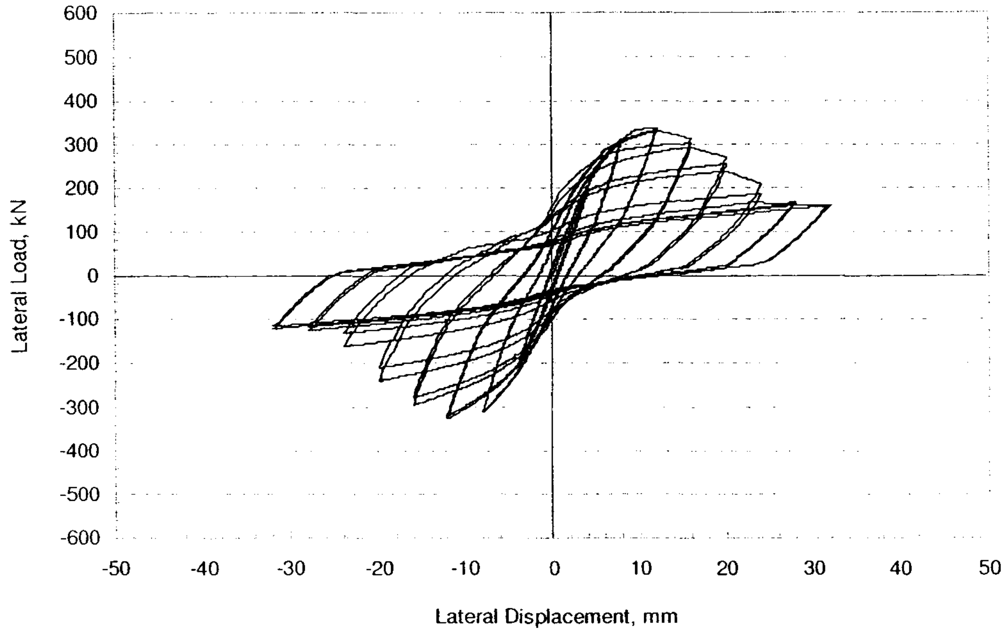

Fig. 6.31 Lateral load-displacement hysteresis curves for specimen # 12 (IDARC 2D-V6.1, 2006)

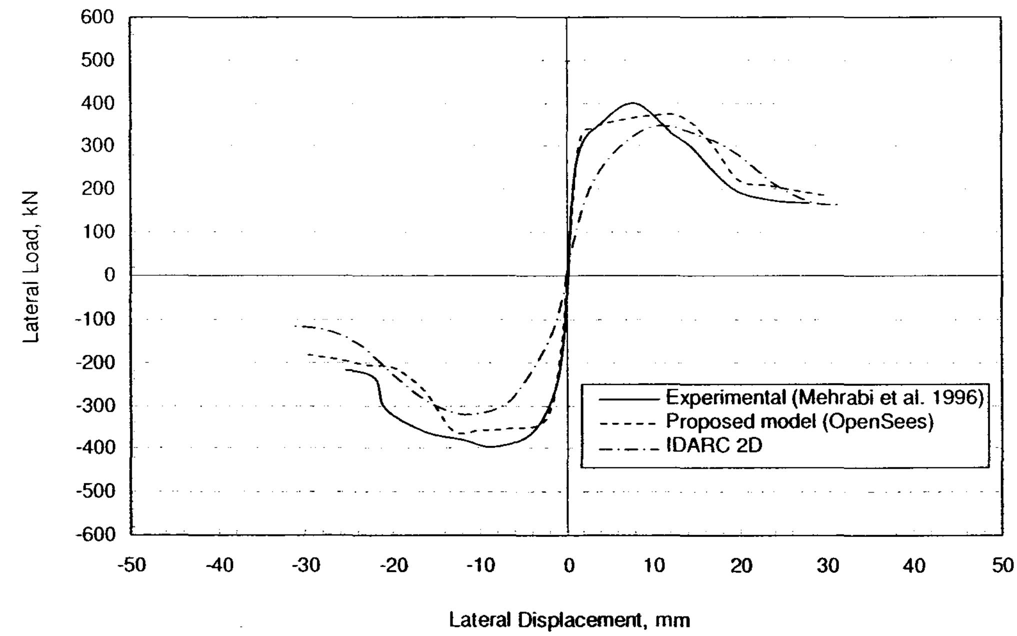

Fig. 6.32 Lateral load-displacement envelopes for specimen # 12

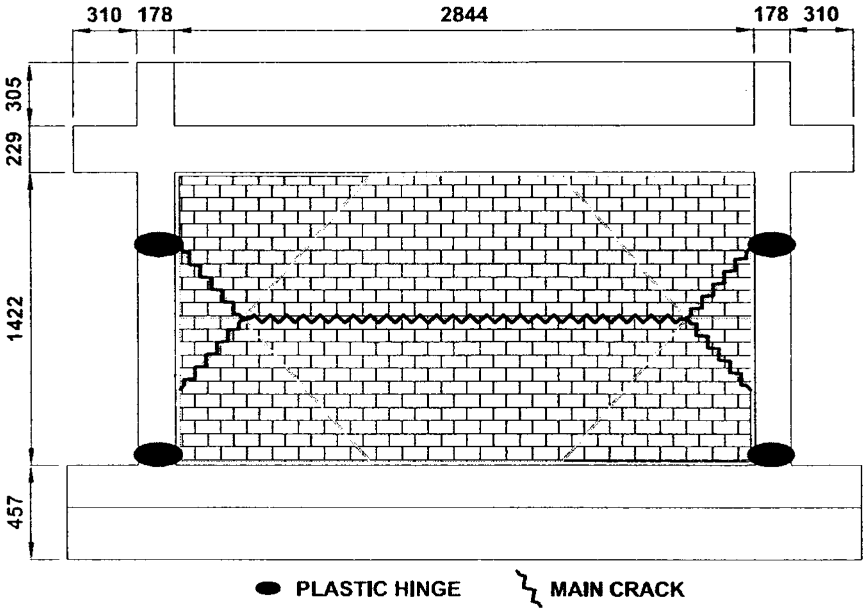

a- Proposed model (OpenSees)

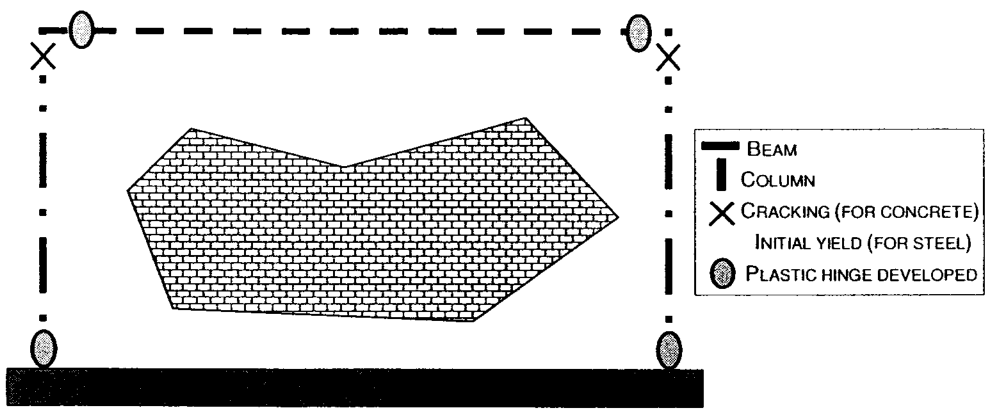

b- IDARC 2D (Versions 6.1, 2006)

Fig. 6-33 Failure mechanism of specimen # 12

The resistance of an infilled frame does not seem to depend very much on the aspect ratio of the specimen in the range of variation considered in their study. However this observation may not be valid if the change of aspect ratio leads to a different failure mechanism as discussed in Chapter 5. Furthermore, the distribution of the vertical load between the columns and the beam does not significantly affect the resistance of an infilled frame. Nevertheless, increasing the total vertical load by 50% can increase the stiffness by 30% and the maximum resistance by 25%, as shown by specimens 11 and 12.

According to test results by Mehrabi et al. (1996) brittle shear failure was observed in the columns of specimens with weak frames and strong panels. Nevertheless, this generally occurred at relatively large drift levels beyond 1% in most cases. These specimens also exhibited good energy-dissipation capability, which is better than that of a weak frame with weak panel. However, this type of failure is considered brittle in nature and will affect the stability of the structure, and is not repairable. The lateral loads developed by the infilled frame specimens were consistently higher than that of the bare frame. This observation also applies for the least ductile specimen deforming up to a drift level of 2%.

This study indicates that for frames that were properly designed for strong seismic loads, infill panels will most likely have a beneficial influence on its performance. It also indicates that infill panels can be potentially used to improve the performance of existing non-ductile frames.

Studying failure patterns of all specimens and comparing analytical and experimental results, it is observed that in some location of the RC frames the experimental results indicates the formation of shear crack while the proposed model results indicates formations of plastic hinge. This, most likely, happened in the analytical model as a result of overestimation of the confinement of the concrete section due to the effect of ties (transverse rebar). This assumption increases the compressive strength of the concrete which in return increase the shear resistance capacity of the concrete section. This behaviour allowed the formation of plastic hinges and yielding of longitudinal rebar before forming shear cracks in concrete section.

6.3 APPLICATION TWO

Kakaletsis and Karayannis (2008) carried out an experimental program on seven single-story one-bay 1/3-scale specimens of reinforced concrete frames with infills of clay brick and vitrified ceramic brick. The program results provide data for the evaluation of the influence of different opening shapes and different infill compressive strengths on the surrounding frames. The program included testing of: bare frame, frame specimens with solid weak and solid strong infills, frame specimens with concentric window opening, and frame specimens with concentric door opening with weak and strong infills. In this section two infill frames only were analyzed, the first frame "frame # S" which is RC frame with weak infill, while the second frame "frame # SI" is RC frame with strong infill. The configuration, cross-sections of the members, and design details of the frame specimens are shown in figure 6.34. The reinforced concrete frame represents a typical ductile concrete construction, built in accordance with the currently applicable codes and standards in Greece which are very similar to EC2 (1992) and EC8 (1991).

Masonry infills had a height/length ratio H/L = 2/3 and were constructed with two selected brick types cut into two halves in conformance to the test scale. The configuration is shown in figure 6.35. The "weak" common clay brick usually used in Greece had a thickness of 60 mm, while the "strong" vitrified ceramic brick that proved to be important for the specimen behaviour had a thickness of 52 mm. A typical mortar mix was used for the two types of infills with portions 1 : 1 : 6 of cement : lime : sand, respectively, and produced mechanical properties similarly to type M1 mortar according to EN 998-2 standard (BS EN 998-2:2003). Masonry properties were chosen in such a way to produce the desired lateral strength of the two types in a magnitude $V_{w,u}$ equal to 27.36 or 25.58 kN which is lower than that of the lateral strength of the frame F_f equal to 42.48 kN. This closely represents actual construction practice in Greece.

Supplementary material tests were conducted on concrete, reinforcing steel and masonry samples. The mean compressive strength of the frame concrete was 28.51 MPa. Yield stress of longitudinal and transverse steel was 390.47 and 212.2 MPa, respectively.

the compressive strength of the "weak" masonry prisms was lower than that of the "strong" ones while the shear strength of the bed joints in the "weak" and "strong" specimens compared with the same of the full size infills height / length ratio (H/L = 2/3) were almost identical.

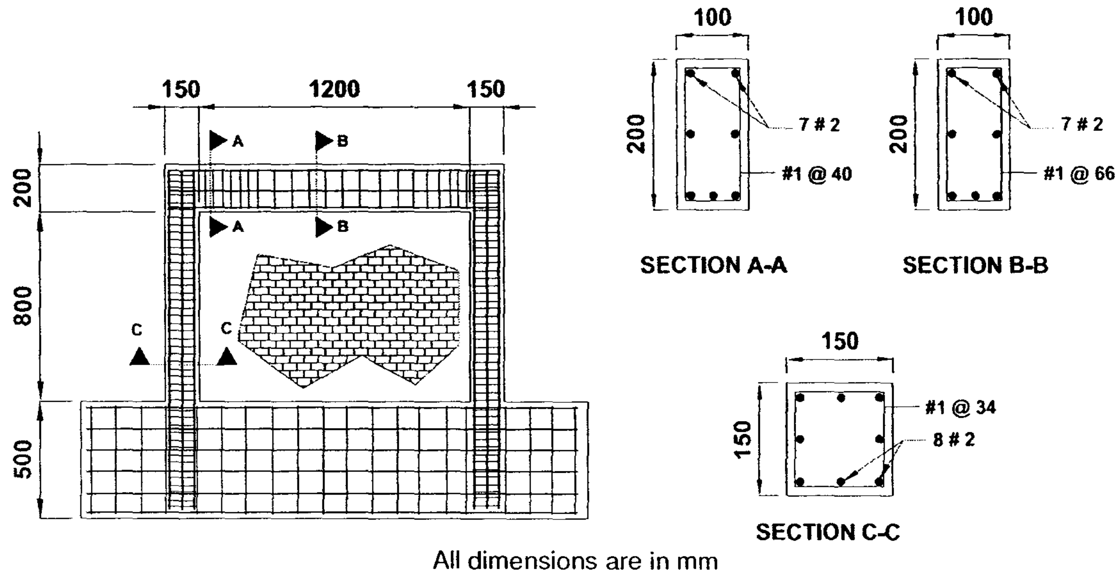

Fig. 6.34 Design details for the RC frame, Kakaletsis and Karayannis (2008)

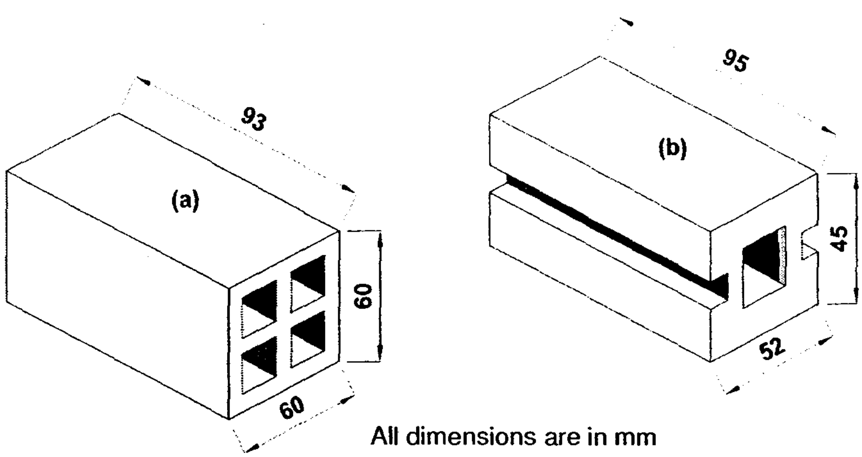

Fig. 6.35 Masonry units: (a) Hollow; (b) Solid.

Kakaletsis and Karayannis (2008)

The test setup is shown in figure 6.36(a). The lateral load was applied by means of a double action hydraulic actuator. The vertical loads were exerted by hydraulic jacks that were tensioning four strands at the top of the column whose forces were maintained constant during each test. The level of this axial compressive load per column was set 50 kN (0.1 of the ultimate load). The loading sequence comprises full cycles of gradually increasing displacements. Two full loading cycles were applied at each displacement level (figure 6.36(b)). The loading cycles started from ductility level μ = 0.8 which corresponds to amplitude equal to ±2 mm (the displacement of yield initiation for the system is considered as ductility level μ = 1).

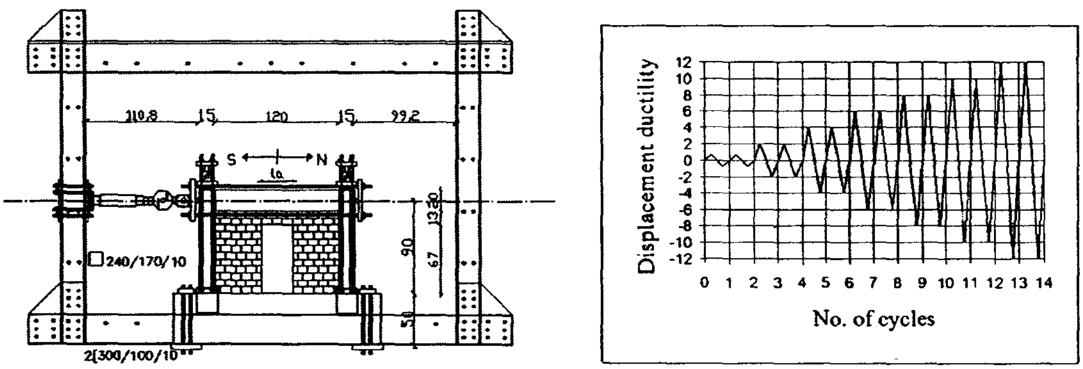

(a) (b)

All dimensions are in cm

Fig. 6.36 (a) Test setup and (b) loading program

Kakaletsis and Karayannis (2008)

Specimens "S" and "IS" are two identical RC frames with solid weak and solid strong infills, respectively. The two specimens were analyzed using the proposed OpenSees model. Each specimen was subjected to one fully reversed displacement cycles at each amplitude level. The amplitude level was 2.0 mm, similar to that used throughout the experimental program. In the developed model, the masonry wall was modeled using 10 quadrilateral isoparametric elements connected on the prescribed failure planes with contact zero-length elements. The proposed model and boundary conditions are presented in figure 6.37.

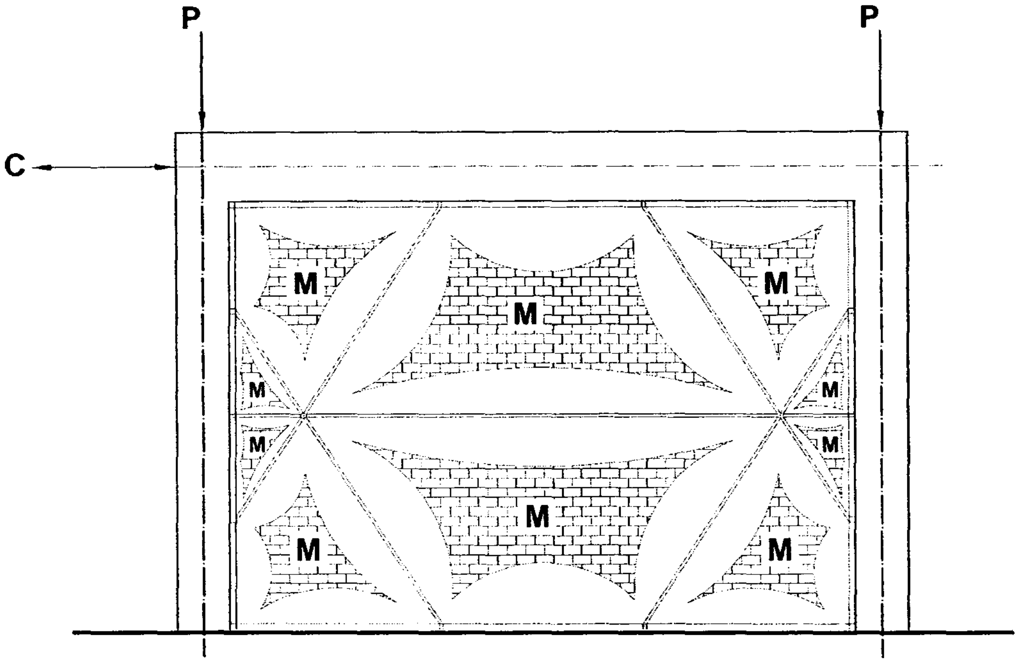

Fig. 6.37 Proposed model and boundary conditions for specimen "S" and "IS"

6.3.1 Frame with Weak infill

The hysteresis curves for specimen "S" as recorded during experimental program by Kakaletsis and Karayannis (2008) and the proposed model are shown in figures 6.38 and 6.39, respectively. The load-displacement envelop for the two results are shown in figure 6.40.

The analytical and experimental results for specimen "S" show that the maximum lateral displacement equals 81.46 kN and 88.7 kN respectively. The displacement at maximum lateral resistance was 10 mm. The behaviour of specimen showed faster stiffness and strength degradation with respect to specimen "IS". Secant initial stiffness of specimen "S" was 20.71 kN/mm according to experimental results and 31.8 kN/mm according to the analytical results.

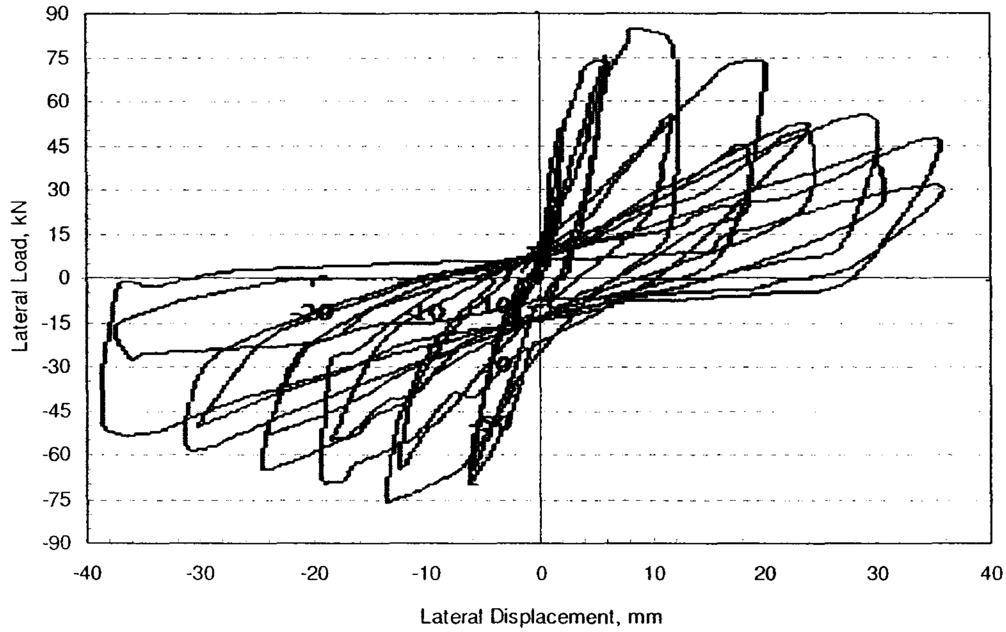

Fig. 6.38 Lateral load-displacement hysteresis curves for specimen "S" (Kakaletsis and Karayannis, 2008)

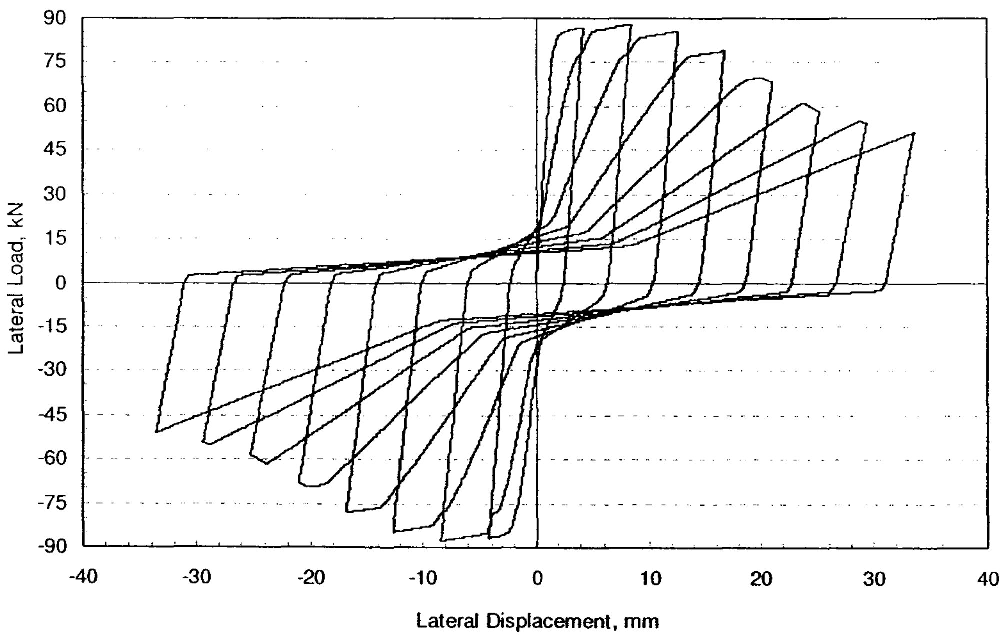

Fig. 6.39 Lateral load-displacement hysteresis curves for specimen "S" (Proposed model-OpenSees)

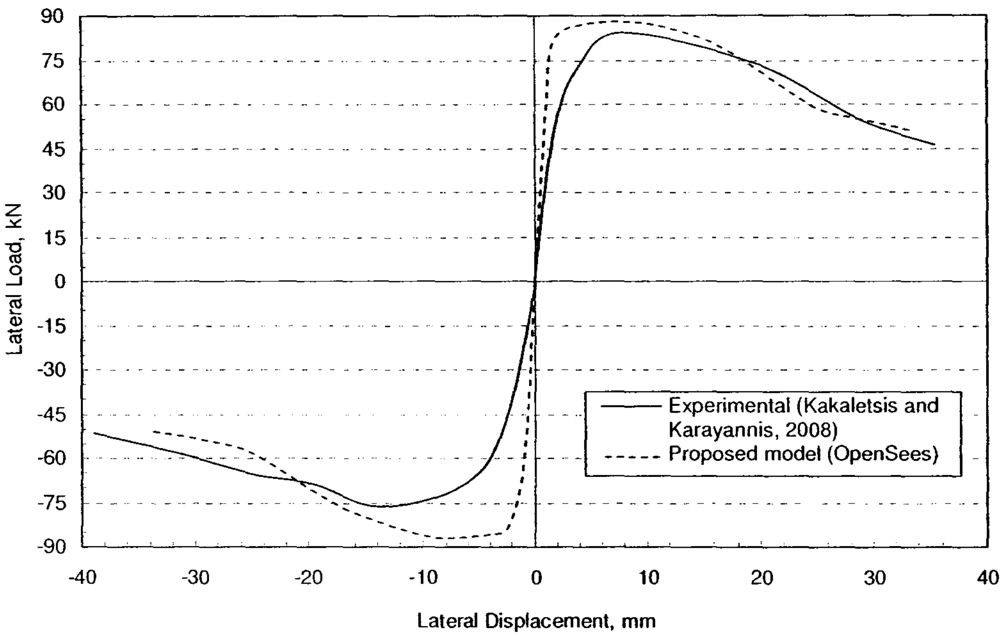

Fig. 6.40 Lateral load-displacement envelopes for specimen "S"

6.3.2 Frame with Strong-infill

The hysteresis curves for specimen "IS" from the experimental data and analysis using the proposed model are presented in figures 6.41 and 6.42, respectively. Envelop of the two hysteresis curves is shown in figure 6.43.

Experimental results of specimen "IS" (RC frame with strong infill) showed that the maximum lateral load resistance equals to 72.92 kN at lateral displacement of 12.32 mm. The analytical results using the proposed model showed that the lateral resistance of specimen "IS" equals to 108.7 kN at lateral displacement of 15 mm. there are significant variation between the experimental and analytical results for this specimen. However, the experimental results appear to be incorrect, since the lateral load resistance of the same RC frame with weak infill was 81.47 kN which was higher than the case of strong infills. The corresponding displacement was 8.31 mm.

The secant initial stiffness of specimen 'IS" resulted from experimental and analytical analysis was 21.84 kN/mm and 27.6 kN/mm, respectively.

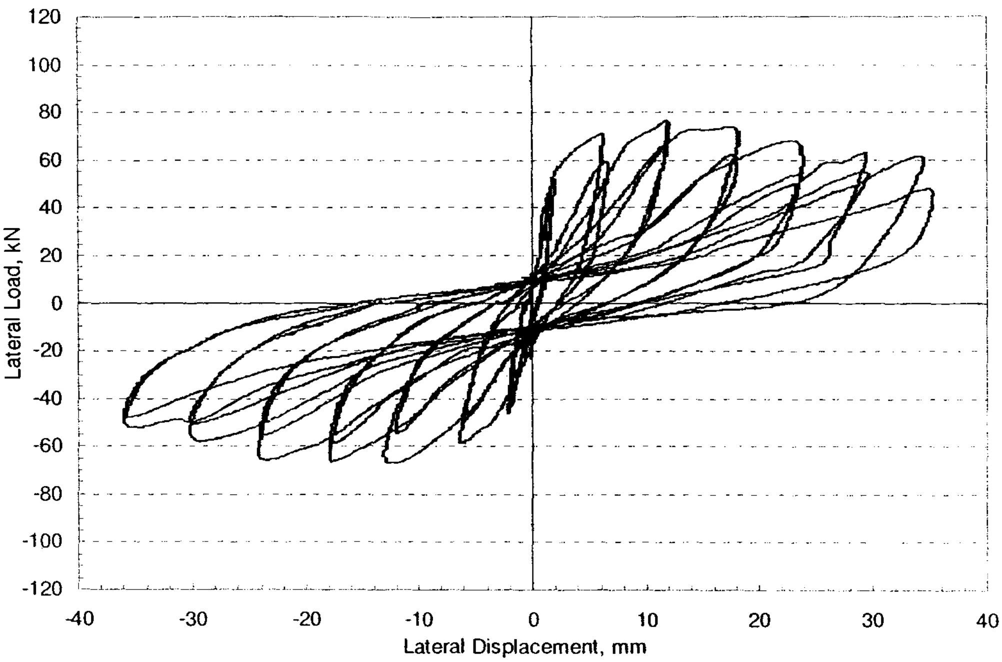

Fig. 6.41 Lateral load-displacement hysteresis curves for specimen "IS" (Kakaletsis and Karayannis, 2008)

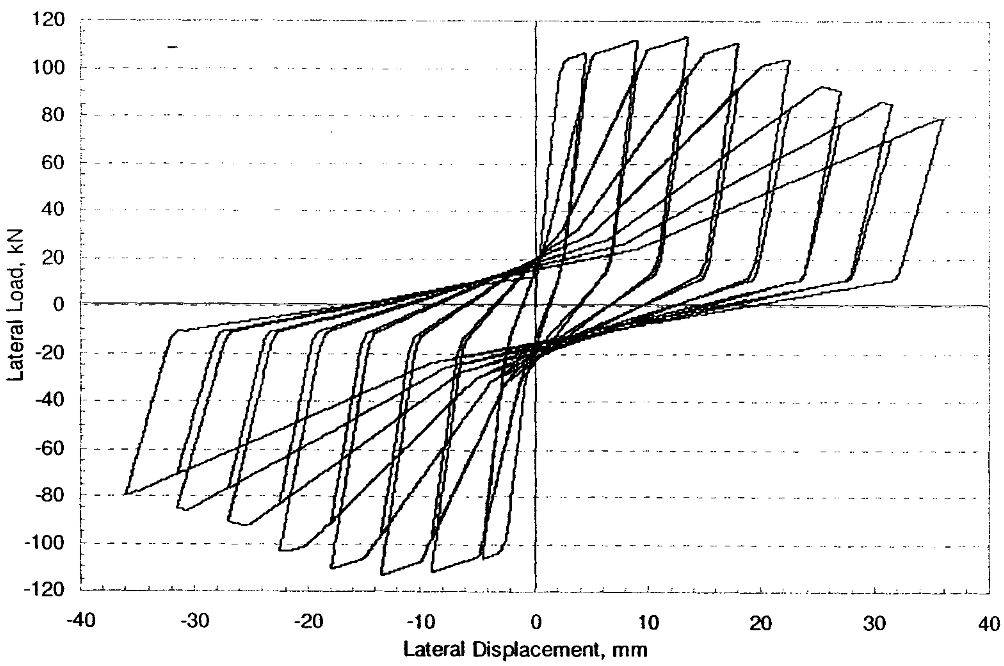

Fig. 6.42 Lateral load-displacement hysteresis curves for specimen "IS" (Proposed model-OpenSees)

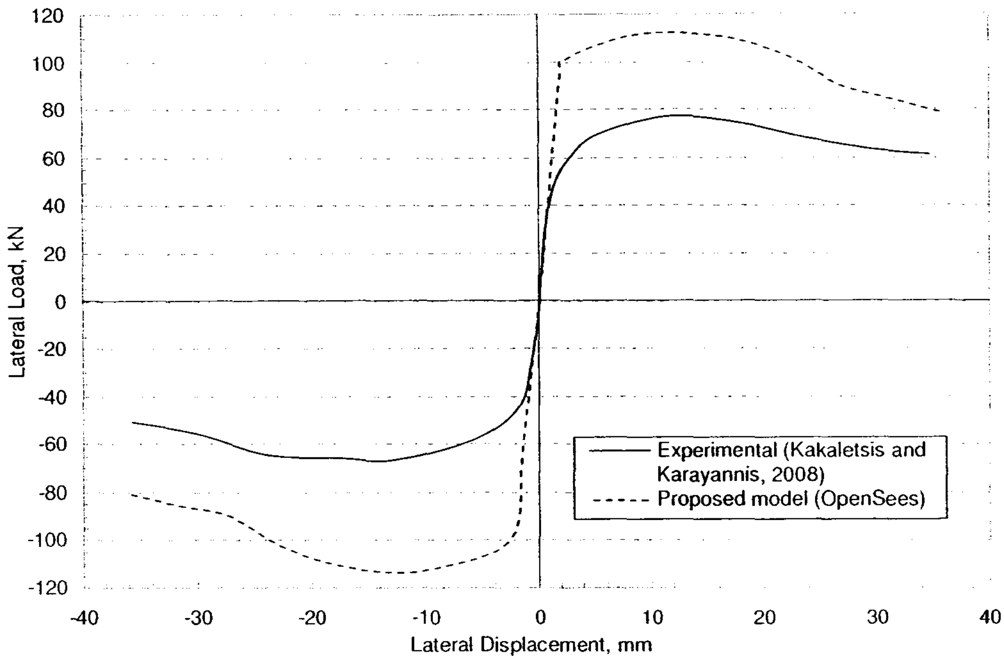

Fig. 6.43 Lateral load-displacement envelopes for specimen "IS"

6.3.3 Failure Patterns

The failure patterns for the experimental and proposed model for specimen "S" and "IS" were presented in figures 6.44 and 6.45, respectively. The experimental results showed that, The nonlinear behaviour of specimens "S" and "IS" was initiated by the cracking of the infill. First cracks appeared in the form of inclined cracks in the top compression corners with approximately a 45° angle and were later joined by horizontal sliding cracks developed along the bed joints near the mid height of the panel at a drift 3%. Then plastic hinges were developed at the top and the bottom of the columns, at a drift 4 to 11%, respectively, while the lower portions of the column were braced by the bottom segment of the wall and flexural cracks formed in the columns. However, as shown by the damage patterns of specimens, the failure of the weak solid infill specimen "S" (figure 6.41(a)) was dominated by internal crushing in the infill, at a drift 19%, while the failure of the strong solid infill specimen "IS" (figure 6.45(a)) was dominated by sliding of the infill along its bed joints at drift of 14%. Failure modes for both specimens "S" and "IS" were mode-C, as shown in figures 6.44 and 6.45.

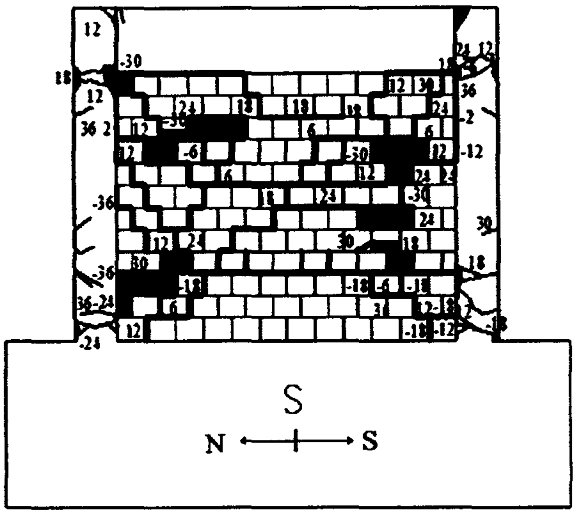

a- Kakaletsis and Karayannis, 2008)

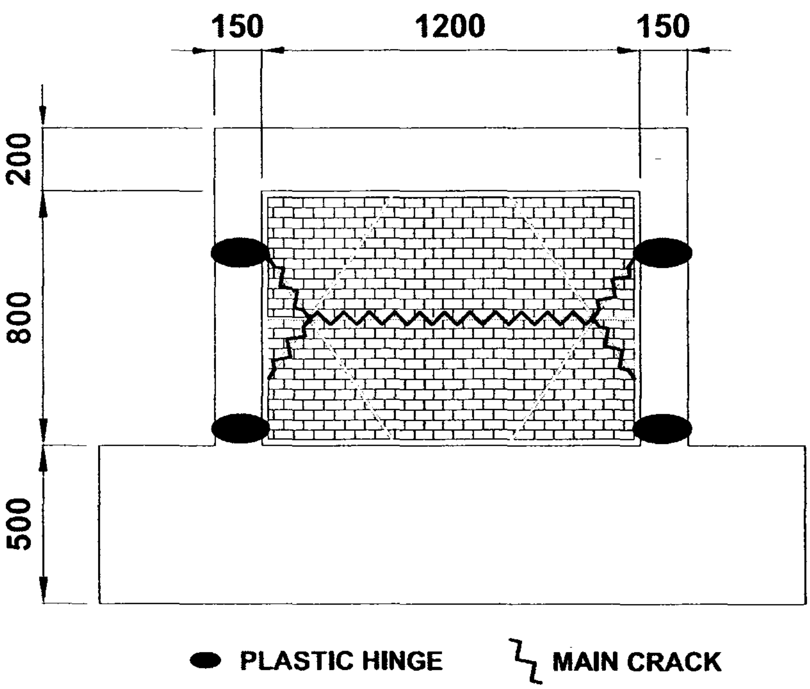

b- Proposed model (OpenSees)

Fig. 6.44 Failure mechanism of specimen "S"

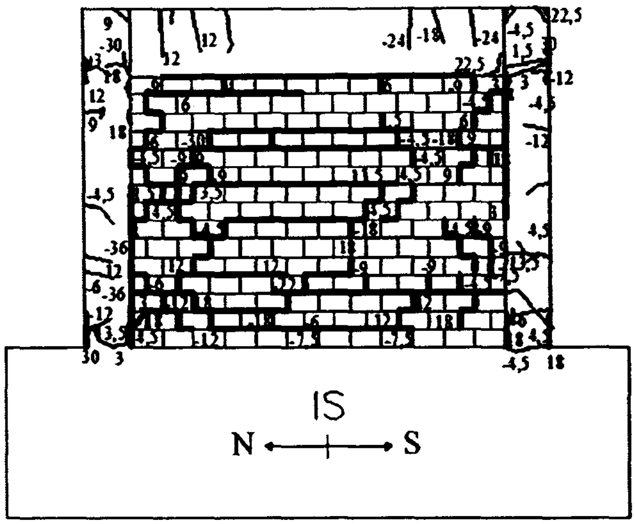

a- Kakaletsis and Karayannis, 2008)

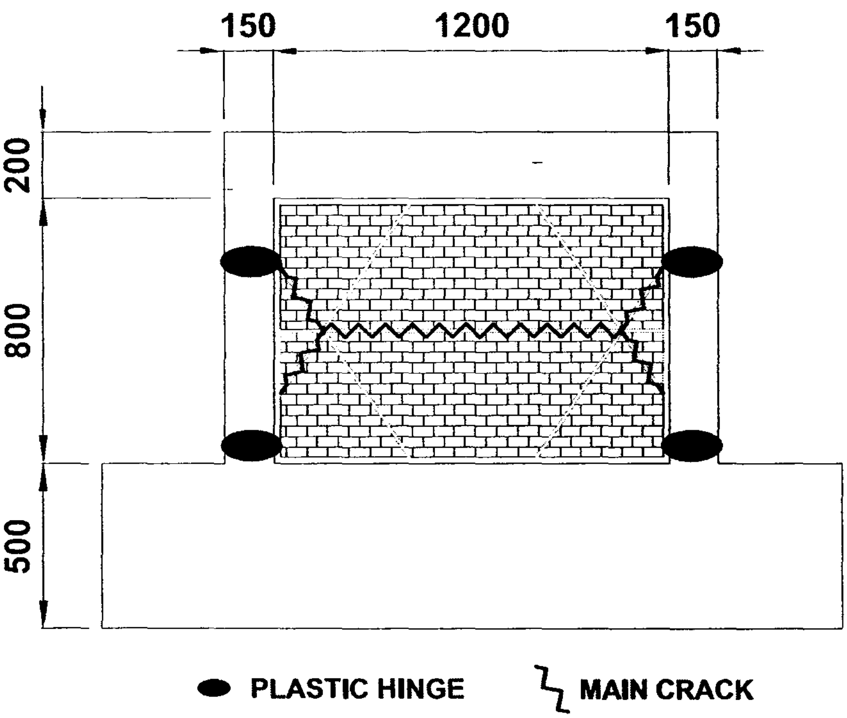

b- Proposed model (OpenSees)

Fig. 6.45 Failure mechanism of specimen "IS" (strong infill)

The proposed model indicates that the cracks in the infill panel started as a diagonal crack near the corner of the loaded point in direction of mid-height of the panel. This diagonal crack was followed by a sliding crack at the mid-height failure surface, and then followed by another diagonal crack in the opposite direction of the loaded point. Plastic hinges in the RC frame were located near the upper end of the column (near the beam-column connection) and at the bottom of the columns (just above the support point). These locations are similar to the locations observed during the test. The behaviour of specimens "S" and "IS" was similar but at different load and displacement levels, as shown in figure 6.46. Analysis of the infilled frames using the proposed model closely represents the test results.

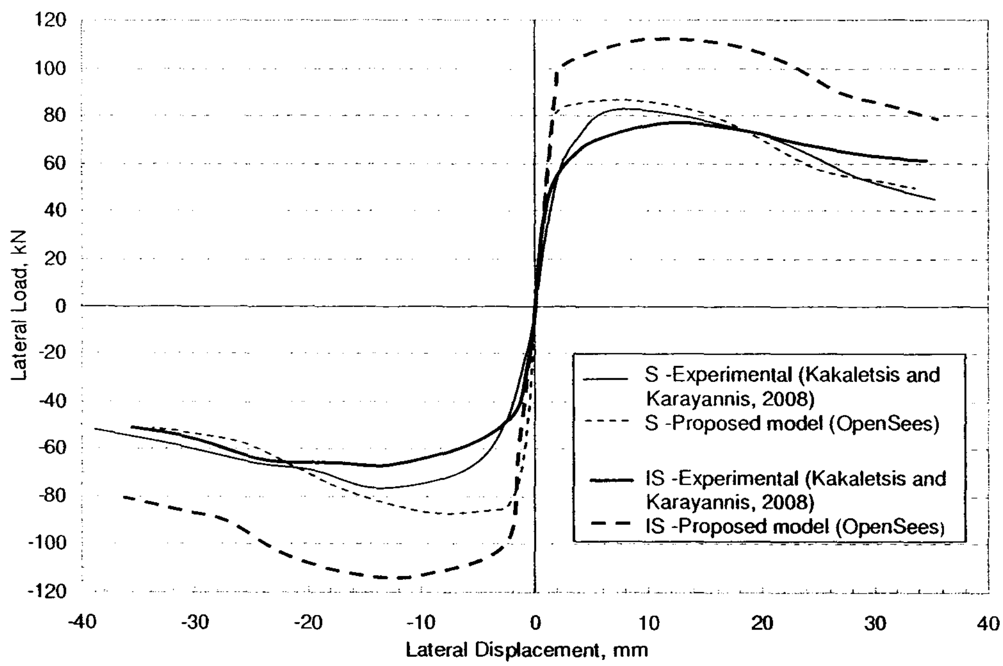

Fig. 6.46 Lateral load-displacement envelopes for specimens "S" and "IS"

Test specimen "S" (frame with weak infill) and "IS" (frame with strong infill) had the same aspect ratio (H/L = 2/3). Comparing the failure patterns of the two specimens and frames with the same aspect ratios and boundary conditions in Chapters 4 and 5, it is observed that frames with aspect ratio of 2/3 could have failure Mode-C or Mode-E according to the height of the frame and type of frame (Strong or weak). The cyclic nature of the loading routine of specimens "S" and "IS" could affect of the failure of mortar and masonry units in the infilled frame, which in return will affect the failure mode of the surrounding frame. However, the observed failure patterns of specimens "S" and "IS" are in good agreement with the conclusion reached in Chapters 4 and 5.

This page is intentionally left blank

CHAPTER 7

CONCLUSIONS AND RECOMMENDATIONS

7.1 SUMMARY

The objective of this research was to develop a practical and economical technique applicable for global analysis of general three-dimensional reinforced concrete infilled frames under lateral loads. Novel finite element model for the infill and the surrounding frame was developed using a special finite element configuration to represent the masonry panel. Prescribed failure planes in different directions were defined depending on the observed failure mode of masonry panels. Moreover, contact elements were used on the failure planes to connect the panel elements, and between the panel elements and the boundary reinforced concrete frame. Different material models were used to represent the behaviour of concrete, reinforcing steel, mortar joints and inclined saw-tooth cracks in the infill panel. Different material models were also used to describe the behaviour through and perpendicular to the prescribed failure planes.

The proposed finite element model was verified against results from experimental and analytical studies conducted by others. Various frame configurations, reinforcement details, boundary conditions and material properties were considered to verify the capability of the proposed model to simulate the behaviour of different frames. The overall behaviour presented by the Load-deflection relationship, failure point and failure mode were compared with the experimental and analytical results. Satisfactory agreement with the previously published results was obtained.

The new model was used to investigate the effect of different parameters on the behaviour of infilled frame. These parameters include; relative infill/concrete strength, infill strength (weak/strong infill), RC frame strength (weak/strong frames), aspect ratio of the infill panel, configuration of the RC frame and boundary conditions of the RC frame. Conclusions and observations were obtained from investigating the effect of different parameters on the behaviour of infilled frame.

The proposed model was applied to analyze the behaviour of infilled frames subjected to cyclic loads. Infilled frames with different loading routines, strength and boundary conditions were investigated. Hysteretic loops obtained by using the new model were verified against experimental and analytical results and good correlation were obtained. The failure modes and crack patterns were compared with the experimental results and good agreements were obtained. The proposed model failed to capture some shear cracks in the RC frames as per the experimental results.

7.2 CONCLUSIONS

Based on the verification of the proposed finite element model against experimental and analytical results and from studying the effect of different parameters on the behaviour of infilled reinforced concrete frames the following conclusions were reached:

- The new finite element model described in this study was verified against the experimental and analytical results by different authors. Infilled frames with different configurations, boundary conditions, material properties and masonry strength were investigated through verification stage of this study and satisfactory agreement was obtained.
- The numerical results have shown that the model can capture and predict the overall behaviour, crack patterns and failure mechanisms of the infilled reinforced concrete frame structures subjected to in-plane monotonic loading.
- It was found that the effect of relative masonry/concrete strength has no effect on the failure mode. However, relative masonry/concrete strength has an effect on the maximum displacements and maximum loads that can be resisted by the infilled RC frames.
- The two frames; one with flexible beam and one with stiff lower beam showed change in the failure mechanism from Mode-E at aspect ratio more than or equals to approximately 0.75 to Mode-C at aspect ratios less than approximately 0.75. The change in the failure mechanism was observed at aspect ratios close to the points of peak displacements in the maximum displacement-aspect ratio relationships.

- Although frames of lower flexible beam had less reinforcement than frames of stiff lower beam, frames of first group dissipate more energy than the frames of the second group for the same aspect ratios. Moreover, resistance of the second group of frames to the lateral load was higher than the resistance of first group of frames for all aspect ratios. However, the loss of strength of frames of the second group of frames was faster than the loss of strength of the first group of frames.

- Two different groups of RC frames infilled with the same type of infill were analyzed to investigate the effect of different aspect ratios on the behaviour of infilled frames. The first group was strong frame and the second group was weak infill frames. It was found that type of RC frame, strong or weak, has small effect on the failure mechanism of the infilled frame. Moreover, type of RC frame has effect of approximately 25% on the overall strength of the infilled frame. However, the most important factor that affects the failure mechanism of infilled RC frames is the aspect ratio of the infill pane.

- There was numerical instability when analyzing frames with height more than 7.00 m, and the proposed model failed to solve the problems. This may be, due to one of the following reasons; 1) the relatively large size of the masonry element; 2) the small dimension of the columns and beams sections with respect to the over all dimensions of the infilled frames; 3) the high aspect ratio of the infilled frame especially for small spans.

- Results of the proposed model were verified for infilled RC frames under cyclic loading. Different aspect ratios, frame types (strong and weak), different loading conditions and different infill types are considered throughout the verification process. The proposed model showed satisfactory accuracy for representing the cyclic behaviour of infilled frames under cyclic loading. The developed model can also predict the failure mechanism of different frames and different boundary conditions.

- Results of the proposed finite element were compared with the results of IDARC-2D model for infilled RC frames. Solving a one story infilled RC frame under cyclic load using IDARC-2D model takes between 5-to-7 minuets, while solving the same problem using proposed model takes between 10-to-12 minutes. The IDARC model consider the infill panel as one element, that is may be the reason why it takes shorter time to solve the same problem. Although the proposed model is relatively time consuming but it can predict the failure mode and crack patterns better than the IDARC-2D model.

- As a final note, the proposed model is simple, efficient and has an adequate accuracy. Finally, it should be noted that the present analysis and conclusions were based on a limited numbers of problems. To establish general conclusion on the behaviour of infilled RC frame more investigations are needed.

7.3 RECOMMENDATIONS FOR FUTURE RESEARCH

Future investigations are needed in the following area:

1- The proposed model was investigated under static and cyclic lateral loads. The model may be examined to study its capability to simulate the behaviour of infilled RC frames under general dynamic loads.

2- Investigate the use of infill to enhance the lateral resistance of exciting RC frame.

3- All verification problems under static or cyclic loads and parametric studies were applied to single story-single bay frames. The model need to be investigated when implemented in a multi-story, multi-bay infilled RC frame.

4- The proposed model configuration does not allow the presence variety of openings within the infill panel. The configuration of the proposed finite element model needs to be enhanced to allow including openings with different sizes and shapes.

5- Mortar strength was not on of the parameters included in this research. Further studied need to be carried out to study the effect of mortar strength on the behaviour and failure modes of infilled frames.

6- Study the reflection of results and conclusions on the current masonry code previsions.

7- This research was concerned with the strength of masonry panel and its effect on the surrounding RC frames in the in-plane direction. Further investigations should be carried out to improve the proposed model to include the strength of masonry panel in the lateral direction.

8- Improve the proposed model to simulate some missing shear cracks and plastic hinges when compared with the experimental results.

9- Finally, a better material model for masonry element can be used to improve the behaviour of the element to simulate the actual behaviour of masonry panel.

This page is intentionally left blank

REFERENCES

ACI (318);" Building code requirements for reinforced concrete', American Concrete Institute, 1989, Detroit, USA.

Al-Chaar G., Issa M. and Sweeney S.; "Behaviour of Masonry-nfilled Nonductile Reinforced Concrete Frames", Journal of Structural Engineering, ASCE, 2002, Vol. 128, No. 8,: 1055-1063.

Anderson J. C. and Townsend W. H.; "Models for RC frames with degrading stiffness", Journal of Structure Engineering Division, ASCE, 1977, Vol. 103(ST12):2361-2376.

Atkinson R.H., Amadei B.P., Saeb S., Sture S., "Response of masonry bed joints in direct shear"; Journal of Structure Engineering, ASCE 1989; Vol. 115(9):2276–96.

Bard Y., "Nonlinear parameter estimation", Academic press, 1974, New York, USA.

Benedetti, D., Carydis, P., and Pezzoli, P.,''Shaking table tests on 24 simple masonry buildings.'' Earthquake Engineering and Structural Dynamics, 1998, Vol. 27(1), 67–90.

Bertero V.V. and Brokken S.; "Infills in seismic resistant building", Journal of Structural Engineering ASCE, 1983, Vol. 109(6): 1337-1361.

British Standards Institute, BS EN 998-2:2003; "Specification for mortar for masonry. Masonry mortar", published October 30, 2003.

CEN TC 250,"Design of masonry structures-Part 1-1: General rules for buildings-Rules for reinforced and unreinforced masonry (ENV 1996-1-1)" Eurocode 6, CEN Technical Committee 250/SC6, Brussels 1995.

Chen W. F.; "*Plasticity in Reinforced Concrete*", McGraw-Hill Book Company, New York, 1981.

Chen W. F. and Han D. J.; "*Plasticity for Structural Engineering*", Springer-Verlag, New York, 1988.

Chiou Y. J., Tzeng J. C., and Liou Y. W.; " Experimental and analytical study of masonry infilled frames", Journal of Structural Engineering, ASCE, October 1999, Vol. 125(10): 1109-1117.

Choubey U. B.; "Behaviour of infilled frames under cyclic loads", Ph.D. thesis, submitted to Indian Institute of Technology (IIT), Delhi, 1990.

Chrystormou C. Z., Gergley P., Abel J. F.; "Nonlinear seismic response of infilled steel frames", Proceeding of 10^{th} World Conference On Earthquake Engineering, A. A. Balkema, Rotterdam, the Netherlands, 1992, Vol. 8: 4435-4437.

Colangelo F.; "Pseudo-dynamic seismic response of reinforced concrete frames infilled with non-structural brick masonry", Earthquake Engineering and Structural Dynamics, 2005, Vol. 34: 1219-1241.

Combescure D. and Pegon P.;" Application of the local-to-global approach to the study of infilled frame structures under seismic loading", Nuclear Engineering and Design, 2000, Vol. 196: 17-40.

Dawe J. L., Seah C. K., and Liu Y.;"A computer model for predicting infilled frame behaviour", Canadian Journal of Civil Engineering, 2001, Vol. 28: 133-148.

Dhanasekar, M., Page, A. W., and Kleeman, P. W.; ''the failure of brick masonry under biaxial stresses'' Proceedings, American Concrete Institute, ACI (Part 2), 1985, Vol. 79: 295-313.

Dolsek M. and Fajfar P.;" Mathematical modelling of an infilled RC frame structure based on the results of pseudo-dynamic tests", Earthquake Engineering and Structural Dynamics, 2002; Vol. 31: 1215–1230.

Dolsek M. and Fajfar P.; "Inelastic spectra for infilled reinforced concrete frames" Earthquake Engineering and Structural Dynamics, 2004, Vol. 33: 1395-1416.

Dymiotis C., Kappos A., and Chryssanthopoulos M.; "Seismic Reliability of masonry-infilled RC frames", Journal of Structural Engineering, ASCE, March 2001, pp 296-305.

Eurocode 2 (EC2) ENV 1992 Design of concrete structures, 1992.

Eurocode 8 (EC8) "Structures in seismic regions, Part 5, Foundations, Retaining Structures, Geotechnical Aspects" Draft, January 1991.

Federov V. V. and Hackl P.;" Model-oriented design of experiments", In: lecture notes in statistics, 1997, Vol. 125, Springer-Verlag, NY.

Fiorato A. E., Sozen M. A. and Gamble W. L.; "An investigation of the interaction of reinforced concrete frames with masonry filler walls" Report UILU-ENG-70-100, Department of Civil Engineering, University of Illinois, Urbana-Champaign IL, USA. 1970.

François M. and Royer-Carfagni G., "Structured deformation of damaged continua with cohesive-frictional sliding rough fractures", European Journal of Mechanics A/Solids, 2005, Vol. 24: 644-660.

Gambarotta L. and Lagomarsino S.; "Dynamic Models for the seismic response of brick masonry shear walls. Part I: the mortar joint model and its applications", Earthquake Engineering and Structural Dynamics, 1997, Vol. 26: 423-439.

Ghosh A. K. and Made A. M.;"Finite Element Analysis of Infilled Frames", Journal of Structural Engineering, ASCE, 2002, Vol. 128 (7): 881-889.

Goodman R. E., Taylor R. L., and Brekke T. L.; "A model for the mechanics of jointed rock", Journal of the Soil Mechanics and Foundations Division (ASCE), 1968, Vol. 94(SM3): 637-659.

Gopalaratnam V. S., Shah S. P.; "Softening response of plain concrete in direct tension". American Concrete Institute, ACI, 1985; Vol. 82: 310–23.

Halphen B. and Nguyen Q. S., "*Sur les matériaux standards*", généralisés. J. Mécanique, 1975, Vol. 14 (1): 38-63.

Hendry A.; "Structural Brickwork", Macmillan, London, 1981.

Holmes M.; ''Steel frames with brickwork and concrete infilling'', Proceeding, Institute of Civil Engineering, Structural Building, 1961, Vol. 19: 473-478.

Hughes T. JR.; "The finite element method", linear static and dynamic finite element analysis. Englewood Cliffs, NJ: Prentice-Hall, 1987.

IDARC 2D Version 6.1, February 2006. User's Guide.
http://civil.eng.buffalo.edu/idarc2d50/, Accessed September 2007.

Ignatakis C., Stavrakakis E., and Penelis G.,"Analytical model for masonry using the finite element method." Proceedings of international conference on Structural Repair and Maintenance of Historical Buildings, Florence, Italy, Birkhauser, 1989, 511–523.

Jefferson A. D. and Mills N. R., "Fracture and shear properties of concrete construction joints from core samples", Journal of Materials and Structures, 1998; Vol. 31: 595–601.

Kakaletsis D. J. and Karayannis C. G.; "Influence of masonry strength and openings on infilled R/C frames under cycling loading", Journal of Earthquake Engineering, 2008, Vol. 12: 197-221.

Kappos A. J., Stylianidis K. C., and Michailidis C. N.; ''Analytical models for brick masonry infilled R/C frames under lateral loading'', Journal of Earthquake Engineering, 1998-b, Vol. 2(1):59–87.

Kappos A. J., Dymiotis C., and Chryssanthopoulos M. K.; "Seismic Reliability of Masonry-Infilled RC Frames", Journal of Structural Engineering, ASCE, 2001, Vol. 127: 296-305.

Kappos A. J., Penelis G. G, and Drakopoulos C. G.; "Evaluation of Simplified Models for Lateral Load Analysis of Unreinforced Masonry Buildings", Journal of Structural Engineering, ASCE, 2002, Vol. 128(7): 890-897.

Karsan I. D., Jirsa O.; "Behaviour of concrete under compressive loadings" Journal of Structural Engineering, ASCE, 1969; Vol. 95: 2543–63.

Klingner R. E. and Bertero V. V.; "Infilled frames in earthquake-resistant construction", Report EERC/76-32, Earthquake Engineering Research Center, University of California, Berkeley, CA, USA 1976.

Lee H. S. and Woo S. W.;"Effect of masonry infills on seismic performance of a 3-storey R/C frame with non-seismic detailing", Earthquake Engineering and Structural Dynamics 2002, Vol. 31: 353-378.

Liauw T. C. and Kwan K. H.; ''Plastic theory of non-integral infilled frames'', Proceedings of Institute of Civil Engineering, 1983, Vol. 75: 379-396.

Liauw T. C. and Kwan K. H.;" Nonlinear behaviour of non-integral infilled frames", Journal of Computer and Structure, 1984, Vol. 18(3): 551-560.

Liauw T. C. and Kwan K. H.;"Unified plastic analysis for infilled frames", Journal of Structural Engineering (ASCE), 1985, Vol. 111(7): 1427-1448.

Lofti H. R. and Shing P. B.;" An appraisal of smeared crack models for masonry shear wall analysis", Journal of Computer and Structures, 1991, Vol. 41(3): 413-425.

Lourenco P.B. and Ramos L.F., "Characterization of the cyclic behavior of dry masonry joints", Journal of Structural Engineering, ASCE, 2004, Vol. 130(5): 779–86.

Luenberg D. G.;" Linear and nonlinear programming", Addison-Wesley publishing company, 1989, Reading, PA, USA.

Madan A., Reinhorn A. M., Mander J. B. and Valles R. E.; "Modeling of masonry infill panels for structural analysis", Journal of Structural Engineering, ASCE, 1997, Vol. 123(10): 1295-1302.

Mainstone R. J., Weeks G. A.; "The influence of bounding frame on the racking stiffness and strength of brick walls", Proceedings of the 2nd International Conference on Brick Masonry, Stoke-on-Trent, UK, 1970: 165-171.

Mander J. B., Nair B., Wojtkowski K. and Ma J,;" Experimental study on the seismic performance of brick-infilled steel frames with and without retrofit", Technical report NCEER-93-0001, National conference for earthquake engineering, 1993, State University of New York, Buffalo, New York.

Mehrabi A. B.; ''Behavior of masonry-infilled reinforced concrete frames subjected to lateral loadings.'' PhD thesis, University of Colorado, Boulder, Colorado, (1994).

Mehrabi A. B., Shing P. B., Schuller M. P. and Noland J. L.; "Performance of masonry-infilled R/C frames under in-plane lateral loads", Report CU/SR-94–6; Department of

Civil, Environmental, and Architectural Engineering, University of Colorado, Boulder CO, USA. 1994.

Mehrabi A. B., Shing P. B., Schuller M. P. and Noland J. L.; "Experimental evaluation of masonry infilled RC frames", Journal of Structural Engineering, (ASCE), 1996, Vol. 122(3): 228-237.

Mehrabi A. B., Shing P. B.; "Finite Element Modeling of Masonry-Infilled RC Frames", Journal of Structural Engineering, ASCE, 1997, Vol. 123(5): 0604-0613.

Morbiducci R.; "Nonlinear parameter identification of models for masonry', International Journal of Solids and Structures, 2003, Vol. 40: 4071-4090

Mosalam K. M.; "Modeling of the non-linear seismic behaviour of gravity load designed infilled frames", 1995 EERI Student Paper, Los Angeles, California, 1996.

Mosalam K. M., White R. N. and Gergely P.; "Static response of infilled frames using quasi-static experimentation" Journal of Structural Engineering (ASCE), 1997, Vol. 123(11): 1462-1469.

Ngo D. and Scordelis A. C.; "Finite element analysis of reinforced concrete beams", Journal of American Concrete Institute, ACI, 1967; Vol. 64(3): 152–163.

Oliveira D. V. and Lourenc P. B.; "Implementation and validation of a constitutive model for the cyclic behaviour of interface elements", Journal of Computers and Structures, 2004, Vol. 82: 1451-1461.

OpenSees, 2006. Command Language Manual
http://opensees.berkeley.edu/OpenSees/manuals/usermanual/index.html, Accessed November 2006.

Page A. W.; "Finite element model for masonry", Journal of structural Division, ASCE, 1978, Vol. 104(8): 1267-1285.

Page A. W., "A non-linear analysis of the composite action of masonry walls on beams", Proceedings of the Institution of Civil Engineers, Part 2, 1979, Vol. 67: 93-110.

Page A. W. and Ali S. S.;" Finite element model for masonry subjected to concentrated loads", Journal of Structural Engineering, ASCE, 1988, Vol. 114(8): 1761-1783.

Penelis G., Sarigiannis D., Stayrakakis E., and Stylianidis K., ''A Statististical evaluation of damage to buildings in the Thessaloniki Greece earthquake of June 20, 1978.'' Proceedings of the 9th World Conference on Earthquake Engineering, Tokyo-Kyoto, Japan ,1988.

Pietruszczak S. and Niu X.; "A mathematical description of macroscopic behaviour of brick masonry", International Journal of Solid Structures, 1992, Vol. 29(5): 531-546.

Polyakov S. V.; "Masonry in framed buildings (Godsudarstvenoe Isdatel' stvo Literatury Po Stroidal stvui Architecture. Moscow, 1956)", Translated by Cairns G. L. in 1963. National Lending Library for Science and Technology, 1956, Boston Spa, Yorkshire, U.K.

Polyakov S. V.; "On the interaction between masonry filler walls and enclosing frame when loaded in the plane of the wall", Earthquake Engineering, Earthquake Engineering Research Institute, EERI, San Francisco, California, 1960, pp. 36-42.

Powell G. H. and Paul F. C.; "3D beam-column element with generalized plastic hinges", Journal of Engineering Mechanics, ASCE, 1986, Vol. 112(7): 627-641.

Reinhardt H.W.; "Fracture mechanics of an elastic softening material like concrete", Heron 1984; Vol. 29(2): 3–41.

Saatcioglu M., Mitchell D., Tinawi R., Gardner N. J., Gillies A. G., Ghobarah A., Anderson D. L., and Lau D.; "The August 17, 1999, Kocaeli (Turkey) earthquake - damage to structures", Canadian Journal of Civil Engineering, 2001; 28: 715–737.

Saneinejad A., and Hobbs B.; "Inelastic design of infilled frames", Journal of structure engineering, ASCE, 1995, Vol. 121(4): 634-650.

Seah C.K., "A universal approach for the analysis and design of masonry infilled frame structures" Ph.D. thesis, Department of Civil Engineering, University of New Brunswick, Fredericton, N.B, 1998.

Seah C. K., Liu Y., and Dawe J.L.; "Behaviour of masonry infilled walls" Proceedings of the 11th International Brick/Block Masonry Conference, Tongji University, Shanghai, China, 1997, 940-948.

Singh H., Paul D. K., and Sastry V. V.; "Inelastic dynamic response of reinforced concrete infilled frames", Journal of Computers and Structures; 1998, Vol. 69: 685-693.

Shing B. and Mhrabi A. B.; "Behaviour and analysis of masonry-infilled frames", Proceedings, Structural Engineering Materials., 2002, Vol. 4: 320-331.

Sorenson H. W.;" Parameter estimation: Principles and Problems", Marcel Dekker, 1980, New York, USA.

Stafford-Smith B.; "Lateral stiffness of infilled frames", Journal of the Structural Division, ASCE, 1962, Vol. 88(ST6): 183-199.

Stafford-Smith B.; "Behaviour of square infilled frames", Journal of the Structural Division, ASCE, 1966, Vol. 92(ST1): 381-403.

Stafford-Smith B.; "The composite behaviour of infilled frames In Tall buildings", Edited by A. Coull and B. Stafford-Smith, Pergamon Press, London, U.K., 1967a, pp. 481-493.

Stafford-Smith B.; "Methods of predicting the lateral stiffness and strength of multi-storey infilled frames", Building Science, 1967b, Vol. 2: 247-257.

Stafford-Smith B. and Carter C.; "A method of analysis for infilled frames", Proceedings of the Institution of Civil Engineers, 1969, Vol. 44: 31-48.

Stankowski T, Runesson K, Sture S., "Fracture and slip of interfaces in cementitious composites. I: characteristics", Journal of Engineering Mechanics, ASCE, 1993; Vol. 119(2): 292–314.

Stutcliffe D. J., Yu H. S. and Page A. W.; "Lower bound limit analysis of unreinforced masonry shear wall", Computer and Structures, 2001, Vol. 79: 1295-1312

Tarr A. C.; "Reinforced Concrete Structures In Seismic Zone", World Seismicity Map, American Concrete Institute, ACI, Detroit, 1977.

UBC (1991) Uniform Building Code. International Conference of Building Officials, Whittier, California, USA.

Valiasis T. N. (1989); ''Experimental investigation of the behaviour of RC frames infilled with masonry panels and subjected to cyclic horizontal load-Analytical modeling of the masonry panel.'' PhD thesis, Aristotle University of Thessaloniki (in Greek).

Weaver W. and Gere J. M.; "Matrix analysis of framed structures", 2nd ed. D. Van Nostrand, New York, 1980.

Weaver W., and Johnston P.R.; "Finite elements for structural analysis" Prentice-Hall, Inc., Englewood Cliffs, New Jersey, 1983.

Wood R. H.; "Plasticity, composite action and collapse design of unreinforced shear wall panels in frames'' Proceedings of the Institute of Civil Engineering, Part 2, 1978, Vol. (65): 381-411.

Zarnic R., and Gostic S.; "Non-linear modelling of masonry infilled frames", Proceedings of the 11th European Conference on Earthquake Engineering, Paris, France. 1998.

Zarnic R., Gostic S., Crewe A. J., and Taylor C. A.; "Shaking table tests of 1:4 reduced-scale models of masonry infilled reinforced concrete frame buildings", Journal of Earthquake Engineering and Structural Dynamics, 2001; Vol. (30): 819-834.